GEOLOGY OF THE TELESCOPE PEAK QUADRANGLE, CALIFORNIA

AND

LATE MESOZOIC REGIONAL METAMORPHISM, DEATH VALLEY AREA, CALIFORNIA

Thesis by

Theodore Charles Labotka

In Partial Fulfillment of the Requirements

for the Degree of

Doctor of Philosophy

California Institute of Technology

Pasadena, California

1978

(Submitted May 24, 1978)

ACKNOWLEDGMENTS

Many people have helped me, both physically and mentally, during the tenure of this study. Arden L. Albee allowed me the freedom to take my own direction in the thesis, and his criticism prevented me from making far-fetched conclusions and considerably improved this final output. Jo Laird and Robert Powell listened freely to my random thoughts on petrology and geology in my attempts to coagulate a coherent thesis. Leon Silver has shown a continued interest in the geology of the Panamint Mountains and has instilled in me an interest in the regional geology of the southwestern United States. Lauren Wright guided me through the geology of the southern Death Valley area; I have had many fruitful discussions with him and Bennie Troxel about the geologic evolution of Death Valley, and they kindly provided me a copy of their geologic map of the Funeral Mountains. Marvin Lanphere and Douglas McDowell have spent time with me in the field and discussions with them helped formulate the synthesis of the geology of the Telescope Peak Quadrangle.

I have benefited from discussions with Scott Baldridge, David Beaty, Robert Dymek, and James Quick about the application of microprobe analysis to petrologic problems. Arthur Chodos has helped make microprobe analysis less of a chore through his efforts in maintaining a first-rate facility and has helped immensely in computer programming.

George Richmond, and Jim and Norma Weston made Happy Canyon pleasant.

Field work was supported by a Geological Society of America Penrose Bequest grant to me, and analytical work was supported by a National Science Foundation grant EAR75-03416 A03 to A. L. Albee.

ABSTRACT

The Telescope Peak Quadrangle lies in the central Panamint Mountains which form the western boundary of Death Valley, California. The oldest rocks in the quadrangle consist of an 1800 m.y. complex of augen gneiss, quartzofeldspathic gneiss, and muscovite-biotite schist. These rocks were intruded approximately 1400 m.y. ago by porphyritic quartz monzonite in the World Beater Dome area. The earlier Precambrian rocks are unconformably overlain by the later Precambrian Pahrump Group. The Pahrump Group is comprised of the Crystal Spring Formation, Beck Spring Dolomite, and Kingston Peak Formation. These formations show variations in thicknesses and lithologies within the quadrangle which indicate that the Pahrump Group was deposited in a dynamic environment. The lithologies and thicknesses of the Crystal Spring Formation and Beck Spring Dolomite indicate that most of the quadrangle was underlain by a platform of earlier Precambrian basement which stood above sea level in the World Beater Dome area (World Beater Island) and which dropped off into deeper water near Tuber Canyon. The distribution of locally derived conglomerates in the lower Kingston Peak Formation and the presence of a local unconformity at the base indicate that at the end of Beck Spring Dolomite deposition, World Beater Island and adjacent areas to the north were uplifted, and the lower Kingston Peak Formation was deposited in eastern and western basins separated by the uplift. Continued deposition buried the uplift, and upper units in the Kingston Peak Formation include diamictite which grades northward into fine-grained

greywacke, pillow basalt interbedded in the diamictite, micaceous limestone, conglomerate, and argillite. The Pahrump Group is unconformably overlain by later Precambrian Noonday Dolomite, Johnnie Formation, Stirling Quartzite and Cambrian and Precambrian Wood Canyon Formation. The rocks were regionally metamorphosed at low pressure and intruded by leucocratic, muscovite-bearing granite about 80 m.y. ago. Folding occurred after this metamorphism and a north-northwest-trending anticline and World Beater Dome were formed. Retrograde metamorphism accompanied the folding event. Subsequently, low-angle normal faults developed, the Miocene Little Chief stock was intruded, large masses of monolithologic breccia formed, and the Panamint Mountains were uplifted along the Panamint Valley fault zone.

Regional metamorphic terrains in the Panamint Mountains and in the Funeral Mountains show marked differences in the physical conditions attained during metamorphism. The Panamint Mountains exhibit low pressure regional metamorphism, and the characteristic assemblages developed in pelitic schists are andalusite + staurolite + biotite and andalusite + cordierite + biotite. Isograds based on the appearance of sillimanite in pelitic rocks and tremolite and diopside in calcareous rocks indicate a westward increase in metamorphic grade toward an 80 m.y. muscovite granite pluton. A higher pressure metamorphic terrain was developed in the Funeral Mountains, and mineral assemblages in pelitic rocks are characterized by the presence of kyanite. Garnet, staurolite, and kyanite isograds have been delineated and show that the grade increases toward the structual culmination of the Funeral Mountains. Migmatites occur in the highest grade

area (sillimanite + garnet + biotite + muscovite + quartz), and the metasedimentary sequence was intruded by muscovite granite. The reaction

chloritoid → staurolite + garnet + chlorite

is recorded in the Funeral Mountains, but in the Panamint Mountains the coexistence of chloritoid + biotite indicates that the garnet + chlorite join became unstable prior to the breakdown of chloritoid. Microprobe data on coexisting mineral assemblages, chemographic analysis of mineral facies in pelitic schists, and available experimental data indicate that the extremes in physical conditions attained during metamorphism were ~3 kb, ~600°C in the Panamint Mountains and ~8.5 kb, ~700°C in the Funeral Mountains. The sequence of tectonic and metamorphic events in the two areas is similar, but the facies series represent greatly different P/T gradients.

Assemblages in calciferous schist from the low pressure environment in the Panamint Mountains are characterized by quartz + epidote + calcic amphibole + chlorite + biotite in the tremolite zone and by quartz + epidote + calcic amphibole + garnet + biotite, quartz + epidote + diopside + calcic amphibole, and quartz + epidote + diopside + grossular in the diopside zone. Muscovite or microcline are common additional phases. Assemblages which occur in quartz + epidote + muscovite or quartz + epidote + microcline rocks are potentially useful for delineation of metamorphic grade and distinction between lower and higher pressure facies series. The compositions of calcic amphiboles formed in a low pressure environment generally fall in the series tremolite-pargasite and are related to the continuous break-

down of epidote and chlorite.

TABLE OF CONTENTS

page

FIGURES

page

TABLES

1

INTRODUCTION

This thesis presents the results of mapping and a synthesis of mapping by others in the central Panamint Mountains and the results of petrologic investigation on the regionally metamorphosed rocks in the Panamint and Funeral Mountains, Death Valley area, California. The presentation is divided into three sections.

The first section describes the results of several years of mapping and thought about the geology of the Telescope Peak Quadrangle, California. Marvin A. Lanphere (1962) mapped the Wildrose Canyon area, Arden L. Albee mapped in the vicinity of World Beater Dome (Lanphere, Wasserburg, Albee, and Tilton, 1964), and S. Douglas McDowell (1967) mapped in the vicinity of the Little Chief stock. In addition, Albee, Lanphere, and McDowell (1971) reconnoitered the geology of the remainder of the quadrangle and R. Smith (1976) mapped young faults in Panamint Valley. I mapped the northwestern part of the quadrangle in greater detail and compiled the other authors' work with mine onto a 1:48,000 base. The map (Plate I), cross sections (Plate II), and correlation of map units (Plate III) are folded in the back of the thesis, and the description of map units is located in the appendix. The stratigraphy, structure, an outline of the metamorphism, and geologic history of the Telescope Peak Quadrangle are synthesized and presented in part I.

Parts II and III describe the petrology of the regionally metamorphosed rocks in the Death Valley area. In part II the development of mineral assemblages in siliceous dolomite and pelitic schist from the low pressure terrain in the Panamint Mountains is contrasted with the development in the higher pressure terrain in the Funeral Moun-

tains. Pelitic schist comprises only a small amount of the metamorphic rock types in the Panamint Mountains. However, pelitic schist assemblages are emphasized in this discussion, because they have been extensively studied elsewhere and hence, the pressure-temperature regime during metamorphism is generally described in terms of mineral assemblages in pelitic schist.

The more abundant rock type in the Panamint Mountains is calciferous schist and part III describes the petrology of calciferous schist metamorphosed in a low pressure environment. Mineral assemblages in calciferous schist have not been studied as extensively as pelitic schist assemblages, and consequently the development of assemblages with increasing grade is poorly understood. The mineral assemblages which occur in the Panamint Mountains suggest a sequence of prograde metamorphic reactions, but retrograde metamorphism was superimposed and isograds based on these reactions cannot be mapped. The suggested sequence of reactions and mineral assemblages is, nonetheless, a potentially valuable indicator of metamorphic grade.

GEOLOGY OF THE TELESCOPE PEAK QUADRANGLE, CALIFORNIA

INTRODUCTION

The Telescope Peak Quadrangle encompasses the central Panamint Mountains which form the western boundary of the central part of Death Valley, California (Figure 1). The Panamint Mountains are a north-trending range with a tremendous amount of relief. Telescope Peak, 11,049 feet above sea level, is the highest point, and it lies only about 25 km west of the lowest point in Death Valley, 282 feet below sea level. The lowest elevations within the quadrangle are in Panamint Valley at approximately 1040 feet above sea level. The topography is rugged along the east side of the range crest and along the western margin of the range. West-flowing streams are deeply incised near the western margin, but the canyons widen toward the divide, and the heads of many drainages occur in broad, high parks.

The climate in the Death Valley region is desert and the vegetation at the lower elevations is sparse and is characterized by creosote, desert holly, and plants of the buckwheat family. The higher elevations of the Panamint Mountains receive substantial precipitation, and the west-draining, spring-fed streams flow nearly year-round. Mesquite and willow occur in the canyons and near springs. At higher elevations, sagebrush, mountain mahogany, pinyon, juniper, limber pine and bristlecone pine grow. In general, the rugged topography, dry climate, and sparse vegetation allow good exposures of rock.

Access to the range is principally from the west. A gravel road runs along the east side of Panamint Valley, and jeep trails are located in Tuber, Surprise, Happy, and Pleasant Canyons. Most are washed out by the frequent, summer flash floods and are rebuilt only

Figure 1: Location of the Telescope Peak Quadrangle (TPQ) and Chloride Cliff Quadrangle (CCQ), eastern California.

UNITED STATES
DEPARTMENT OF THE INTERIOR
GEOLOGICAL SURVEY

DEATH VALLEY NATIONAL MONUMENT AND VICINITY

CALIFORNIA-NEVADA

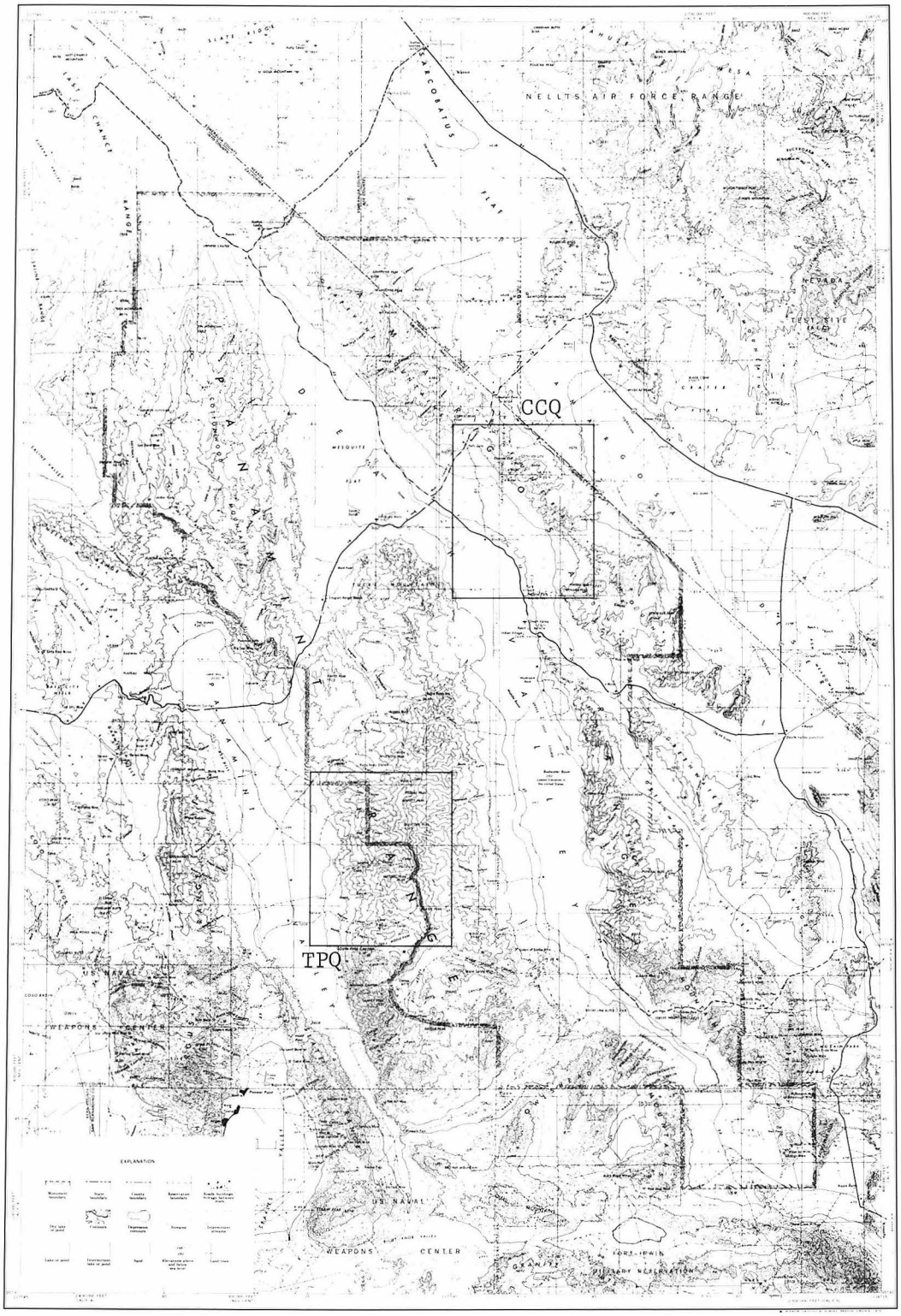

when there is sufficient interest in a mining venture in the mountains. A paved road serves Wildrose Canyon and is maintained by the National Park Service. A gravel road runs along the west side of Death Valley and jeep trails run up Hanaupah Canyon and Butte Valley.

There are no permanent settlements in the Telescope Peak Quadrangle, but a number of miners live in Ballarat, a once active mining town, and in Happy, Pleasant, and Jail Canyons. Indian Ranch, a reservation at the mouth of Hall Canyon, caters to the occasional tourist, and a ranger station is located in Wildrose Canyon.

The Panamint Mountains have elicited considerable economic interest because of the numerous silver and gold deposits, and Panamint City, located in upper Surprise Canyon, was a major silver mining district in the 1870's. The Panamint Mountains hold considerable geologic attention because they contain the westernmost exposures of known Precambrian rocks in central California and contain the easternmost Sierra Nevada-type plutonic rocks. In addition, the tremendous relief across the mountains is maintained by Quaternary faulting.

Murphy (1930, 1932) carried out the first detailed studies of the geology of the Panamint Mountains. He described the geology of the Panamint City Mining District and reconnoitered the geology of the Telescope Peak area. Murphy divided the late Precambrian strata into several formations with local names.

White (1940) mapped two small areas in Wildrose Canyon because of the presence of possibly economic antimony deposits. Hopper (1947) mapped a strip of the Emigrant Canyon Quadrangle to the north and recognized the presence of the Johnnie Formation, Stirling Quartzite, and

Wood Canyon Formation, as well as younger formations which are not exposed in the Telescope Peak Quadrangle. Maxson (1950) investigated the physiography of the Panamint Range and described an old erosion surface of moderate relief, later uplifted by displacement on the Panamint Valley Fault Zone and severely dissected.

Johnson (1957) mapped a portion of the Manly Peak Quadrangle to the south and recognized the presence of the Kingston Peak Formation and Noonday Dolomite in the Panamint Mountains. Albee and Lanphere (1962) correlated the rock units described by Murphy (1932) with the Pahrump Group and Noonday Dolomite of Hewett (1940), and Labotka and Albee (1976, 1977) outlined the depositional environment of the Pahrump Group exposed in the Telescope Peak Quadrangle.

Detailed geologic mapping in the Telescope Peak Quadrangle began in 1958 when Lanphere (1962) mapped the Wildrose Canyon area. In 1962 A. L. Albee directed the California Institute of Technology Geology Summer Field Camp and he, with B. Carter, S. Curtis, and R. Hooke, mapped the upper Pleasant and Happy Canyons area. Lanphere, Wasserburg, Albee, and Tilton (1964) described the geology and strontium isotopic characteristics of the World Beater Dome. R. Smith (1976) mapped in Panamint Valley and described the deformation of Pleistocene Lake Panamint, and Hooke (1965) estimated the amount of eastward tilting of Death Valley based in part on alluvial fan morphology on the east side of the Panamint Mountains. McDowell (1967) mapped the Little Chief stock and its environs, and Albee, Lanphere, and McDowell (1971) provided a generalized geologic map of the Telescope Peak Quadrangle for the revised edition of the Death Valley Sheet of the Geologic Atlas of

California (in press).

Additional mapping by the author was carried out in the northwest part of the area where a number of structural and stratigraphic complexities occur. This report synthesizes this new work with the work of other authors, and a unified description of the geology of the Telescope Peak Quadrangle is presented.

STRATIGRAPHY

EARLIER PRECAMBRIAN ROCKS

The oldest rocks exposed in the Telescope Peak Quadrangle are crystalline gneiss, schist, and granite which crop out in the core of a north-northwest-trending anticline and along the western margin of the Panamint Range south of Happy Canyon. These old crystalline rocks are represented by three principal types. The first, and possibly oldest type, is a sequence of metasedimentary micaceous schist and leucocratic, quartzofeldspathic gneiss. The second is a grey, biotite-rich augen gneiss which contains inclusions of micaceous schist. The third rock type is a grey porphyritic quartz monzonite which has intruded the augen gneiss in the World Beater Dome area.

The earlier Precambrian micaceous schist and quartzofeldspathic gneiss are exposed along the western margin of the range south of Happy Canyon and in the core of a major anticline in Surprise, Hall, and Jail Canyons. Murphy (1932) included these rocks in his Panamint Metamorphic Complex. Schistose rocks predominate in the western margin area and also occur in Surprise Canyon. The dominant lithology in these areas consists of light-grey, micaceous quartzite and feldspathic quartzite. The rocks have a well developed foliation which is principally defined by the parallel alignment of flattened or sheared quartz grains. This cataclastic texture is particularly evident in the vicinity of the west-dipping fault which separates the earlier Precambrian rocks from later Precambrian strata (the South Park Canyon fault of Johnson, 1957). Elsewhere, the parallel alignment of micas defines the foliation. Dark, biotite-rich schist and local hornblende-schist layers

are interbedded with the quartzite. These dark schist layers dominate the earlier Precambrian metasedimentary rocks in Surprise Canyon. In Surprise Canyon, where the earlier Precambrian biotite schist sequence dips steeply east, the sequence is apparently "overlain" by quartzofeldspathic gneiss. This leucocratic gneiss comprises the outcrops of earlier Precambrian rocks in Hall and Jail Canyons. The gneiss exhibits a moderately developed foliation, and the stratiform appearance of the gneiss suggests that it may have been bedded. The major phases which comprise the leucocratic gneiss are quartz, microcline, plagioclase, and muscovite. The apparent bedded nature of the gneiss suggests that the protolith may be a felsic, volcanic rock, but deformation and recrystallization have obliterated the original texture of the rock.

Visually estimated modes of representative samples of the metasedimentary rocks and quartzofeldspathic gneiss are listed in Table 1.

The two other earlier Precambrian rock types, the augen gneiss and the porphyritic quartz monzonite, occur in World Beater Dome in Happy and Pleasant Canyons. Murphy (1932) originally called these rocks World Beater Porphyry, but Lanphere and others (1964) distinguished the augen gneiss and the quartz monzonite and renamed the rocks which occur in this dome the World Beater Complex. Lanphere and others (1964) describe in detail the petrography and structural characteristics of these two rock types in their study on the isotopic characteristics of the World Beater Complex. The augen gneiss is a medium to dark grey, biotite-rich, quartz monzonitic orthogneiss. Coarse augen (up to 4 cm) of potassium feldspar megacrysts and of quartz + plagioclase segregations, a high biotite content (10 to 25 vol%), and inclusions of quartz-

TABLE 1: MODES AND COMPOSITIONS OF EARLIER PRECAMBRIAN ROCKS

	METASEDIMENTARY ROCKS			QUARTZOFELDSPATHIC GNEISS	QUARTZ MONZONITE	AUGEN GNEISS
	Mouth of Pleasant Canyon	South Park Canyon	Surprise Canyon	Surprise Canyon	near Stone Corral,	Pleasant Canyon
	CP 117*	CP 427c*	PML 273*	PML 271*	CP 346**	CP 93R**
Quartz	88	54	30	10	39	36
Plagioclase	5	0	20	40	25.5	21
Microcline-microperthite	5	15	0	40	13.5	25
Biotite	0	10	35	tr	8	5
Muscovite	1	10	0	tr	12	12
Hornblende	0	0	10	0	0	0
others	op	z, ch, op, ap	ep, op, ap, t	ep, ap, sph, z	ap, op, z	ap, op, z

SiO_2	73.40	71.72
TiO_2	0.20	0.51
Al_2O_3	13.60	13.68
Fe_2O_3	0.42	00.77
FeO	1.81	2.99
MnO	0.03	0.04
MgO	0.49	0.87
CaO	0.40	0.79
Na_2O	2.21	2.36
K_2O	5.94	4.38
P_2O_5	0.13	0.13
H_2O^+	0.67	1.05
H_2O^-	0.04	0.05
Total	99.34	99.33

ch = chlorite, op = opaque, ap = apatite, ep = epidote, sph = sphene, z = zircon, t = tourmaline

* visually estimated mode

** mode calculated from chemical composition

Figure 2: Earlier Precambrian World Beater Complex, Pleasant Canyon

a) biotite augen gneiss

b) intrusive relation between quartz monzonite and augen gneiss

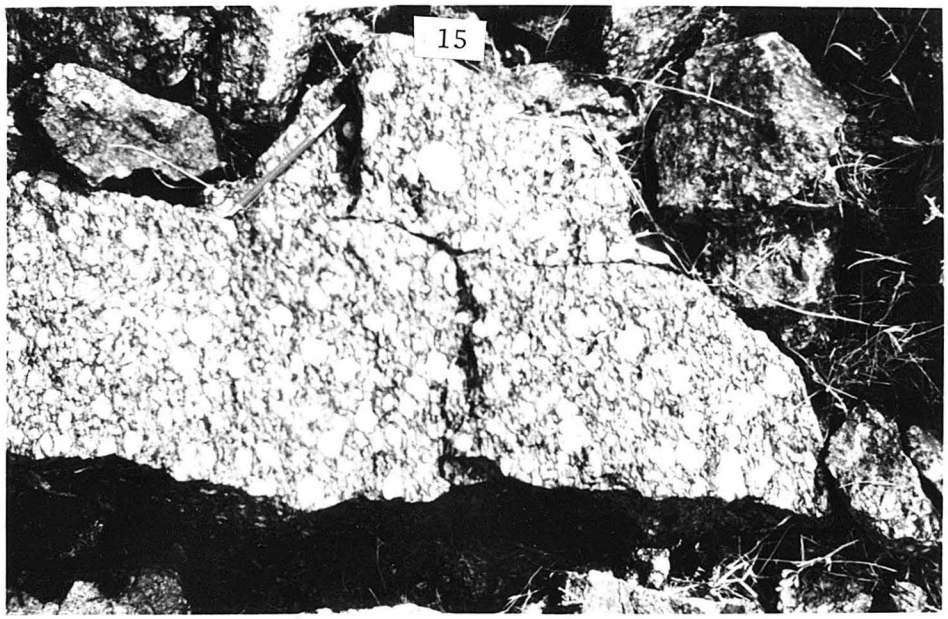

a

b

biotite-muscovite schist distinguish this unit from all other Precambrian rocks (Figure 2a). The relative age relations between the augen gneiss and the metasedimentary rock sequence are unclear, but inclusions of mica schist in the augen gneiss suggest that it intrudes the paragneiss and schist.

The grey augen gneiss was intruded by a light grey, equigranular to porphyritic quartz monzonite. The rock has a non-foliated, hypidiomorphic granular texture and contains megacrysts of tabular potassium feldspar. This granite crosscuts the foliation in the augen gneiss, and in many places the augen gneiss is pervasively invaded by the granite (Figure 2b). Augen gneiss and granite are represented by one map unit, the World Beater Complex. Modes and chemical analyses of representative samples of the augen gneiss and the quartz monzonite are taken from Lanphere and others (1964) and listed in Table 1.

Uranium-lead ages were obtained from zircon separates from the augen gneiss and the grey quartz monzonite by Lanphere and others (1964). The isotopic systems were greatly disturbed during the Mesozoic but they indicate that the augen gneiss is approximately 1790 m.y. old and the cross-cutting quartz monzonite is about 1350 m.y. old. Potassium-argon and rubidium-strontium ages obtained from pegmatites which cut across metarhyolite in the Warm Spring area (southeast side of the Panamint Mountains) give ages ranging from 1660 to 1730 m.y. (Wasserburg and others, 1959). $^{207}Pb/^{206}Pb$ ages obtained from zircon separates from the metarhyolite and a granitic gneiss in the same area are 1720 and 1780 m.y. respectively (Silver and others, 1961). No isotopic age data are available from the metasedimentary sequence, but the inclu-

sions of mica schist in the augen gneiss suggest that the quartzite-schist sequence is older than the augen gneiss.

LATER PRECAMBRIAN ROCKS — PAHRUMP GROUP

Introduction

The later Precambrian Pahrump Group occupies a unique position in the stratigraphic sequence of the Death Valley area, California. These are the oldest deposits in the southwest Great Basin which were not metamorphosed and strongly deformed prior to late Paleozoic and Mesozoic tectonic events. The Pahrump Group marks the inception of grossly continuous sedimentation through the Paleozoic, and because the Pahrump is extensively exposed in the Panamint Mountains an opportunity is provided to study the environment of the initial deposits in the Cordilleran Geosyncline.

These later Precambrian sedimentary rocks were first described in the Panamint Mountains by Murphy (1932). He applied the term Panamint Metamorphic Complex to the oldest and more highly metamorphosed rocks in the Panamint Mountains (Figure 3). He assigned overlying rocks to Marvel Dolomitic Limestone, Surprise Formation, and Telescope Group (Figure 3). Subsequently, Hewett (1940) defined the Pahrump Group in the Kingston Range and divided the group into Crystal Spring Formation, Beck Spring Dolomite, and Kingston Peak Formation. The Kingston Peak Formation was recognized in the southern Panamint Mountains by Johnson (1957), and he correlated this formation with the Surprise Formation and the lower part of the Telescope Group of Murphy (1932). Albee and Lanphere (1962) recognized the presence of earlier Precambrian base-

Figure 3: STRATIGRAPHIC NOMENCLATURE FOR THE PAHRUMP GROUP

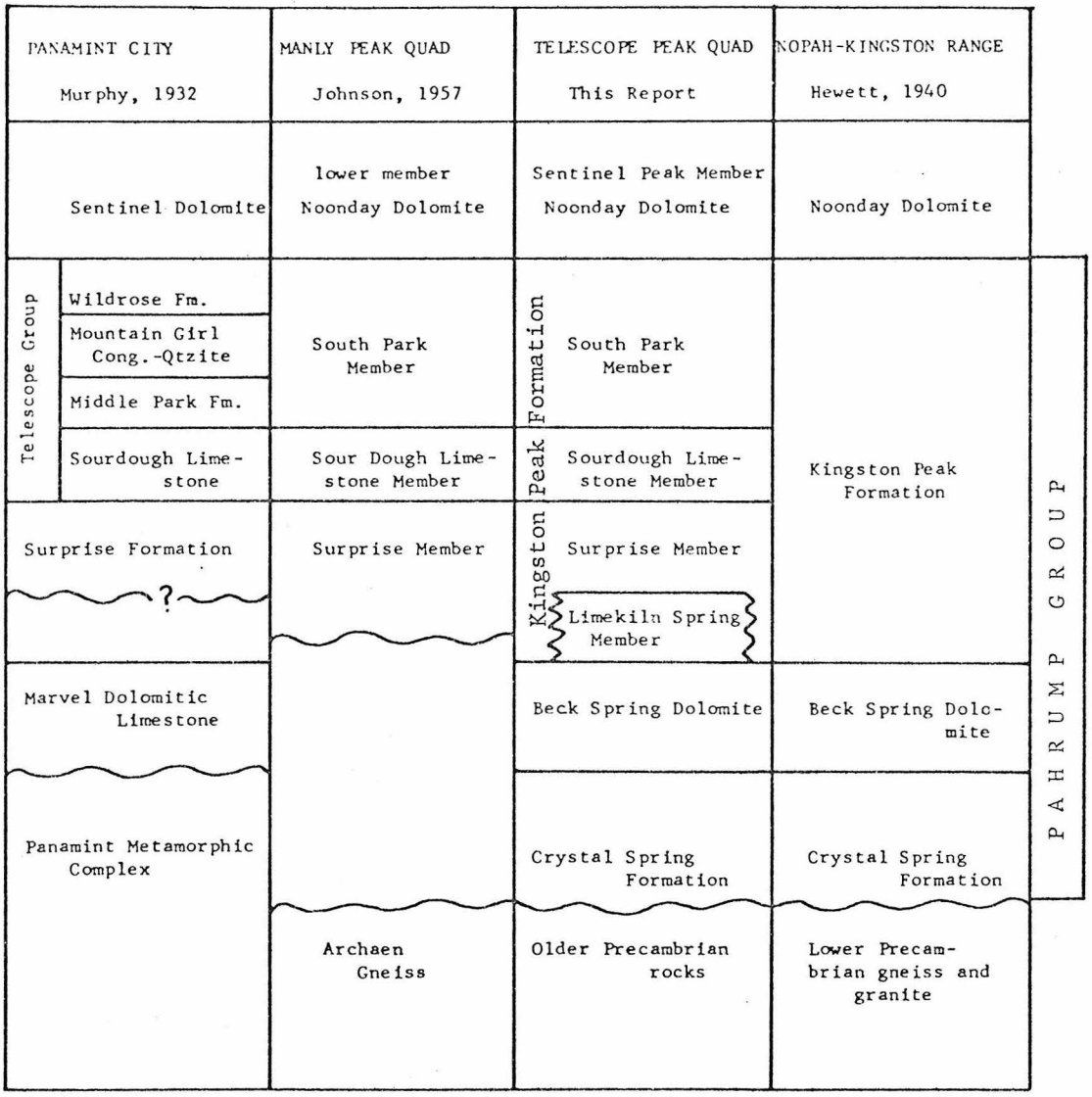

ment and the Pahrump Group in the Telescope Peak Quadrangle, and they correlated the earlier Precambrian basement and the Crystal Spring Formation to the Panamint Metamorphic Complex, and the Beck Spring Dolomite to the Marvel Dolomitic Limestone. Widespread use of Hewett's (1940) nomenclature has lead to the abandonment of Murphy's formational names.

The detailed mapping which allowed the correlation of the Panamint Metamorphic Complex of Murphy (1932) with the Pahrump Group and earlier Precambrian basement revealed a complex change in the lithologies and thicknesses of the Pahrump Group over relatively small distances. Late Mesozoic and Tertiary folds and faults are superimposed on the Precambrian rocks, and these structures confuse the stratigraphic relations. Structural and geographic features frequently referred to in the following descriptions are indicated in Figure 4. Particularly important features are the north-northwest-trending anticline and the associated World Beater Dome. Stratigraphic sections are incomplete and highly faulted on the west side of this feature. Even on the east flank of the structure unfaulted sections are rare. Measured sections on the east flank are derived from Albee and Lanphere (1962) (Pleasant Canyon and Sentinal Peak), Johnson (1957) (a South Park-Redlands Canyon composite), and Murphy (1932) (Surprise Canyon). Additional sections were measured in Tuber and Jail Canyons, and the descriptions of the sections in Surprise Canyon and on Sentinal Peak were supplemented.

Stratigraphic sections on the west flank of the anticline are incomplete. Partial sections were measured in lower Surprise Canyon but most thicknesses are calculated from the map distribution. Errors

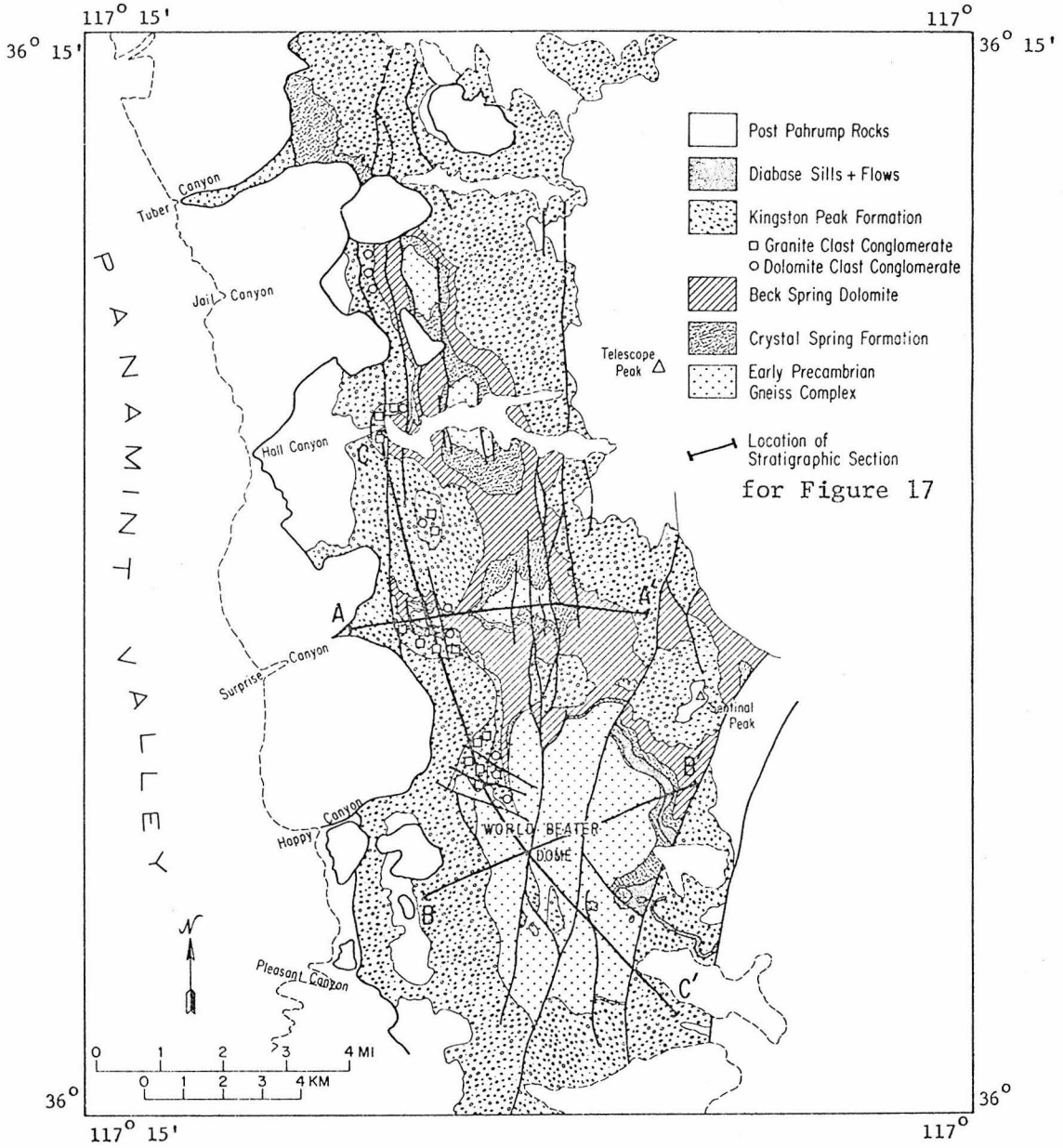

Figure 4: Generalized geology of the Pahrump Group, Telescope Peak Quadrangle.

are difficult to estimate because many contacts are gradational and because many units change in thickness over very small distances. Calculated thickness is also subject to errors in contact locations and in dip. However, the arguments are based on large changes in thicknesses and errors as large as 20% (in the worst cases) are tolerable.

The late Mesozoic metamorphism makes textural analysis difficult, but the metamorphic rocks do preserve many primary sedimentary structures, particularly millimeter-scale bedding and graded bedding. Despite later metamorphism and deformation, the changes in thicknesses and in the overall lithologies of the constituent units allow a first order determination of the paleogeography during the late Precambrian.

Crystal Spring Formation

The Crystal Spring Formation is the oldest of the formations which comprise the Pahrump Group. The Crystal Spring Formation was defined by Hewett (1940) for exposures in the Kingston Range and was correlated to part of the Panamint Metamorphic Complex by Albee and Lanphere (1962). Like most of the lithologic units in the central Panamint Mountains the thickness of the Crystal Spring Formation is variable. The Crystal Spring Formation is 200 to 300 m thick in most places, but in Tuber Canyon where the base is not exposed the formation appears to be greater than 1000 m thick. The formation thins toward World Beater Dome and is absent on the west and southwest flanks of the dome.

A complete section is exposed on the southwest side of Sentinal Peak (Figure 5). The formation contains 18 m of light grey quartzite which contains quartzite clasts at the base. The quartzite is overlain

Figure 5: Stratigraphic Sections of the Pahrump Group, Panamint Mountains.

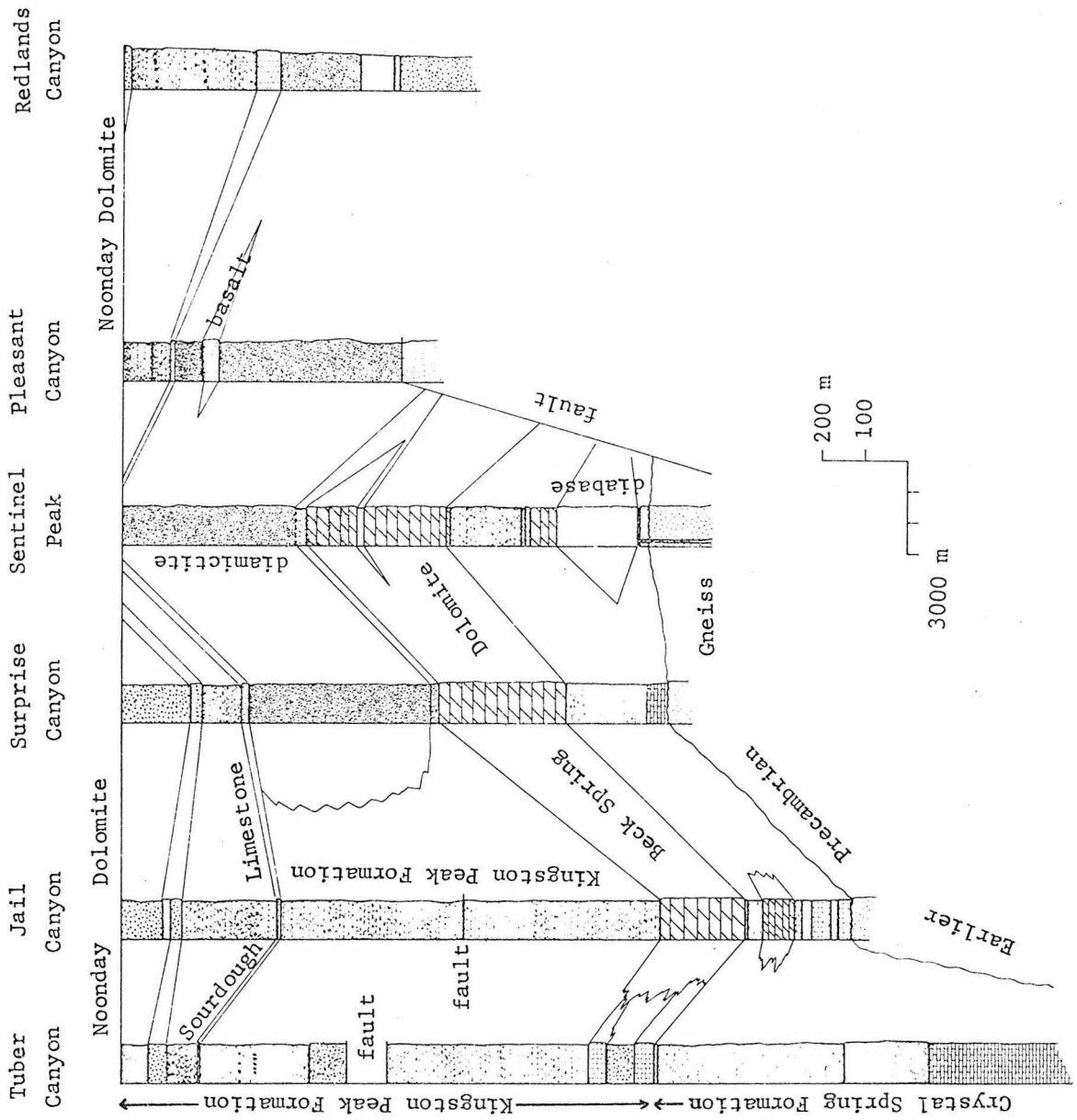

by about 60 m of light grey dolomite and 200 m of blue-grey micaceous quartzite which is interbedded with argillite and dolomite in the upper 15 m. The section was intruded by a 180 m thick diabase sill and its feeder dike.

Between Surprise and Jail Canyons the Crystal Spring Formation is characterized by dark brown-weathering, micaceous carbonate (calcite marble) overlain by dark grey argillite, quartz-rich arenite, and muscovite-biotite schist. The marble comprises approximately the lower third of the formation.

In the Crystal Spring section measured in Jail Canyon (Figure 5) a lower unit, about 130 m thick, consists of rock types similar to those found to the south and includes dark-weathering micaceous marble, micaceous arenites, dark biotite schists, and amphibolite. This unit is overlain by 75 m of light tan dolomite marble. The marble is medium-bedded and contains thin interbeds of siliceous dolomite marble and arenite. The marble is overlain by 30 m of quartz-rich schist and 6 to 10 m of quartzite.

In Tuber Canyon, rocks which are here correlated with the Crystal Spring Formation comprise a section which is more than three times as thick as the Crystal Spring section exposed immediately to the south. The base is not exposed but the lowest unit consists of at least 305 m of dark brown-weathering marble similar to the dark brown marbles in the lower part of the Crystal Spring Formation. The marble contains what appear to have been chert nodules (nodular quartz segregations which have tremolite reaction rims) and massive amphibolite layers in the upper part. The marble unit is overlain by a southward thinning

wedge which consists of quartz arenite, amphibolitic schist, and white calcite marble. A middle unit consists of 210 m of flaggy micaceous quartzite. Blue-grey graphitic schist and quartzite occur at the top of the section. These rocks occur in the core of the north-northwest trending anticline, and folding may have exaggerated the true thickness.

In contrast to the apparently thick section of Crystal Spring Formation in Tuber Canyon, the formation is very thin or absent on the west and south flanks of World Beater Dome. Here the only rocks recognized as Crystal Spring Formation are white quartzite and quartzite-clast conglomerate which in most places are less than 5 m thick. Rocks assigned to the Kingston Peak Formation lie unconformably over the quartzite or rest on the older Precambrian basement. The 200 to 300 m of Crystal Spring Formation exposed on the east side of the dome thin and pinch out westward over the dome.

Beck Spring Dolomite

The Marvel Dolomitic Limestone of Murphy (1932) was correlated to the Beck Spring Dolomite by Albee and Lanphere (1962), and it lies conformably on the Crystal Spring Formation throughout most of the Telescope Peak Quadrangle. Like the Crystal Spring Formation, the thickness of the Beck Spring Dolomite varies considerably. On the east flank of the anticline 200 to 300 m are exposed, but on the northwest side of World Beater Dome the formation is only about 30 m thick and it is absent south of Happy Canyon.

On Sentinal Peak, the Beck Spring Dolomite consists of generally massive-bedded, blue-grey sandy dolomite. Oolitic dolomite is common

in the massive-bedded sequence, but near the top thinly laminated and stromatolitic dolomite, intraformational dolomite breccia, and intertongues of quartz-rich arenite and argillite are abundant (Figure 5). Similar interfingering of dolomite and siliceous clastic rocks occur in the upper Beck Spring Dolomite along the western margin of the anticline. In many places no suitable continuous carbonate horizon serves to separate Beck Spring Dolomite from the overlying, dominantly non-carbonate-bearing Kingston Peak Formation. This leads to the definition of a transitional "Limekiln Spring Member" of Kingston Peak Formation, described below.

In contrast to the gradational nature of the upper contact on the margins of the anticline, the upper contact of the Beck Spring Dolomite is sharp on top of the structural high. In Surprise Canyon, Beck Spring Dolomite is in angular discordance with the overlying Kingston Peak Formation on top of a structural high, but it interfingers with the Kingston Peak Formation on the flank of this same structure (Figure 6).

In and south of lower Happy Canyon Beck Spring Dolomite is less than 30 m thick and laps over the Crystal Spring Formation. The Beck Spring is dominantly a breccia and it pinches out just south of Happy Canyon. This breccia which occurs on top of World Beater Dome consists of angular dolomite clasts set in a dolomitic matrix and is suggestive of a shoal breccia.

Beck Spring Dolomite is also absent in the Tuber Canyon section where Crystal Spring rocks are overlain by thinly laminated, siliceous calcite marble interbedded with quartz arenite and fine-grained meta-

Figure 6: Stratigraphic relations between Beck Spring Dolomite and Kingston Peak Formation, lower Surprise Canyon.

a) Beck Spring Dolomite (light) interfingering with dark clastic rocks of Kingston Peak Formation.

b) Angular unconformity between Beck Spring Dolomite (light) and overlying Kingston Peak Formation (dark). Crystal Spring Formation is blocky cliff-former beneath Beck Spring Dolomite.

a

b

greywacke. This metalimestone and arenite sequence is continuous upward into Kingston Peak Formation with no apparent stratigraphic break. Isolated out crops in the floor of Tuber Canyon show Beck Spring Dolomite interbedded with quartz-rich arenite and grey limestone and suggest a facies change from dolomite to the clastic sequence.

Kingston Peak Formation

The lithology of the Kingston Peak Formation (Hewett, 1940) varies considerably within the Death Valley area although conglomerate and pebbly mudstone units are ubiquitous. Within the Telescope Peak Quadrangle lateral lithologic heterogeneity occurs with respect to distribution, size and composition of clasts in conglomerates.

This lithologic heterogeneity and variations in thickness are particularly acute in the lower Kingston Peak Formation. Johnson (1957) divided the Kingston Peak Formation into the Surprise, Sourdough Limestone, and South Park members which he correlated to the Surprise Formation, Sourdough Limestone, Middle Park, Mountain Girl Conglomerate-Quartzite, and Wildrose Formations of Murphy (1932) (Figure 3). In addition, the Limekiln Spring member is defined here as a unit which is transitional to the underlying Beck Spring Dolomite.

Limekiln Spring Member

The Limekiln Spring Member encompasses the greatest variation in lithology and thickness in the Kingston Peak Formation and records a dynamic environment of deposition. The unit is here named for the exposures near Limekiln Spring in Surprise Canyon. The unit is extensively and almost exclusively exposed along the western margins of the

anticline and World Beater Dome. However, the arenaceous rocks which interfinger with Beck Spring Dolomite on Sentinal Peak are also included in this member.

The lower contact intertongues with the Beck Spring Dolomite except in lower Surprise Canyon and south of Happy Canyon where the Limekiln Spring Member rests unconformably on Beck Spring Dolomite, Crystal Spring Formation, and earlier Precambrian basement. The upper contact is defined as the top of a calcareous quartzite extensively exposed in the western part of the range. This definition of the Limekiln Spring Member is largely operational because the unit is isolated from most of the rest of the Kingston Peak Formation by the anticline. Time-equivalent strata most certainly exist on the east side of the anticline and in Tuber Canyon, but the lateral gradation to these equivalents is unknown. Certainly, the axis of the present anticline and dome separated an eastern from a western depositional environment, and arguments based on the first appearance of overlying diamictite suggest that although there is a great accumulation of Limekiln Spring strata, equivalent rocks east of the anticline are quite thin.

The Limekiln Spring Member has been subdivided into several lithologic units which are shown in Figure 7, a larger scale detail of Plate 1. The three major units are an arkosic unit which occurs at the base of the member in the Hall Canyon area, a heterogeneous unit which consists predominantly of pelitic and amphibolitic schists and metagreywacke, and a quartzite and calcareous quartzite unit which occurs at the top of the member. The volumetrically abundant argillaceous layer contains within it conglomerates, breccias, and dolomite beds whose

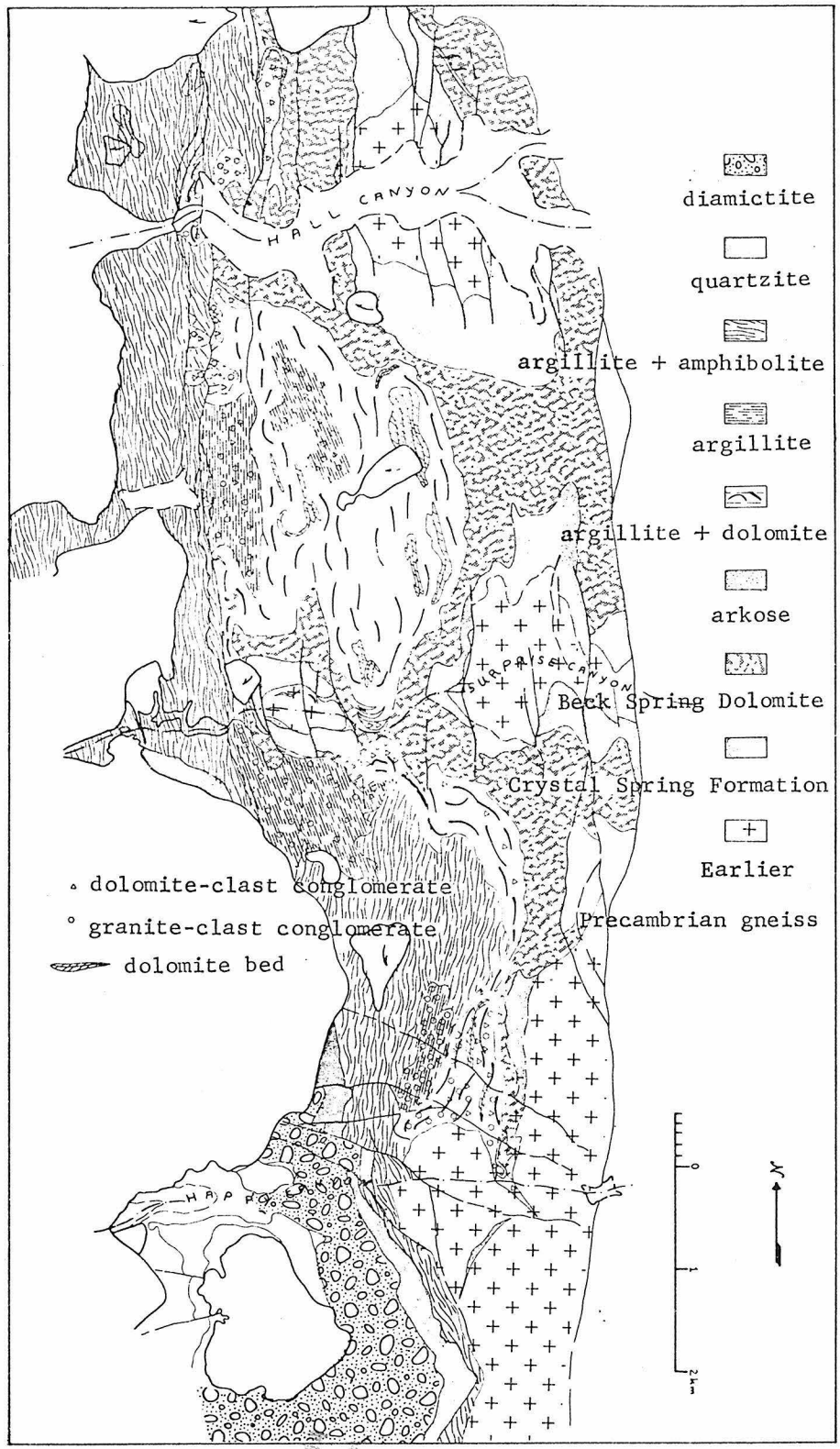

Figure 7: Distribution of lithologies within the Limekiln Spring Member, west-central Panamint Mountains.

distribution is also indicated in Figure 7.

The arkosic unit occurs at the base of the Limekiln Spring Member in the Hall and Jail Canyon areas. The unit is about 170 m thick in Jail Canyon and it pinches out just north of Surprise Canyon. The arkosic unit is comprised of a variety of lithologies which include dolomite, breccia, amphibolite, feldspathic quartzite, arkose, and arkosic conglomerate (Figure 8). The lithologies occur in 5 to 10 m thick layers which are intimately interbedded. The breccia consist of large blocks of dolomite up to several meters across, set in a green amphibolitic matrix (presumably a calcareous mud), and these breccias are interbedded with dolomite similar in appearance to the Beck Spring Dolomite. A second type of conglomerate consists of leucocratic granitic pebbles and cobbles set in a dark arenaceous matrix, interbedded with dark arenite (Figure 8). This conglomerate is considerably more abundant to the south and is described below. The third rock type is arkose or arkosic conglomerate; a component which distinguishes the arkosic unit from the rest of the Limekiln Spring Member. The arkose is coarse-grained and contains boulders of granite. The arkose is restricted to the west side of the anticline, pinches out to the south. The north and west limits are unknown, but it does not occur in the Tuber Canyon section.

Except for the arkose, the rock types which occur in the argillaceous unit are similar to those in the arkosic unit. The predominant rock type is dark brown-weathering fine-grained metagreywacke, amphibolitic schist, and pelitic schist. This unit also interfingers with Beck Spring Dolomite, and dolomite layers are common in the lower part

Figure 8: Lithologies within the Limekiln Spring Member.

a) Arkosic unit, Hall Canyon. Dark layer at bottom of cliff is a mafic sill; cliff consists of interlayered dolomite, dolomite-clast conglomerate, and arkose.

b) Granitic clast conglomerate, Hall Canyon. Large boulder is ∿0.5 m across.

c) Dolomite breccia, Surprise Canyon. Large white block is ∿2 m long.

d) Granite clast conglomerate, Surprise Canyon. Unit dips steeply to the right.

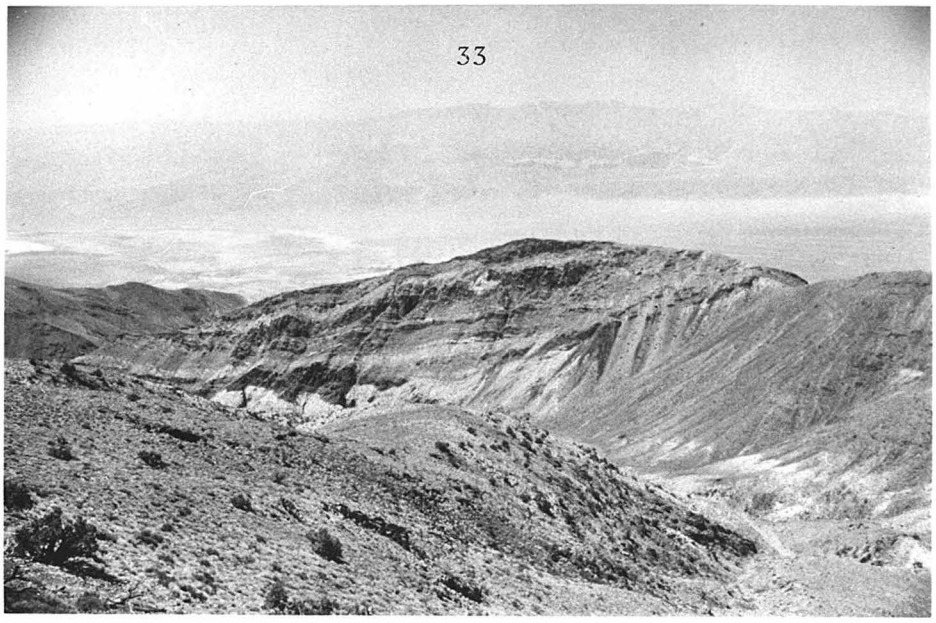

a

b

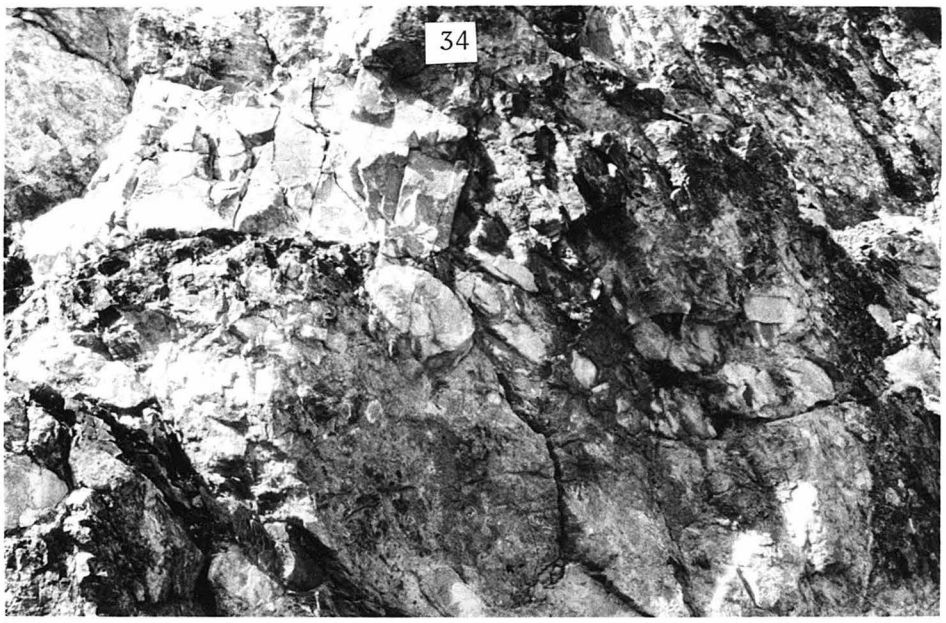

c

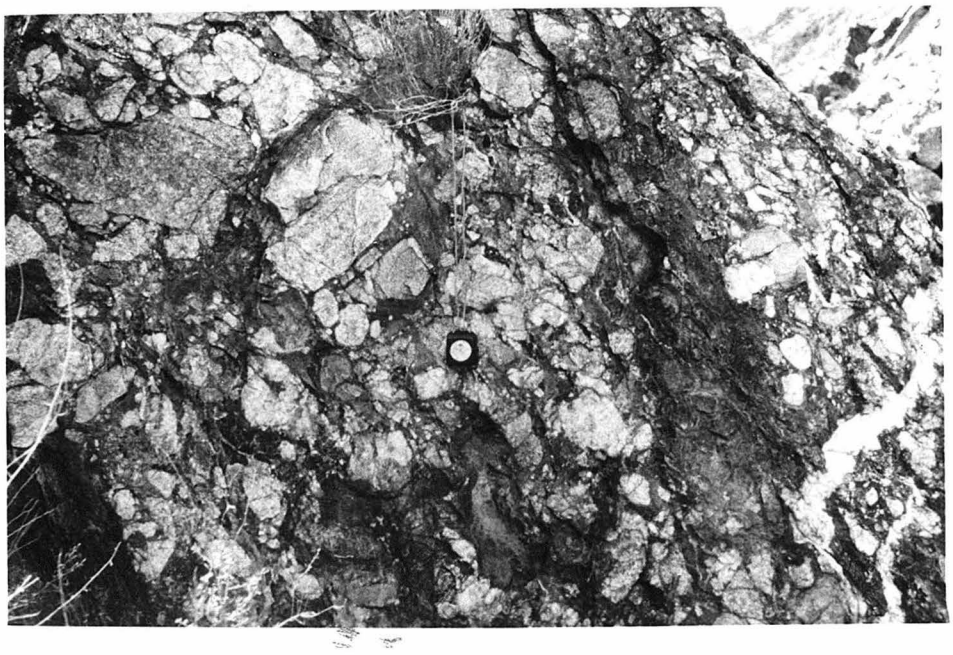

d

of the section. Conglomerate and breccia layers are unevenly distributed within this unit. Dolomite-clast breccias, similar to the ones described above, are interbedded with intertongues of Beck Spring Dolomite (Figure 8) in the trough between the two structural highs in Surprise Canyon and in the adjacent region to the south. Granite-clast conglomerate occurs in great abundance in the region between Happy and Surprise Canyons (Figure 8), and clasts of granitic rock several meters across have been observed. By and large, conglomerate is absent from the argillaceous unit north of Surprise Canyon except in the uppermost exposed section. Figure 7 details the distribution of these rock types and clast types in the Limekiln Spring Member.

The thickness of the argillaceous unit ranges from about 900 m between Happy and Surprise Canyon to 530 m in Hall Canyon. In most places the total thickness is not exposed but irregularities in thickness are readily observed.

The uppermost unit in the Limekiln Spring Member is a 120 to 140 m, thin- to medium-bedded quartzite and calcareous quartzite whose upper contact appears to be conformable with the overlying Surprise Member. The quartzite is light grey but the more calcareous layers weather yellowish-brown.

Surprise Member

The Surprise Member contains one of the most enigmatic rock types in the Death Valley area. Diamictite and associated rocks comprise the Surprise Member in Surprise Canyon and to the south. Approximately 400 m of this member are exposed in Surprise Canyon and on Sentinel Peak,

more than 530 m occur in upper Pleasant Canyon, and Johnson (1957) reports more than 500 m in Redlands Canyon where the base is not exposed.

The lower part of the member south of Surprise Canyon consists of 10-25 m of very fine-grained dark argillite and pelite which is probably equivalent to the Limekiln Spring Member. The argillite is overlain by diamictite which consists of massive, unbedded conglomeratic greywacke and pebbly mudstone. The texture is generally trimodal and consists of angular cobbles, 5 to 10 cm in diameter, sand-sized quartz and lithic grains, and clay-sized dark matrix (Figure 9). Clasts as large as several meters across have been observed and consist of dolomite, quartzite, argillite, granite and granitic gneiss, and diabase. Much of the dolomitic and gneissic clasts have local sources (see discussion).

The matrix is dense black, and the rock resembles basalt, particularly on surfaces where carbonate clasts have weathered out so that the diamictite has a vesicular appearance. Sulphides are abundant and megascopically recognizable pyrite and pyrrhotite are characteristic of the diamictite.

Interspersed within the diamictite section are fine-grained argillite beds which contain graded beds and a few exotic cobbles.

North of Surprise Canyon, the Surprise Member consists almost entirely of a monotonous sequence of thin bedded argillite, micaceous arenite, and fine-grained metagreywacke. Granitic pebble-bearing layers are rare and only three layers were encountered in the section measured in Jail Canyon. Dolomite-clast conglomerates are also uncommon and occur principally in the Kingston Peak Formation exposed in Tuber Canyon.

Figure 9: Lithologies in upper members of Kingston Peak Formation.

a) Diamictite, Sourdough Canyon.

b) Photomicrograph of diamictite from Sentinel Peak (plane polarized light); consists of dolomitic and granitic clasts, 3 to 5 mm in size, ∿0.25 mm quartz sand, and very fine-grained black matrix.

c) Pillow structures in mafic lava flow in Surprise Member, lower Pleasant Canyon.

d) Stretched pebble conglomerate, South Park Member, lower Tuber Canyon.

a

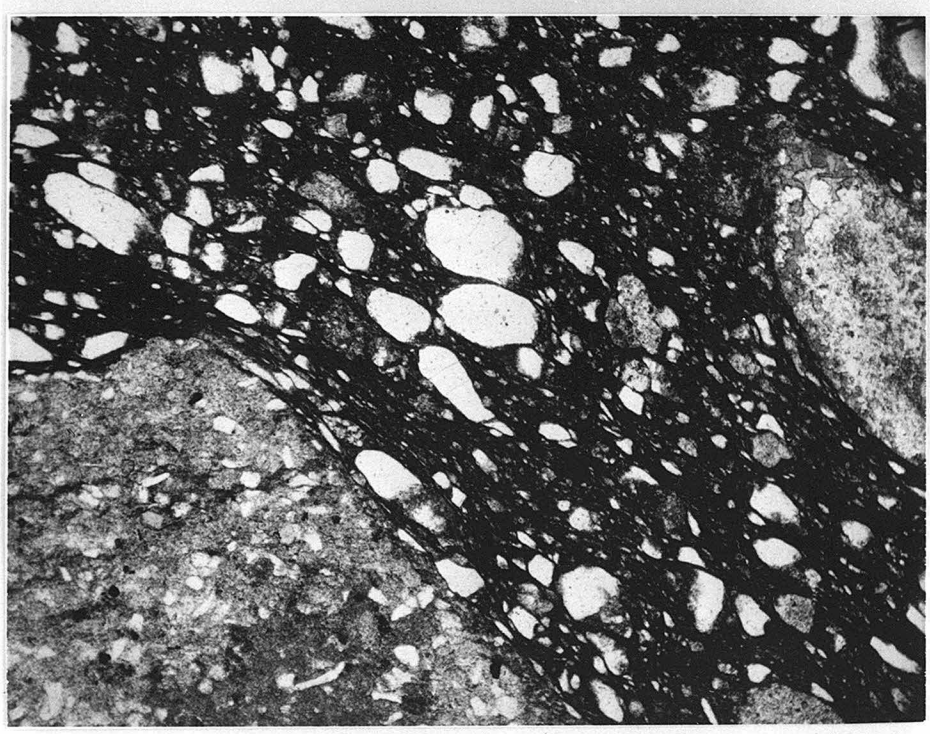

b

1mm

c

d

Thinly laminated siliceous limestone is an important component north of Hall Canyon. In Hall Canyon a 30 m thick limestone (marble) unit which contains clasts of the underlying Beck Spring Dolomite occurs at the base of the Kingston Peak Formation. This carbonate type is very abundant in Tuber Canyon where at least three 30 to 50 m units of this thinly laminated siliceous marble occur in the lower part of the Surprise Member. The marble is characterized by 5 to 10 cm carbonate-rich layers interbedded with quartz-rich layers equally as thick and is distinct from the Sourdough Limestone which does not contain abundant quartzose layers. The carbonate is moderately to strongly deformed and fold hinges and boudins are common. The limestone marble rests on the schist unit of the Crystal Spring Formation and is overlain by the dark arenite which is common in the Surprise Member. The structure of the rocks in this area is complex and the stratigraphy is consequently poorly known. As indicated above, isolated outcrops suggest that this limestone-arenite sequence in the lower Kingston Peak is the stratigraphic equivalent to the Beck Spring Formation, but the transition from the massive dolomite to a clastic carbonate-arenite sequence is obscured as a result of younger tectonic events.

The thickness of the Surprise Member north of Surprise Canyon is difficult to determine directly because the section is greatly faulted. A calculated 427 m of section occur east of the fault to the Sourdough Limestone. The lack of suitable marker horizons in this monotonous section prevent determination of the actual thickness, but the west-side-up normal faulting in this region indicates that 884 m is a minimum estimate for the thickness of the Surprise Member.

Faulting and folding is more intense in Tuber Canyon and the estimate of 1000 m shown in Figure 5 is crude and is based on an estimate of the amount of missing section and of the stratigraphy of the lower 200 m. There are at least 700 m of continuous, non-repeated section present.

In upper Pleasant Canyon and in lower Pleasant, Happy, and Tuber Canyons, mafic volcanic rock or its metamorphosed equivalent are interbedded within the diamictite and micaceous arenite of the Surprise Member ~100 m below the Sourdough Member. The mafic rock contains abundant pillow-like structures (Figure 9), and in the less metamorphosed upper Pleasant Canyon locality, the upper part of the mafic unit consists of a breccia with quartzofeldspathic clasts in the basaltic matrix and of basaltic blobs in a siliceous matrix. Whatever the origin of the diamictite, the extrusion of basaltic pillow lava indicates that at least part of the unit was deposited in a subaqueous environment.

Sourdough Limestone Member

The Sourdough Limestone is a generally thin, but persistent unit which separates the Surprise Member from the South Park Member. The unit consists of a thinly-laminated, light- and dark-grey, micaceous limestone, and varies in thickness from 50 m in the Manly Peak Quadrangle (Johnson, 1957) to less than 10 m. Much of this change in thickness may be due to later deformation; the laminae are often spectacularly folded in the thicker sections. Penecontemporaneous folds and slumps occur in places at the top, and dark clastic rocks from the overlying South Park Member are folded into the Sourdough Limestone.

South Park Member

The stratigraphy of the South Park Member is considerably more uniform than any of the lower units of the Pahrump Group, although thickness varies due to the unconformity at the top. From 80 to 250 m of thin-bedded argillite and pelitic schist rest on top of the Sourdough Limestone (Middle Park Formation of Murphy, 1932). Locally, the rock has a spotted appearance due to the presence of altered cordierite porphyroblasts. Scattered pebbly layers occur near the top of the argillite.

This argillite is overlain by 30 to 100 m of what Murphy (1932) called Mountain Girl Conglomerate-Quartzite. The lower part is dominated by conglomerate which is comprised of quartzite clasts in a reddish to black matrix. The rock is clast-supported and clasts are generally no larger than 10 cm. Far from the anticline axis, the cobbles are well rounded and spherical, but in most places the conglomerate is deformed. The stretched, white quartzite clasts in a dark matrix give the rock a spectacular appearance (Figure 9). Granule conglomerate and lithic greywacke are interbedded within the conglomerate, and the conglomerate unit grades upward into fine- to medium-grained, white to pink micaceous, feldspathic quartzite. This conglomerate-quartzite unit is locally overlain by up to 150 m of pebbly mudstone and calcareous argillite (Wildrose Formation of Murphy, 1932). The unconformity at the base of the overlying Noonday Dolomite has cut out this upper unit in most places and the conglomerate-quartzite unit typically occurs at the top of the Pahrump Group.

LATER PRECAMBRIAN ROCKS — NOONDAY DOLOMITE

Noonday Dolomite rests disconformably on the Kingston Peak Formation in the Telescope Peak Quadrangle. Angular discordance is slight, and is observed only by the truncation of upper units in the Kingston Peak Formation. This truncation is most marked on Sentinel Peak where Noonday Dolomite appears to rest on the Surprise Member of the Kingston Peak Formation. Elsewhere in southern Death Valley area the disconformity is marked by Noonday Dolomite sitting on Beck Spring Dolomite, Crystal Spring Formation, and earlier Precambrian rocks (Wright and others, 1974).

The age of the unconformity is probably late Precambrian because the lowest occurrence of lower Cambrian fossils is in the upper part of the Wood Canyon Formation, about 2000 m above the base of the Noonday Dolomite (Diehl, 1974). Noonday Dolomite, Johnnie Formation, and Stirling Quartzite are considered to be Precambrian in age, but there is no convenient stratigraphic marker to separate probable Precambrian rocks from probable Paleozoic rocks.

The rocks here recognized as comprising the Noonday Dolomite of Hazzard (1937) were first described by Murphy (1932) as the Sentinel Dolomite, Radcliff Formation, and Redlands Dolomitic Limestone. The Noonday Dolomite is extensively and nearly continuously exposed just west of the crest of the range where the threefold subdivision is easily recognized. Outcrops also occur on Tuber Ridge, in Hanaupah Canyon, and along the western flank of the World Beater Dome.

A section of Noonday Dolomite was measured in Hanaupah Canyon. The lowest member of the Noonday Dolomite, the Sentinel Peak Member

(after the Sentinel Dolomite of Murphy, 1932), consists of 30 m of medium grey, very siliceous limestone which occurs in 5 to 15 cm thick beds, overlain by 30 m of massive, grey to white dolomite. Thin irregular laminae, tubes and eyes filled with sparry calcite, and small mounds of possible algal origin are common in this member.

The middle part of the Noonday Dolomite is named the Radcliff Member (after the Radcliff Formation of Murphy, 1932) and lies conformably on top of the Sentinel Peak Member. In Hanaupah Canyon the Radcliff Member is approximately 225 m thick and consists of thinly laminated, grey, pink, green, or brown crystalline limestone interlaminated with dark greenish grey or grey argillaceous limestone and argillite. The proportion of argillite is greater in the lower part of the member where lenses of conglomerate also occur. The conglomerate consists of argillite clasts in an argillaceous matrix.

The upper member of the Noonday Dolomite is called the Redlands Member (after the Redlands Dolomitic Limestone of Murphy, 1932), and in Hanaupah Canyon the Redlands Member consists of massive, light grey dolomite, approximately 160 m thick.

Several sections of Noonday Dolomite in the Panamint Mountains are shown in Figure 10 and illustrate the lateral variations in lithologies within the formation. The Sentinel Peak Member consists of massive dolomite of probable algal origin throughout the Panamint Mountains, but the thickness ranges from about 140 m in the Pleasant Canyon area to less than 50 m in the Wildrose Canyon area. A massive dolomite everywhere occurs at the base of the Noonday Dolomite but in many places near Wildrose Canyon the Sentinel Peak Member is too thin to map sepa-

Figure 10: NOONDAY DOLOMITE - JOHNNIE FORMATION

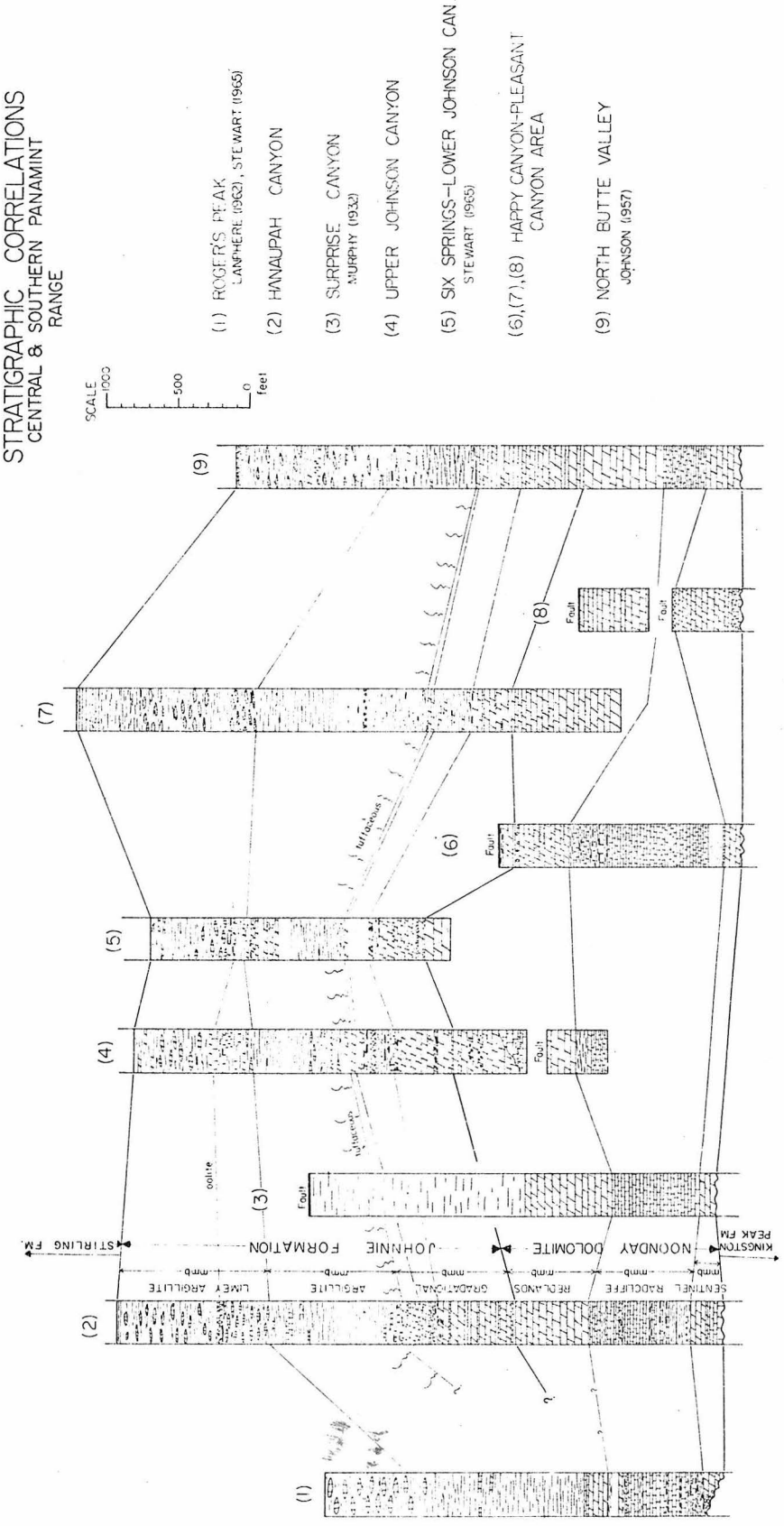

rately.

The Radcliff Member is comprised of a variety of lithologies. In the southern part of the area, near Butte Valley, the member consists almost entirely of thinly laminated limestone and only a small proportion of argillite. In the exposures of the Radcliff Member north of Happy Canyon, argillite is a major lithology and in many places the interlaminated argillite and limestone are spectacularly deformed into tight, passive-flow folds. Penecontemporaneous conglomerate in which dolomite clasts and minor argillite clasts are embedded in a dark green, calcareous, argillaceous matrix is prominent in exposures near Wildrose Canyon. The thickness of the Radcliff Member ranges from 100 to 250 m.

The Redlands Member ranges from 130 to 260 m thick and the relative proportion of clastic debris varies from south to north. North of Surprise Canyon the Redlands Member is massive dolomite and contains abundant algal structures, but in Johnson and Pleasant Canyons quartz and carbonate sandstone with calcareous matrix is abundant, and some layers are locally conglomeratic. The clastic carbonate grains range from silt-to medium sand-sizes and quartz grains, generally well rounded, range from fine sand-to pebble-sized. Crossbedding in the calcareous sandstone is well developed, and in places the sandstones are composed of 85% quartz. The lateral gradation from dolomite to sandy dolomite is observed, and in the Pleasant Canyon region where sandy dolomite and calcareous sandstone are abundant, the distinction between the Noonday Dolomite and the overlying Johnnie Formation is nebulous. The lower part of the Johnnie Formation contains dolomite beds similar in appearance to the dolomite in the Noonday Dolomite, and the base of the

Johnnie Formation is defined as the base of the lowest occurring orthoquartzite bed which interrupts the massive dolomite sequence (Hazzard, 1937). Thus, in some places there is no practical mapping boundary between the two formations.

The distribution of Noonday Dolomite and equivalent strata in the southern Death Valley region is outlined by Williams and others (1974) and Wright and others (1978). There the Noonday Dolomite is comprised of a lower, algal dolomite member and an upper dolomite member. The lower dolomite member contains mound-like structures which had as much as 200 m of relief across them. The upper dolomite member consists of a greater variety of lithologies. Thin-bedded dolomite and argillite filled the deep areas between the mounds of the lower member. The majority of the member consists of algal dolomite which contains abundant stromatolites, tubes, and eyes. Farther south, clastic debris becomes abundant, and a transition from the platform facies Noonday Dolomite to a basinal equivalent occurs. The basinal equivalent is comprised of breccia, arkosic sandstone, siltstone, and shale, interbedded limestone and dolomite and dolomite-quartz sandstone (Williams and others, 1974). Tentative correlation of Noonday Dolomite in the Panamint Mountains to the southern Death Valley area suggests that the Sentinel Peak Member corresponds to the lower dolomite member, and the Redlands Member corresponds to the upper dolomite member. It is not certain whether the Radcliff Member correlates to the thin-bedded part of the upper dolomite member which fills the intermound areas or whether it correlates to the basinal clastic wedge.

LATER PRECAMBRIAN ROCKS — JOHNNIE FORMATION

The Johnnie Formation of Nolan (1929) is correlated by Stewart (1970) to rocks which Murphy (1932) termed Hanaupah Formation and Death Valley Formation. The Johnnie Formation has been divided into two mappable units in the Telescope Peak Quadrangle, a 150 to 330 m thick gradational member overlain by a 400 to 650 m thick argillaceous member. In addition, the argillaceous member can be divided into a lower, green argillite unit and an upper calcareous argillite unit throughout most of the quadrangle. The lower contact is gradational to the Noonday Dolomite, and the Johnnie Formation is conformably overlain by arkose and quartzite of the Stirling Quartzite. A complete section of Johnnie Formation is exposed in Hanaupah Canyon and is described in detail (McDowell, 1967) (Figure 10).

> The basal unit of the gradational member is 183 m thick and consists of 20 to 30 m intervals of light yellow-brown or brown weathering, massive gray dolomite with some sandy dolomite containing quartz grains of silt- or fine-sand size, and rare limestone beds, alternating with 2 to 3 m intervals of dark red-brown weathering, cross-bedded, coarse-grained gray orthoquartzite or dolomitic quartzite. The interval between the quartzite beds increases downward. Algal-like heads occur only in the uppermost dolomite beds of this unit.
>
> The middle unit consists of 40 m of dark red-brown weathering, brown, gray or blue-gray, 1 to 2 m cross-bedded quartzite beds and rare medium red-brown weathering, brown sandy dolomite. The member forms a distinctive dark band in outcrop and makes an excellent mapping horizon.
>
> The upper unit of the gradational member is 45 m thick and consists of less than 3 m thick beds of light brown or yellow-brown weathering, medium gray or blue-gray dolomite, sandy dolomite, limestone, and sandy limestone. The quartz sand beds are cross-bedded. One dark gray, thinly laminated, limestone bed occurs 30 m from the top of the member.
>
> The argillite member is 360 m thick and is made up dominantly of gray-green weathering, gray, green or gray-green very thinly laminated micaceous argillite. In the basal 80 m, 20 to 30 percent of the rock is dark yellow-brown weathering, gray or red-gray quartz-sand, crystalline limestone and dolo-

mite. The lower 100 m of the argillite tends to weather red-brown rather than gray-green, and has scattered rusty spots after pyrite(?); its general appearance is suggestive of a rock of tuffaceous origin. In the upper 70 m of the gray-green argillite member, numerous dark brown or medium red-brown weathering, medium-light red-gray crystalline limestone beds and dark gray aphanitic limestone beds are interbedded with the argillite in 2.5 to 10 mm laminations.

The calcareous argillite member is about 300 m thick and consists dominantly of a ripple marked and flute-casted unit in which medium red-gray and rare green, gray-green and purple crystalline limestone lenses less than 20 mm thick or laminations less than 7 mm thick are interbedded with micaceous purple, blue-gray, very thinly-laminated argillite beds less than 12 mm thick. The argillite beds are draped over the elongate limestone lenses, producing sections which look like typical aircraft wing cross-sections. There are also zones in which only the micaceous blue-gray argillite, strongly ripple-marked, occur.

In the top 70 m red-brown weathering, gray or light brown 2 to 20 cm quartzite beds occur and increase in abundance as the Stirling contact is approached. A discontinuous yellow-brown weathering 2 to 3 m dolomite bed often occurs just below the Stirling contact. At a distance of 210 m below the Stirling contact, a 16 m penecontemporaneous conglomerate bed with slabby 15 cm by 60 cm maximum pink crystalline limestone clasts in a medium-dark gray siliceous limestone matrix occurs. This is present throughout the Hanaupah Canyon area and is used locally as a marker bed as it forms a massive dark-brown weathering cliff in the otherwise slabby to platy, lighter-weathering section. The upper contact of the Johnnie Formation with the Stirling Formation is sharp and marks the abrupt break between the darker, finer-grained quartzites and argillites of the Johnnie and the very light-colored, coarser-grained quartzites of the Stirling Formation.

Stewart (1970) divided the Johnnie Formation in the type section in the Nopah Range into several members. The "transitional member" encompasses the lower 162 m of Johnnie Formation and consists of dolomite and sandy dolomite interbedded with quartzite; the "transitional member" corresponds to the lower part of the gradational member in the Panamint Mountains. In the Nopah Range a 160 m thick quartzite member overlies the transitional member and this quartzite appears to correspond to the middle part of the gradational member.

The dolomite in the upper part of the gradational member corresponds to the "lower carbonate-bearing member" in the Nopah Range where the member consists of 5 m of argillite and micaceous sandstone overlain by a 3 m dolomite bed. The "siltstone member" is 230 m thick, of micaceous sandstone, shale, and minor quartzite, and appears to be equivalent to the lower part of the argillite member in the Panamint Range. The upper part of the argillite member corresponds to the "upper carbonate-bearing member" which consists of 160 m of interbedded quartzite, sandy dolomite, and argillaceous sandstone. In the Nopah Range the uppermost 120 m of the Johnnie Formation is called the "rainstorm member" and consists of grey-green to maroon, cross-bedded, ripple-marked, micaceous argillaceous sandstone and minor sandy dolomite. The "rainstorm member" corresponds to the calcareous argillite member in the Panamint Mountains.

A distinctive and persistent oolite bed occurs in the lower part of the "rainstorm member" and this oolite occurs in the same relative stratigraphic position in all described sections east of the Panamint Mountains (Wright and Troxel, 1966; Stewart, 1970). In the Panamint Mountains the oolite bed occurs in Johnson Canyon, and appears to be equivalent to the penecontemporaneous conglomerate in Hanaupah Canyon.

The basal 200-300 feet of the argillite member of the Johnnie Formation in the mapped area is characterized by rusty red-brown or yellow-brown weathering, cliff-forming beds which contain minute cubic cavities in the more argillitic portions which appear to be hematite after pyrite. Within this section, several distinctive light gray or blue-gray, massive, dense "argillite" beds occur which often have irregular close-spaced

fractures filled with a dark brown material to produce a mosaic-textured rock. These break with an almost concoidal fracture, and produce fracture surfaces which in detail are quite hackly and irregular. Their general appearance is that of fine-grained tuffaceous sediments.

Lateral variations in thickness and lithology of the Johnnie Formation are illustrated in Figure 10. The three members can be recognized throughout most of the Telescope Peak Quadrangle, but the upper two members are not distinguished in the Butte Valley area.

Variations within the calcareous argillite member are slight. On the east slope of the range, the small red-gray lenses which give the member its distinctive ripple-marked appearance are almost wholly of crystalline limestone, while on the west side of the range these same lenses are wholly quartzose and consist of fine to medium-grained quartz grains in a siliceous matrix. Carbonates are very rare to the west of the range divide. The thickness ranges from 265 to 400 m.

The oolite bed which occurs near the base of the calcareous argillite member has a very erratic distribution. As noted above a 1 m bed of thinly laminated dolomite with 0.5 to 2 mm oolites occurs in lower Johnson Canyon. In middle Johnson Canyon the oolite bed is represented by clasts of oolitic dolomite in a penecontemporaneous conglomerate. Elsewhere the same stratigraphic horizon is represented by penecontemporaneous conglomerate with non-oolitic clasts.

The middle, argillite member ranges from 230 to 400 m thick. The unit thickens southward and the grain size increases from silt to medium sand. Pebble conglomerate occurs locally. Where the unit is more highly metamorphosed a weak slaty cleavage is developed and 1 mm spherical

chlorite segregations and cordierite porphyroblasts occur. The tuffaceous portion of the member appears the same throughout the range.

The thickness of the gradational member ranges from 125 to 250 m. Dolomite layers contain greater proportions of clastic debris to the south and this increase in debris parallels the change from massive dolomite to dolomitic sandstone in the underlying Redlands Member of the Noonday Dolomite. In regions west of the range crest where metamorphic grade is greater, the sandy dolomitic layers contain tremolite and the pelitic layers contain andalusite and biotite.

LATER PRECAMBRIAN ROCKS — STIRLING QUARTZITE

The Stirling Quartzite (Nolan, 1929) conformably overlies the Johnnie Formation and the contact between them is sharp. The lower 100 to 150 m of Stirling Quartzite consists of medium- to coarse-grained feldspathic quartzite and conglomerate. The quartzite is massive and white at the base but reddish brown-weathering in the upper part of the section. The remainder of the Stirling Quartzite consists almost entirely of crossbedded quartzite which contains minor siltstone and thin bedded dolomite near the top. Approximately 130 to 200 m above the base there are two 25 m thick argillite units separated by 15 m of quartzite. The argillite is purple in color and it stands out against the reddish brown quartzite. In the northeast corner of the quadrangle the unit contains 5 to 10 mm andalusite porphyroblasts and the unit is cut by veins of andalusite and pyrophyllite.

The top of the Stirling Quartzite is exposed only in the northeast corner of the quadrangle where the thickness of the Stirling Quartzite

is approximately 500 m. Stewart (1970) measured 850 m of Stirling Quartzite in the Emigrant Canyon Quadrangle and Johnson (1957) reports at least 300 m of quartzite in the Manly Peak Quadrangle.

LATER PRECAMBRIAN TO CAMBRIAN ROCKS — WOOD CANYON FORMATION

In the northeast corner of the quadrangle an incomplete section of Wood Canyon Formation (Nolan, 1929) overlies the Stirling Quartzite. The lower part of the formation consists of greenish brown and yellowish brown, thin bedded shale and sandstone which is interbedded with 0.5 to 1 m thick dolomite beds. The lower contact is gradational to the top of the Stirling Quartzite in which thin shale and dolomite beds occur. The majority of the Wood Canyon Formation consists of thin- to medium-bedded quartzite which is interbedded with minor, thin shale and dolomite. The Wood Canyon Formation in the Telescope Peak Quadrangle is incomplete and faulted, but Hunt and Mabey (1966) estimate a thickness of 860 m in Blackwater Wash, approximately 17 km to the north.

TERTIARY ROCKS

Monolithologic Breccia

The west face of the Panamint Range from Wildrose Canyon to Happy Canyon is composed of great masses of megabreccia. Smaller masses of breccia also occur on the crests of west trending ridges south of Surprise Canyon and south of Pleasant Canyon. These deposits consist of material derived primarily from the Kingston Peak Formation, although Beck Spring Dolomite, Noonday Dolomite, and Cretaceous granitic rock are also represented. The deposits which form the gateway to Surprise Canyon consist of finely crushed and pulverized Kingston Peak Formation and

support a badlands-type topography consisting of knife-sharp ridges and steep-walled gullies. Although the rocks are extremely crushed, there is no great mixing of different rock types, and in places ghost bedding occurs. The source location of the breccia is easily recognized and the breccia masses are interpreted to be large landslides (see section on structure). The larger masses rest on a surface which dips from about 40° west to horizontal, and this surface is believed to be a slide surface upon which the breccia developed.

The monolithologic breccia is believed to be Pliocene in age. Between Jail and Hall Canyons a desert pavement surface of low relief has been developed on the breccia and is now at an elevation of 4000 feet above sea level. This surface corresponds to the Pliocene "Darwin Arid Senesland" of Maxson (1950). Additionally, near Wildrose Canyon the breccia is unconformably overlain by the Plio-Pleistocene Nova Formation (see below) and an upper age limit for the breccia of Pliocene is indicated. The lower age limit for breccia is not well constrained, the youngest rocks which occur as clasts within the breccia are Cretaceous. The breccia is believed to be younger than Miocene because there is no evidence that the breccia was ever mantled by volcanic rocks which would have been derived from the Little Chief stock. A small patch of breccia north of Hall Canyon rests on top of a dacite sill which if the sill is related to the Little Chief stock also suggests that the breccia formed later than 12 m.y. ago (see section on Little Chief stock).

Monolithologic breccia which is comprised of Noonday Dolomite clasts occurs in isolated remnants on top of west-trending ridges south of Pleasant Canyon and in the Manly Peak Quadrangle (Johnson, 1957). The

breccia nearly everywhere rests on Sourdough Limestone, and the breccia is locally overlain by old alluvial deposits. This breccia may be correlated to the larger, range front breccia masses, particularly if the overlying alluvium was deposited during the formation of the Pliocene erosion surface. The Noonday Dolomite breccia must have been much more extensive because no immediate source for the breccia now exists.

Nova Formation

In the Wildrose Canyon area the monolithologic breccia is overlain disconformably by alluvial fan deposits which Hopper (1947) called the Nova Formation. A 1 to 2 m thick dark grey limestone occurs at the base, and the limestone is overlain by an undetermined thickness of alluvial silt, sand, and gravel. The unit is much more extensively exposed north of the Telescope Peak Quadrangle where the gravels are tilted as much as 30° to the east. Hall (1971) divided the Nova Formation into three units and called the lower part Fanglomerate #3. Hall (1971) noted that the fanglomerates are intercalated with monolithologic breccia which is similar to, but not as volumetrically abundant as the breccia in Telescope Peak Quadrangle. He also recognized fresh-water limestones which appear to have filled depressions in the fan. Hall (1971) describes basalt flows which are interbedded near the top of Fanglomerate #3 and which range in age from 5 to 4 million years. A Pliocene age for the fanglomerate is indicated.

QUATERNARY ROCKS -- LANDSLIDE DEPOSITS, ALLUVIUM, AND PLAYA LAKE DEPOSITS

Young landslide breccias are abundant in the Telescope Peak Quad-

rangle and are commonly superimposed on the older breccias. The distinction between Pliocene breccia and younger landslide breccia is based on the nature of the lower contact and the "texture" of the brecciated material. The older breccias have planar, west-dipping contacts and are comprised of finely crushed but unmixed rock. Younger landslide deposits have irregular lower contacts which dip down the present slope, the parent rocks are broken into angular fragments, and diverse lithologies are commonly mixed together.

Unconsolidated alluvial silts, sands, and gravels are divided into older and younger deposits. The older alluvium is distinguished from presently accumulating alluvium by the dissection of the older. The older alluvium occurs along the eastern side of Panamint Valley where it was uplifted by Quaternary faulting along the Panamint Valley fault zone. Older dissected alluvium also occurs in the canyons as elevated terrace remnants. Alluvium and playa lake silts and clays are accumulating not only in Panamint Valley but also in the broad upper reaches of most of the west-draining canyons. The broad valleys and moderate relief in the upper reaches of these canyons was related by Maxson (1950) to the Pliocene "Darwin Arid Senesland" (see discussion of geologic history).

INTRUSIVE IGNEOUS ROCKS

METADIABASE DIKES AND SILLS

Mafic dikes and sills intrude the older Precambrian rocks and the Pahrump Group in the Telescope Peak Quadrangle where they are metamorphosed to greenstone and amphibolite. Most of the sills intruded along contacts between formations and the sills are generally less than 50 m thick. A sill of diabase approximately 200 m thick was intruded into the Crystal Spring Formation on the east flank of World Beater Dome, and metamorphosed basaltic pillow lava occurs within the Surprise Member of the Kingston Peak Formation. Although no crosscutting relations which might indicate more than one age of intrusion were observed, the presence of diabase clasts in the Kingston Peak Formation below the pillow lava indicates at least two periods of igneous activity during the Precambrian in the Death Valley region.

Throughout the Death Valley region, diabase sills and dikes intruded the carbonate rocks of the Crystal Spring Formation. The contact metamorphic aureoles contain talc-bearing assemblages, and the Death Valley area is a leading talc-producing region (Wright, 1968). The age of diabase emplacement is believed to be pre-Kingston Peak Formation and possibly pre-Beck Spring Dolomite (Wright, 1968), but radiometric age determinations have been unsuccessful because the diabase is considerably altered. A diabase dike sample from the World Beater area gave a K-Ar date of 377 m.y. (Lanphere and others, 1964) which reflects alteration during the Mesozoic metamorphism. Wrucke and Shride (1972) suggested a correlation of the Pahrump diabase to diabase in late Precambrian rocks of the Grand Canyon area and if diabase sills were emplaced at the same

time over this large region, the diabase may be 1100 m.y. old (Silver, 1960).

HALL CANYON PLUTON

The prominant cliff-forming unit exposed on the west slope of the Panamint Mountains at the mouth of Hall Canyon is a leucocratic, muscovite-bearing granitic pluton and is informally named Hall Canyon pluton. This particular granitic rock is most extensively exposed at the mouths of Hall Canyon and Jail Canyon, but small, isolated areas crop out in Wildrose Canyon, Tuber Canyon, and Surprise Canyon as well. The contacts with the country rocks, invariably the Kingston Peak Formation, are nearly always concordant and dip slightly west in Hall Canyon and steeply west in Jail Canyon. The western contact of the pluton is obscured by the monolithologic breccia, and so the form of the pluton is not well known. The smaller exposures in Surprise, Tuber, and Wildrose Canyons generally exhibit discordant, crosscutting contacts with apophyses of granitic rock injected into the host rock.

Plagioclase, quartz, and microcline-microperthite comprise 90 percent of the rock. Plagioclase is typically the most abundant phase and occurs both as phenocrysts and as matrix grains. Phenocrysts reach 1 cm in size and locally exhibit oscillatory zoning. Plagioclase composition ranges from $An_{.003}\ Ab_{.990}\ Or_{.007}$ to $An_{.181}\ Ab_{.809}\ Or_{.010}$. Microcline also occurs as a phenocryst phase but the relative abundance of microcline and plagioclase is variable. Microcline generally constitutes less than 20% of the rock, but in the smaller bodies in Wildrose Canyon microcline phenocrysts are much more abundant. The composition of micro-

cline is $An_{.000}$ $Ab_{.050}$ $Or_{.950}$. Approximately 7% of the granitic rock is comprised of muscovite with the composition $K_{0.95}$ $Na_{0.05}$ $Fe_{0.25}$ $Mg_{0.11}$ $Al_{1.83}$ $(Al_{0.81}$ $Si_{3.19})$ O_{10} $(OH)_2$. Muscovite occurs as subhedral to euhedral books ranging from 1 mm to 10 mm in diameter and appears to be a primary magmatic phase. Secondary white mica also occurs in altered rocks and appears to be replacing plagioclase. Mafic phases generally comprise less than 3% of the rock. Brown biotite (Table 2) occurs in most localities but small rounded garnet grains are also present in some of the smaller, isolated exposures. The biotite is commonly altered to chlorite and trace amounts of epidote are also observed. Modes, phase compositions, and normative mineral compositions of several samples of the Hall Canyon Pluton are listed in Table 2.

Near the margins of the large plutonic exposure, the granitic rock is strongly foliated parallel to the contact. The foliation is defined by the parallel alignment of muscovite plates and planar orientation of long axes of feldspar phenocrysts set in a fine-grained quartz-rich matrix. Phenocrysts are somewhat rounded, some show possible rotation, and the matrix is a granular mosaic of equant quartz grains which have some interlocking boundaries as well as straight, polygonal boundaries. Coarser grained quartz is invariably flattened parallel to the foliation, and edges appear to be recrystallizing to the fine-grained matrix. The well developed foliation indicates that deformation accompanied or followed intrusion, but the small, isolated body of granitic rock in Surprise Canyon is unfoliated and preserves a fine-grained, primary igneous texture. Thus, a complex sequence of intrusion, deformation, and continued intrusion may have occurred.

TABLE 2: MODE, PHASE COMPOSITIONS, AND CALCULATED BULK COMPOSITION OF PML 179 and P 101, HALL CANYON PLUTON

	PML 179, lower Surprise Canyon								P 101, lower Tuber Canyon						
	Quartz	Plag	Micr	Musc	Gar	Ap	other	Bulk Composition	Quartz	Plag	Micr	Musc	Gar	Ap	Bulk Composition
(2178 pts)									(1455 pts)						
Vol %	27.5	45.8	18.7	7.5	tr	0.3	0.2	100	35.9	46.9	10.2	6.7	0.2	0.1	100.0
ρ	2.65	2.63	2.56	2.77					2.65	2.63	2.56	2.77	4.30	3.20	
wt %	28.1	46.2	18.4	7.4				100.1	36.0	46.7	9.8	7.1	0.3	0.1	100.0
SiO_2	100	70.18	64.80	48.15	38.07			76.1	100	68.57	65.11	46.76	37.49		77.8
TiO_2				0.0	0.07			0.0				0.22	0.05		0.0
Al_2O_3		19.78	17.92	29.15	21.35			14.25		22.02	18.33	34.34	21.18		14.6
FeO		0.11	0.19	5.42	23.61			0.4		0.0	0.16	3.04	22.25		0.3
MnO				1.42	19.52			0.1				0.0	18.08		0.1
MgO				0.0	0.0			0.0				0.17	0.35		0.0
CaO		0.21	0.0	0.0	0.58			0.1		2.24	0.0	0.0	1.39	54.19	1.1
Na_2O		11.49	0.62	0.60				5.2		10.72	0.06	0.83			5.1
K_2O		0.05	16.07	10.81				3.8		0.08	16.12	10.60			2.4
H_2O				4.43				0.3				4.04			0.3
Total		101.83	99.60	100.0	103.2			100.25		103.63	99.78	100.0	100.79		101.7

q	28.3	cor	1.5	q	33.4	cor	1.9
or	22.3	hy	0.8	or	13.9	hy	0.6
ab	46.6			ab	45.0		
an	0.5			an	5.1		

Figure 11: Granitic rocks in Telescope Peak Quadrangle.

a) Hall Canyon pluton (light), north of mouth of Surprise Canyon.

b) Little Chief stock from head of Surprise Canyon.

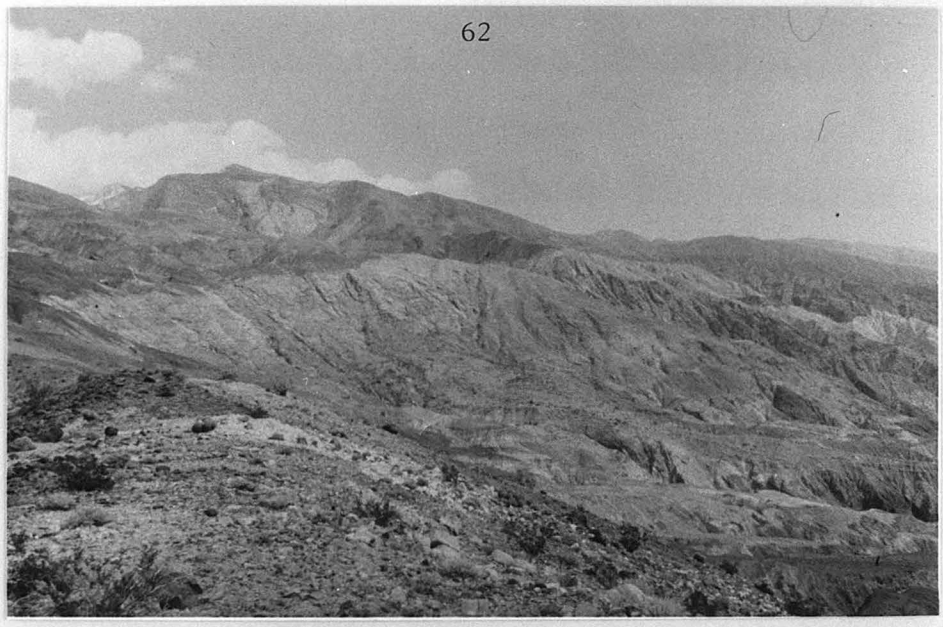

a

b

Gravity data of Hunt and Mabey (1966) indicate a relatively low gravity anomaly centered over the Wildrose-Nemo Canyons area, as compared to topographically comparable areas in which Precambrian rocks are exposed. They suggest the presence of granitic rock underlying this portion of the Panamint Mountains. A cursory examination of the granitic pluton exposed in the Skidoo region in the Emigrant Canyon Quadrangle showed that this pluton is also composed of a leucocratic, muscovite-bearing granite which has concordant intrusive contacts. It is possible that the Skidoo pluton and the Hall Canyon pluton are related, and that much of the Harrisburg Flat area may be underlain by this granitic rock.

Muscovite separated from an exposure of this granite in Wildrose Canyon is used as an internal standard for potassium-argon analysis (P-207) and has yielded ages of 81 to 83 m.y. derived by K-Ar and Rb-Sr techniques (Lanphere and Dalrymple, 1967; Dalrymple and Lanphere, 1971).

LITTLE CHIEF STOCK AND RELATED DIKES

The Little Chief stock (Murphy, 1932) is exposed near the crest of the range between Hanaupah and Johnson Canyons. The structure, mode of emplacement, and crystallization history of the stock are described by McDowell (1967, 1974, 1978).

The Little Chief stock is composite and consists of a south and a north "phase". The north phase exhibits a chilled margin at the border of the south phase, and both phases contain inclusions of an older phase near their mutual contact. Stock-country rock contacts are almost everywhere steep, and vary from vertical to steeply outward or inward dipping. The country rock is deformed by the intrusion of the stock, and in many

places, the stock is sheathed by carbonate rocks of the Noonday Dolomite.

The stock is composed of hornblende-biotite granite porphyry which contains phenocrysts of plagioclase and sanidine up to 10 mm in diameter set in a fine-grained groundmass of quartz, alkali feldspar, and plagioclase. Sanidine phenocrysts are coated with a rim of plagioclase which gives the rock a Rapikivi texture. Table 3 lists representative modes of the Little Chief stock. McDowell (1978) describes the complex rimming relations observed in feldspar phenocrysts, and he interpreted the complex zoning in terms of the history of crystallization. At an early stage of crystallization the magma assimilated dolomitic wall rocks and the liberated CO_2 elevated the fluid pressure and caused fracturing of the roof rocks and emplacement of dikes. The magma then ascended into its present position which was approximately one kilometer below the surface. At this time the magma probably vented to the surface.

Rhyolite porphyry dikes associated with the Little Chief stock occur in swarms. These dikes invade the shallow-dipping normal faults and are crosscut by the stock itself. High angle "trap door" faults which formed during the intrusion of the stock also offset the low angle faults. Because similar low angle faults along the east face of the range offset Tertiary volcanic rocks (Hunt and Mabey, 1966), the Little Chief stock is probably Tertiary in age. Stern and others (1966) report a 12 m.y. age obtained from a granite porphyry boulder collected from the mouth of Hanaupah Canyon and believed to have been derived from the Little Chief stock. The cluster of late Tertiary ages reported by Stern and others (1966) obtained from dike and volcanic rocks near the mouth

TABLE 3: TYPICAL MODES OF THE MAJOR PHASES OF THE LITTLE CHIEF STOCK*

	North phase interior	North phase exterior	South phase
PHENOCRYSTS			
Sanidine	10	15	12
Sodic oligoclase replacing sanidine	0	10	6
Oligoclase rims on sanidine	11	0	0
Plagioclase	21	6	7
Hornblende	3	1	4
Biotite	2	3	1
Other minerals	2	1	1
Total phenocrysts	49	36	31
GROUNDMASS			
Alkali feldspar	28	29	37
Quartz	19	32	24
Plagioclase	3	2	7
Other minerals	1	1	1
Total groundmass	51	64	69

Note: Values in volume percent.

*from McDowell (1978)

of Hanaupah Canyon is consistent with a Tertiary age for the stock.

STRUCTURE

The structure of the central Panamint Mountains is dominated by a north-northwest-trending anticline which includes World Beater Dome and an asymmetric anticline north of the dome. Rocks on the east flank of the anticline dip gently east, and the east slope of the Panamint Mountains is a dip slope, interrupted by the Little Chief stock. The anticline is cut by numerous faults of several ages. The oldest are a series of north-trending, high angle faults which in part probably predate the development of the anticline. Younger faults include shallow-dipping normal faults, faults associated with the intrusion of the Little Chief Stock, and faults which form the Panamint Valley fault zone.

PRE-LATE TERTIARY STRUCTURES

North-Trending Faults

West of the range crest, steeply dipping faults are generally north-trending and dip vertically or steeply west. Deviations in trend occur in some faults in the southern and southeastern part of the quadrangle where faults strike north-northeast and north-northwest. In addition, a set of faults which strike west-northwest occurs in lower Happy Canyon.

There is a network of north-trending faults west of the range crest which extends the length of the quadrangle, and one single fault which runs through the middle of World Beater Dome has been mapped for approximately 15 miles (25 km) along strike. Despite the relatively small offset across them, north-trending faults are prominent in the Telescope Peak Quadrangle.

Offsets across these faults are primarily dip-slip although the

absolute displacement is complex. Many faults exhibit a reversal in the sense of displacement along strike. Offset across a fault is indicated by the fault's position relative to the core of the anticline, but the axis of the anticline trends north-northwest, across the trend of faulting. Faults thus show a scissors-type offset along strike, and the maximum stratigraphic separation observed is approximately 800 m.

The north-trending fault which separates earlier Precambrian rocks along the west face of the range from later Precambrian rocks has a much shallower west-dip than the other north-trending faults. Johnson (1957) called this fault the South Park Canyon fault, and the shallow west-dip with older Precambrian rocks on the hanging wall gives a reverse fault geometry. It is suggested below that the present geometry may be due to a post-faulting, folding episode.

Because the north-trending faults have a scissors-type offset, these faults are believed to predate the development of the north-northwest-trending anticline. Some direct evidence supports this contention. On top of the western structural high in Surprise Canyon a north-trending fault displaces Beck Spring Dolomite and older rocks, but the displacement is truncated at the Kingston Peak contact, and the Kingston Peak Formation buries the faulted rocks. Thus, at least one north-trending fault is Precambrian in age. These high-angle faults are presumed to be inherited from an old fracture pattern in the basement which were activated during the late Precambrian, during the formation of the north-northwest-trending anticline, and even during the intrusion of the Little Chief stock (McDowell, 1974).

North-Northwest-Trending Anticlines, Domes, and Associated Faults

The structural culmination of the Panamint Mountains trends approximately 20° west of north and consists of a series of anticlines and domes. The core of the structural high is occupied by earlier Precambrian basement, except in Tuber Canyon where Crystal Spring Formation resides in the core. The anticline is cut by the north-trending faults, and canyons which cut across the anticline give the outcrop pattern an impression of en echelon domes.

The domes and anticlines are asymmetric; east flanks dip gently east, but west flanks dip steeply west and are locally overturned (Figure 12). This asymmetry is repeated on a smaller scale south of lower Hall Canyon where Beck Spring Dolomite occupies the cores of smaller domes. On the west flank of World Beater Dome the steeply dipping sedimentary mantle is thrown into a complementary open syncline. In the Manly Peak Quadrangle, this broad anticline-syncline couple dominates the structure (Johnson, 1957). The west flank of the broad syncline is truncated by a west-dipping, apparently reverse fault which Johnson (1957) named the South Park Canyon fault. The moderate dip of this fault sets it apart from the other north striking faults, and the timing of its displacement relative to the formation of the folds is not clear (see below).

Numerous minor folds are associated with the north-northwest anticline, particularly on the west flank of the structure. A zone of disharmonic folding is developed along a north trend, between the structural high and the Cretaceous Hall Canyon pluton (Figure 13). Within this zone which is up to 100 m wide amphibolitic layers in the lower Kingston

Figure 12: Overall structure in the Panamint Mountains.

a) Gently dipping east flank of anticline, Hall Canyon. From lower right to upper left: Beck Spring Dolomite, Kingston Peak Formation, Noonday Dolomite, Johnnie Formation.

b) Steeply dipping west flank of anticline, Surprise Canyon. Steeply west dipping Limekiln Spring strata separated from less steeply dipping strata by a zone of disharmonic folding. Late Tertiary slide mass in background.

a

b

Figure 13: Smaller scale structures on west flanks of anticline.

a) Zone of disharmonic folding, Surprise Canyon.

b) Fold in Crystal Spring Formation, Tuber Canyon.

a

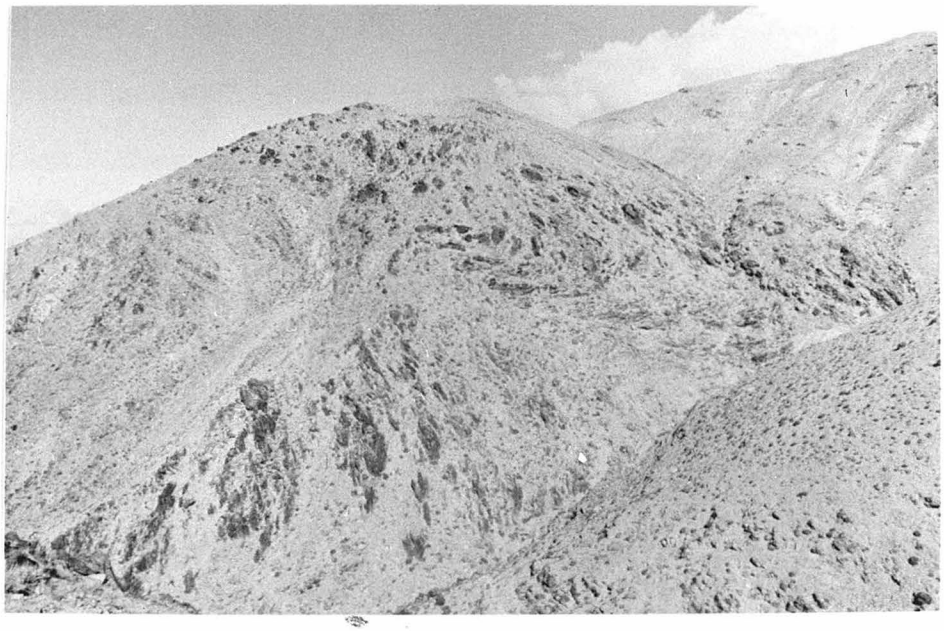

b

Peak Formation are disharmonically folded along north-northwest axes and roughly horizontal axial planes. This zone separates steeply west-dipping strata on the east from more gently west-dipping strata on the west, but the stratigraphic separation is confined within the Limekiln Spring Member of the Kingston Peak Formation.

A lineation is also well developed along the west flank of the anticline. Cobbles within the lower Kingston Peak Formation are stretched and have lengths up to about 10 times the diameter. The long axes of cobbles plunge in the range 20°/N10W to 40°/S. A mineral lineation is also well developed and is defined by the parallel alignment of hornblende and white mica pods. The plunge of the lineation ranges from 15°/N20W to 15°/S20E.

The lower limit of the time of folding and associated faulting is the 80 m.y. age of the Hall Canyon pluton. Tangible evidence for this lower limit is minimal; the granite is deformed along its margin (see description of pluton above) and it is displaced in a few places by faults associated with folding which suggest that intrusion predated deformation. The principal argument stems from the metamorphism. Two periods of metamorphism are recognized. The older is related to the intrusion of the granite, and the second is a retrograde event which exhibits greatest effects in the cores of the folds and the development of the lineation. Hence, folding occurred after intrusion of the granite and regional metamorphism of the country rock.

It is possible that folding occurred shortly after the primary metamorphic event because the small unfoliated bodies of granite cross-cut strata deformed during the folding event. Such an effect could

arise by deformation prior to the complete consolidation of the Hall Canyon pluton during which the folding reactivated intrusion of late stage liquids. No crosscutting relations within the granitic pluton were observed and such a mechanism and timing sequence can only be postulated.

The upper limit for the time of folding is the age of low angle faulting. As discussed below, low angle normal faults cut the folds, and the faults are probably pre-Miocene in age.

Reactivation of old, north-trending faults during the folding event is suggested, but the reverse fault (South Park Canyon fault) exposed along the west front of the range south of Happy Canyon complicates this simple structural history. In the Manly Peak Quadrangle this fault is intruded by a granodiorite which has been thoroughly metamorphosed (Johnson, 1957). Johnson suggested a Triassic age for the granodiorite and indicated that all contacts are intrusive. This fault was not re-activated during post-metamorphic folding. These relations imply that there was a post Noonday Dolomite (youngest rock cut by the fault), pre-Triassic (?) granodiorite faulting episode, and that the present reverse fault geometry may be the result of post-Cretaceous folding.

The fault dips 30° west where it cuts Noonday Dolomite (south of Pleasant Canyon), but steepens down dip to 40° west in and north of Pleasant Canyon where the fault cuts the Surprise Member of the Kingston Peak Formation. This down dip steepening is consistent with the folding of an originally steeply dipping fault on the limb of a syncline.

LATE TERTIARY STRUCTURES

Low Angle Normal Faults

Low angle normal faults crop out extensively along the east slope of the Panamint Mountains in the northeast corner of the quadrangle. In addition several isolated fault blocks occur on the ridges on the west slope of the range.

The low angle faults on the east slope have dips which range from 45° west to nearly horizontal. One individual fault even changes dip along strike from moderate to low. Displacement across these faults is nearly everywhere normal; even where the faults are nearly flat, younger rocks are placed over older. Offsets across the faults are generally less than 200 m. These low angle faults have no apparent stratigraphic control; the faults dip west, but the rocks dip east. The flat faults are not confined to a bedding plane.

Low angle faults crop out extensively along the east foot of the Panamint Range, to the east and northeast of Telescope Peak Quadrangle, and Hunt and Mabey (1966) called this extensive fault network the Amargosa Thrust Complex. Hunt and Mabey (1966) believed that these faults had a complex history which started with Cretaceous or Jurassic thrusting, early Tertiary intrusion, and Late Tertiary folding and gravity sliding. The Mesozoic thrusting was believed to be large scale, east to west, gravity sliding of rock off of a high eastern plateau. These faults are reinterpreted to be Tertiary structures (see Geologic History) which were active after the Late Cretaceous folding episode and after mid-Tertiary volcanism, but prior to the intrusion of the Little Chief stock. The faults along the east foot of the Panamint Mountains both

cut felsite dike swarms and are intruded by plugs and sills of felsite of Late Tertiary age (Stern and others, 1966). In the Telescope Peak Quadrangle these low angle faults are invaded by rhyolite dikes and are cut by structures related to the intrusion of the 12 m.y. Little Chief stock.

Several relatively small, isolated fault blocks occur on the ridges on the west slope of the range. These "klippen" occur on each major ridge north of Hall Canyon, and south of Nemo Canyon (Lanphere, 1962). The faults which bound the blocks are generally gently west-dipping, but in places (particularly on Tuber Ridge) the faults appear to have a spoon shape in which fault planes are curved and dip east at the western edge of the fault block. The individual blocks may have once been part of one large fault block, but the elevations of the flat faults are not the same and the rocks on the hanging walls are of different ages (middle Kingston Peak Formation near Hall Canyon, Crystal Spring, Beck Spring, and lower Kingston Peak in Jail-Tuber Canyon area, and Noonday Dolomite and Johnnie Formation on Tuber Ridge). These blocks are probably the remnants of several, once larger fault blocks. The sense of displacement across the faults is hanging wall down to the west (Figure 14), and the locations of source regions for the blocks suggest displacements of approximately 1500 m. The attitude and sense of displacement is similar to those of the faults east of the divide, but the isolated fault blocks may be related to but older than the large masses of monolithologic breccia. The isolated fault blocks cut the structures formed during the Late Cretaceous folding event, and if they are of the same generation as the low angle faults to the east, they are older than

Figure 14: Tertiary low angle, normal faults.

a) Tuber Ridge. Fault places Noonday Dolomite and Johnnie Formation on top of Kingston Peak Formation. Sourdough Limestone is cut by the fault.

b) Jail Canyon. Fault places Kingston Peak Formation on top of Beck Spring Dolomite and Crystal Spring Formation. Note drag fold in Beck Spring-Crystal Spring contact.

a

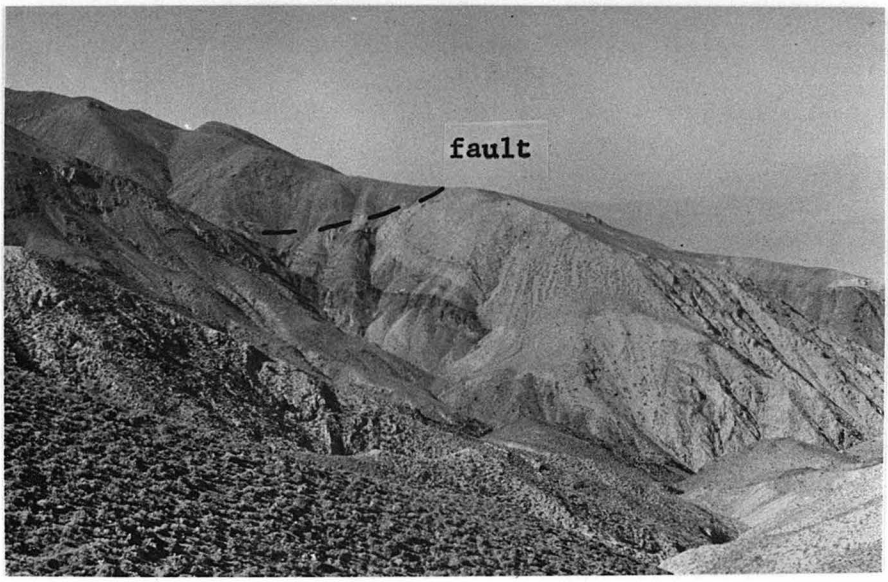

b

the Little Chief stock. If the fault blocks are related to monolithologic breccia they are probably older than the breccia because the coherent nature of the rock in the fault blocks suggests that they formed under greater cover than the breccia.

Little Chief Stock

Structures related to the intrusion of the Little Chief stock are described in detail by McDowell (1974). The most conspicuous effect of the intrusion on the country rocks is the development of a trapdoor defined by vertical faults which ring the stock. The rocks within the bounding faults are uplifted relative to the rocks outside. The greatest displacement occurs on the west side of the trapdoor, and a hinge line of zero displacement is located near the east edge. The trapdoor opens to the west where most of the country rock has been removed above the stock. The stock and the trapdoor faults either crosscut or displace both the earlier north-trending vertical and lower angle west-dipping faults. Dike swarms related to an earlier phase of intrusion which pervasively invade country rocks and the low angle faults are also offset by the trapdoor fault which indicates that the trapdoor formed during the last stages of intrusion. The trapdoor utilized some of the preexisting north-trending vertical faults during displacement.

The east side of the trapdoor is offset by an east-trending tear fault which extends from the inclusion-rich zone in the stock. The displacement across this fault is scissors-like; north side is up near the stock, and a pivot occurs about 3 km east of the stock, east of which the south side is up. This tear fault was probably also a preexisting fault along which the stock was intruded and across which the trapdoor was torn as it was uplifted.

Nearly everywhere carbonate rocks sheathe the stock. In many places, particularly on the southeast side of the stock, the rocks are folded sympathetically with upward emplacement of the stock and greatly thinned.

Slide Masses

Great masses of monolithologic breccia form the western foot of the Panamint Mountains from Wildrose Canyon to south of Happy Canyon. The breccia is comprised predominantly of material derived from the Kingston Peak Formation, and the Kingston Peak Formation forms the footwall of the surface which bounds the breccia throughout much of its length. Where exposed the slide surface is well defined.

The structural setting of the monolithologic breccia shows characteristics similar to those of the low angle normal faults. In general, the breccia was developed on a surface which dips approximately 45° west at the head of the slide and flattens westward to about 5° west. The surface on which the breccia developed does have some irregularities. The slide surface is steeply dipping (45 to 50°) where the breccia rests on granite, but the surface dips less than 30° elsewhere. Between Tuber and Jail Canyons a west-trending bedrock ridge appears to perturb the west-dipping surface. A confused mass of younger landslide material obfuscates the relations between bedrock, an older fault block ("klippe"), and the monolithologic breccia, but there appears to be a window into bedrock on this ridge. It is probable that the geologic relations on this bedrock ridge are more complex than depicted, and in particular the ridge may divide the breccia into two separate masses. The slide sur-

face along most of its extent does not appear to have utilized any one particular bedding plane or other anisotropy during its development. The underlying strata generally dip west and consist of thin-bedded argillite and metagreywacke (Limekiln Spring Member of Kingston Peak Formation). The granitic rock of the Hall Canyon pluton has a steeply west-dipping foliation, particularly near Jail Canyon, and the slide apparently took advantage of these various planes of weakness to develop. Farther to the south, particularly in the Manly Peak Quadrangle, monolithologic breccias (generally of Noonday Dolomite) rest on Sourdough Limestone, and here the top of the limestone may have acted as the weak "break-away" surface along which the breccia developed.

The source and approximate amount of displacement is readily identified in these breccias. Between Happy and Surprise Canyons, brecciated Noonday Dolomite is embedded in crushed Kingston Peak Formation. These rocks are the counterpart to the syncline south of Happy Canyon in which Noonday Dolomite occupies the core. Between Surprise and Hall Canyons the breccia contains crushed granitic rock which is overlain with an approximately horizontal contact by Kingston Peak breccia. This relation corresponds to the contact between the Hall Canyon pluton and Kingston Peak Formation approximately 2500 m to the east. In Jail Canyon the breccia contains a steeply dipping contact between Kingston Peak debris and Beck Spring debris, analogous to a similar contact exposed in bedrock approximately 2000 m up the canyon. The identified source regions for the breccia indicate that the "displacement" of the breccia is approximately 2000 m, down to the west (absolute displacement is approximately 2800 m down the dip of the slide surface).

Figure 15: Late Tertiary - Quaternary faults.

a) Late Tertiary slide mass near mouth of Surprise Canyon. Contact between Kingston Peak Formation (dark) and Hall Canyon pluton (light) is displaced from upper left to lower right.

b) Wildrose Graben.

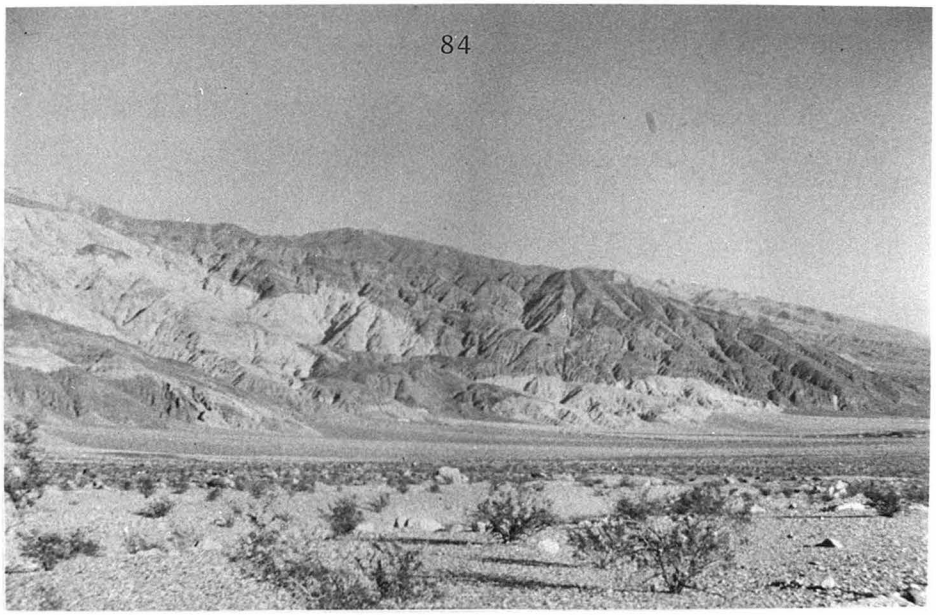

a

b

The shattered and brecciated nature of the material on the hanging wall of the slide surface indicates that although the geometry and sense of displacement is similar to that of the low angle normal fault blocks, formation of the slide mass probably occurred under a shallow cover. The breccia is younger than the displacement on the low angle normal faults, and probably younger than the emplacement of the Little Chief stock. The breccia is at least in part older than the Pliocene (?) Nova Formation, and the "Darwin Arid Senesland" of Maxson (1950).

Quaternary Structures

Young faults are well developed along the east side of Panamint Valley at the margin of the mountain front. This fault network is part of the marginal Panamint Valley fault zone. Both north and south of the Telescope Peak Quadrangle the Panamint Valley fault zone is a comparatively well defined linear array of north-northwest-trending high angle faults (G. I. Smith and others, 1968; R. Smith, 1976) across which vertical warping occurred during Quaternary time (R. Smith, 1976). Evidence for right lateral slip is abundant in northern Panamint Valley and in southern Saline Valley (R. Smith, 1976).

The Panamint Valley fault zone is poorly defined in the Telescope Peak Quadrangle where discontinuous, en echelon, and often antithetic faults are common. The most impressive feature related to the fault zone is Wildrose Graben where older Quaternary gravels are vertically offset about 100 m (Figure 15). An impressive north-facing scarp is exposed at the mouth of Pleasant Canyon and just south of Ballarat where older gravels are uplifted about 120 m.

The prominant reentrant in the mountain front between Pleasant and Wildrose Canyons (Ballarat embayment), the en echelon and often northwest-dipping fault scarps, and common antithetic faults and grabens are attributed by R. Smith (1976) to recent right-lateral shear along the Panamint Valley fault zone. A "pull apart" origin for the central portion of Panamint Valley is suggested (Burchfiel and Stewart, 1966; Smith, 1976).

The dominant, overall vertical component of offset across the Panamint Valley fault zone is east side up. The Fanglomerate #3 of Hall (1971) (equivalent to the lower part of the Nova Formation) in the Panamint Butte Quadrangle is tilted 20 to 40° east, and Hooke (1965) estimated an eastward tilting rate of approximately 0.018°/1000 y on the Panamint block based on alluvial fan morphology.

METAMORPHISM

The rocks which crop out in the central Panamint Mountains have undergone multiple periods of metamorphism. The earlier Precambrian gneiss complex was formed about 1700 to 1800 m.y. ago. Late Precambrian sedimentary rocks were regionally metamorphosed at least twice, and a narrow contact metamorphic aureole was developed at the margins of the Little Chief stock. The detailed petrology of the regionally metamorphosed terrain is described in the next section and the overall characteristics of the metamorphism are only summarized here.

POST-PRECAMBRIAN REGIONAL METAMORPHISM

Effects of regional metamorphism in the Panamint Mountains are recognized over a wide area, from Tucki Mountain in the north to Coyote Canyon in the south (Johnson, 1957). Within the Telescope Peak area argillaceous rocks within the Stirling Quartzite at the northeast edge of the quadrangle show effects of incipient metamorphism, and the degree of recrystallization increases to the west. As described below the metamorphism reaches sillimanite grade, but despite the high grade of metamorphism gross recrystallization did not occur. The grain size of most of the rocks, particularly the metagreywackes, is small. Small scale sedimentary structures, especially centimeter-scale bedding, graded bedding, slump folds, and locally ripples, crossbedding, raindrop impressions are well preserved. Evidence for metamorphic differentiation and metamorphic veins is rare.

The characteristic assemblages developed in pelitic rocks are andalusite + biotite + staurolite and andalusite + biotite + cordierite.

However, pelitic rocks are relatively rare, and the most common assemblage developed in the abundant metagreywackes is quartz + biotite + epidote + plagioclase. Amphibole is an additional constituent in many mafic assemblages. Carbonate rocks contain tremolite- and diopside-bearing assemblages.

The intensity of metamorphism is delineated by isograds based on the stable association of tremolite + calcite at the expense of quartz + dolomite and on the occurrence of diopside relative to quartz + calcite + tremolite (Figure 16). In addition, the transition from andalusite to sillimanite is also defined. These isograds depicted on Figure 16 indicate a westward increase in metamorphic grade toward the vicinity of the Hall Canyon pluton. The coincidence of the highest grade of metamorphism and the position of the Hall Canyon pluton suggest that metamorphism and intrusion occurred simultaneously.

The occurrence of andalusite- and cordierite-bearing assemblages are indicative of low pressure-intermediate metamorphism (Miyashiro, 1961). An estimate of the stratigraphic cover at the time of metamorphism was derived from Hall (1971) and Johnson (1957) (see Part II), and the prevailing lithostatic pressure was about 2.5 to 3.0 kb. Temperature estimates range from about 400°C near the tremolite isograd to about 675°C adjacent to the Hall Canyon pluton (Part II).

A younger regional metamorphic event has affected most of the Telescope Peak area. This second metamorphic event is manifested primarily by chloritization of mafic minerals and sericitization of aluminous minerals. Recrystallization during the second metamorphism was most complete in the core of the anticline. Here, a garnet + chlorite

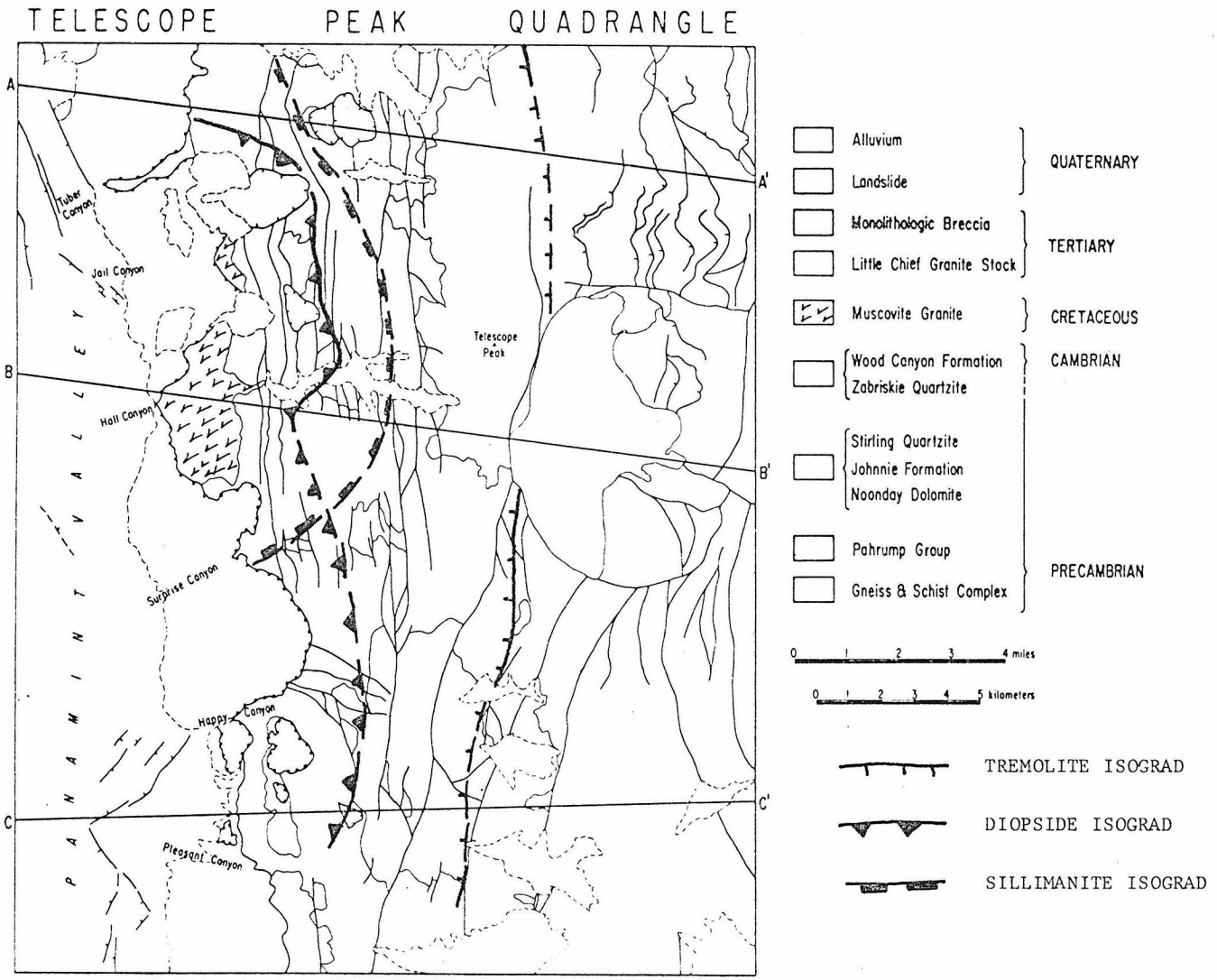

Figure 16: Metamorphic isograds, Panamint Mountains.

assemblage was superimposed on an earlier sillimanite-bearing assemblage, and amphiboles have well-developed secondary rims. A b-axis lineation was developed by the growth of elongate pods of secondary muscovite which formed at the expense of andalusite and sillimanite. This secondary metamorphic event appears to have occurred during the post-intrusive folding episode.

Direct field evidence for the age of metamorphism is lacking; the intensity of metamorphism decreases so that Lower Cambrian Wood Canyon formation is essentially unmetamorphosed. In the Wildrose Canyon area Lanphere (1962) dated muscovite, biotite, and hornblende separated from the Pahrump Group and Noonday Dolomite by the K-Ar method, and he reported ages in the range 79 to 115 m.y. for the metamorphic rocks. Lanphere and others (1964) investigated the strontium isotopic characteristics of the earlier Precambrian World Beater Complex. Despite the Precambrian geologic age of the gneiss Rb-Sr biotite-total rock isochrons indicated ages ranging from 64 to 156 m.y. The high $^{87}Sr/^{86}Sr$ in apatite from these gneisses indicated nearly complete isotopic homogenization during metamorphism, and the range in $^{87}Sr/^{86}Sr$ and $^{87}Rb/^{86}Sr$ for total rock samples indicated that this homogenization had occurred over a large volume of rock. The range in age values for the metamorphic rocks may be due to the superposition of two relatively young metamorphic events. The earlier metamorphism is believed to have occurred about 80 million years ago during the intrusion of the granite, and the second metamorphism occured during the slightly later folding episode.

TERTIARY CONTACT METAMORPHISM

Intrusion of the Little Chief stock was accompanied by contact

metamorphism of the country rock. The contact metamorphic aureole is extremely narrow around most of the stock, and contact metamorphism generally affected less than a few centimeters of rock. In the region of the dike swarm, northeast of the stock, the contact metamorphic effects extend much farther from the stock. Country rocks are predominantly carbonate rocks and diopside- and wollastonite-bearing assemblages occur. Locally, amphibole-bearing assemblages are observed in Kingston Peak Formation.

MINERALIZATION

The Panamint Range was a major silver mining district in the 1870's, and Murphy (1930) estimated that approximately $2 million in silver was produced in Panamint City from 1875 to 1877. Most of the commercially successful mining operations were located in upper Surprise Canyon (Hemlock, Wyoming, and Stewarts Wonder mines), but the Ratcliff mine in lower Pleasant Canyon was a major gold producer around 1900. Today intermittent mining ventures occur in Happy, Surprise, Pleasant and Jail Canyons.

Murphy (1930) described the principal ore-producing veins in the Panamint Silver District and he divided them into three types. Two occur principally in the Kingston Peak Formation and consist of quartz-pyrite-galena veins and quartz-pyrite-pyrrhotite veins. The major silver-producing veins consist of quartz, tetrahedrite, galena, sphalerite, pyrite, and chalcopyrite. These veins are best developed in Beck Spring Dolomite, but they also occur in the Kingston Peak Formation. The major producing veins occur in Beck Spring Dolomite and appear to fill fractures which are oriented either approximately east-west and steeply dipping or parallel to the regional north-trending fault pattern.

The diamictite in the Surprise Member of the Kingston Peak Formation is very dense, black, and contains abundant pyrite, pyrrhotite and chalcopyrite. Although Murphy (1930) believed that the ore deposits are genetically related to the intrusion of the Little Chief Stock, the spatial relation between major ore-producing veins and sulphide-rich Kingston Peak diamictite suggests that the ore may have been derived from the Kingston Peak Formation. Murphy (1930) suggested that ore

deposition occurred during the emplacement of the Little Chief Stock (determined to be Miocene), but no conclusive arguments are made which indicate whether mineralization occurred during emplacement of the granite, or during perhaps one of the earlier metamorphic events.

GEOLOGIC HISTORY AND REGIONAL SETTING OF THE TELESCOPE PEAK QUADRANGLE

The rocks in the Telescope Peak Quadrangle record a complex geologic history which involves the deposition of the late Precambrian Pahrump Group in a tectonically active environment, regional metamorphism and folding of these rocks during the late Mesozoic, and large scale gravity sliding during the Tertiary. However, much of the geologic history of the western Great Basin, particularly the early and middle Mesozoic, is recorded only in the surrounding mountain ranges. Here, the geology of the Telescope Peak area is summarized and integrated with the geology of surrounding regions to provide a coherent picture of what is known and unknown about the tectonic evolution of the western Great Basin.

PRECAMBRIAN HISTORY

The outcrop area of older Precambrian rocks is too limited to provide a clear picture of geologic history prior to the deposition of the Pahrump Group. The pre-Pahrump history involves deposition of sedimentary and possibly volcanic rocks on an unknown basement and intrusion of the proto-augen gneiss. Grey quartz monzonite was intruded in the World Beater area approximately 1400 m.y. ago, but only after the development of the texture in the augen gneiss.

Depositional Environment of the Pahrump Group

The most striking features of the Pahrump Group in the central Panamint Mountains are the stratigraphic changes from east to west across the axis of the domes and from north to south in the Jail-Tuber Canyon areas. The variation in thickness and lithology over short dis-

tances and the presence of locally derived clasts argue for the antiquity of the structural high now represented by domes and for tectonic activity during the deposition of the Pahrump Group.

Both the Crystal Spring Formation and Beck Spring Dolomite thin toward World Beater Dome and dolomite shoal breccia occurs on top of the dome. Despite the erosion that occurred during the initial Kingston Peak deposition, the World Beater area must have stood above sea level during early Pahrump time (World Beater Island). However, in Tuber Canyon, the great increase in thickness of the Crystal Spring Formation and the apparent facies change from Beck Spring Dolomite to a clastic carbonate-arenite sequence suggest a deeper water environment and a large amount of relief on the earlier Precambrian basement.

The pre-Kingston Peak geography envisaged in the Telescope Peak area consists of a relatively stable platform underlain by earlier Precambrian basement. The platform stood above sea level at World Beater Island; supported a carbonate shelf during Beck Spring Dolomite time; and had a northern margin in the vicinity of Tuber Canyon. The northern margin may have been a scarp in the basement, but the lack of coarse detritus in the Crystal Spring Formation suggests that the increase in the sedimentary thickness may be due to a differential rate of subsidence.

Near the end of Beck Spring time, the platform was rejuvenated. World Beater Island and much of the carbonate shelf to the north were uplifted while the region to the west sank. This geography provided a complex depositional environment for the Limekiln Spring Member. Figure 17 illustrates the geometry of the lower Kingston Peak depositional basin. The datum for Figure 17 is intended to be the base of the diamic-

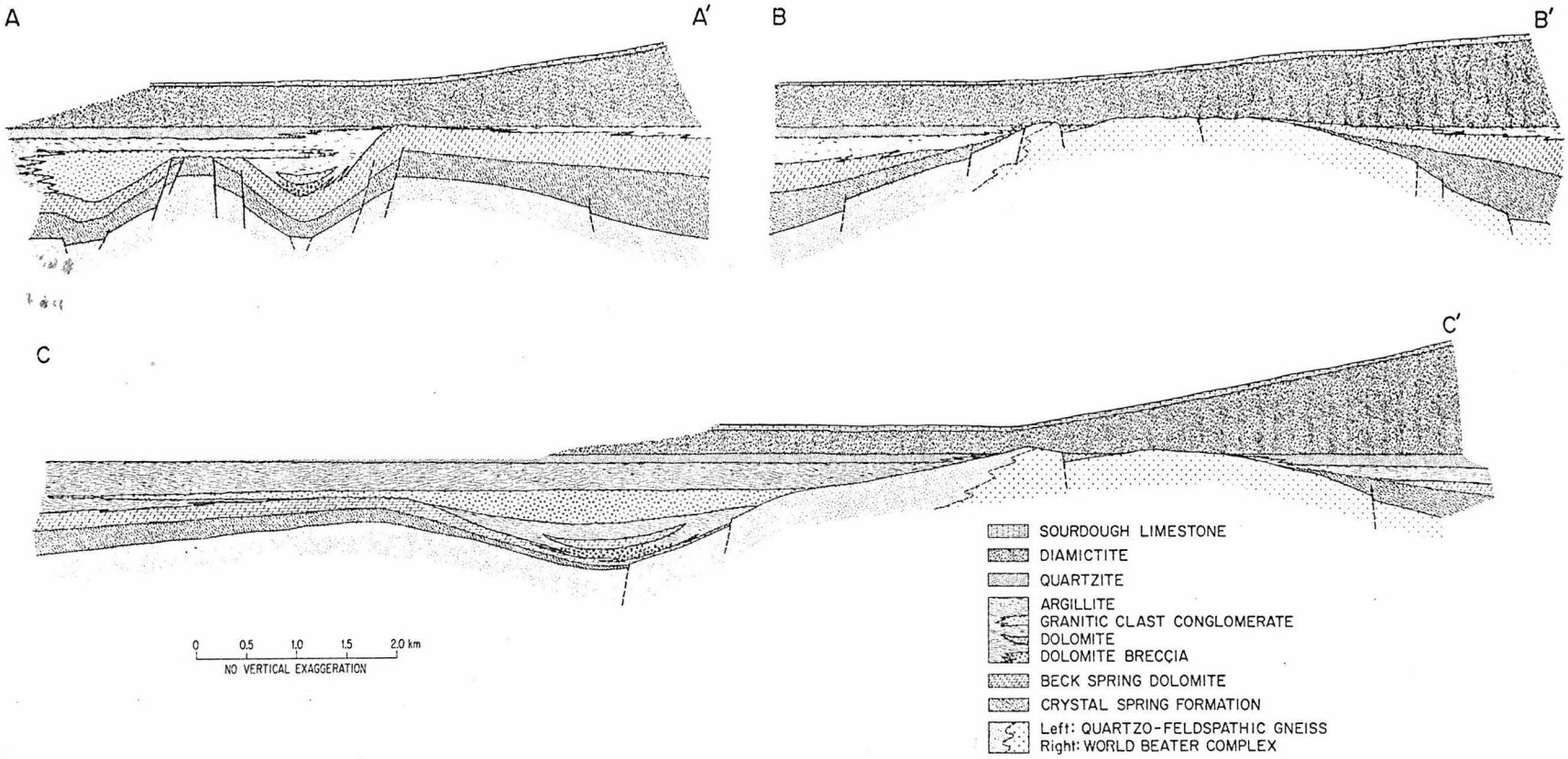

Figure 17: Stratigraphic cross sections of the Pahrump Group. Location shown on Figure 4.

tite, but the facies change from diamictite to argillite north of Surprise Canyon and the absence of the Surprise Member on top of and west of the anticline necessarily renders Figure 17 a cartoon. The uplift of the platform provided a local source for dolomite and granitic clasts to the adjacent down dropped areas. These depressions are largely filled with argillaceous material, although local stabilization must have occurred to allow the development of the dolomite interbeds. Argillite lapped over the conglomerate and eventually the positive areas, and the deposition of the quartzite appears to have eliminated the topographic irregularities on the west side of the high.

The first appearance of the unusual diamictite and associated rocks may represent a time line, and thus, rocks east of the anticline which are equivalent to the Limekiln Spring Member are thin.

The depositional environment of the upper units in the Kingston Peak Formation is not adequately assessed. In particular, the origin and environment of the Surprise Member are unknown, but the peculiar texture and bedding characteristics of the diamictite are suggestive of glacial till (Johnson, 1957). A few thin, graded beds of argillite (often containing exotic "lonestones") do occur, and the presence of pillow structures in basaltic lava indicate that the Surprise Member is at least in part subaqueous and probably marine. The south to north change from diamictite to argillite and greywacke shows that a complex depositional environment must have existed.

The map view of the geography and geology at the end of Beck Spring Dolomite time is shown in Figure 18. Attempts to present quantitative structure contours were fruitless because of the lack of complete

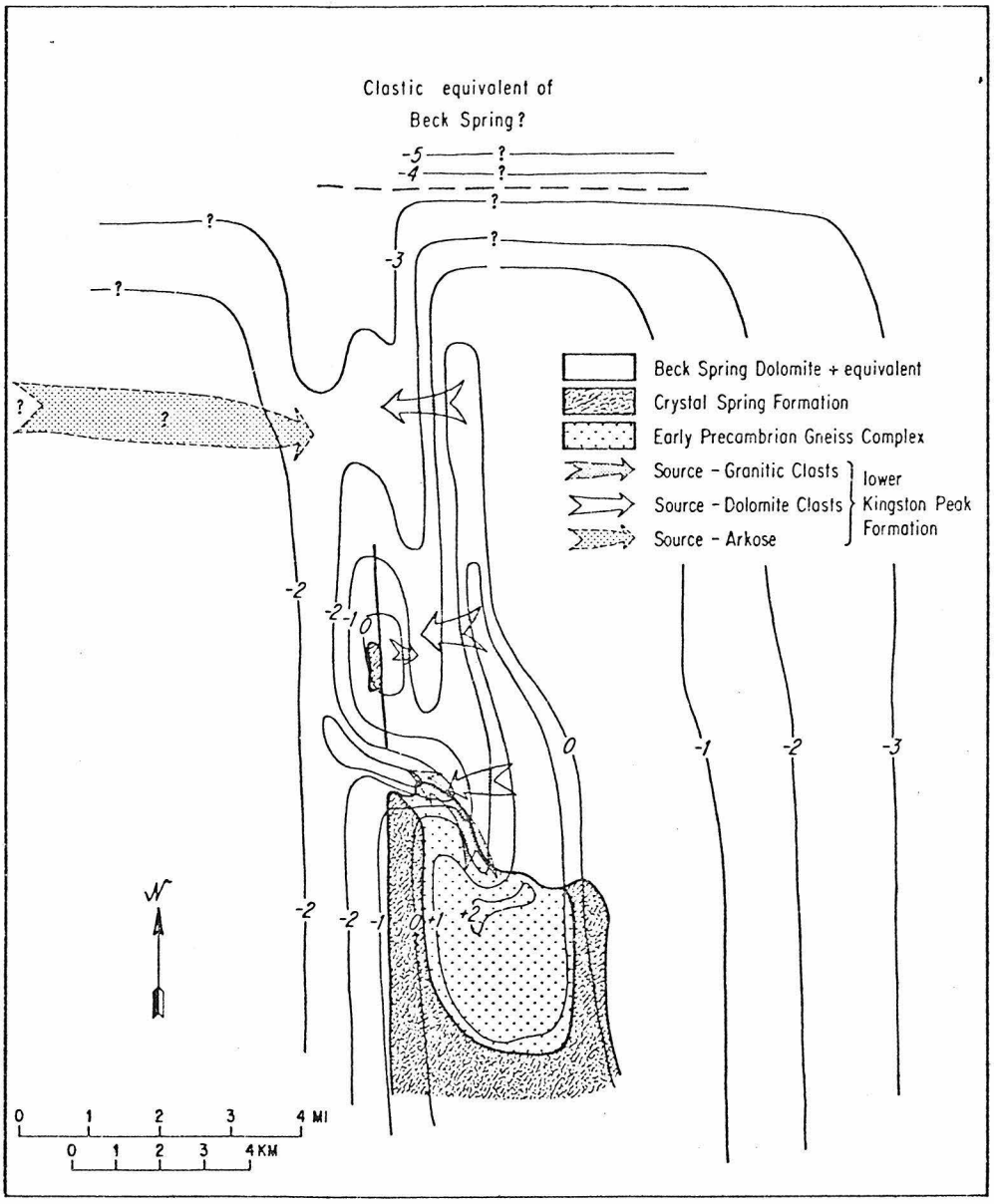

Figure 18: Paleogeography at the end of Beck Spring Deposition. Contours are arbitrary and show only the interpretation of topography; 0 represents sea level.

sections and the later deformation of the Pahrump Group. The contours shown in Figure 18 are arbitrary, although zero is intended to represent sea level, and are used to show only the interpretation of the topography. Source areas and drainage divides are inferred from the distribution of clasts (Figure 7). Sources for the dolomite clasts are particularly obvious in the recognition of the angular unconformity on top of the western high in Surprise Canyon (Figures 7, 15). The granitic clasts are identical to the quartzofeldspathic gneiss which crops out extensively in the basement terrain, but no clasts of the distinctive World Beater Complex were observed. Either the terrain underlain by the World Beater Complex remained covered, or more likely, a drainage divide separated the World Beater Complex from the quartzofeldspathic gneiss complex.

A similar divide is postulated which prevents the delivery of granitic clasts to the trough between the two highs in Surprise Canyon.

Deformation of the basement occurred along the north- and northwest-trending faults which are prominent in the geology. At least one north-trending fault was observed which was buried by lower Kingston Peak rocks. All other faults were reactivated during younger folding.

A source terrain external to the Telescope Peak Quadrangle is indicated for the arkose component in the lower Kingston Peak Formation. The arkose occurs only west of the anticline and it pinches out to the south. A west or northwest source is proposed. The presence of Beck Spring Dolomite clasts up to 3 m in diameter and of clasts of the distinctive World Beater gneiss in the diamictite indicate that World Beater Island continued to be a source after the deposition of the

quartzite, but most of the upper Kingston Peak clastic units must have had sources external to the Telescope Peak Quadrangle.

Intrusion of mafic sills occurred at least as late as earliest Kingston Peak time, and extrusive pillow lava flows occur in the lower Kingston Peak Formation. The presence of diabase clasts in the Kingston Peak below the lava flows indicates that igneous activity must have occurred over a significant period of time.

Regional Significance of the Pahrump Group

The gross stratigraphy exposed in the Telescope Peak Quadrangle records a history of deposition in a Precambrian basin which contained a substantial amount of relief and which was tectonically active during middle Pahrump time. The paleogeography consisted of a deep water basin in the north, a shallow water platform-carbonate shelf, and an island, or the northern part of a peninsula in the south.

The regional extent of the "Panamint platform" is imprecisely known. Johnson (1957) reports that a relatively thin Kingston Peak section rests on earlier Precambrian basement in Goler Wash in the southern Panamint Mountains, and thus, the platform-with-islands probably extended throughout the southern Panamint Mountains.

East and west positive areas are also indicated. An eastern positive area, called the Nopah Upland by Wright and others (1974) occurs in the present site of the Black Mountains. A western positive area is postulated as the source of the arkose in the lower Kingston Peak and was also suggested by L. A. Wright (personal communication) as a source for conglomerates in the Crystal Spring Formation south of Goler Wash.

The regional, pre-Kingston Peak paleogeography in the Death Valley area is illustrated in Figure 19. There is still much uncertainty regarding the paleotectonic elements in this region. Wright and others (1974) outlined evidence for a west-trending trough in the southern Death Valley region which they call the Amargosa Aulacogen. The northern margin of this trough (equivalent to southern edge of Nopah Upland) is well documented, but the southern "Mojave" upland is postulated on the basis of isopachous maps of Crystal Spring Formation (Roberts, 1974) and transport directions for detritus in Crystal Spring Formation (Roberts, 1974) and Noonday Dolomite (Williams and others, 1974). Isopachous maps presented for the Kingston Peak Formation (Wright and others, 1974) and Crystal Spring Formation (Roberts, 1974) suggest that the Amargosa trough shallows to the east and to the west. It is possible that the Panamint Platform extended even farther south than Goler Wash.

Pahrump Group and possibly equivalent rocks also occur in the Tucki Mountain area (Hunt and Mabey, 1966) and in the northern Funeral Mountains (Troxel and Wright, 1968), but the stratigraphy of these rocks is largely unknown.

Figure 19 shows the uplands, shallow water platform areas and deeper water basins suggested by this study and by the others referred to. It is quite apparent that the late Precambrian paleogeography is very irregular and that the relatively simple aulacogen-geosyncline relation originally proposed by Wright and others (1974) is not viable.

Stewart (1972) argues that the initiation of the Cordilleran Geosyncline occurred after the deposition of Belt Supergroup and equivalent strata, and with the deposition of Windermere and equivalent rocks.

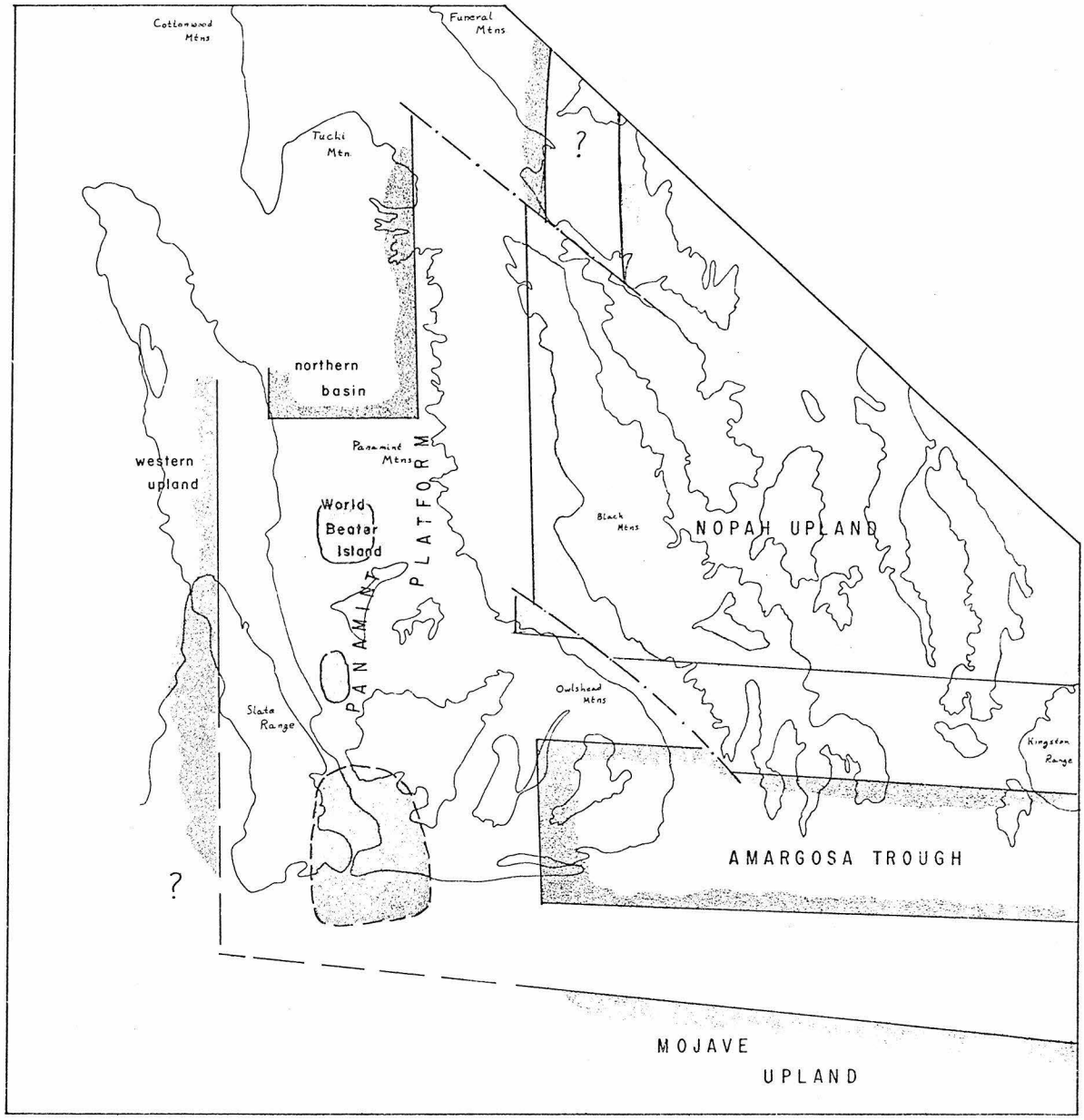

Figure 19: Late Precambrian paleogeography of the Pahrump Group, Death Valley area, California.

Lithologic similarities of the Pahrump Group and overlying strata to Belt Supergroup and Windermere group and equivalents have often been noted (e.g. Stewart, 1972; Crittenden and others, 1971), and in particular the presence of diamictite within these sections is often noted. Diamictite in the Windermere Group and equivalents occurs above an unconformity over the underlying Belt equivalent rocks. Argument by analogy places a major stratigraphic break between Kingston Peak and Beck Spring Dolomite. Rocks equivalent to the Belt Supergroup would be Crystal Spring Formation and Beck Spring Dolomite; Windermere equivalents would be Kingston Peak Formation, Noonday Dolomite, Johnnie Formation, and Stirling Quartzite. Such a correlation does not seem justified for four reasons.

The local unconformity observed between Kingston Peak and Beck Spring rocks occurs well below diamictite-bearing strata, and the intertonguing Beck Spring Dolomite and Kingston Peak strata indicate the local nature of the unconformity and no real absence of time-rock record.

Diamictite first appears above the quartzite unit in the Limekiln Spring Member. Although the diamictite and quartzite appear conformable, the contact may represent a hiatus. However, the distribution of diamictite is capricious, and north of Surprise Canyon the entire lower Kingston Peak consists of monotonous, thin-bedded argillite and fine-grained greywacke. The Pahrump exposed in Tuber Canyon also suggests a continuous sedimentation from the top of the Crystal Spring to the Noonday Dolomite.

Diamictite is unevenly distributed within the Kingston Peak Formation throughout Death Valley. True, massive diamictite and possible

tillite occurs in the Panamint Mountains. Elsewhere the conglomerates are fan deposits (Kingston Range, Hewett, 1956) or turbidites with occasional exotic clasts (Sperry Wash, personal observation). Hence, the first appearance of diamictite is difficult to assess.

The major, regional unconformity which is observed in the Death Valley area occurs between the Kingston Peak Formation and Noonday Dolomite, and not below the Kingston Peak.

The stratigraphic relations within the Pahrump Group indicated by this study are shown in Figure 20a. If the correlation of the Tuber Canyon section to the Pahrump Group is in error, a diastemic relation between Beck Spring and Kingston Peak may exist as shown in Figure 20b. However, the lack of a recognized regional unconformity beneath the Kingston Peak Formation casts doubt on such an interpretation, and a more or less continuous history of sedimentation punctuated with local tectonic uplift is a more accurate description of the Pahrump Group.

The age of the Pahrump Group is not well constrained. The top of the group lies about 2000 m below the lowest occurrence of lower Cambrian fossils in the upper Wood Canyon Formation (Diehl, 1974). The Crystal Spring Formation rests depositionally on the World Beater Complex which is about 1400 m.y. old (Lanphere and others, 1964). Wrucke and Shride (1972) have correlated the diabase sills which occur in the Crystal Spring Formation to those in the Apache and Unkar Groups of Arizona, and they suggested regional diabase sill emplacement at about 1200 m.y. Such a correlation indicates that the Crystal Spring Formation is greater than 1200 m.y. old (Silver, 1960).

In the Telescope Peak area, mafic sills and dikes occur as high as

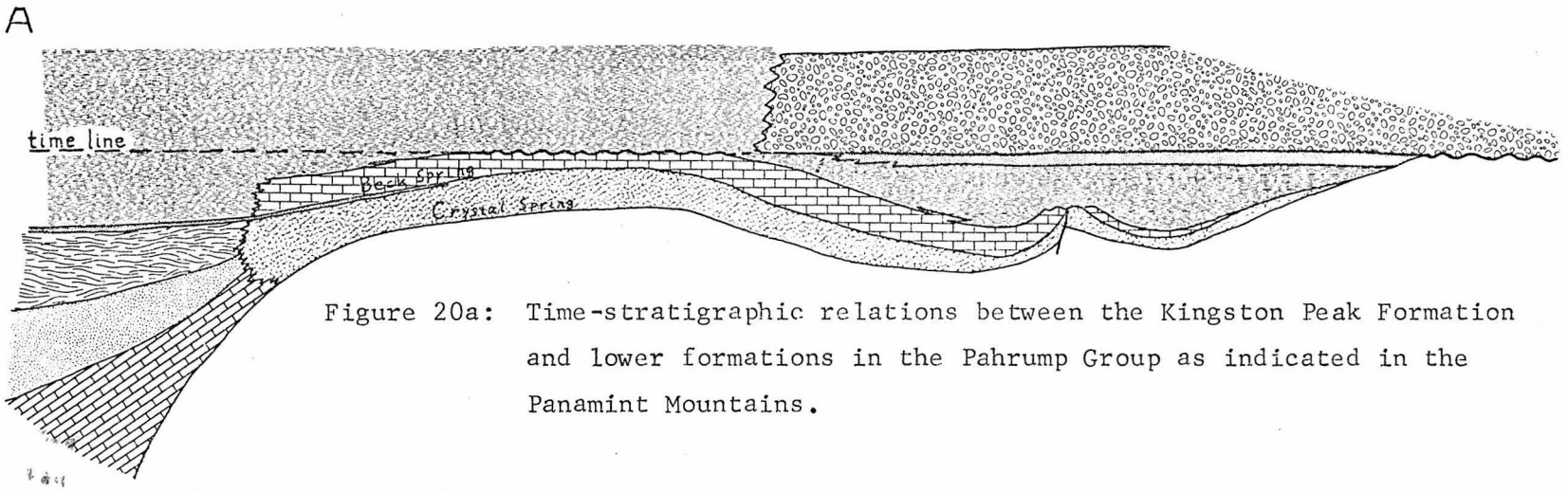

Figure 20a: Time-stratigraphic relations between the Kingston Peak Formation and lower formations in the Pahrump Group as indicated in the Panamint Mountains.

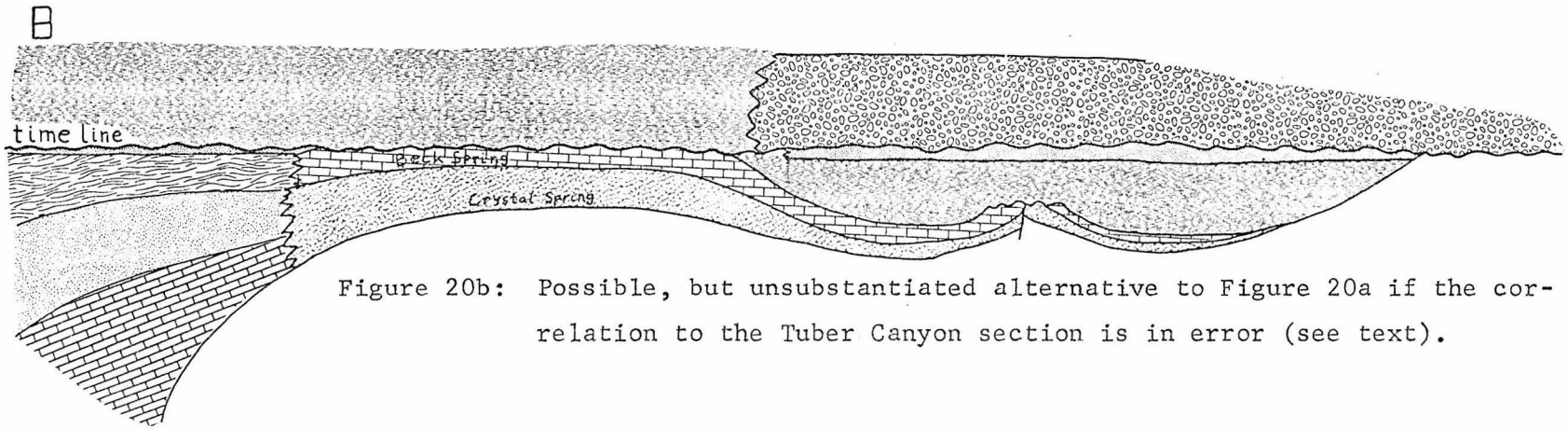

Figure 20b: Possible, but unsubstantiated alternative to Figure 20a if the correlation to the Tuber Canyon section is in error (see text).

the Beck Spring-Kingston Peak contact and basalt flows are interbedded within the Surprise Member of the Kingston Peak Formation. The occurrence of basalt flows in diamictite sections is summarized by Stewart (1972) and this association may represent a single time (∿850 m.y. - Ryan and Belkinsop, 1971).

Such correlations imply that the grossly continuous sedimentation in the Pahrump encompasses a time from greater than 1200 m.y. to less than 850 m.y. old, but these more than 350 million years are represented by only 3000 m of rock, at most. Alternatively, one or both of the age correlations may be in error, or a significant, but unrecognized hiatus may be present in the section.

Stewart (1972) contends that the initiation of the Cordilleran geosyncline is marked by the deposition of diamictite, extrusion of basaltic lava, and the formation of the northwest paleoslope characteristic of Paleozoic sedimentary trends. If the opening of the Cordilleran ocean was accomplished by continental rifting, as proposed by many people (e.g. Stewart, 1972; Burchfiel and Davis, 1975; Gabrielse, 1972), the initial deposits are most likely to record a microenvironment dominated by local provenance and irregular basins of deposition. Only when the local environments are integrated can the overall northwest paleoslope be established. It is believed that the initiation of the Cordilleran geosyncline occurred after the intrusion of 1400 m.y. granitic rocks (Silver and others, 1977) when ensislic basins were developed in which Crystal Spring, Belt, Apache, Big Cottonwood rocks were deposited (Silver and others, 1977; Stewart, 1972; Harrison and others, 1974 [Harrison and Reynolds (1976) feel that the Belt Supergroup was deposited at the edge

of an ancient continental margin]). Episodic, vertical deformation, compatible with rifting, occurred at the end of Beck Spring Dolomite time, and at the end of Kingston Peak time.

PALEOZOIC AND MESOZOIC HISTORY

Regional uplift occurred after the deposition of the Pahrump Group and the disconformity at the base of the Noonday Dolomite truncates some of the upper units in the Kingston Peak Formation. Rocks of the latest Precambrian Noonday Dolomite, Johnnie Formation, Stirling Quartzite, and Cambrian Wood Canyon Formation were deposited on top of this disconformity. There is no evidence for any disconformities within this stratigraphic section.

Evidence for the Paleozoic history of the Telescope Peak area is lacking, but relatively complete Paleozoic sections are extensively exposed to the north (Hall, 1971, Hunt and Mabey, 1966) which indicate a relatively quiescent period of dominantly carbonate sedimentation after the middle Cambrian.

The next geologic event recorded in the Telescope Peak Quadrangle occurred in the late Cretaceous when the Precambrian rocks were regionally metamorphosed and intruded by muscovite-bearing granite. This regional metamorphism was followed by a deformational event which produced the north-northwest-trending anticlines and World Beater Dome. The formation of these structures was accomplished in part by reactivation of the older north-trending faults, and was accompanied by a second metamorphic event.

The Mesozoic history of the Death Valley region is considerably

more complex than the geology exposed in the Telescope Peak Quadrangle indicates. Prior to the Late Cretaceous metamorphism one or more periods of thrusting and intrusion occurred. An extensive network of thrusts crops out in the White and Inyo Mountains (Inyo Thrust of Stevens and Olson, 1972), in the Last Chance Range (Last Chance Thrust of Stewart and others, 1966), in the Hunter Mountain area (Racetrack Thrust of McAllister, 1958), in the Cottonwood Mountains (Lemoigne Thrust of Hall, 1971), in the Argus Range (Argus-Sterling Thrust of Moore, 1974), and the Slate Range (Layton Well Thrust of Smith and others, 1968). Most of these faults either displace or are intruded by Mesozoic grantic rocks (Figure 21). Dunne and others (1978) summarize the Mesozoic history of the White-Inyo Mountains region. At least two periods of thrusting are separated by an episode of intrusion. The Last Chance, Racetrack, Lemoigne thrusts displace Permian strata but are intruded by granitic rocks of the Hunter Mountain pluton (approximately 175 m.y.). The more westerly Swansea and Argus-Sterling thrusts displace Triassic marine and Triassic to lower Jurassic volcanic strata as well as granitic rocks approximately 160 to 180 m.y. old. The upper age limit on the younger thrust system is placed by the 150 m.y. old Independence dike swarm which intrudes the Swansea thrust.

In the eastern Mojave Desert, Burchfiel and Davis (1971 and 1977) describe an extensive history of thrusting and intrusion which commenced in the Triassic and continued into the Cretaceous. Stevens and others (1974) suggested that the Panamint Mountains rest on the upper plate of a thrust fault, the Butte Valley thrust, and this implies that the Precambrian rocks in the Death Valley area are allochthanous. The Butte

Figure 21: Regional geology of eastern California. From California Division of Mines and Geology, Geologic Data Map no. 2, Geologic Map of California (1977).

PRECA
Conglomerate, shale, sandstone, limestone, dolomite, marble, gneiss, horn-
fels, and quartzite; may be Paleozoic in part.
OWENS
LAKE
ZONE
FAULT
ZONE

Valley fault is nearly everywhere intruded by 150 m.y. granitic plutons, but where it is not, the Butte Valley fault is a high angle normal fault (Johnson, 1957).

Thus, after the depositions of Triassic marine strata (as suggested by Johnson, 1957, and Stewart and others, 1966) and before the late Cretaceous metamorphism exhibited in the Panamint Mountains, the Telescope Peak area was involved to an unknown extent in a late Triassic thrusting episode, an early to middle Jurassic period of intrusion, a middle to late Jurassic thrusting episode, a late Jurassic period of intrusion, and perhaps an even younger thrusting episode.

The latest Mesozoic history appears to be recorded in the Panamint Mountains, Tucki Mountain, and the Funeral Mountains. This period of history is characterized by regional metamorphism followed by regional folding and doming. The Panamint Mountains seem to represent a deeper level of the late Mesozoic crust than is exposed in regions to the west. Events which correspond to regional metamorphism must include emplacement of Cretaceous batholithic rocks of the Sierra Nevada (Evernden and Kistler, 1970), but the relative position of the regionally metamorphosed terrain to the batholith is unclear.

TERTIARY AND QUATERNARY HISTORY

During the Tertiary, deformation occurred along low angle normal faults, quite in contrast with the earlier styles of deformation. Displacement across low angle faults occurred both before and after the emplacement of the Little Chief stock. The younger monolithologic breccias may have formed in response to the inception of displacement

along the Panamint Valley fault zone. A relatively stable period after the formation of the monolithologic breccia allowed the development of the Pliocene erosion surface. Renewed displacement along the Panamint Valley fault zone uplifted the Panamint Range and caused dissection of the old erosion surface. Substantial uplift had occurred prior to the development of late Pleistocene Lake Panamint (Smith, 1976).

The setting of the Panamint Mountains during the Tertiary and the relations between the Panamint Mountains and adjacent mountain blocks are not clear. The Tertiary is dominated by uplift and denudation of the metamorphic terrains in the Panamint, Black, and Funeral Mountains (Hunt and Mabey, 1966). This uplift is coupled with the inception of extensional tectonics as exemplified by the hypabyssal intrusion of felsic igneous rocks and great eastward tilting of blocks along rotational faults (Wright and Troxel, 1973). The great east-west extension appears to be coupled in turn with the inception of regional right-lateral shear which is manifested in the Panamint Valley and Death Valley fault zones (Burchfiel and Stewart, 1966).

This extensional tectonic regime is represented in the central Panamint Mountains by low angle normal faults, Little Chief stock, and late Tertiary monstrous landslides. Late Tertiary and Quaternary deformation involved uplift and eastward tilting of the Panamint Mountains along the Panamint Valley Fault Zone, but the degree to which the central Panamint Mountains was affected by this deformation is unclear. In the Panamint Butte Quadrangle Plio-Pleistocene Nova Formation is tilted 20 to 40° east, but these rocks appear to be in a block which is separated from the central Panamint Mountains by an old strand of the

Panamint Valley fault (Smith, 1976). Smith (1976) indicates that the maximum present uplift rate of the Panamint block is about 1.5 mm/y, but the amount of eastward tilting is not determined. The principal deformation across the Panamint Valley Fault Zone occurs as right-lateral displacement and is probably responsible for the present geometry of Panamint Valley (Smith, 1976).

Intriguing problems yet remain. What is the extent to which the Precambrian block was involved in early and middle Mesozoic thrusting? Are the Precambrian rocks in the Death Valley area allochthanous or do they occur in a fenster, an island in a sea of thrusts? To what degree was the Panamint Block tilted to the east during the Tertiary and Quaternary? The restoration of any eastward tilt forces the late Mesozoic asymmetric anticline to be overturned to the west and indicates an east to west tectonic transport, a most unusual environment of deformation for the Cordillera. A final question, one addressed in Part II, what is the relation between the regional metamorphism exhibited in the Panamint and Funeral Mountains to the intrusive activity in the Sierra Nevada?

LATE MESOZOIC REGIONAL METAMORPHISM, DEATH VALLEY AREA, CALIFORNIA

INTRODUCTION

Regional metamorphism has affected the Precambrian and Paleozoic rocks in the Death Valley area, particularly in the Panamint and Funeral Mountains where the Pahrump Group and overlying formations have attained the amphibolite facies. The isotopic data of Lanphere (1962) and Lanphere and others (1964) indicated that regional metamorphism in the Panamint Mountains occurred during the late Mesozoic. The age of metamorphism in the Funeral Mountains is largely undetermined, but it is quite likely that metamorphism in the Panamint and Funeral Mountains was contemporaneous.

Andalusite-bearing assemblages in the Panamint Mountains are in sharp contrast to kyanite-bearing assemblages in the Funeral Mountains on the east side of Death Valley. The two regional metamorphic terrains appeared to have formed under different physical conditions and this study was undertaken to document the facies series represented by the two terrains and to contrast the development of mineral assemblages in pelitic schists. The following discussion is divided into three sections, the first describes the petrology of the Panamint metamorphic terrain, the second describes the petrology of the Funeral metamorphic terrain, and the third contrasts the development of mineral assemblages in pelitic schists and proposes a possible tectonic environment of metamorphism.

Samples were collected from the Panamint and Funeral Mountains in order to supplement previously collected samples from the Wildrose Canyon area (Lanphere, 1962), the Little Chief stock area (McDowell, 1967), the World Beater Dome area (Lanphere and others, 1964), and

others collected during reconnaissance of the Panamint and Funeral Mountains metamorphic terrain by A. L. Albee. Because of the diverse sedimentary and igneous rocks in the Panamint Mountains, samples were collected to provide as wide a range in bulk composition and metamorphic grade as possible. In the Funeral Mountains, sampling was concentrated on the abundant pelitic schists because carbonate rocks and amphibolitic schists are not as common or widespread as they are in the Panamint Mountains.

Nearly all samples were examined in thin section in order to identify mineral assemblages and textures. Complementary x-ray powder diffraction methods were used to distinguish the phyllosilicates muscovite and talc in carbonate rocks, and to determine the presence of muscovite, paragonite, and pyrophyllite in low-grade argillites from the Panamint Mountains. Similar x-ray diffraction analysis has not yet been performed on Funeral Mountains samples. Carbonate rocks were stained with alizarin red in order to distinguish calcite from dolomite.

Samples which showed the least amount of low grade alteration and which are comprised of multiple-phase assemblages were selected for detailed study.

Chemical analyses were obtained with a Materials Analysis Corporation model 5-SA3 electron microprobe. Standard operating conditions are 15 kV accelerating potential, 50 namp sample current on brass, 30 sec peak counting time, and maximum spot diameter of 20 μm. Counting time was increased to a maximum of 120 sec in order to maintain a 1% standard deviation for counts on elements of low concentration. Spot size was varied according to the size and nature of the mineral analyzed.

Large spot sizes were used for analysis of feldspars and micas in order to minimize the volatilization of alkalis. Data were accumulated with three automated wavelength dispersive spectrometers, and data were reduced on line with PDP 8/L computer using the technique of Bence and Albee (1968) and the correction factors of Albee and Ray (1970). The analyzed elements were chosen according to the mineral as described in Table 4. CO_2 and $H_2O + O_2$ were calculated for carbonate and hydrous minerals by the methods of Chodos and others (1973). The chemical analysis was normalized to a formula for the particular mineral as described in Table 4.

Reproducibility of analysis was monitored by replicate analyses of the standard minerals McGetchen garnet, P-80 anorthite, Leilenkopf sanidine and P-238 hornblende. Precision of the garnet and sanidine analyses in the Caltech lab was found to be about 1.5 times the counting error (Champion and others, 1975). Standard errors for the reported analyses are taken to be 2% on elements whose abundance is greater than 10 wt % and 10% on minor elements. Detection limit on the microprobe under these conditions is approximately 0.05 wt %.

Samples which were chosen for analysis were examined in thin section, and based on textural relations, points on mineral grains were selected for analysis. Textural relations which affected the choice of analysis locations include mutual mineral contacts and inclusions in porphyroblasts, and large mineral grains such as garnet and amphibole were analyzed for chemical zoning. Analyses are reported here in terms of formula proportions. Complete chemical analyses may be obtained from the author upon request.

TABLE 4

MINERAL	ANALYZED ELEMENT																NORMALIZATION	FERRIC IRON
	Si	Ti	Al	Cr	Fe	Mn	Mg	Ca	Na	K	F	Cl	Zn	Zr	Ce	Ba		
Amphibole	X	X	X	X	X	X	X	X	X	X	X	X					I Σ (cations - K) = 15 II Σ (cations - K - Na) = 15 III Σ (cations - K - Na - Ca) = 13	46 - total pos. charge
Aluminosilicate	X	X	X		X				X	X							Σ cations = 3	all ferric
Biotite	X	X	X		X	X	X	X	X	X	X	X	X				Σ (cations - K - Na - Ca) = 7	22 - tot. pos. chg.
Chlorite	X	X	X	X	X	X	X	X	X		X	X	X				Σ (cations - Na - Ca) = 10	28 - tot. pos. chg.
Chloritoid	X	X	X		X	X	X	X			X		X				Σ cations = 8	24 - tot. pos. chg.
Cordierite	X	X	X		X	X	X	X	X	X							Σ (cations - K - Na) = 11	36 - tot. pos. chg.
Epidote Minerals	X	X	X		X	X	X	X			X				X		Σ cations = 8	3 - (Al + Ti)
Feldspar	X	X	X		X		X	X	X	X						X	Σ cations = 5	
Garnet	X	X	X	X	X	X	X	X									Σ cations = 8	2 - (Al + Ti + Cr)
Mica	X	X	X		X	X	X	X	X	X	X	X	X				Σ (cations - K - Na - Ca) = 6	22 - tot. pos. chg.
Pyroxene	X	X	X	X	X	X	X	X	X								Σ cations = 4	12 - tot. pos. chg.
Opaque oxide	X	X	X	X	X	X	X						X	X			I Σ cations = 2 (rhombohedral) II Σ cations = 3 (spinel)	stoichiometry
Sphene	X	X	X		X	X	X	X			X				X		Σ cations = 3	
Carbonate					X	X	X	X									Σ cations = 2	

LOW PRESSURE REGIONAL METAMORPHISM, PANAMINT MOUNTAINS

INTRODUCTION

The Panamint Mountains are a fault block range which form the western boundary of central Death Valley. The internal structure of the range is dominated by a north-northwest-trending anticline which contains earlier Precambrian gneiss in the core. The later Precambrian Pahrump Group which overlies the gneiss dips gently east on the east flank of the anticline and generally steeply west on the west flank. The later Precambrian Noonday Dolomite, Johnnie Formation, and Stirling Quartzite generally occur on the east limb of the structure (Figure 22). Isotopic data of Lanphere (1962) and Lanphere and others (1964) indicate that metamorphism occurred during the late Mesozoic, and arguments presented in Part I and substantiated here indicate that metamorphism occurred during intrusion of the Cretaceous Hall Canyon pluton; folding occurred later and was accompanied by retrograde metamorphism.

The metamorphosed rocks in the Telescope Peak Quadrangle encompass a wide variety of bulk compositions. The occurrence of andalusite- and cordierite-bearing assemblages indicates that these rocks were metamorphosed under conditions similar to those of the low pressure-intermediate facies series of Miyashiro (1961). It was hoped that the nature of progressive low pressure metamorphism in pelitic schists, siliceous dolomites, and calciferous schists could be ascertained. In particular, calciferous schists are abundant, and many contain interesting, multiple-phase assemblages (for example garnet + grunerite + hornblende + biotite + plagioclase + quartz and garnet + hornblende + epidote + biotite + muscovite + plagioclase + quartz), but the effects of a second, retrograde metamorphic event have made the determination of equilibrium

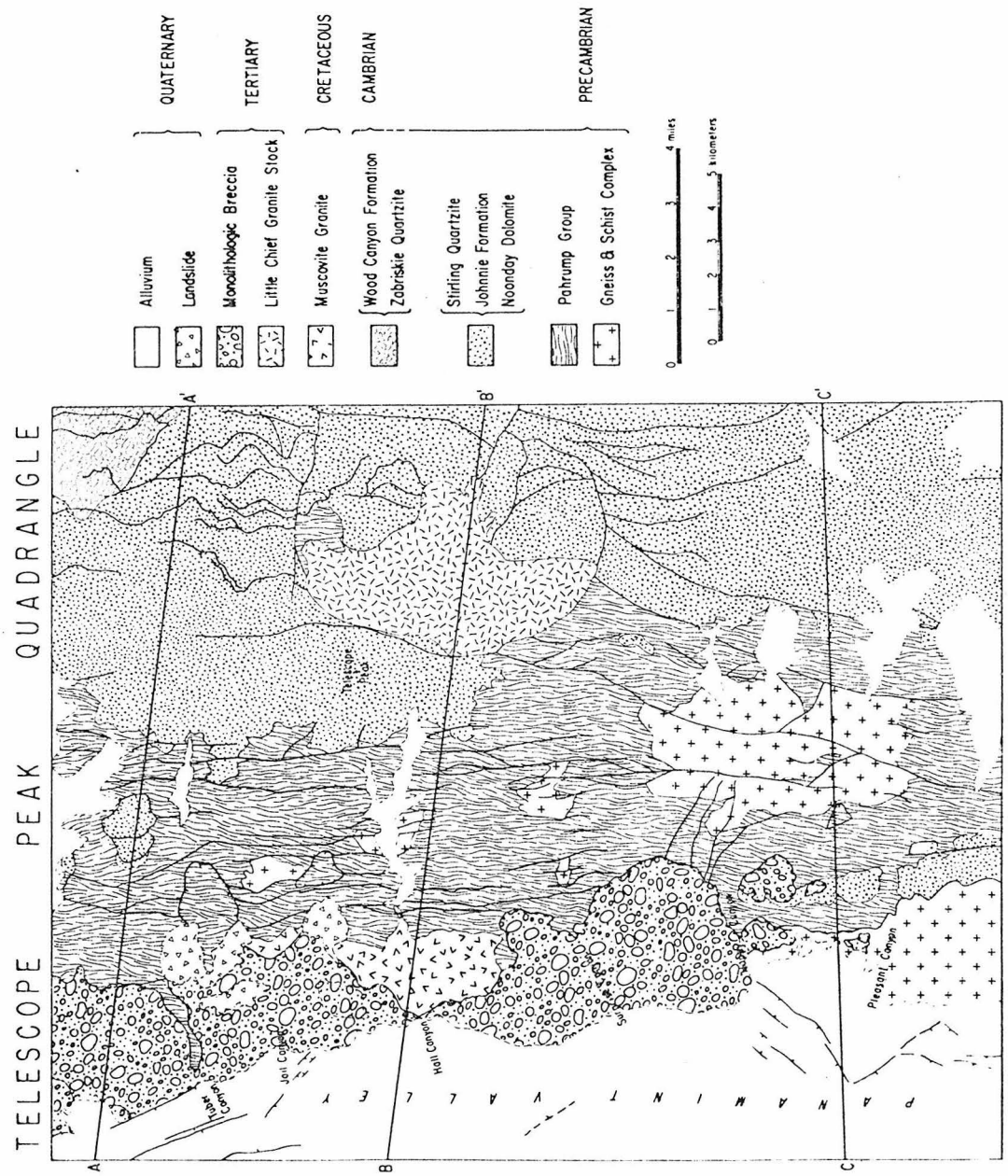

Figure 22a: Generalized geology of the Telescope Peak Quadrangle.

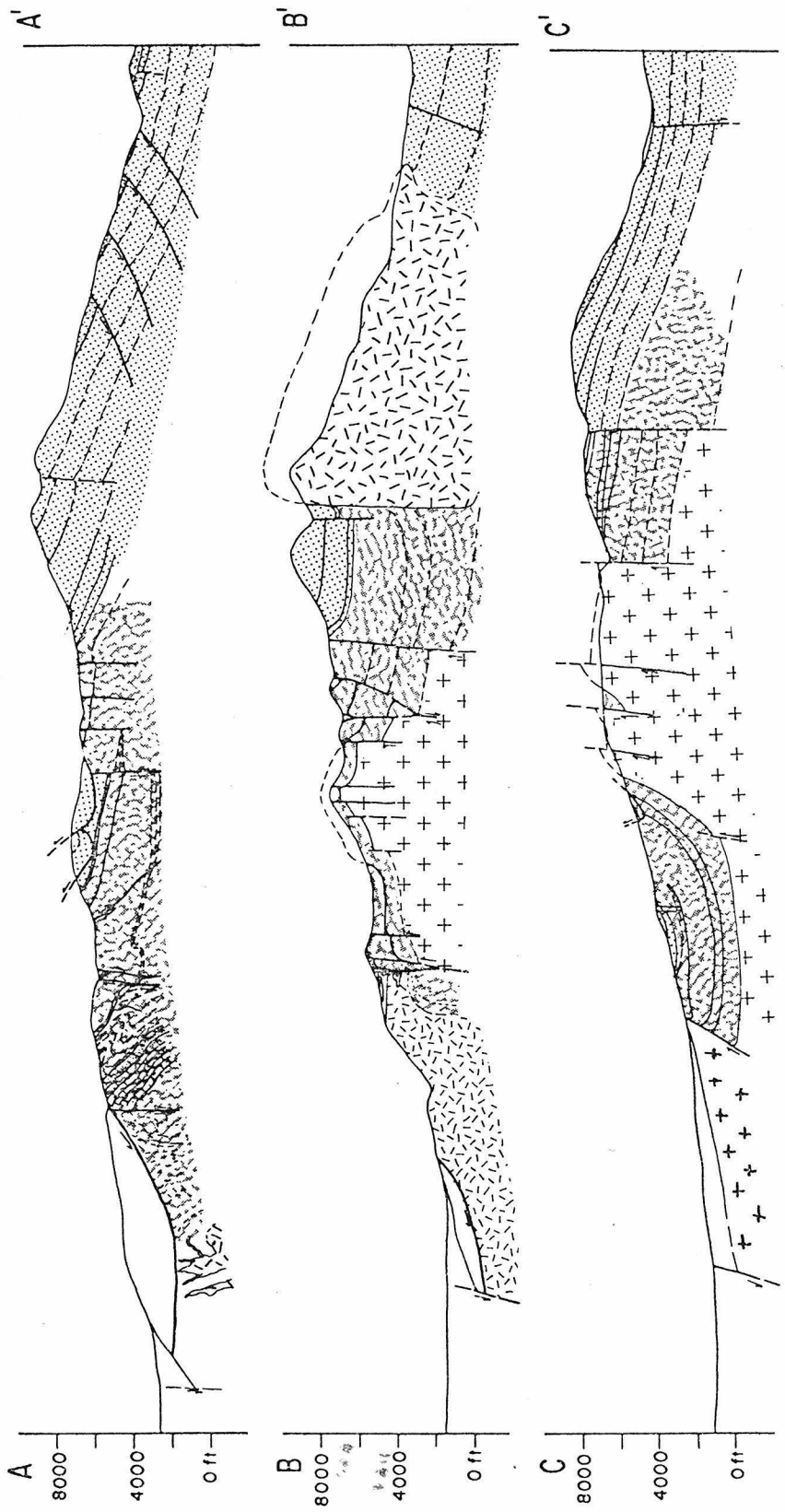

Figure 22b: Geologic cross sections indicated in Figure 22a.

mineral assemblages and compositions very difficult. The elucidation of progressive metamorphic reactions in calciferous schists was less than successful, and the discussion which follows focuses on siliceous dolomite and pelitic schist. Rocks of appropriate pelitic composition are not widely nor uniformly distributed enough to be used for delineation of the familiar metamorphic mineral zones. Mineral assemblages in the abundant carbonate rocks proved more convenient, and tremolite and diopside are used as an index of metamorphic grade.

The textures of the metamorphic rocks are dominated by three features. First, secondary planar fabric (cleavage or schistosity) is weakly developed or is absent. Where a metamorphic foliation is developed in the highest grade areas, the schistosity lies parallel to the bedding. A linear fabric is locally developed along the western margin of the north-northwest-trending anticline which dominates the structure of the central Panamint Mountains. The lineation is principally defined by the long axes of stretched cobbles in the conglomerates, but aligned amphibole grains and white mica pods also occur.

Second, compositional inhomogeneities over distances on the scale of a thin section are preserved. These inhomogeneities are represented by original sedimentary bedding and by clasts in conglomerate. It is surprising that even in rocks which locally contain metamorphic sillimanite small scale sedimentary features such as millimeter-scale bedding and slump folds are preserved. Small, centimeter-sized carbonate clasts in greywacke are easily recognized, even though the carbonate is largely replaced by amphibole. Evidence for metamorphic differentiation, veins, and segregations is almost entirely lacking.

Third, textural features attributable to progressive metamorphic reactions and polymetamorphism are abundant. Inclusions in porphyroblasts, pseudomorphic replacement of porphyroblasts, mineral armoring, and discontinuous compositional zoning in minerals are prevalent. Two periods of metamorphism are recognized. The earlier metamorphism which produced the andalusite- and cordierite-bearing assemblages in pelitic rocks and tremolite- and diopside-bearing assemblages in carbonate rocks was affected by a second, generally retrograde metamorphism. Aluminous minerals are replaced by sericite, mafic minerals are chloritized, amphiboles in calciferous schists are discontinuously zoned from hornblende to actinolite, and so on. The effects of the second metamorphism are developed most strongly in the core of the major anticline where recrystallization of the earlier metamorphic assemblage was nearly complete. Elsewhere, the second metamorphism was very low grade, and its effects made collection of well preserved, earlier metamorphic assemblages frustrating.

ASSEMBLAGES IN SILICEOUS DOLOMITE

Carbonate rocks are abundant in the Panamint Mountains. Beck Spring Dolomite and Noonday Dolomite are largely comprised of siliceous dolomite, micaceous limestone, and dolomitic limestone. In addition, quartz-muscovite limestone occurs in the Kingston Peak Formation and dolomite clasts occur in greywackes in the Kingston Peak Formation.

The low grade and incipiently metamorphosed carbonate rocks are characterized by the assemblage quartz + dolomite and calcite, chlorite, and muscovite are common additional phases. Original sedimentary tex-

tures are well preserved, quartz grains show detrital shapes, intraclasts are recognizable, and probable algal structures are evident.

Generally, on the west side of the range crest, tremolite-bearing assemblages occur. Figure 23 illustrates the distribution of quartz + dolomite assemblages (field observations were confirmed by thin section study) and tremolite + calcite assemblages. In most places the isograd is not well constrained in position because carbonate rocks east of the range divide contain quartz + dolomite and carbonate rocks west of the divide contain tremolite + calcite but the transition occurs in a region of inappropriate rock composition to record the tremolite isograd.

The carbonate rocks in the tremolite zone are coarse-grained and contain tremolite and carbonate grains with maximum dimensions on the order of 1 centimeter. The common mineral assemblages in the tremolite zone are calcite + tremolite + quartz, and calcite + dolomite + tremolite + talc, and quartz + calcite + tremolite + muscovite + zoisite. Tremolite usually occurs in prismatic or bladed form, but asbestiform amphibole is not uncommon in talc-bearing assemblages. Dolomite is usually granular, and calcite tends to be irregular and fills interstices. The blue-grey color of Beck Spring Dolomite which is due to the presence of graphite is lost in the tremolite zone. Graphite is recrystallized into distinct grains in some rocks, but in others graphite is absent.

Wherever identified, talc always appeared to be a secondary mineral derived from the alteration of tremolite. Because talc was formed during retrograde metamorphism, the prograde reaction which is represented by the tremolite isograd is

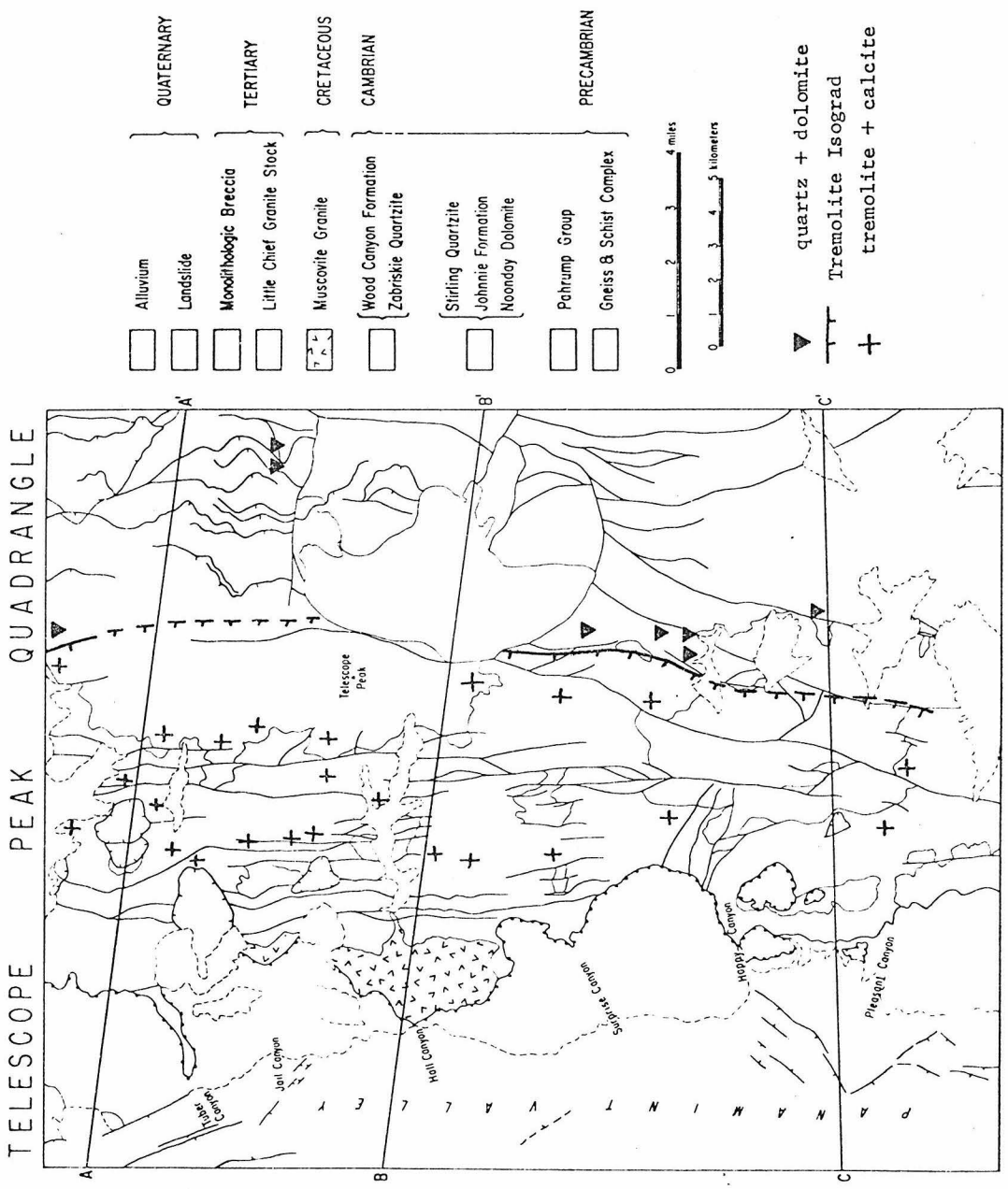

Figure 23: Tremolite isograd

quartz + dolomite = tremolite + calcite.

Figure 24 shows the distribution of diopside-bearing rocks and rocks with the assemblage calcite + tremolite + quartz. The diopside isograd represents the reaction

calcite + tremolite + quartz = diopside.

Many of the diopside-bearing assemblages indicated on Figure 24 occur in calciferous schists which contain the additional components FeO and Al_2O_3. Microprobe analyses of minerals in these assemblages indicate that FeO is preferentially incorporated into chlorite and that pyroxene contains no aluminum. Hence, (Fe, Mg)-calcic clinopyroxene can become stable only after pure Mg-diopside becomes stable. The diopside isograd shown in Figure 24 represents an upper limit on the lower stability limit of calcic clinopyroxene in the Panamint Mountains.

In Jail Canyon and in Tuber Canyon (Figure 24) the assemblages calcite + dolomite + forsterite and calcite + tremolite + forsterite occur, but the forsterite is nearly always altered to serpentine. Thus, the reaction

tremolite + dolomite = calcite + forsterite

is inferred to have occurred locally.

In addition to the carbonate horizons in the Pahrump Group, dolomite clasts are widespread in the Kingston Peak Formation in both the tremolite and diopside zones, and these clasts have developed reaction rims against a siliceous, micaceous matrix. Most clasts which are smaller than 1 cm are completely altered to amphibole but larger ones have preserved a dolomite core. The dolomite is rimmed by a zone which consists of calcite + tremolite and which is about 1/3 the clast radius

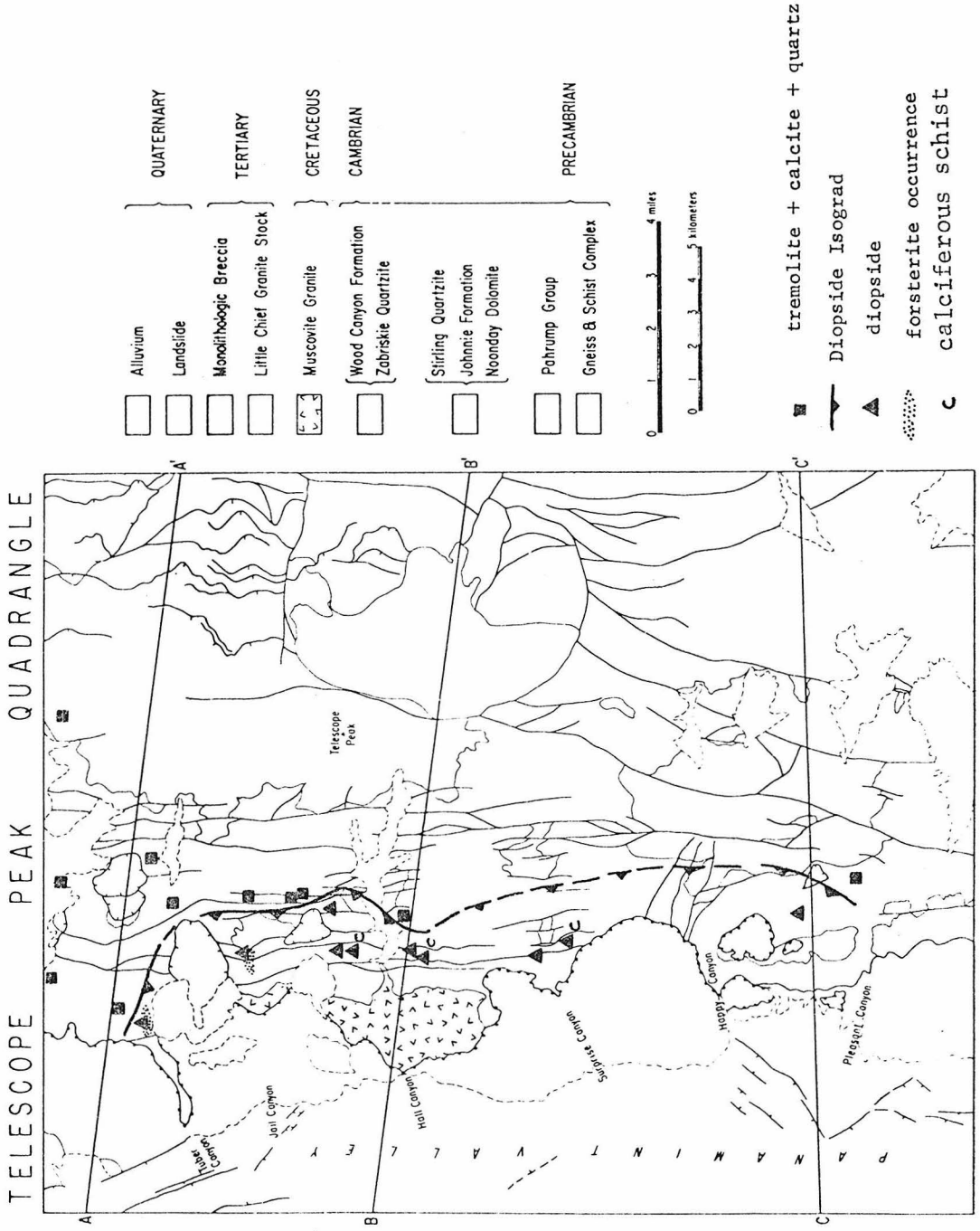

Figure 24: Diopside isograd.

in thickness. This inner zone is rimmed by a thinner zone which consists entirely of tremolite. Zoning in the host rock around the clasts is also common, but boundaries are not as sharp as they are in the clast. A thin, discountinuous rim of diopside is developed adjacent to clasts which occur in the diopside zone, and the entire calcsilicate assemblage is surrounded by a diffuse zone rich in microcline (+ epidote + quartz) within the biotite-rich rock matrix. The reactions which appear to have occurred during the metasomatic alteration of the dolomite clasts are

$$\underset{\text{(core)}}{\text{dolomite}} + SiO_2 + H_2O = \underset{\text{(zone 1)}}{\text{calcite}} + \underset{\text{(zone 1)}}{\text{tremolite}} + CO_2$$

$$\underset{\text{(zone 1)}}{\text{calcite}} + SiO_2 + H_2O + MgO = \underset{\text{(zone 2)}}{\text{tremolite}} + CO_2$$

$$\underset{\text{(matrix)}}{\text{phlogopite}} = \underset{\text{(zone 3)}}{\text{microcline}} + MgO + H_2O$$

Silica is provided by the abundant quartz in the matrix and MgO is provided by breakdown of biotite. The textures in carbonate rocks are illustrated in Figure 25.

ASSEMBLAGES IN CALCIFEROUS SCHISTS

Calciferous schist is the most abundant rock type in the Panamint Metamorphic terrain. The characteristic assemblage which comprises these rocks is biotite + epidote + plagioclase + quartz. Amphibole, chlorite, and calcite are common additional phases. The grain size in calciferous schist is generally small, and small-scale sedimentary features, such as laminated bedding and graded bedding are preserved. Amphibole generally occurs as larger, porphyroblastic grains which are compositionally zoned. Dark green hornblende commonly exhibits patchy

Figure 25: Textural features in metamorphosed siliceous dolomite, Panamint Mountains.

a) Prismatic tremolite in dolomite + calcite matrix, CP 468 (crossed nicols).

b) Interstitial calcite (with dark outlines) and granoblastic dolomite, PML 1a (plane polarized light).

c) Reaction rims on a dolomite clast (left) in Kingston Peak Formation. Post-metamorphic deformation caused the sheared calcite zone, PML 245 (crossed nicols).

d) Forsterite (clear high relief) altered to serpentine (clear, low relief) in dolomite + calcite matrix, PML 250m (plane polarized light).

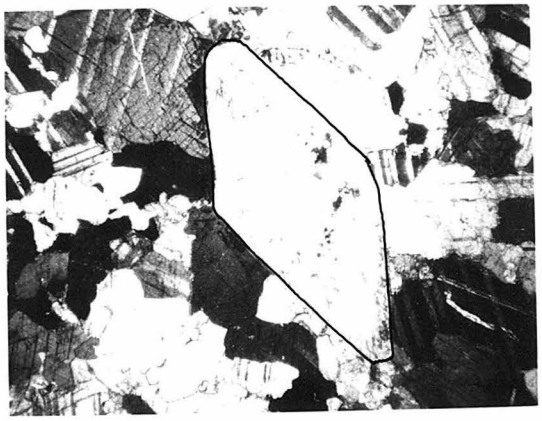

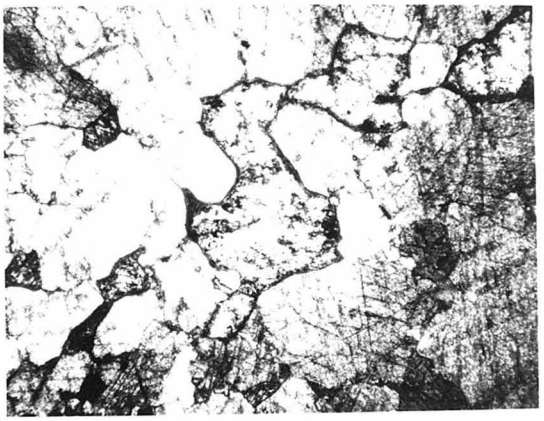

b

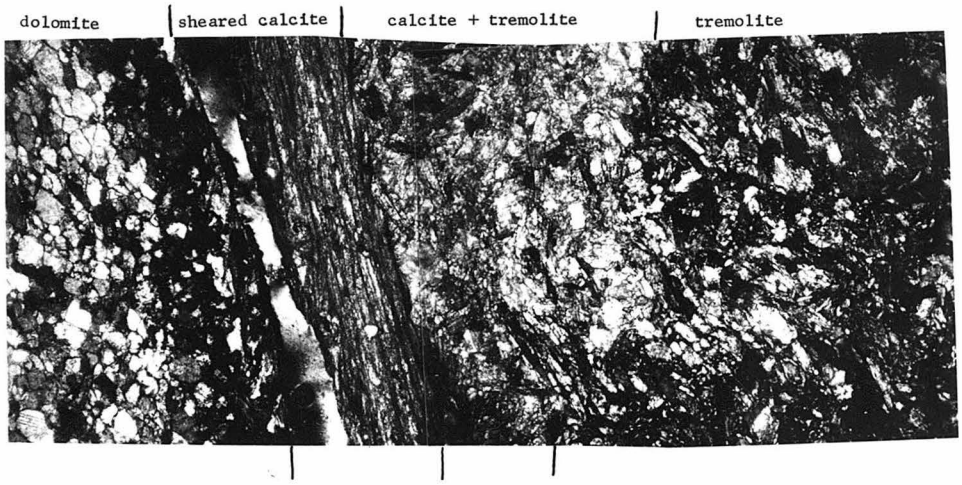

1 mm

d

intergrowths and rims of colorless actinolite, a texture attributable to polymetamorphism. Polymetamorphic textures are typical in calciferous schist; biotite is altered to chlorite and plagioclase is replaced by epidote and white mica. The effects of retrograde metamorphism are difficult to separate from the prograde effects, but amphibole preserves a range in composition which allows the determination of the mechanism responsible for this compositional variation. The substitutional mechanism recorded in amphibole composition is described in a later section.

The diagnostic assemblage in calciferous schist from the tremolite zone is quartz + plagioclase + biotite + epidote + calcic amphibole + calcite + chlorite + muscovite + ilmenite. Most assemblages in the tremolite zone do not contain all of these phases and in particular calcic amphibole is generally absent. A greater variety of mineral assemblages occurs in the diopside zone. These include quartz + epidote + plagioclase + biotite + calcic amphibole + garnet + muscovite + ilmenite, quartz + epidote + plagioclase + biotite + calcic amphibole + chlorite + (ilmenite or sphene), quartz + epidote + plagioclase + diopside + calcic amphibole + microcline, quartz + epidote + plagioclase + diopside + grossular + microcline, and quartz + plagioclase + biotite + calcic amphbiole + grunerite + garnet. The compositions of the constituent phases in these assemblages are described in a later section.

ASSEMBLAGES IN PELITIC SCHIST

Introduction

Rocks which contain diagnostic mineral assemblages in the system

Al_2O_3-K_2O-FeO-MgO are relatively uncommon and are restricted to the lower Stirling Quartzite, Johnnie Formation, and discontinuous layers within the Kingston Peak and Crystal Spring Formations. The majority of the rocks in the Telescope Peak Quadrangle are calcium-rich, and epidote-bearing assemblages are common. Epidote does not coexist with any mineral more aluminous than garnet or chlorite, and although calcium-poor pelitic schist has a limited distribution, diagnostic assemblages are abundant enough to characterize the response of pelitic schist to low pressure regional metamorphism.

Low grade rocks which occur outside the tremolite zone are very fine-grained and retain textural features indicative of detrital sedimentary rocks. The most common assemblage in these low grade rocks is quartz + sericite + chlorite + calcite + magnetite. In the Kingston Peak Formation, biotite is an abundant additional phase, and pyrite and pyrrhotite occur in the black, graphitic diamictite. Spotted pelites occur in the Kingston Peak Formation in upper Pleasant Canyon. The spots are generally rounded and appear to have grown across bedding with no disruption of layering. Figure 26a shows that in CP 58b graded bedding is well preserved and a spot has grown across the layering. The spots consist of a quartz mosaic with carbonate, chlorite, biotite, and muscovite, and the matrix is comprised of quartz + biotite + muscovite + ilmenite. Although the minerals which constitute the spots are unlike the alteration products of cordierite which occur at higher grades, the habit suggests that these spots were cordierite.

Higher grade pelitic assemblages were collected from five localities which are illustrated on Figure 27. The first occurs in the

Figure 26: Textural features in lower grade pelitic schists, Panamint Mountains.

a) Spotted argillite in Kingston Peak Formation. Spot grew across fine, graded layering, PML 58b (plane polarized light).

b) Andalusite porphyroblast which grew across layering in Stirling Quartzite, Wildrose Peak CP 455a (crossed nicols).

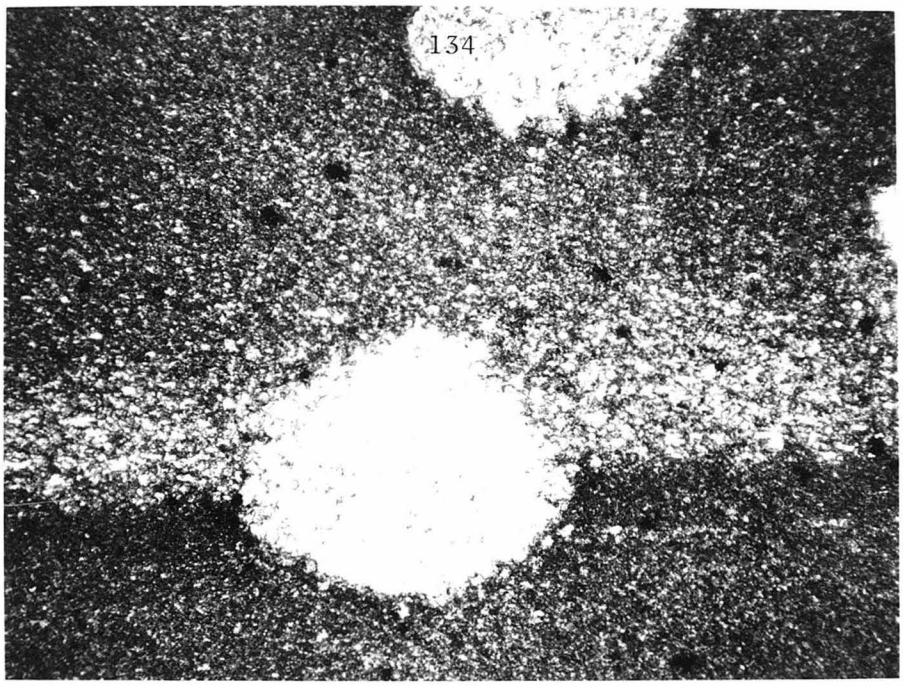

a

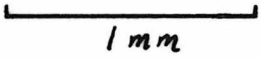

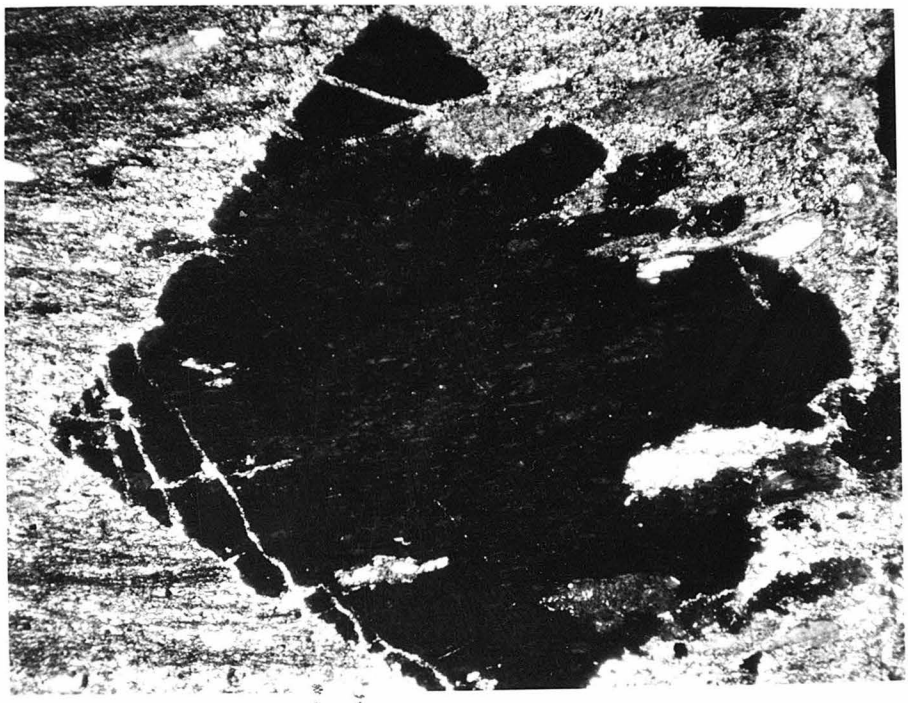

b

Stirling Quartzite near Wildrose Peak in the northeast corner of the Telescope Peak Quadrangle. The second occurs in the lower Kingston Peak Formation near the head of Surprise Canyon. The third occurs on the west side of the divide between Wildrose and Hall Canyons in the Johnnie Formation. The fourth is on Tuber Ridge where the Johnnie Formation occurs in a fault block. The fifth location occurs in the Crystal Spring Formation in Tuber Canyon.

Several samples from these localities were analyzed by electron microprobe techniques in order to determine the distribution of elements among coexisting phases. The samples which were analyzed, their mineral assemblages, and locations are listed in Table 5.

Nearly all of the minerals which occur in these rocks can be described in terms of the oxide components SiO_2, Al_2O_3, FeO, MgO, K_2O, and H_2O. Quartz + muscovite-bearing assemblages may be plotted on the plane Al_2SiO_5-FeO-MgO. As long as H_2O is a boundary value component and if any additional components introduce additional phases, such diagrams are phase diagrams in which three-phase assemblages are invariant under constant T, P, and a_{H_2O} conditions (Thompson, 1957).

Stirling Quartzite - Wildrose Peak

Two aluminous, purple argillite layers occur in the Stirling Quartzite near Wildrose Peak (Figure 27). Most of the rocks in these layers contain the assemblage andalusite + chlorite + muscovite + quartz + hematite. Andalusite occurs as 1 to 5 mm rectangular porphyroblasts in a fine-grained matrix (Figure 26b). Andalusite contains abundant hematite inclusions, and in hand specimen the porphyroblasts are black

TABLE 5: ANALYZED PELITIC SCHISTS, PANAMINT MOUNTAINS

SAMPLE	ASSEMBLAGE													LOCATION
	QTZ	MUSC	BIO	GA	CH	CTD	CD	ST	AND	SIL	PLAG	OP	OTHERS	
CP 455a	X	X			X				X			hem	ppy rut	1
CP 503	X	X			X	X			X			hem	ppy rut	1
CP 9a	X	X	X	X		X		X				ilm		2
CP 9b	X	X	X	X		X		X				ilm		2
CP 9d	X	X	X			X						ilm		2
CP 474a	X	X	X		X			X	X		X	ilm		3e
CP 474g	X	X	X		X				X		X	ilm		3e
PML 126	X	X	X		r			X	X		X	ilm		3a
CP 33b	X	X	X					X	X		X	ilm		3b
PML 130	X	X	X					X	X		X	ilm		3d
PML 131	X	X	X		X		X				X	hem		3d
PML 133	X	X	X		X		X				X	hem		3d
PML 134	X	X	X		X		X				X	ilm		3d
PML 143	X	X	X		X		X				X	hem		3d
CP 32b	X	X	X		X						X	hem mag		3c
PML 141a	X	X	X					X	X		X	ilm		4
PML 140f	X	X	X					X	X		X	ilm		4
PML 140c	X	X	X						X		X	ilm	all	4
PML 107a	X	X	X		r		X		X		X	ilm		4
CP 497d	X	X	X					X	X		X	ilm		4
CP 43	X	X	X	X	X		X				X	ilm	all	4
PML 140e	X		X		r		X	X	X		X	ilm		4
PML 244d	X	X		r	r	r						ilm		5
PML 250b	X	X	r	r	r					X		ilm		5
PML 250c	X	X	r	r	r			X		X		ilm		5
PML 250e	X	X		r	r	r				X		ilm		5
PML 250g	X	X			r	r		X		X		ilm		5

ppy = pyrophyllite, hem = hematite, ilm = ilmenite, mag = magnetite, rut = rutile, all = allanite; r = mineral formed during retrograde metamorphism; location corresponds to Figure 27.

All minerals except quartz were analyzed.

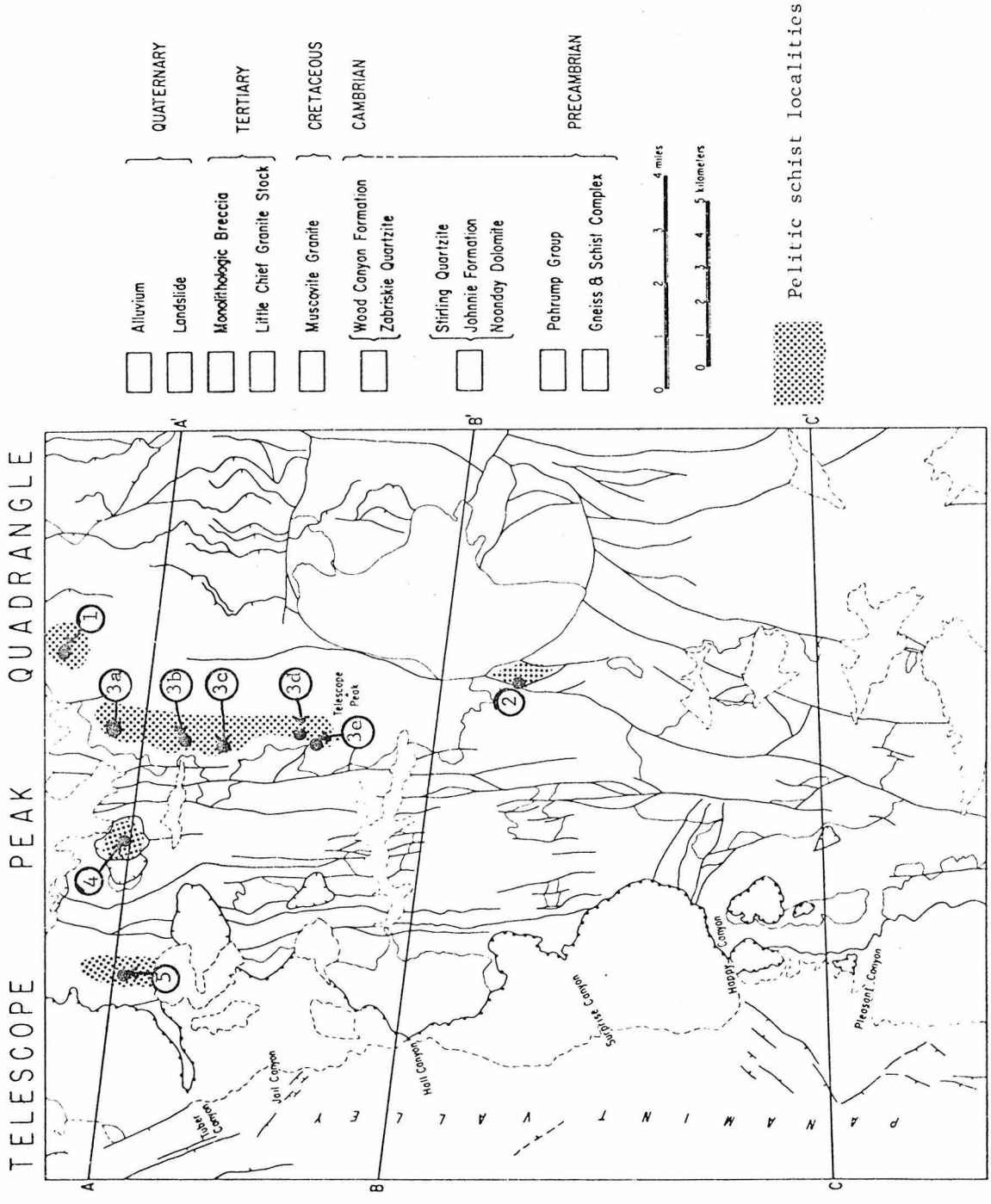

Figure 27 : Pelitic schist sample localities.

and set in a grey matrix. Muscovite occurs in pods and is commonly interleaved with chlorite. Near Wildrose Peak this unit is extensively cut by veins which consist of andalusite, pyrophyllite, and hematite, and in thin section, the andalusite in the quartzite is altered along cracks to pyrophyllite. The aluminum phosphate lazulite is a common accessory and also appears to be an alteration product of andalusite. The alteration is attributable to the retrograde metamorphic event. Sample CP 503 contains the assemblage andalusite + chloritoid + chlorite + muscovite + quartz + hematite + rutile, and the composition of andalusite + chlorite + chloritoid is shown on Figure 28a. The rock contains abundant hematite, and the presence of andalusite may be due to the higher oxidation state of iron. The chlorite which coexists with chloritoid shows a wide range in Mg/(Mg + Fe). Only two small grains of chloritoid occur in sample CP 503, and no chlorite occurs in the vicinity of either grain. The equilibration volume around the chloritoid grains is probably small and the equilibrium partition of Mg over Fe between chlorite and chloritoid is uncertain. Under these low grade conditions, though, the chloritoid-chlorite join appears to be stable.

Kingston Peak Formation - Upper Surprise Canyon

Pelitic layers occur within the lower Kingston Peak Formation near the head of Surprise Canyon (Figure 27) which contain chloritoid-bearing assemblages. The assemblage quartz + muscovite + biotite + garnet + staurolite + chloritoid comprises samples CP 9a and CP 9b. The grain size in these rocks is small. Chloritoid plates are recognizable in hand sample. The plates are randomly oriented, approximately 2 mm

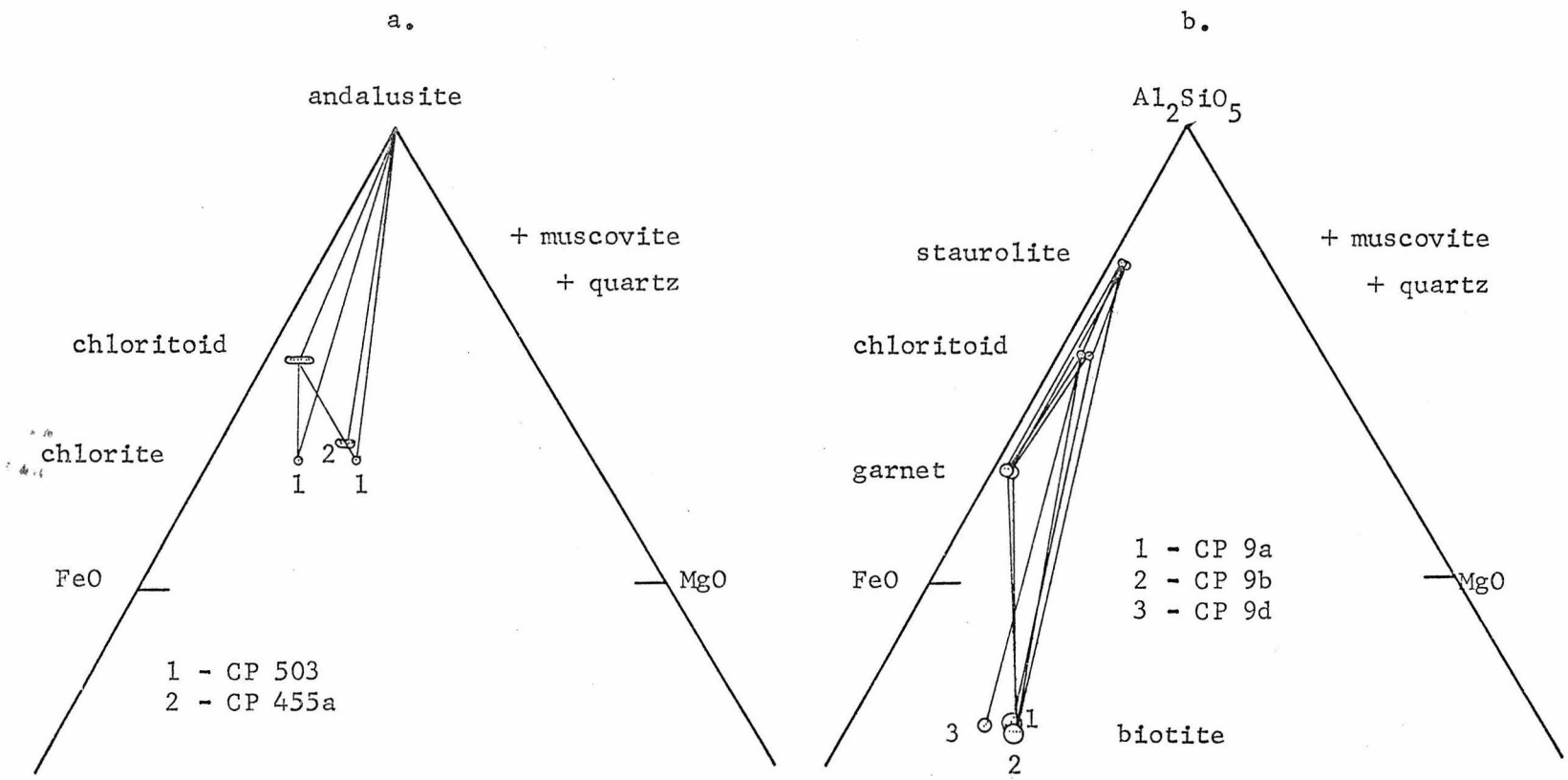

Figure 28: Analyzed pelitic assemblages from a) Stirling Quartzite, Wildrose Peak and b) Kingston Peak Formation, head of Surprise Canyon.

in diameter, and inclusions of quartz define an hourglass pattern. Staurolite forms rectangular grains less than 2 mm long, and garnet occurs as 0.5 mm rounded grains which are free from inclusions. Muscovite and biotite are very fine grained, and muscovite defines a weak foliation which is generally oriented parallel to bedding (Figure 29a).

The composition of coexisting phases in samples CP 9a, 9b, and 9d are shown on Figure 28b, and Albee (1972) reported analyses on CP 9a. The aluminous minerals chloritoid and staurolite coexist with biotite to the exclusion of chlorite. The only samples collected from this locality have the assemblage garnet + chloritoid + staurolite + biotite or chloritoid + biotite, and the nature of the distribution of elements in more magnesium-rich compositions is unknown.

The assemblage garnet + chloritoid + staurolite + biotite appears to contain an extra phase for an arbitrary choice of P, T, and a_{H_2O}. Garnet contains approximately 4 wt % MnO and staurolite contains 1.0 to 1.5 wt % ZnO, and even though the zinc and manganese contents are small, they may be sufficient to stabilize an "extra" phase. Alternatively, it is possible that the activity of water is buffered by the four-phase assemblage. The general lack of four-phase assemblages elsewhere indicates that if water is an initial value component in upper Surprise Canyon area, the behavior is local.

Johnnie Formation - Range Divide Between Wildrose and Hall Canyons

The pelitic layers in the Johnnie Formation west of the crest of the Panamint Range between Wildrose and Hall Canyons contain a variety of assemblages. The assemblages which characterize the pelitic schists

Figure 29: Textural features in higher grade pelitic schists, Panamint Mountains.

a) Garnet + staurolite + chloritoid + biotite schist, Kingston Peak Formation, Surprise Canyon, CP 9a (crossed nicols).

b) Cordierite + biotite + chlorite schist, Johnnie Formation, near Roger's Peak, PML 143 (crossed nicols). Cordierite forms rounded porphyroblasts, chlorite occurs as plates, biotite is in groundmass.

c) Altered hexagonal porphyroblast enclosed by andalusite poikiloblast, CP 474g (crossed nicols).

d) Poikiloblastic andalusite and porphyroblastic books of biotite, Johnnie Formation near Telescope Peak, CP 474g (crossed nicols).

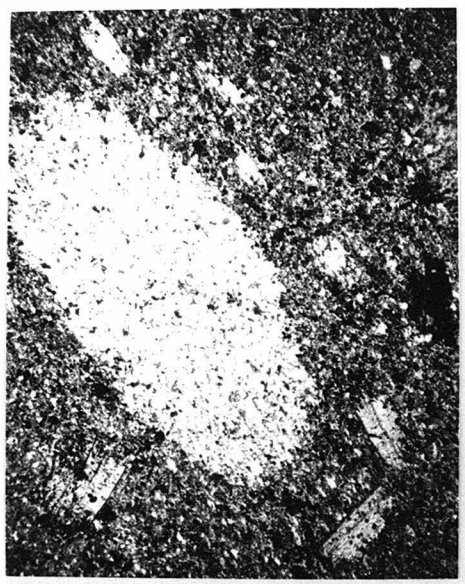

b 1mm

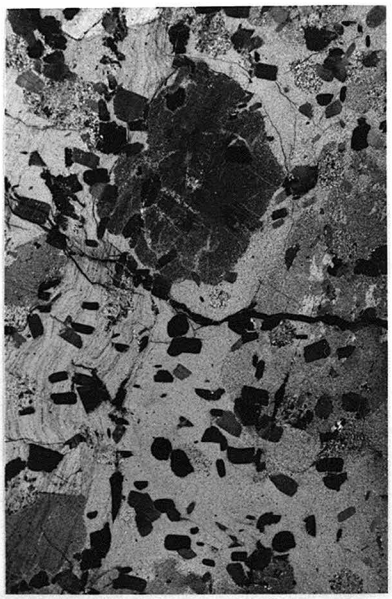

d 1cm

a 1mm

c 1mm

in this region are

andalusite + staurolite + biotite + quartz + musocovite + albite + ilmenite

andalusite + chlorite + biotite + quartz + muscovite + plagioclase + ilmenite

cordierite + chlorite + biotite + quartz + muscovite + plagioclase + Ti-hematite.

Andalusite forms large rectangular parallelipipeds and contains many inclusions of quartz, biotite, and staurolite. Within the andalusite poikiloblasts there are areas of inclusion-free andalusite which possibly reflect an early period of slow growth followed by an accelerated growth rate. Staurolite occurs as inclusions in many such porphyroblasts where staurolite is absent from the matrix. Staurolite does not occur as porphyroblasts, but is usually small, ragged appearing, and contains abundant quartz inclusions. Biotite is orange to reddish brown and forms thick, randomly oriented books (Figure 29d). Albite occurs in the assemblage staurolite + andalusite + biotite and forms rounded porphyroblasts which contain a modest number of quartz inclusions in the core.

Cordierite-bearing rocks are much finer grained than the andalusite-bearing ones, and cordierite is the only recognizable mineral in hand specimen. Cordierite is spherical, approaches 5 mm in diameter, and contains numerous quartz and mica inclusions. Biotite in these cordierite rocks is fine-grained and green; chlorite forms 0.5 mm plates, is green in color, and shows normal, first order birefringence. The magnesium-rich assemblage cordierite + biotite + chlorite is one of

the few that contain hematite, and the abundance of hematite may be the factor which causes the appearance of such magnesium-rich minerals. Plagioclase is about An_{30} in composition and occurs as very fine grains in the quartz-mica matrix.

All of these rocks show abundant evidence for both progressive metamorphic reactions and polymetamorphism. Most assemblages have suffered a second retrogressive metamorphic event. Biotite is nearly completely altered to chlorite, and cordierite is altered to an aggregate of sericite and chlorite. Andalusite nearly always shows some alteration along the rims to sericite and is in many cases completely altered to fine-grained white mica.

Staurolite inclusions in andalusite porphyroblasts which occur in a staurolite-free matrix indicates that during progressive metamorphism a continuous reaction such as

staurolite + muscovite = andalusite + biotite

occurred. Growth of andalusite engulfed and isolated staurolite from the matrix. In a few samples hexagonal porphyroblasts, now completely altered to quartz + muscovite + chlorite, are poikilitically enclosed by andalusite (Figure 29c). The original nature of the porphyroblast is uncertain, but the form and alteration products are suggestive of cordierite, and a progressive metamorphic reaction of the form

cordierite = andalusite + chlorite

is also indicated.

Several samples which were relatively unaltered during retrograde metamorphism were analyzed (see Table 5). The assemblages andalusite + staurolite + biotite, andalusite + chlorite + biotite, and cordierite +

chlorite + biotite are represented, and their compositions are illustrated in Figure 30a. The general consistency of partition is noted; the more iron-rich compositions contain staurolite, the more magnesium-rich contain cordierite, and those intermediate in Mg/(Mg + Fe) contain chlorite. Biotite coexists with all other phases, including andalusite.

Areas enclosed by the assemblages staurolite + andalusite + biotite and andalusite + biotite + chlorite overlap, an apparent discrepancy which obviates the assumption of equilibrium. The compositions of the offending staurolite + biotite + andalusite assemblage were derived from inclusions in andalusite because matrix biotite is altered to chlorite. Hence the biotite composition reflects conditions prior to its isolation from the matrix, and the discrepancy is more apparent than real. In addition, these samples were collected from an area of about 4 square miles and variations in T and a_{H_2O} can only be expected over such a large area. In support of such a hypothesis, three cordierite + chlorite + biotite assemblages collected from the same outcrop have essentially identical compositions. The fourth cordierite + chlorite + biotite assemblage (PML 134) which represents a significantly more iron-rich composition contains muscovite only as inclusions in cordierite and cannot legally be represented on this projection.

Johnnie Formation - Tuber Ridge

The Johnnie Formation also occurs in an isolated fault block near the western, higher grade portion of the tremolite zone. The block itself occurs in the tremolite zone, but one sample collected from a calcsilicate layer within the block contains the assemblage diopside +

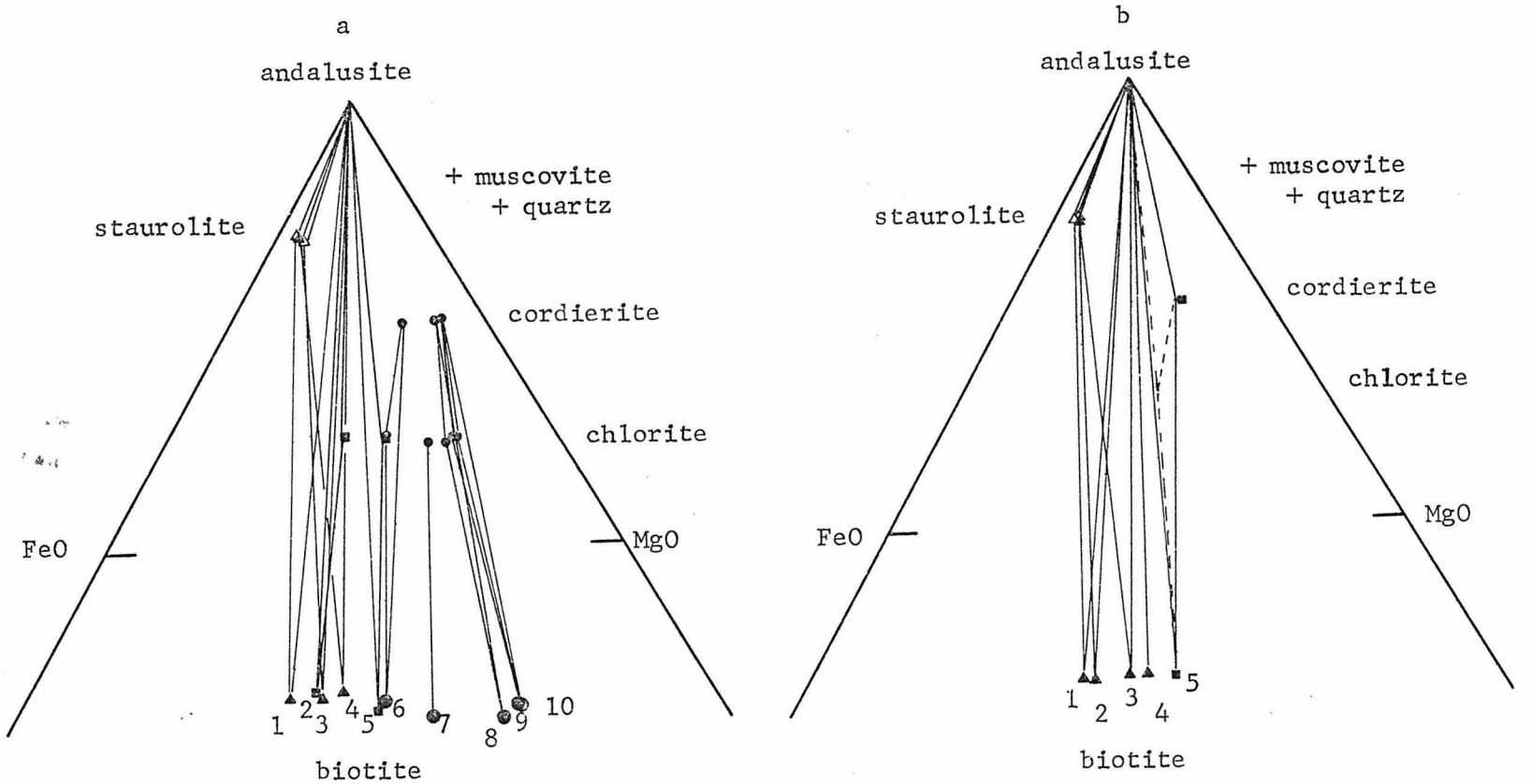

1 - PML 130
2 - CP 474a
3 - CP 33b
4 - PML 126
5 - CP 474g
6 - PML 134
7 - CP 32b
8 - PML 143
9 - PML 133
10 - PML 131

1 - PML 140f
2 - CP 497d
3 - PML 141a
4 - PML 140c
5 - PML 107a

Figure 30: Analyzed pelitic assemblages from the Johnnie Formation from a) range crest and b) Tuber Ridge.

tremolite + clinozoisite. The pelitic assemblages which occur in this block are

andalusite + staurolite + biotite + muscovite + quartz + plagioclase + ilmenite

andalusite + cordierite + biotite + muscovite + quartz + plagioclase + ilmenite

andalusite + cordierite + staurolite + biotite + quartz + plagioclase + ilmenite

garnet + biotite + cordierite + chlorite + quartz + plagioclase + ilmenite.

Retrograde metamorphism was extensive, and few minerals survived unaltered. However, progressive metamorphic reactions are again indicated. The best example occurs in CP 43 with the assemblage cordierite + garnet + biotite + chlorite; muscovite occurs only as inclusions in cordierite, and the matrix consists of biotite + chlorite. A reaction such as

chlorite + muscovite = cordierite + biotite

is indicated.

The mineral assemblages from Tuber Ridge locality which were analyzed are shown in Figure 30b. As in the lower grade locality andalusite + staurolite + biotite is a common assemblage. The more magnesium-rich compositions are accommodated by andalusite + cordierite + biotite in preference to chlorite-bearing assemblages. One rock (CP 43) which contains muscovite only as inclusions in cordierite contains chlorite with $Mg/(Mg+Fe) \simeq 0.55$ and retrograde chlorite in andalusite + cordierite + biotite + muscovite (PML 107a) and andalusite + cordierite + staurolite + biotite (PML 140e) assemblages also has an Mg-value of about 0.55.

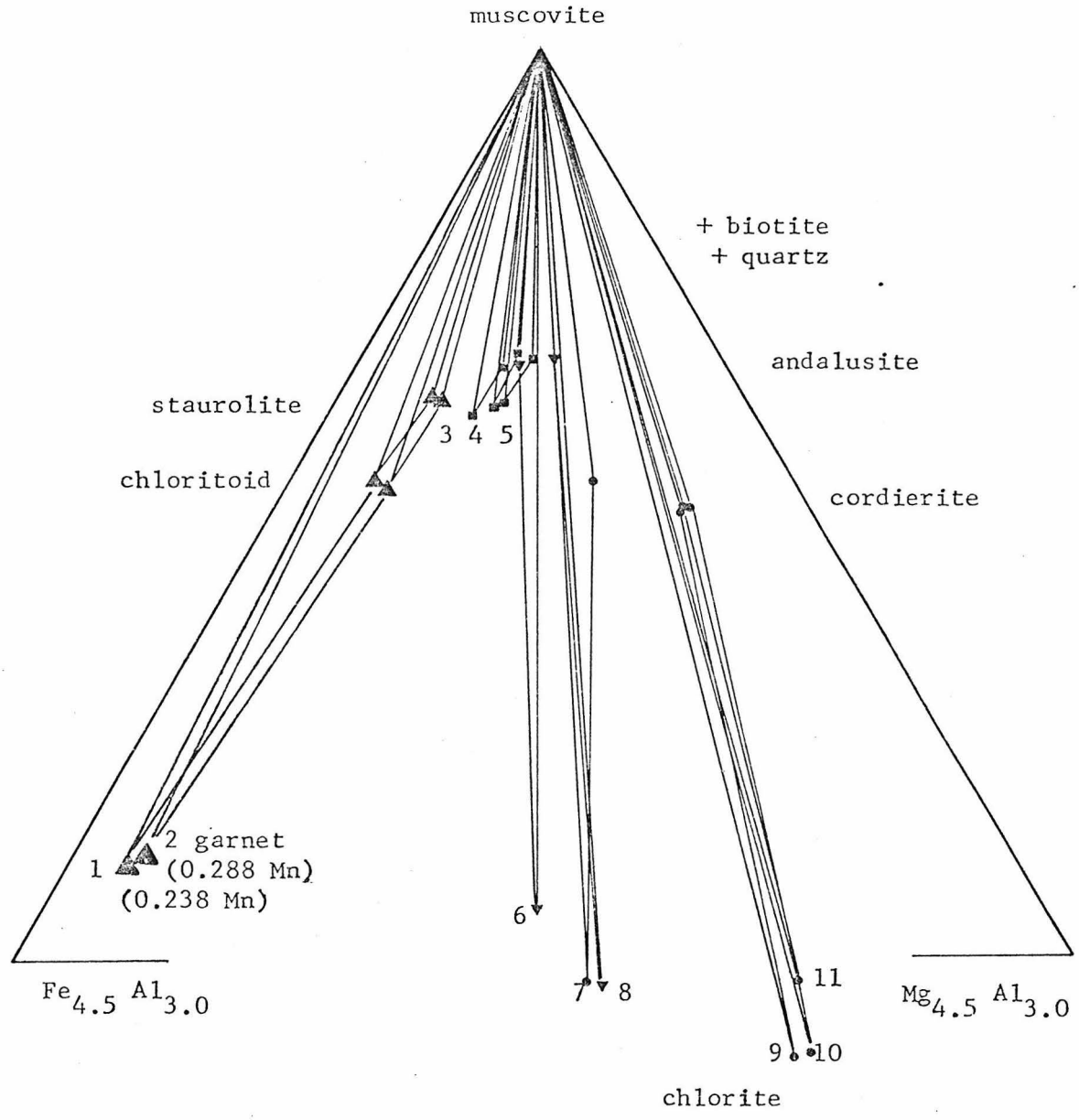

1 - CP 9a
2 - CP 9b
3 - PML 130
4 - CP 33b
5 - PML 126
6 - CP 474a
7 - PML 134
8 - CP 474g
9 - PML 143
10 - PML 131
11 - PML 133

Figure 31a: Lower grade pelitic assemblages which coexist with biotite + quartz.

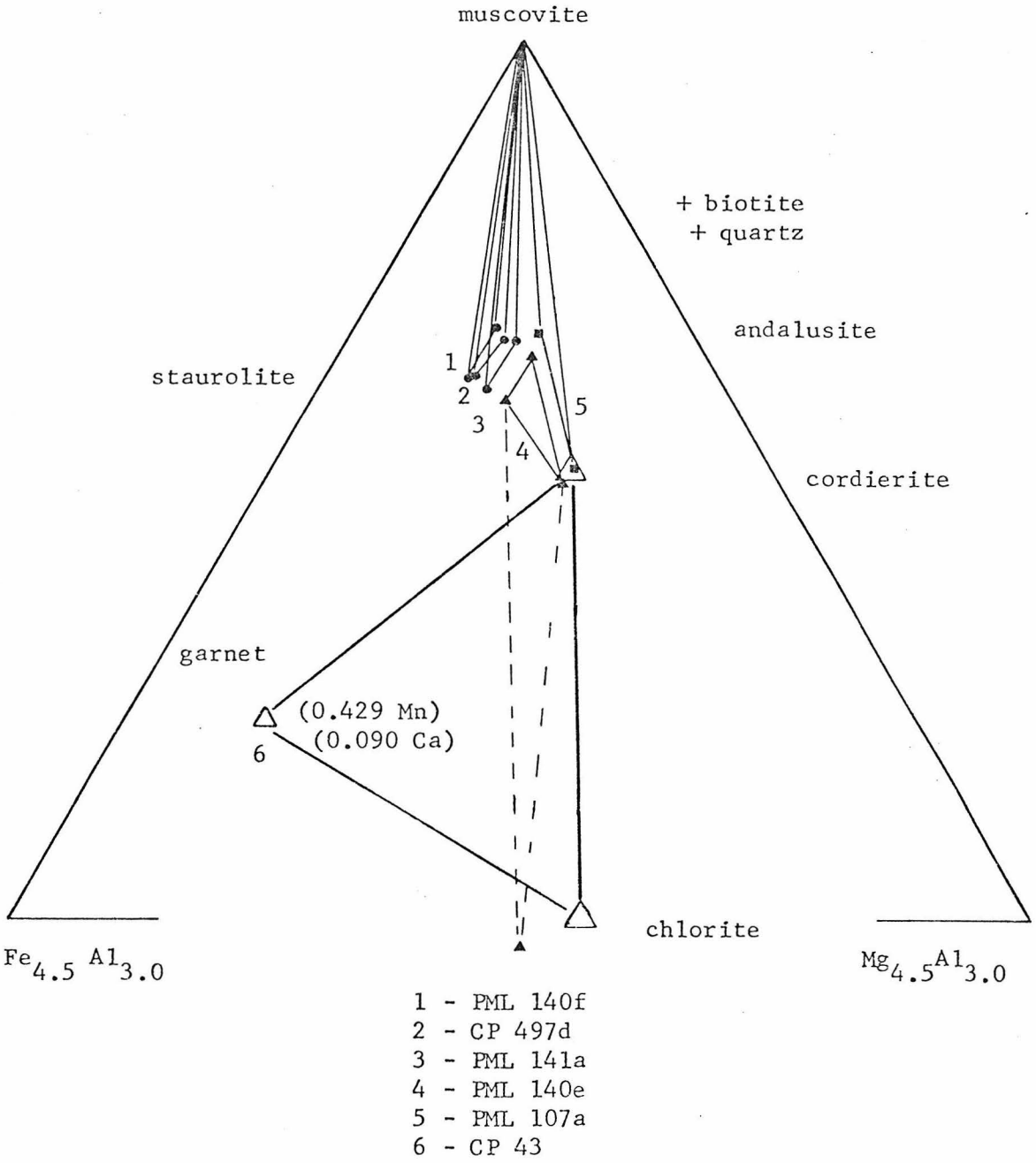

1 - PML 140f
2 - CP 497d
3 - PML 141a
4 - PML 140e
5 - PML 107a
6 - CP 43

Figure 31b: Higher grade pelitic assemblages which coexist with biotite + quartz.

It is suggested that the maximum stability limit of chlorite + muscovite + quartz is realized at this Mg-value of 0.55.

Biotite is a ubiquitous phase in pelitic schist assemblages, whereas prograde continuous reactions such as

muscovite + cordierite = andalusite + biotite

consume muscovite, and samples CP 43 and PML 140e do not contain muscovite. In Figure 31, the compositions of minerals in quartz + biotite assemblages are plotted on the plane $KAl_2(AlSi_3)O_{10}(OH)_2$ - $Fe_{4.5}Al_{1.5}(Al_{1.5}Si_{2.5})O_{10}(OH)_8$ - $Mg_{4.5}Al_{1.5}(Al_{1.5}Si_{2.5})O_{10}(OH)_8$. Points were projected from observed biotite compositions onto this plane using the linear algebraic methods outlined by Greenwood (1975). In Figure 35b, the muscovite-free assemblages biotite + quartz + andalusite + cordierite + staurolite and biotite + quartz + cordierite + garnet + chlorite from the Tuber Ridge locality are plotted. The garnet which coexists with cordierite in sample CP 43 contains 25 mole % spessartine and 5 mole % grossular, and the presence of garnet in this sample is probably due to a high manganese content.

Crystal Spring Formation - Tuber Canyon

The effects of the second metamorphic event are most clearly seen in the pelitic schists from the Crystal Spring Formation (Figure 27). Here the schists are coarse-grained and contain the assemblages garnet + chlorite + biotite + muscovite + quartz + ilmenite and garnet + chlorite + chloritoid + muscovite + quartz + ilmenite. The muscovite is very coarse-grained, and occurs in elliptical pods. The muscovite includes grains of staurolite and sillimanite (Figure 32). The evidence is

Figure 32: Polymetamorphic schist from Crystal Spring Formation, Tuber Canyon, PML 250c.

a) Retrograde assemblage garnet + biotite (dark) + chlorite (light plates) (plane polarized light).

b) Relic staurolite (fibrous) and staurolite (dark, high relief) enclosed in muscovite (plane polarized light).

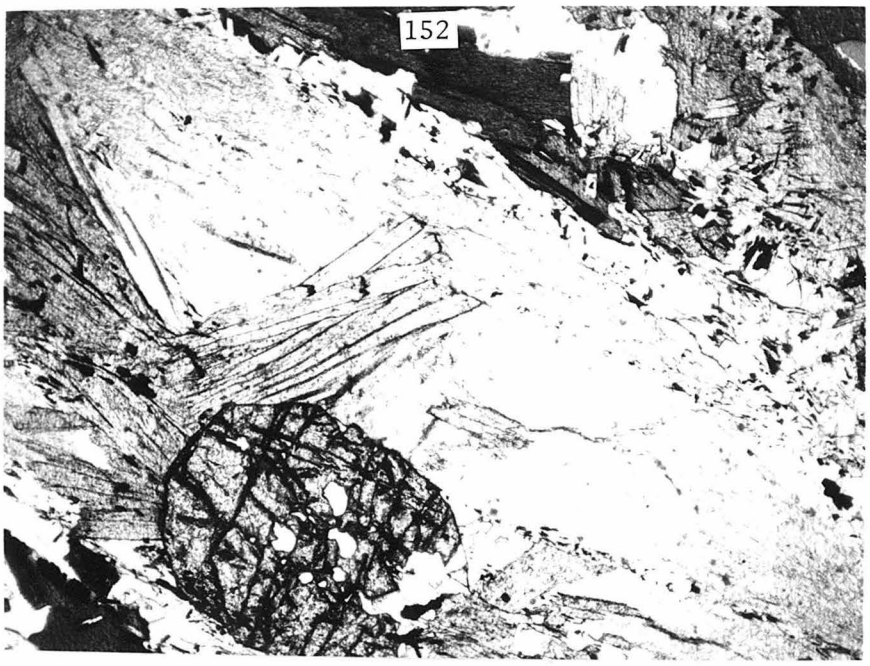

a

1 mm

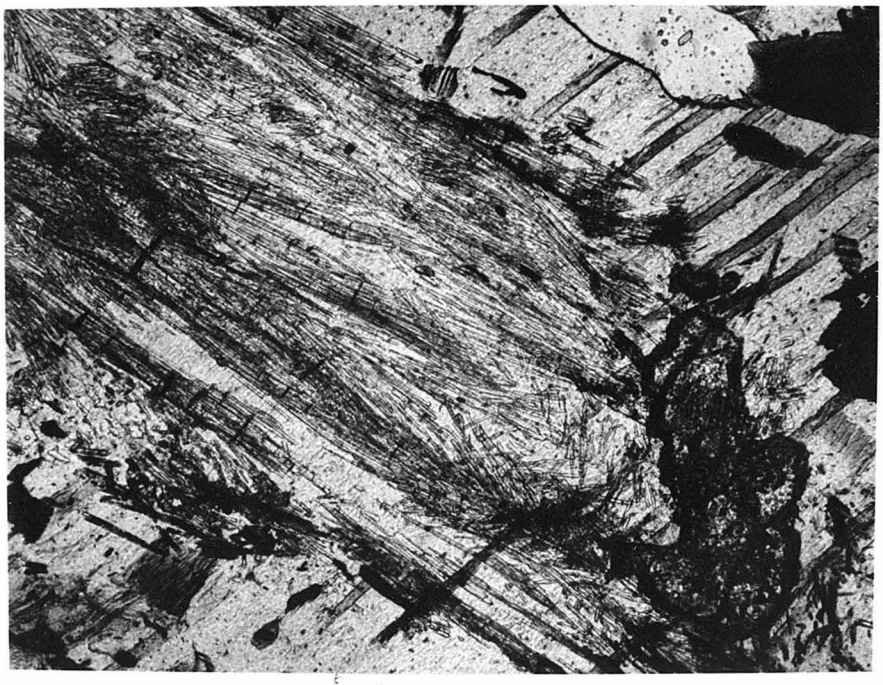

b

0.5 mm

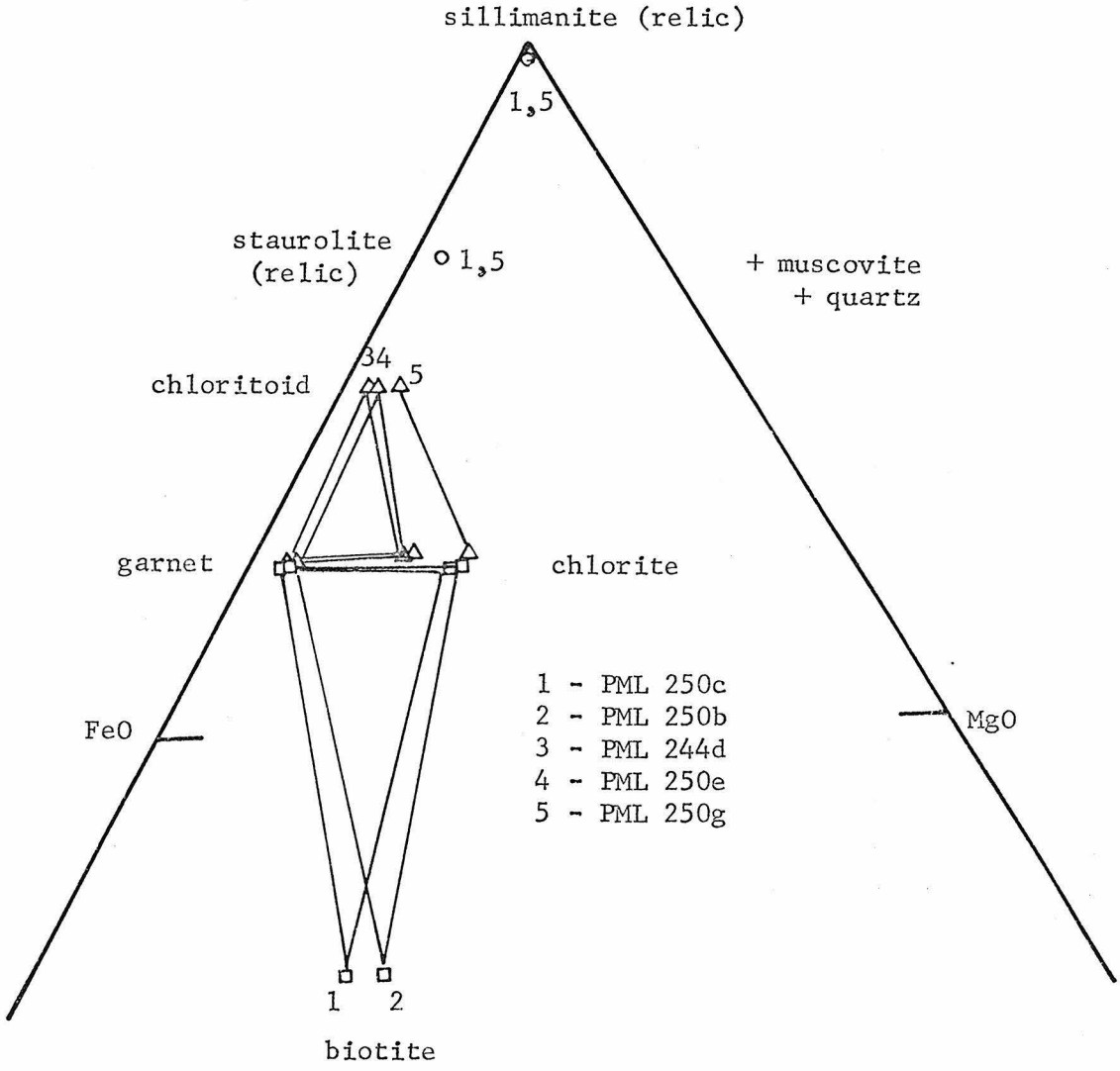

Figure 33: Analyzed retrograde assemblages from Tuber Canyon.

unequivocal; the earlier metamorphic event produced a sillimanite + staurolite + biotite assemblage which nearly completely recrystallized to the garnet + chlorite + (biotite or chloritoid) assemblage during the second event. The compositions of these assemblages are shown on Figure 33. The composition of relic staurolite and sillimanite which occurs as inclusions in coarse grained muscovite are also shown. The primary assemblage, formed during the earlier event had to have been sillimanite + staurolite + biotite. A surprising feature of these secondary assemblages is the coexistence of garnet + chlorite + muscovite + quartz, an association which is nowhere else exhibited by any of the primary metamorphic assemblages.

Sillimanite Isograd

Many pelitic rocks in the Kingston Peak Formation and Crystal Spring Formation occur in the vicinity of the diopside isograd. Most all are composed of the assemblage aluminosilicate + biotite + muscovite + plagioclase. In such rocks the transition from andalusite to sillimanite is recorded. Unfortunately, these aluminosilicate minerals are most often represented by white mica pseudomorph due to the retrograde metamorphism. Figure 34 compares andalusite and sillimanite to their respective pseudomorphs, and in Figure 35 the distribution of these minerals and pseudomorphs is used to define a sillimanite isograd.

PARTITION OF ELEMENTS AMONG COEXISTING PHASES

The distribution of elements among coexisting minerals within any of the sample localities is consistent. Apparent discrepancies such as crossing tie lines or "extra" phases are attributable to local

Figure 34: Andalusite and sillimanite in Kingston Peak Formation, west side of anticline, Panamint Mountains.

a) Andalusite (large white) and altered staurolite (?) (small rectangles) in dark, biotite-rich matrix, CP 109 (plane polarized light).

b) Altered andalusite (grey fibrous mica pseudomorph), PML 83 (plane polarized light).

c) Fibrous sillimanite in quartz + biotite matrix, PML 227 (plane polarized light).

d) Altered fibrous sillimanite in a biotite-rich matrix, PML 49a (plane polarized light).

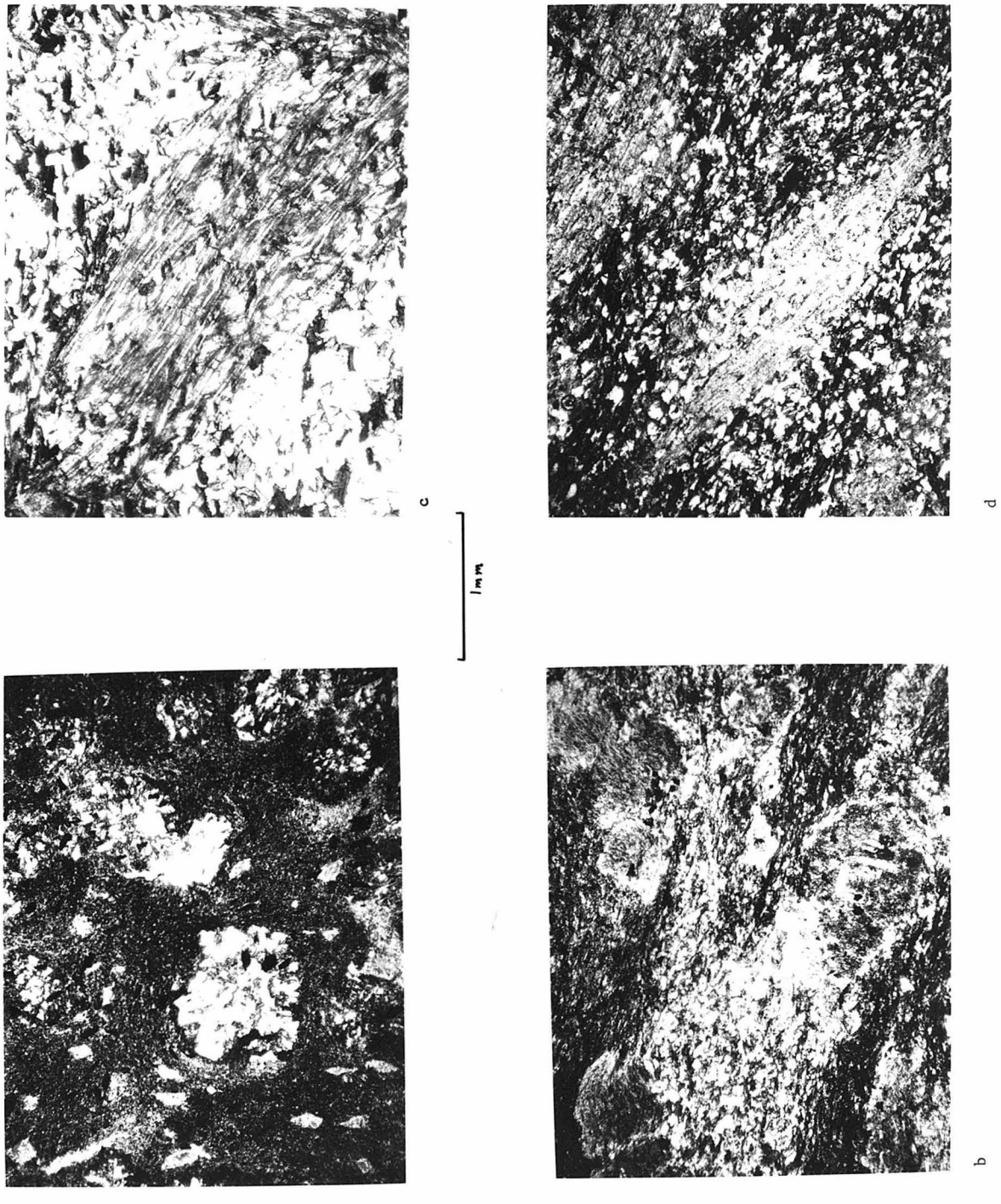
c
d
1mm
b

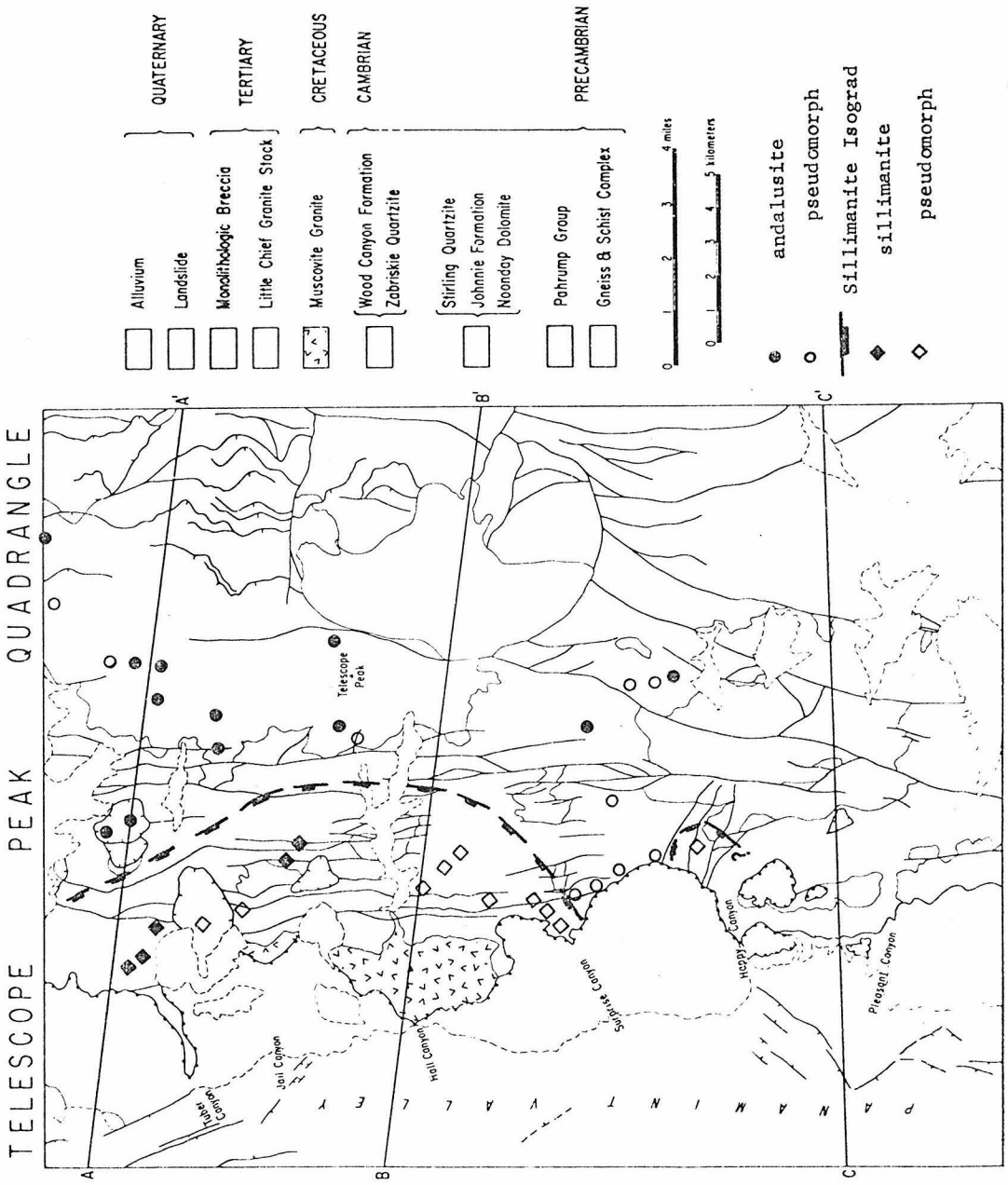

Figure 35: Sillimanite isograd.

variations in the intensive thermodynamic parameters, to the use of inclusions in altered rocks, or to the presence of additional components. Despite the limited availability of unaltered samples, an approach to chemical equilibrium is suggested. This suggestion warrants a closer examination of the relative partition of iron over magnesium in mafic phases, the partition of potassium, aluminum, and magnesium + iron among potassic phases, and the nature of the saturating sodium, calcium, and iron-titanium phases in order to substantiate the indication of equilibrium.

The partition of iron, magnesium, manganese, and zinc among coexisting mafic phases is illustrated in Figure 36. Several features are noted. Garnet is more iron-rich than any coexisting phase, and cordierite is the most magnesium-rich. The Mg/Fe values for coexisting staurolite and chloritoid are nearly identical, but staurolite appears to be more iron-rich phase. Only two samples from the same outcrop were analyzed, and a conclusive argument regarding the relative partition of iron and magnesium cannot be made. Albee (1973) similarly concluded that staurolite is more iron-rich than coexisting chloritoid. Chlorite is always slightly more magnesium-rich than coexisting biotite. Figure 37 illustrates that there is little or no systematic dependence of K_D on the amount of octahedral aluminum, and no matter what the composition of the rock which contains the biotite + chlorite assemblage, biotite is always slightly more iron-rich than coexisting chlorite. The order of iron enrichment cordierite < chlorite < biotite was also observed by Guidotti and others (1975), and the relative enrichment is always such that chlorite occurs on the iron-rich side of the bio-

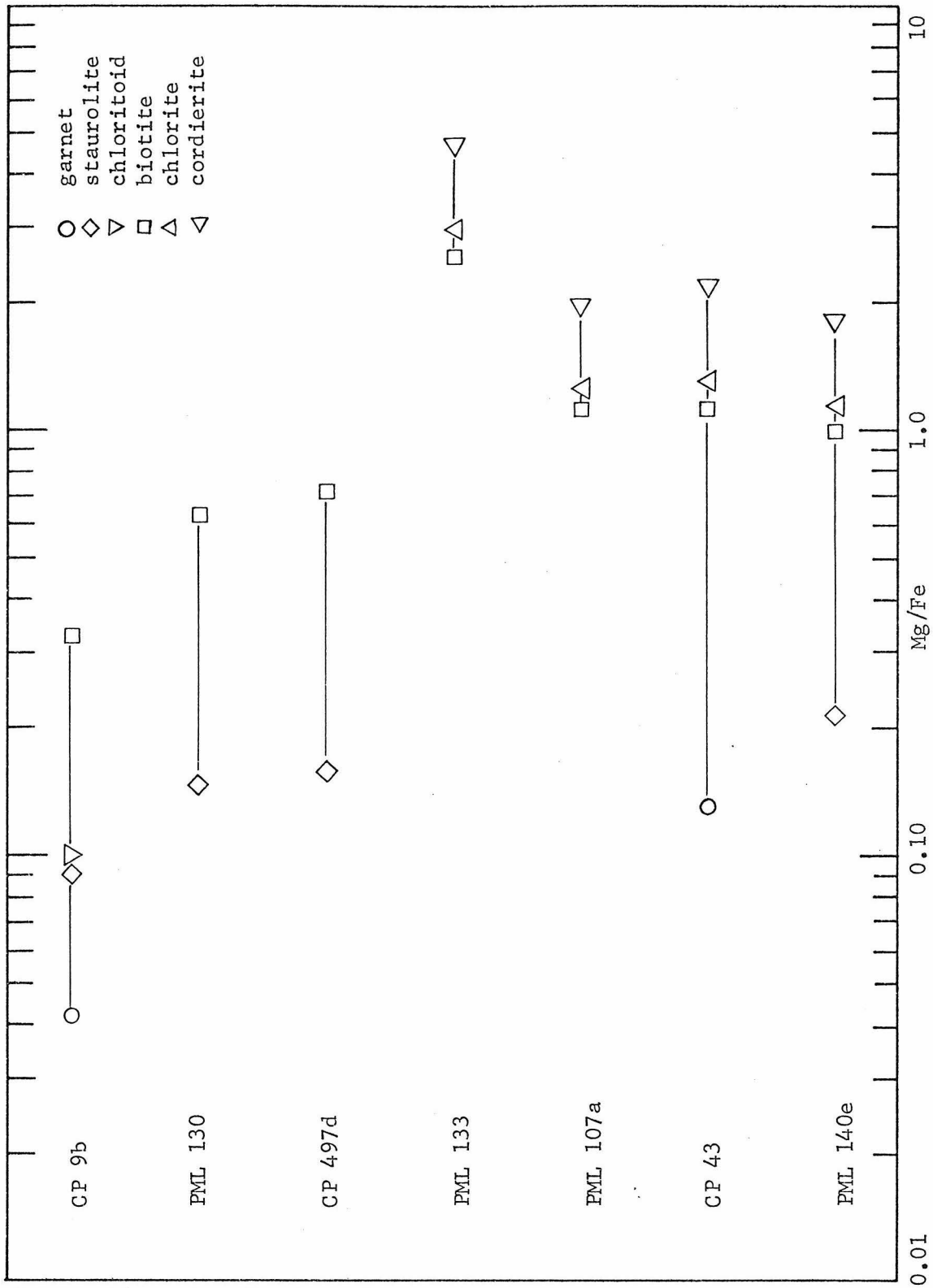

Figure 36 a: Distribution of Fe and Mg between coexisting phases.

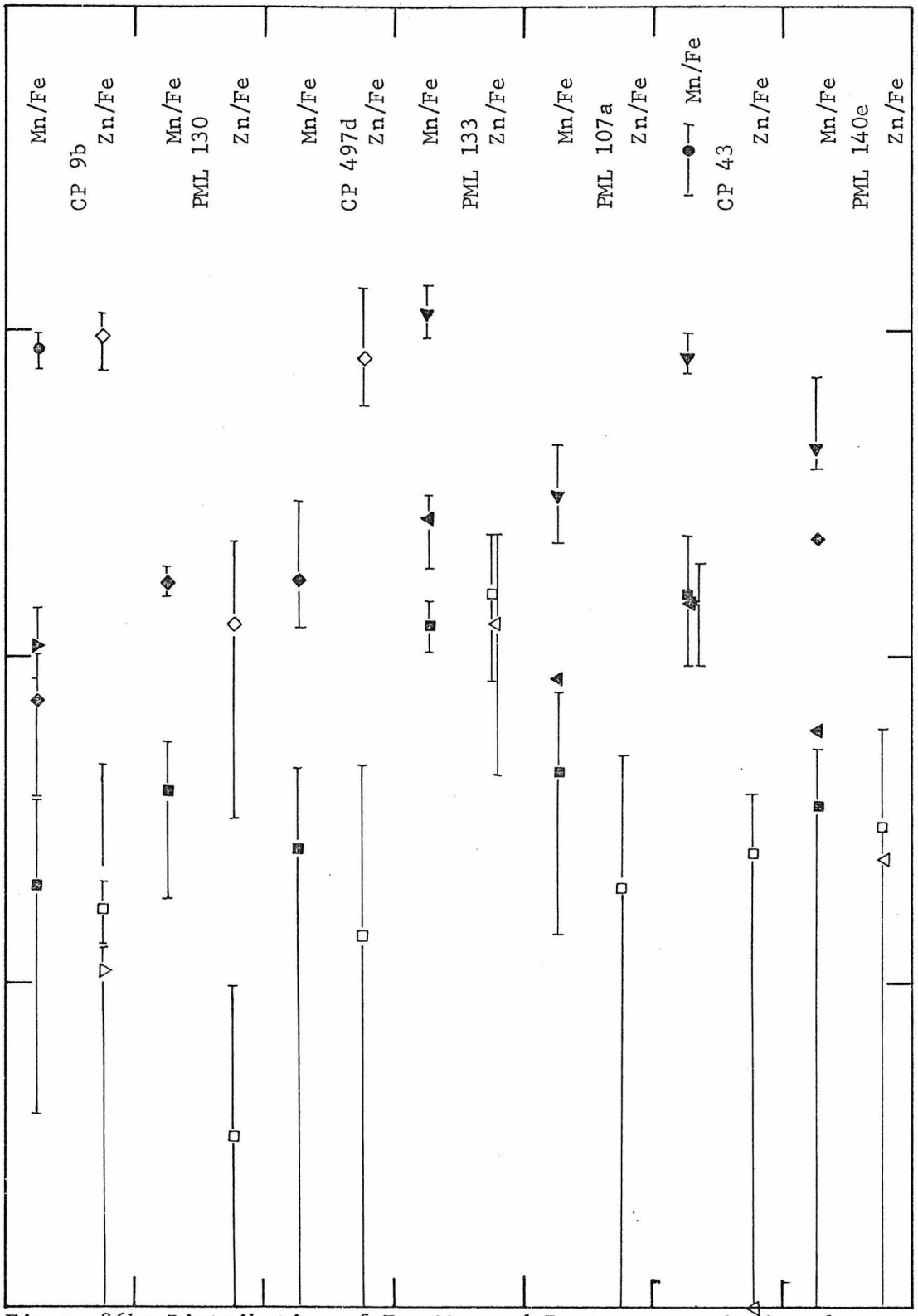

Figure 36b: Distribution of Fe, Mn, and Zn among coexisting phases.

COMPOSITION OF COEXISTING CHLORITE AND BIOTITE, PANAMINT MOUNTAINS

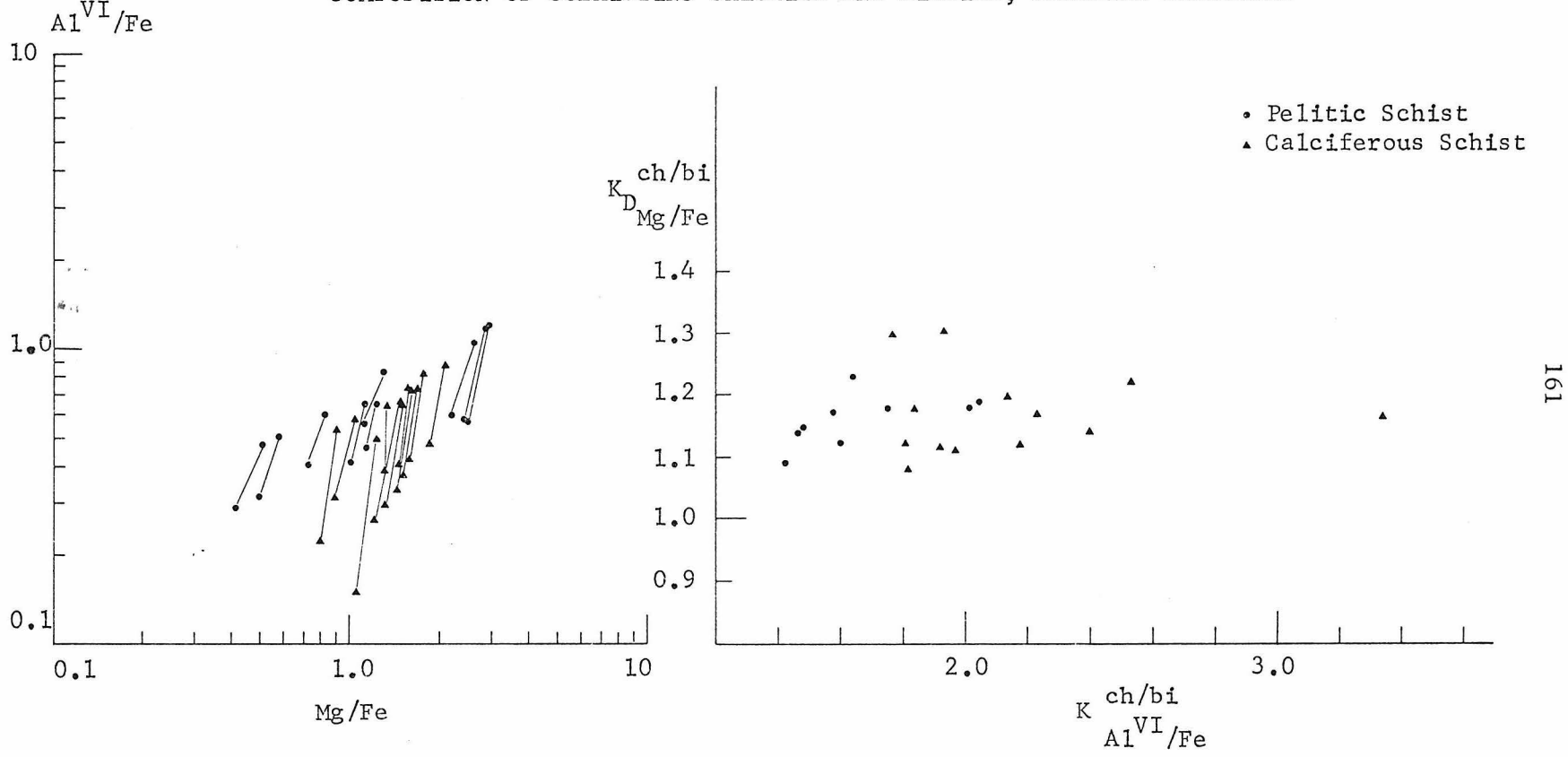

Figure 37

tite-cordierite join. The relative increase of Mg/Fe is garnet < staurolite ≤ chloritoid < biotite < chlorite < cordierite. Manganese and zinc occur in very small amounts in most phases. Garnet may be very manganiferous and is the most manganese-rich of any coexisting phase. Cordierite also concentrates manganese, but most other phases contain amounts of manganese too small to be precisely measured. The apparent increase in Mn/Fe is biotite < chlorite < staurolite < chloritoid < cordierite < garnet. Zinc occurs in appreciable amounts only in staurolite.

Muscovite, biotite, and chlorite occur in a variety of assemblages which occur in calciferous schists as well as pelitic schists. The amount of aluminum in these minerals may vary by the coupled substitution $Al^{IV} + Al^{VI} \rightleftarrows Si^{IV} + FM^{VI}$ or $3FM^{VI} \rightleftarrows 2Al^{VI} + \square$ ($\square \equiv$ vacancy). Figures 38, 39, and 40 illustrate the amount of Al^{VI} and Al^{IV} in chlorite, biotite and muscovite. In general, the minerals from pelitic assemblages coexist with andalusite, whereas those from calciferous schists coexist with epidote. In almost all cases, chlorite, biotite, and muscovite from aluminous pelitic schists contain more total aluminum than those same minerals which occur in the low aluminum calciferous schists. The differences in chemistry of these minerals are attributable to both coupled substitutions. The line in each figure represents the substitution $Al^{IV} + Al^{VI} \rightleftarrows Si^{IV} + FM^{VI}$, but very few points fall on the line. Points which fall on the high Al^{IV} side of the line contain ferric iron which substitutes for Al^{VI}, and points which fall on the high Al^{VI} side contain excess Al^{VI} generated by the substitution $3FM^{VI} \rightleftarrows 2Al^{VI} + \square$.

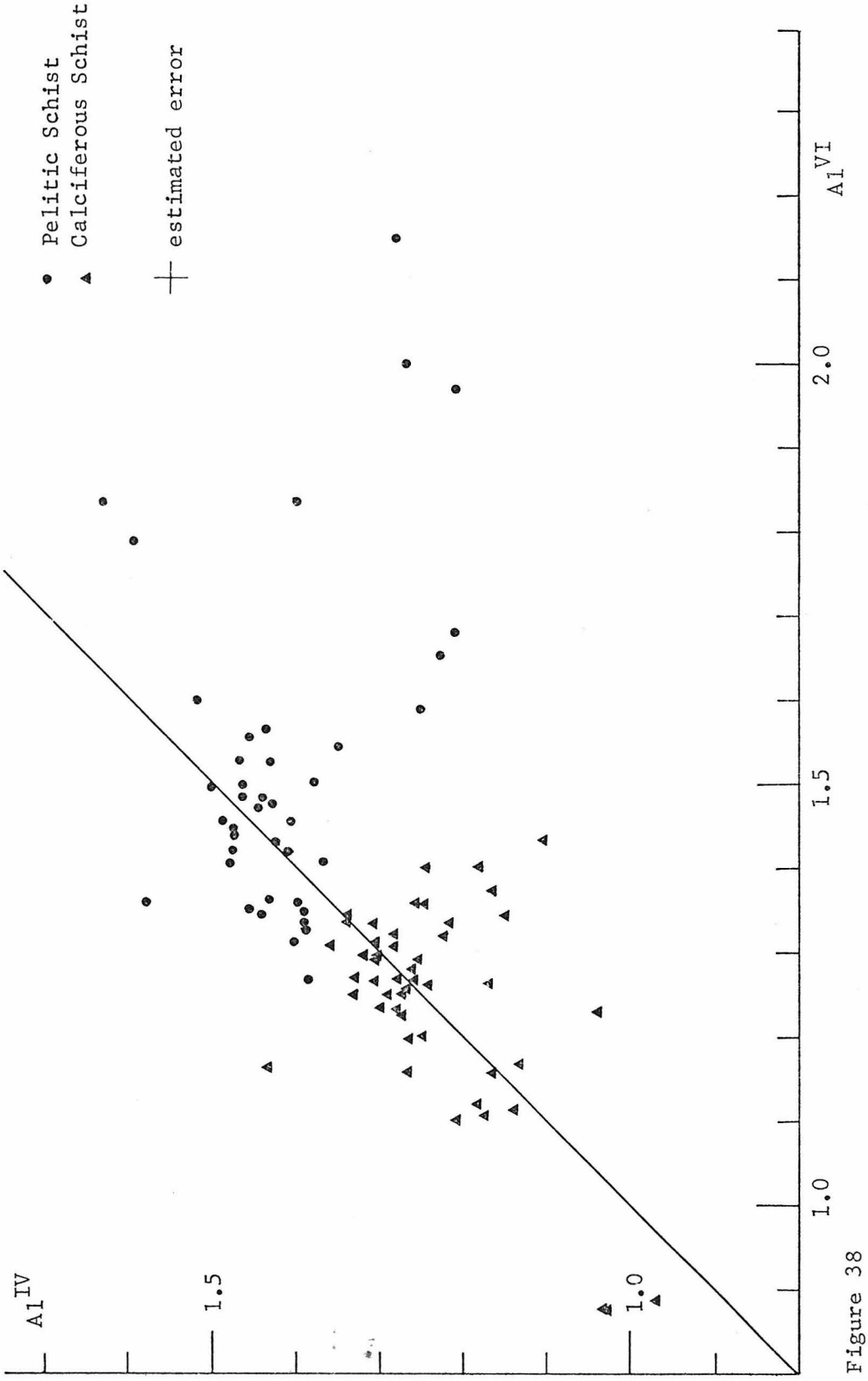
COMPOSITION OF CHLORITE, PANAMINT MOUNTAINS
Pelitic Schist
Calciferous Schist
estimated error
Al IV
Al VI
1.0
1.5
2.0
1.0
1.5

Figure 38

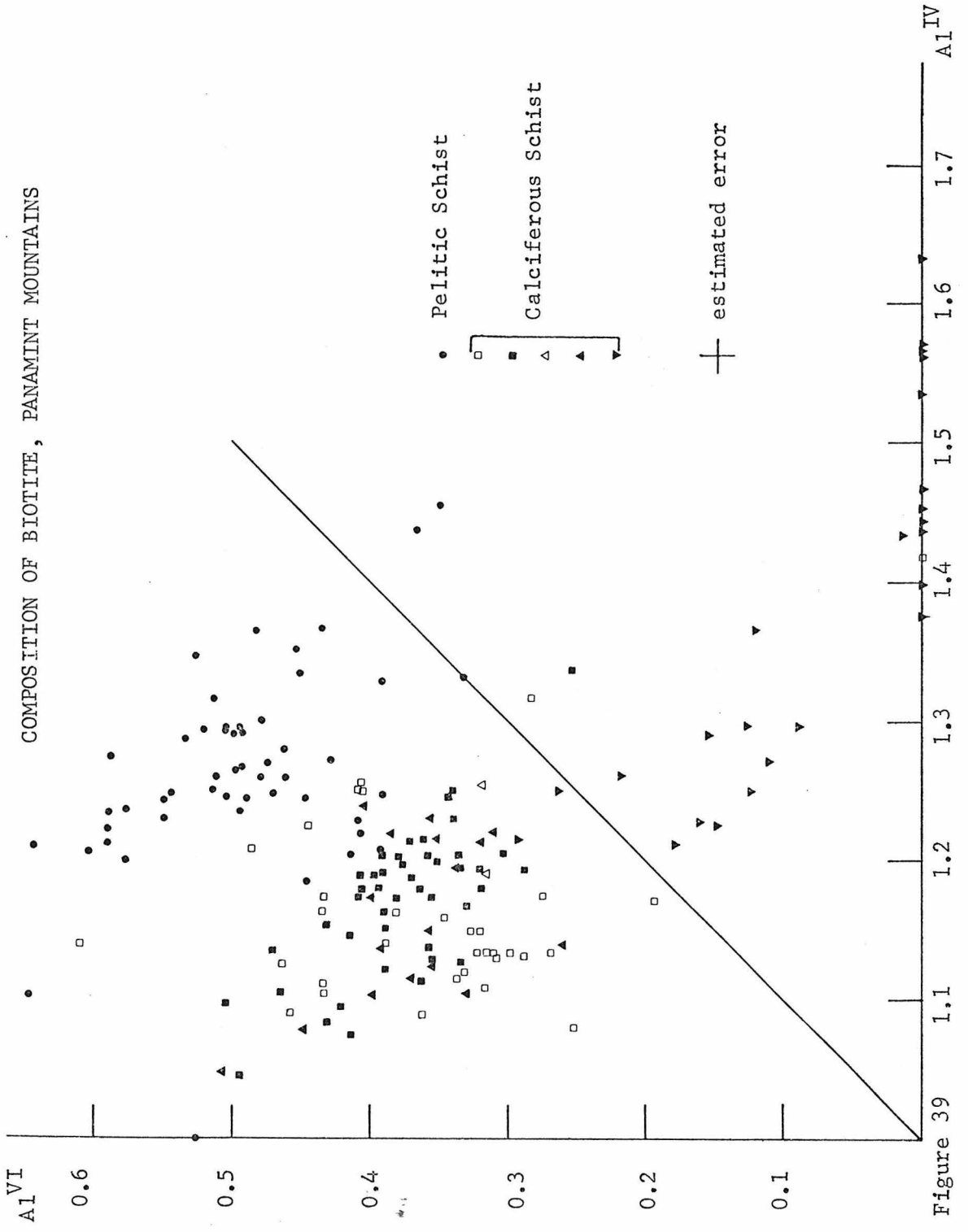
COMPOSITION OF BIOTITE, PANAMINT MOUNTAINS
Pelitic Schist
Calciferous Schist
estimated error
Al^{VI}
0.6
0.5
0.4
0.3
0.2
0.1
1.1
1.2
1.3
1.4
1.5
1.6
1.7
Al^{IV}

Figure 39

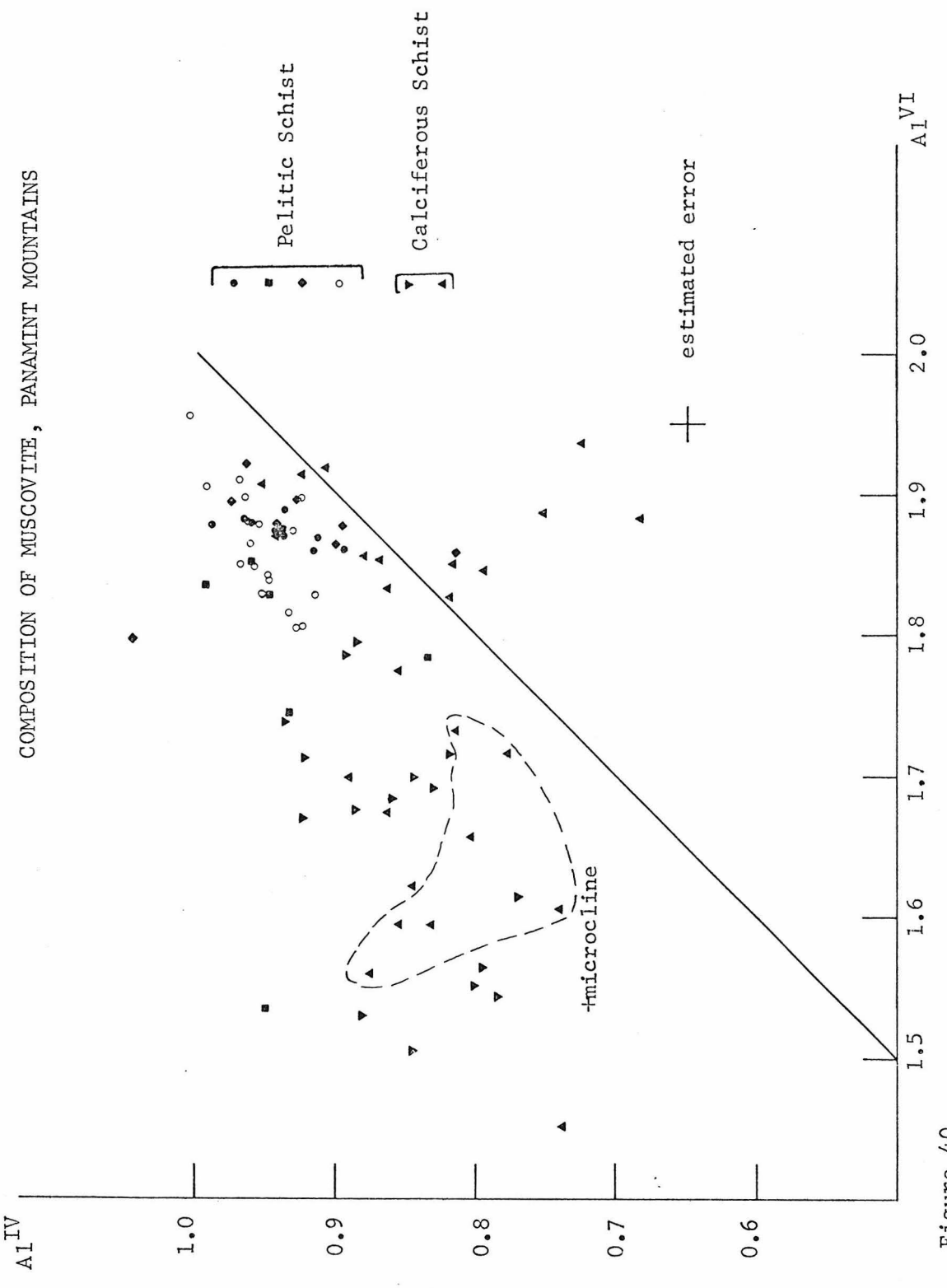
COMPOSITION OF MUSCOVITE, PANAMINT MOUNTAINS
Pelitic Schist
Calciferous Schist
estimated error
+microcline
Al^{IV}
Al^{VI}
1.0
0.9
0.8
0.7
0.6
1.5
1.6
1.7
1.8
1.9
2.0

Figure 40

The compositions of coexisting muscovite and biotite are illustrated in Figure 41. For clarity only selected analyses are shown. The biotite and muscovite from pelitic schists which coexist with andalusite contain the most aluminum. Of the muscovite and biotite which occur in calciferous schists, those which coexist with microcline contain the least amount of aluminum, and muscovite contains a maximum amount of Fe + Mg ("phengite"). The relative partition of aluminum and iron + magnesium is regular, predictable, and consistent with the attainment of equilibrium.

Sodium and calcium are additional components in all pelitic rocks and these elements are principally accommodated by plagioclase. In addition, sodium substitutes for potassium in muscovite and biotite, and paragonite is a possible sodium-saturating phase. Although a systematic search for paragonite by x-ray diffractometry was not performed, paragonite was not encountered during microprobe analyses of white mica in pelitic schists. Figure 42 illustrates the amount of sodium which substitutes for potassium in muscovite. Muscovite which occurs in pelitic schists contains appreciably more sodium than muscovite in calciferous schists. Plagioclase which coexists with muscovite in pelitic schists has compositions generally in the range An_{25} to An_{35}. Albite (An_3 to An_5) occurs in the assemblage andalusite + staurolite + biotite (PML 130) and plagioclase as calcic as An_{55} occurs in the higher grade assemblages PML 140c and CP 43. Figure 43 illustrates the myriad of plagioclase compositions from Panamint assemblages. In principal, the sodium-rich muscovite in pelitic schists should coexist with sodium-rich plagioclase, whereas the more potassium-rich micas should

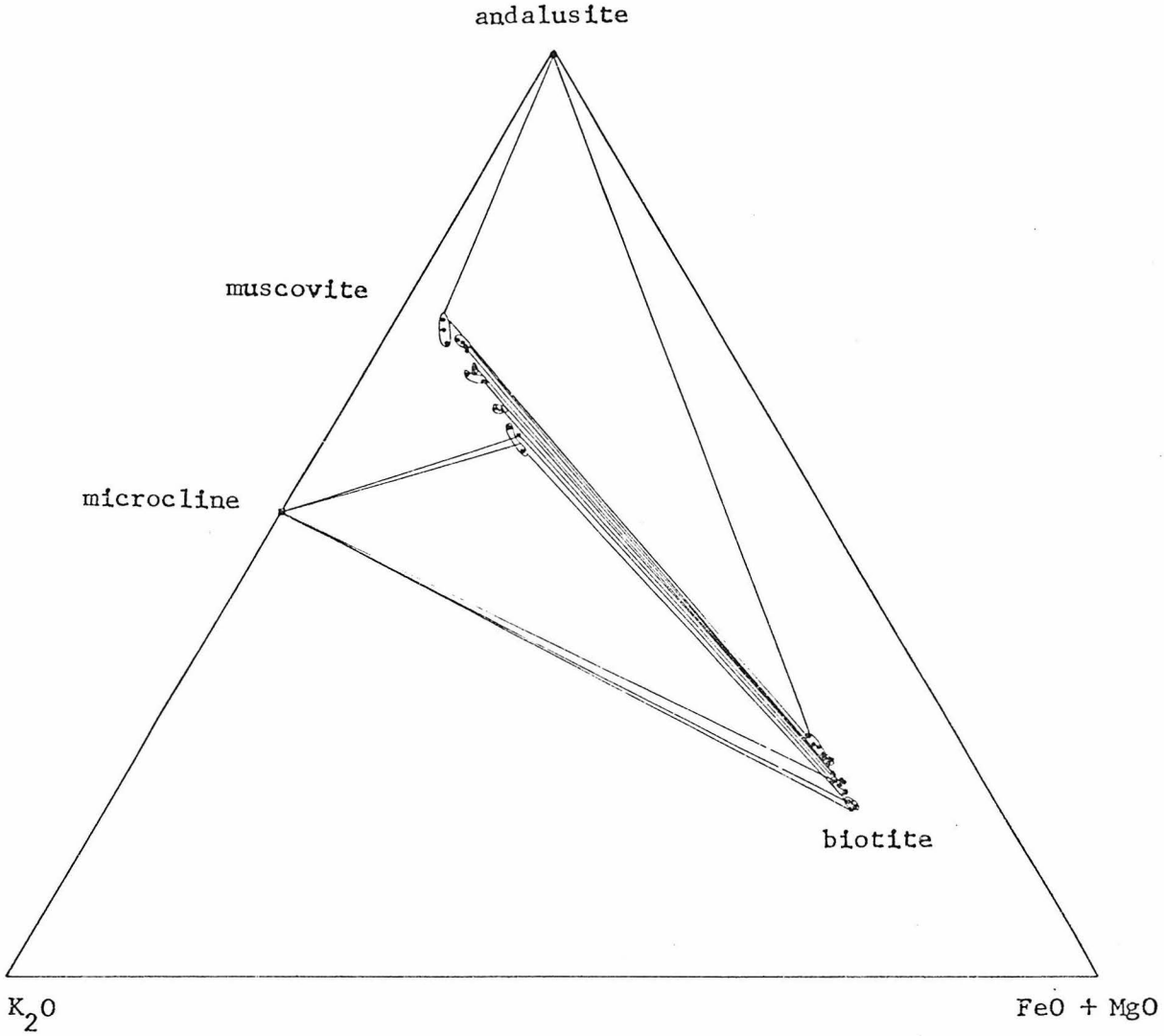

DISTRIBUTION OF Al_2O_3 and FeO + MgO BETWEEN COEXISTING MUSCOVITE AND BIOTITE
PANAMINT MOUNTAINS

Figure 41

Figure 42 SODIUM AND SILICON IN MUSCOVITE, PANAMINT MOUNTAINS

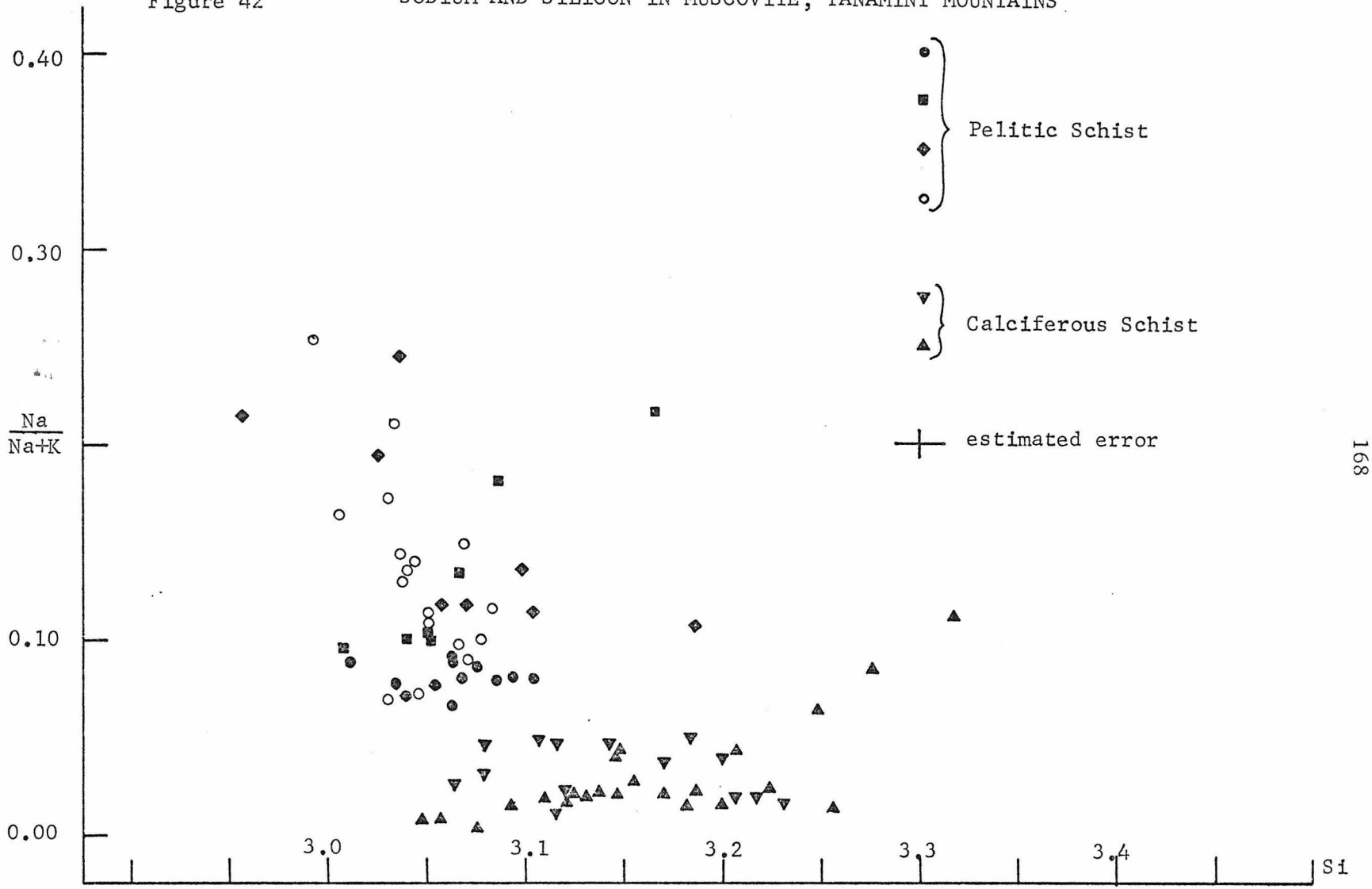

Figure 43a
COMPOSITION OF PLAGIOCLASE, PANAMINT MOUNTAINS

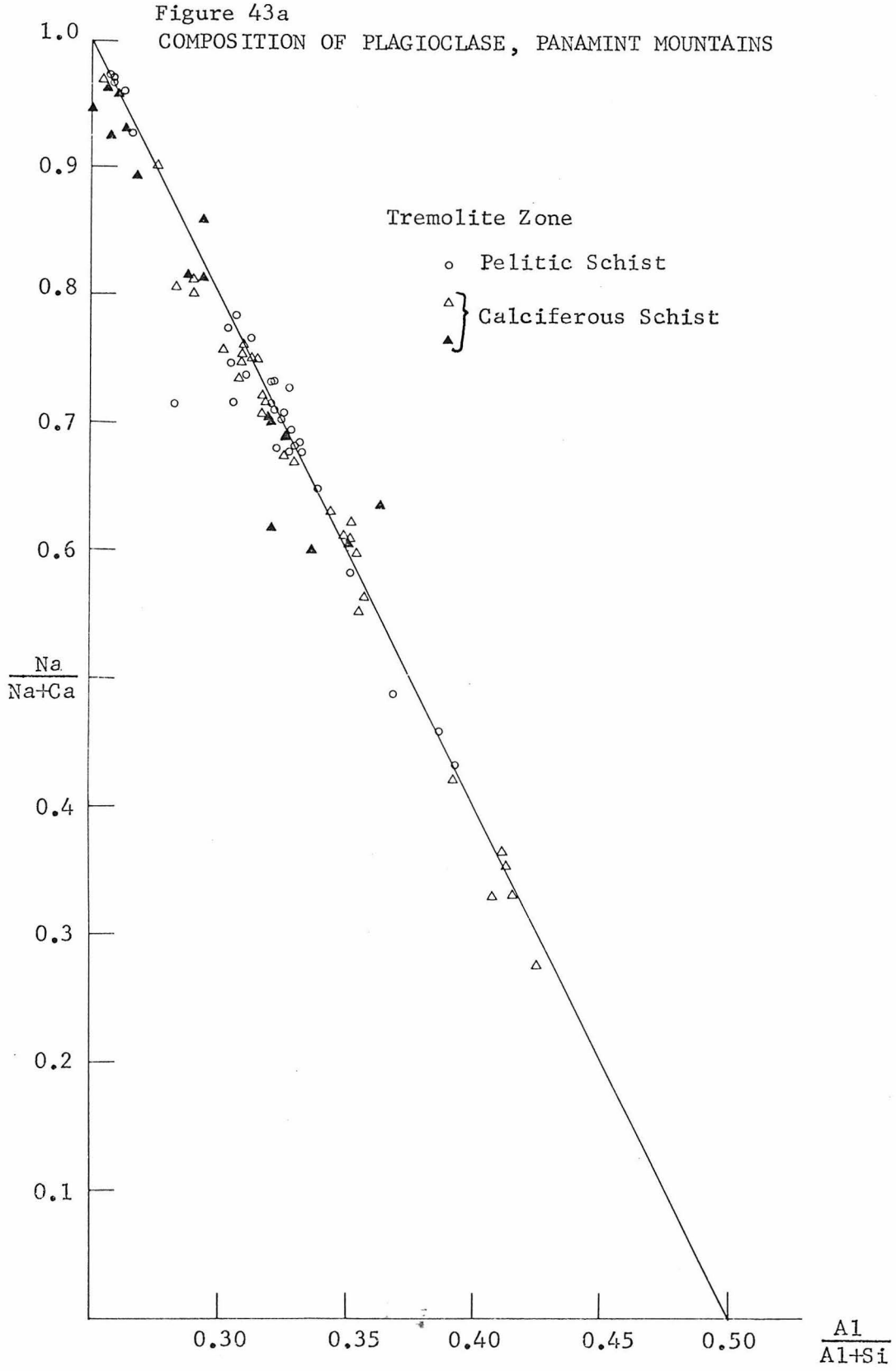

Figure 43b

COMPOSITION OF PLAGIOCLASE, PANAMINT MOUNTAINS

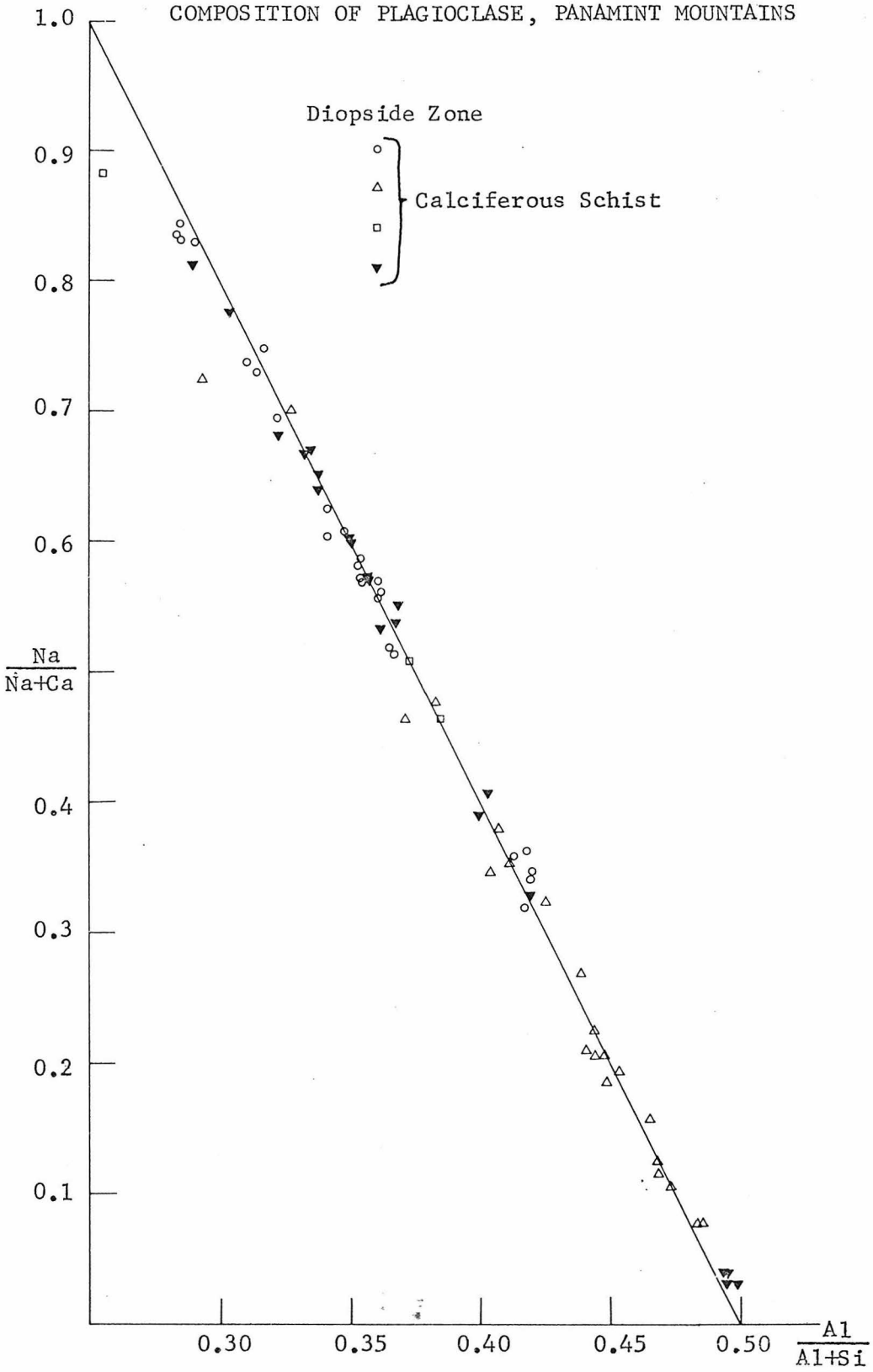

coexist with more calcic plagioclase. The wide range in plagioclase compositions which are observed, even within one sample, prevents determination of this relation. Low-sodium muscovite coexists with plagioclase as sodic as An_{20} and as calcic as An_{90}. This effect is probably related to two processes, the change in partition of Na/(Na + Ca + K) between muscovite and plagioclase with a change in grade, and the superposition of two metamorphic episodes.

A titanium phase occurs in all assemblages and in all assemblages but two the saturating phase is ilmenite. Titaniferous hematite occurs in the assemblage cordierite + chlorite + biotite, and rutile occurs in the low grade assemblage andalusite + chloritoid + chlorite. In general, ferric iron content in pelitic schists from the Panamint Mountains is low, and hematite occurs only in the assemblages andalusite + chloritoid + chlorite and cordierite + chlorite + biotite. Magnetite is observed only in the low grade assemblage chlorite + biotite.

AKFM Facies Series

The relative consistency in partition of Fe, Mg, and Al among coexisting phases in pelitic schists from the Panamint Mountains indicates that equilibrium was approached during metamorphism. Even though the occurrence of pelitic schists is limited, enough information is available to characterize the metamorphism of pelitic schist under low pressure conditions. Figures 44 and 45 illustrate the proposed sequence of reactions responsible for the low pressure metamorphism of pelitic schists. The greatest uncertainty in this sequence is the relation of chloritoid-bearing assemblages to cordierite and chlorite assemblages.

AKFM PELITIC SCHIST ASSEMBLAGES

PANAMINT MOUNTAINS

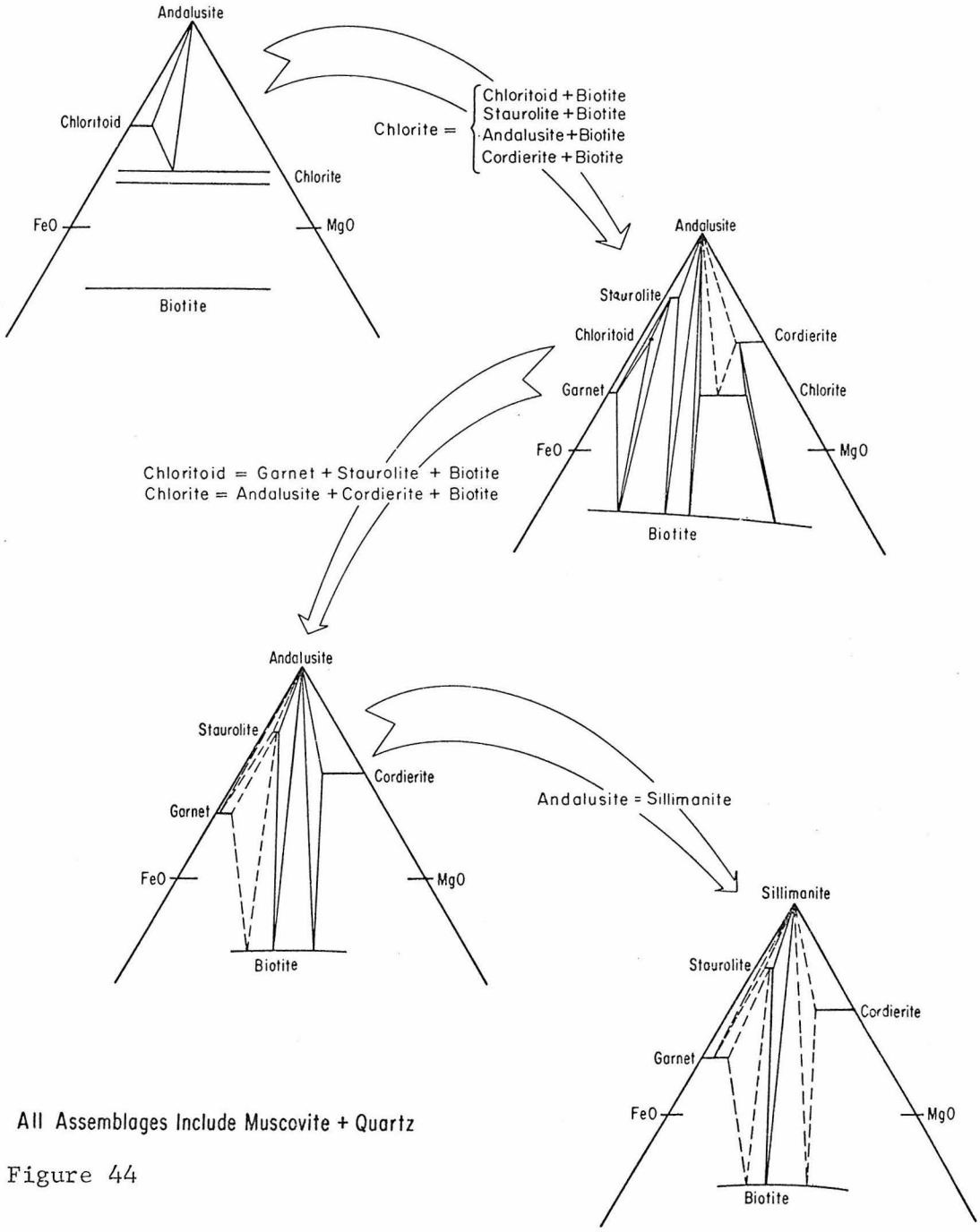

All Assemblages Include Muscovite + Quartz

Figure 44

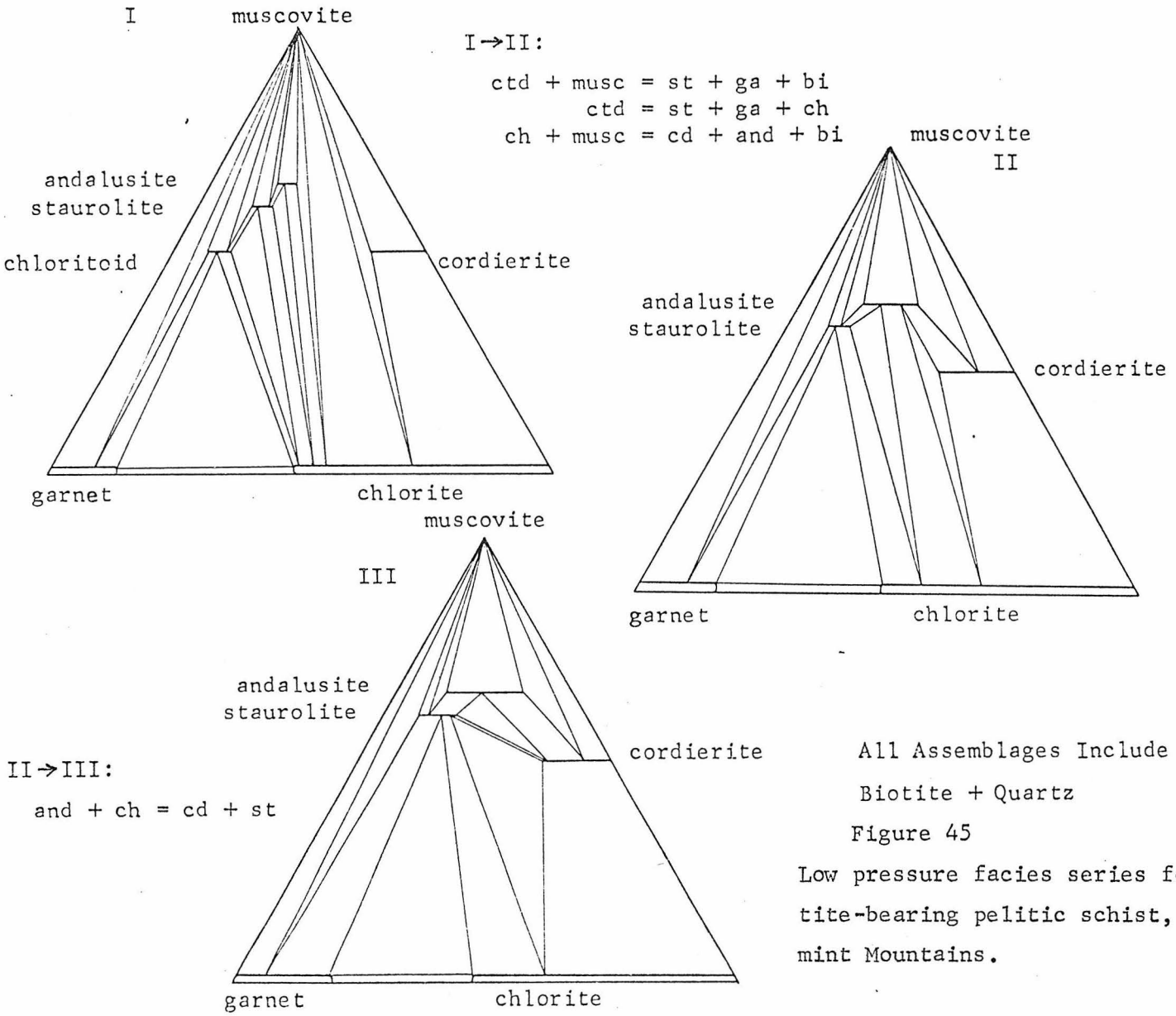

All Assemblages Include Biotite + Quartz

Figure 45

Low pressure facies series for biotite-bearing pelitic schist, Panamint Mountains.

In particular, the breakdown of chloritoid relative to any other reactions is unknown. Figures 44 and 45 are drawn to indicate that chloritoid is stable when andalusite + biotite is stable. The most striking feature is the apparent "rapidity" over a small change in metamorphic grade with which chlorite + muscovite + quartz becomes unstable. Outside the tremolite zone chlorite appears stable over a wide range in compositions. Inside the isograde the association chlorite + muscovite + quartz breaks down over nearly the entire range in Mg/(Fe + Mg) and the favored association is biotite + aluminous mineral. In fact, biotite coexists with nearly every other mineral. The general destruction of chlorite is accomplished by a series of reactions which depend on the Mg/(Fe + Mg) of the rock.

$$\text{chlorite + muscovite + quartz} = \begin{cases} \text{chloritoid + biotite + } H_2O \\ \text{staurolite + biotite + } H_2O \\ \text{andalusite + biotite + } H_2O \\ \text{cordierite + biotite + } H_2O \end{cases}$$

Chlorite is always more Mg-rich than biotite, but not as much as cordierite, and so the terminal reaction which places an upper limit on the stability of the association chlorite + muscovite + quartz must be

$$\text{chlorite + muscovite + quartz = andalusite + biotite + } H_2O.$$

Assuming that the composition of the retrograde chlorite which is present in the assemblage andalusite + cordierite + biotite is the terminal composition of chlorite, the reaction may be quantified:

$$15[FeTiO_3] + 550.3[(Fe_{2.07}Mg_{2.55}Mn_{0.02}Al_{1.35})(Al_{1.46}Si_{2.54})O_{10}(OH)_8] +$$

ilmenite chlorite

$$62.5[K(Fe_{0.05}Mg_{0.04}Ti_{0.01}Al_{1.90})(Al_{0.98}Si_{3.02})O_{10}(OH)_2] + 339.5[SiO_2] =$$

muscovite quartz

$$109.5[Al_2SiO_5] + 62.5[K(Fe_{1.22}Mg_{1.25}Ti_{0.09}Al_{0.43})(Al_{1.27}Si_{2.73})O_{10}(OH)_2] +$$

andalusite biotite

$$350.3[(Fe_{0.66}Mg_{1.31}Mn_{0.02})Al_4Si_5O_{18}] + 10[Fe_{0.96}Mn_{0.04}TiO_3] + 2201[H_2O].$$

cordierite ilmenite

The mineral compositions are derived from actual analyses of PML 107a and the reaction is written so that manganese released from chlorite and titanium absorbed by biotite is balanced by an appropriate change in amount and compositions of ilmenite. The effect of the difference in sodium content between biotite and muscovite is neglected, but because muscovite is more sodium-rich than biotite, an increase in the albite content of plagioclase also accompanies this reaction.

PHYSICAL CONDITIONS OF METAMORPHISM

The Panamint Mountains exhibit andalusite- and cordierite-bearing assemblages which are indicative of the low pressure-intermediate facies series of Miyashiro (1961). Quantification of the intensive thermodynamic parameters which attended metamorphism is attempted utilizing geologic, experimental, and theoretical arguments.

The total rock pressure is assumed to be the lithostatic pressure due to the stratigraphic column. At the time of metamorphism (late Mesozoic) the entire column from Precambrian through Triassic is assumed to have been present and the thicknesses of the individual

units is believed to be similar to those measured in the Panamint Butte (Hall, 1971) and Manly Peak (Johnson, 1957) Quadrangles. Table 6 lists these units and thicknesses, and the lithostatic pressure is found to be 2.3 kb at the top of the Johnnie Formation, 2.6 kb on top of the Pahrump Group, and 3.0 kb on top of the earlier Precambrian basement. These pressures are fully consistent with stability of andalusite indicated by the experimental work of Holdaway (1971) and Anderson and others (1977).

The transition from andalusite to sillimanite is recorded within the Pahrump Group, and the temperature indicated by this transition derived from Holdaway (1971) at a pressure of 2.75 Kb is 575°C. Most other temperature estimates which may be bracketed by experimental stability limits of mineral assemblages are subject to the uncertainty in fluid phase composition.

Temperature estimates were based on the distribution of iron and magnesium between garnet and biotite. An exchange reaction is independent of the composition of the fluid. The distribution coefficient K_D $(=[X_{Mg}/X_{Fe}]^{gar}/[X_{Mg}/X_{Fe}]^{bio})$ is a very weak function of pressure and depends most strongly on temperature (Kretz, 1961; Albee, 1965b). Temperatures were calculated for garnet-biotite pairs from the oxygen isotopic calibration of Goldman and Albee (1977), and Figure 46 shows the distribution of values derived from this geothermometer. The results agree remarkably well with the direction of increasing metamorphic grade and with the temperature indicated by the sillimanite isograd. The garnet-biotite pair near the tremolite isograd gives a low value of 418°C, and the sample collected at the contact with the muscovite-

TABLE 6: STRATIGRAPHIC COLUMN PANAMINT RANGE

AGE	FORMATION		THICKNESS (m)
Triassic	Warm Spring	(Johnson, 1957)	1333
"	Butte Valley	"	1333
Permian	Owens Valley	(Hall, 1971)	800
"	Keeler Canyon	"	608
Pennsylvanian	Lee Flat Limeston	"	217
Mississippian	Perdido	"	250
"	Tin Mountain	"	
Devonian	Lost Burro	"	500
"	Hidden Valley Dolomite	"	133
Ordovician	Eureka Quartzite	"	117
"	Pogonip Group	"	500
Cambrian	Nopah	"	450
"	Bonanza King	"	1000
"	Carrara	"	333
"	Zabriskie	(Hunt & Mabey, 1966)	137
Cambrian-Precambrian	Wood Canyon	"	758
Precambrian	Stirling Quartzite	"	667
"	Johnnie	(this report)	1333
"	Noonday Dolomite	"	
"	Pahrump Group	"	1667
	Total		12,137

TABLE 7: TEMPERATURE CALCULATED FROM GARNET-BIOTITE PAIRS PANAMINT MOUNTAINS

SAMPLE	GARNET			BIOTITE				TEMPERATURE °C	
	Mg/Fe	X_{Mn}	X_{Ca}	Mg/Fe	X_{Fe}	X_{Ti}	X_{Al}^{VI}	G-A	F-S
CP 9a	0.049	0.077	0.005	0.326	0.754	0.030	0.200	418	521
CP 401	0.094	0.249	0.090	0.608	0.622	0.046	0.152	524	529
CP 43	0.142	0.239	0.051	1.133	0.469	0.025	0.201	526	473
McD 350a	0.213	0.070	0.350	0.961	0.510	0.041	0.116	597	646
PML 195a	0.216	0.106	0.165	1.229	0.449	0.038	0.129	625	567
PML 39 interior	0.165	0.112	0.187	0.727	0.579	0.052	0.108	656	655
PML 39 matrix	0.153	0.114	0.185	0.839	0.544	0.045	0.129	438	578
PML 225b	0.250	0.021	0.096	0.836	0.545	0.032	0.121	680	773
PML 250c	0.066	0.048	0.019	0.423	0.703	0.031	0.151	422	531
PML 250b	0.074	0.030	0.022	0.497	0.668	0.030	0.170	426	518

X_{Fe}^{bi} = Fe/Fe + Mg; all other X_i = i/3 (i = formula proportion of cation i)

G-A: Goldman and Albee (1977):

$$\ln K_D = -0.177(\pm0.010)[1000\ \ln\alpha] - 1.22(\pm0.14)X_{Ca}^{G} + 1.40(\pm0.09)X_{Fe}^{B} + 0.942(\pm0.109)X_{Ti}^{B} - 1.59(\pm0.21)X_{Al}^{B} - 0.492(\pm0.068)$$

F-S: Ferry and Spear (1977): $\ln K_D = -\frac{2266}{T} + 0.960$

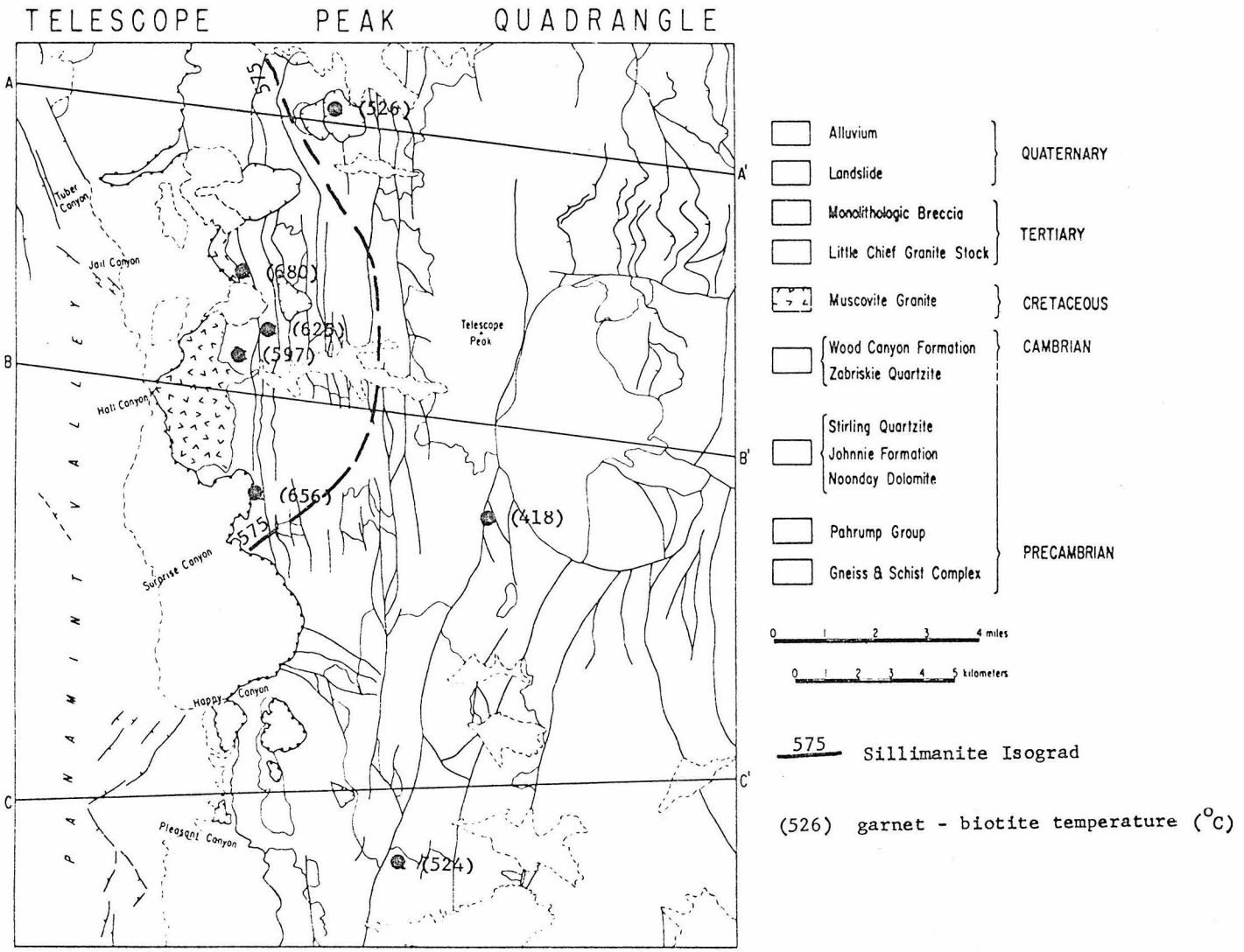

Figure 46: Distribution of temperatures calculated from Goldman and Albee (1977).

TABLE 8: ACTIVITY OF WATER, PANAMINT MOUNTAINS

SAMPLE	MUSCOVITE X_{par}	PLAGIOCLASE X_{ab}	T* °C	F_{H_2O} bars	a_{H_2O}
PML 126	0.120	0.668	425	287	0.493
PML 130	0.200	0.960	425	187	0.321
PML 140f	0.210	0.962	525	811	0.829
PML 141a	0.114	0.763	525	731	0.747

*assumed temperature; $P_s = P_f = 2500$ b

f_{H_2O} calculated from paragonite + quartz = andalusite + albite + H_2O

granite gives the highest value of 680°C. One sample, PML 39, shows reequilibration at lower temperatures. The pair: (biotite included in garnet) and (garnet interior) gives a value of 656°C while the pair: (biotite in matrix)-(garnet rim) gives a value of 438°C. In Table 7 the temperatures calculated from Goldman and Albee (1977) are compared to temperatures calculated from the experimental calibration of Ferry and Spear (1977). The agreement is generally not good and differences of as much as 140°C are noted. Garnet which occurs in the Panamint Mountains is very manganese- and calcium-rich and the effect of Mn on K_D can be large (Albee, 1965b). Hence, the calibration of Goldman and Albee (1977) is believed to more closely represent conditions of metamorphism than the manganese- and calcium-free calibration of Ferry and Spear (1977).

The occurrence of water-poor assemblages at relatively low grades suggests that the composition of the fluid phase during metamorphism may have been the controlling factor for reaction. A great percentage of the stratigraphic column consists of carbonate rocks and decarbonation reactions may provide substantial amounts of CO_2 to the fluid. Calcite is a very common phase in the calciferous schists, and its presence suggests that a_{CO_2} was high. Some reactions which may occur in calciferous schist have been studied experimentally by Hewitt (1973, 1975) and Hoschek (1973):

muscovite + calcite + quartz = microcline + anorthite + CO_2 + H_2O and

phlogopite + calcite + quartz = microcline + tremolite + CO_2 + H_2O.

The assemblage muscovite + biotite + microcline + hornblende + calcite + quartz + plagioclase occurs in calciferous schists and a knowledge of

P, T, and effects of solid solution on the end member phases allows the calculation of the composition of the fluid phase. However, there are great uncertainties in temperature estimates and in activity-composition relations and such a calculation was not attempted. The occurrence of this assemblage indicates that the fluid phase contained substantial amounts of CO_2 (Hewitt, 1975).

The assemblage grossular + epidote + diopside + quartz also occurs in calciferous schists, and the experimental data on the stability of grossular at 2 Kb (compiled by Storre and Nitsch, 1972) indicate that if wollastonite is not stable, grossular is limited to assemblages which coexist with very water-rich fluids ($X_{CO_2} < 0.05$) between 500 and 600°C.

Mineral assemblages in the siliceous dolomites do not provide much diagnostic information on T-X_{CO_2} for two reasons. First, data on experimental systems are quite conflicting. Skippen (1974) suggests on the basis of both experiment and calculation that assemblages involving calcite + talc should become prominent at higher pressures, but Slaughter, Kerrick, and Wall (1975) suggest just the opposite. Second, even in situations in which X_{CO_2} is buffered by a reaction, most common reactions proceed over a wide range in T and X_{CO_2}. Interpolating the data of Skippen (1974) and Slaughter and others (1975), conditions at the tremolite isograd may range from T≈450°C, $X_{CO_2} \simeq 0.5$ to T ≈ 500°C, $X_{CO_2} \simeq 0.9$. The temperature derived from the garnet-biotite pair in upper Surprise Canyon (418°C ± 15°) suggests the lower temperature end of this range. In general, sillimanite first occurs in the tremolite zone. This suggests that diopside first appears at temp-

eratures in excess of 575 °C at about 2.75 kb. A crude interpolation of the data of Slaughter and others (1975) and Skippen (1974) suggests that the fluid phase in carbonate rocks at the diopside isograd may have had X_{CO_2} between 0.5 and 0.8. The control on the relative positions of the diopside and sillimanite isograds is loose, and they even cross in Surprise Canyon, so the fluid composition probably varied beyond this range. The local occurrence of forsterite in Tuber and Jail Canyons suggests that the temperature may have been higher than 575 °C, but values of T and X_{CO_2} are also largely undefined.

A limited amount of experimental data exists on a multivariant reaction which occurs among the phases in the assemblage quartz + muscovite + plagioclase + andalusite. This assemblage is common in the pelitic schist from the Johnnie Formation, and the activity of water was calculated from the reaction

$$\text{paragonite + quartz = albite + andalusite + } H_2O.$$

The equilibrium constant is given by

$$\log_{10}K = -\frac{4171}{T} + 7.94 + \frac{0.0555(P-1)}{T} \quad \text{(Ghent, 1975).}$$

$$\log_{10}K = \log f_{H_2O} + \log X_{alb}^{plag} - \log X_{par}^{musc} + \log\gamma_{ab}^{plag} - \log\gamma_{par}^{musc}.$$

$$RT \ln\gamma_{par}^{mica} = (1-X_{par})^2(W_{Na} + 2(W_K - W_{Na})X_{par}).$$

$W_{Na} = 3082.1 + 0.0822P + 0.1698T$, $W_K = 4163.9 + 0.1259P + 0.3954T$ (Eugster and others, 1972). For $X_{ab}^{plag} > 0.5$, $\gamma_{ab}^{plag} = 1.0$ (Orville, 1972). The calculation was performed with an assumed pressure of 2500 b ($P_f = P$) and assumed temperatures of 425°C (PML 126 and PML 130) and 525°C (PML 140f and PML 141a). The results, shown in Table 8, strongly

suggest that a great proportion of the fluid phase consists of volatiles other than H_2O, but the lack of a carbon-species buffer (e.g. graphite) prevents determination of the prominent gaseous species in the fluid.

The evidence suggests that throughout the Telescope Peak Quadrangle, the fluid phase contained substantial amounts of CO_2. The local occurrence of grossular-bearing assemblages indicates that the coexisting fluid was locally water-rich. The composition of the fluid probably varied over large regions; CO_2 was abundant in carbonate rocks and less abundant but prevalent in siliceous rocks.

The extremes in pressure-temperature conditions realized during the metamorphism of the Panamint Mountains are shown in Figure 48. The relation between this P-T path and experimental determination of relevant equilibria is also shown. The observed mineral assemblages and estimated P-T path are compatible with the stability of andalusite low temperatures, the persistence of staurolite into the sillimanite zone, the stable coexistence of andalusite + albite, and the breakdown of chlorite in the stability field of andalusite.

The principal effects of the second metamorphism, outlined above, are the restabilization of muscovite + quartz + chlorite in formerly high grade rocks and the stable association of garnet + chlorite + muscovite + quartz. During the primary metamorphism the association garnet + chlorite apparently was not stable in contrast to the occurrence of garnet + chlorite in retrograde mineral assemblages. Temperature estimates based on the K_D for garnet-biotite of Goldman and Albee (1977) (Table 5) are 422 and 425°C for two retrograde samples; these are comparable to the temperatures derived for the garnet + staurolite +

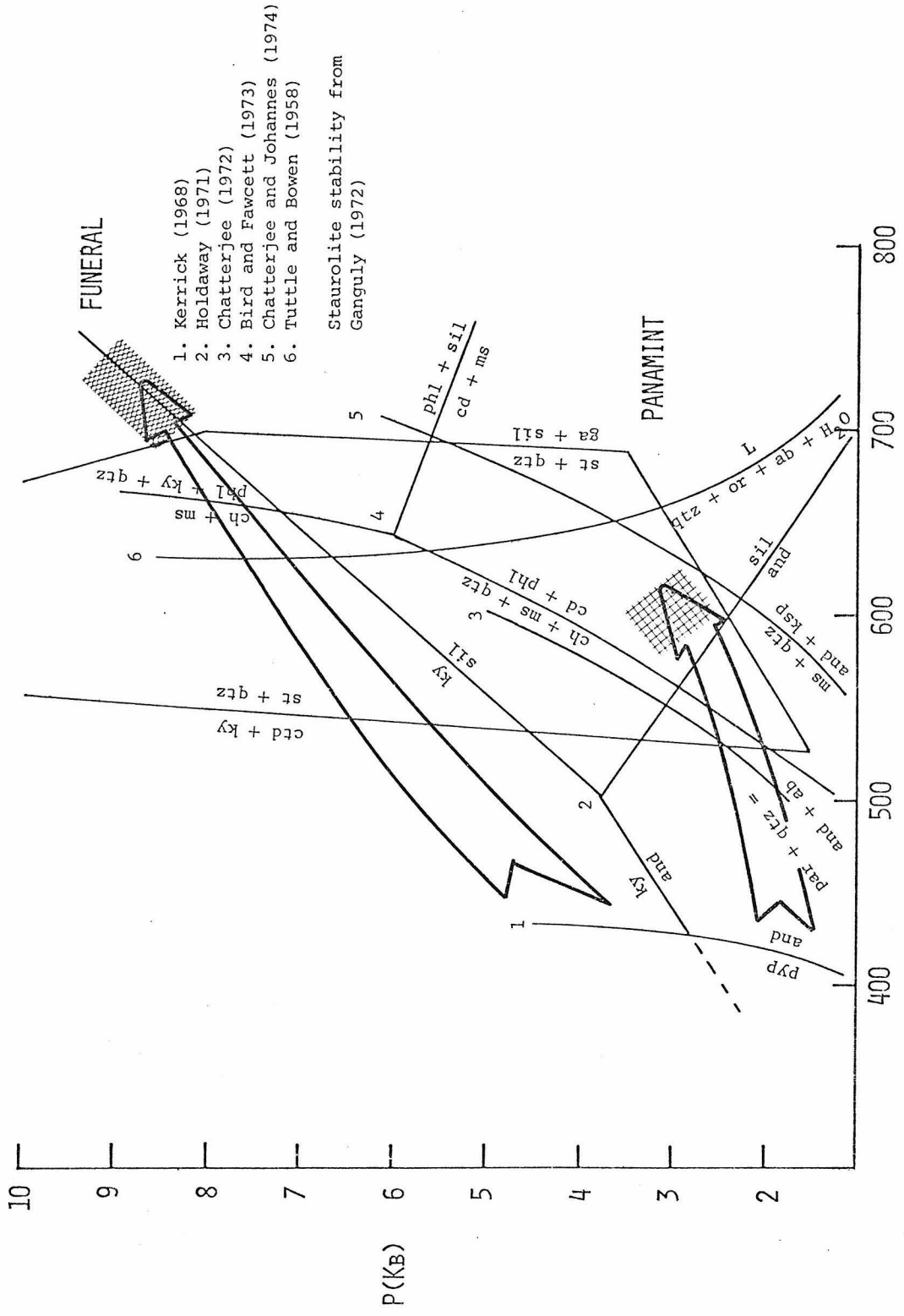

Figure 47 :
P/T path of metamorphism, Panamint Mountains.

chloritoid + biotite assemblage near the tremolite isograd. This apparent discrepancy in mineral assemblages formed at the same temperature may be explained by analysis of the reaction

garnet + chlorite = biotite + chloritoid

which relates the two assemblages. As shown in a later section, the slope of this reaction in $P_T = P_{H_2O}$ - T space is small and a change in pressure due to the different stratigraphic position of the rock bearing these assemblages may be sufficient to cross the reaction plane. Alternatively, or in addition, the low activity of water suggested for the primary metamorphic event may be responsible for the stabilization of the less hydrous assemblage chloritoid + biotite over garnet + chlorite. The alteration of andalusite to pyrophyllite near Wildrose Peak indicates that temperature was less than about 425° C during retrograde metamorphism (Kerrick, 1968).

The spatial relation between the primary metamorphic isograds and the Cretaceous muscovite granite is clear, and although it is unlikely that the heat from the intrusion caused the metamorphism, a genetic relation between intrusion and metamorphism is indicated. Metamorphism of the Panamint Mountains and intrusion of the muscovite-granite occurred in a thermal regime with a low dp/dT. Mineral assemblages in pelitic schists are significantly different from those formed in the Funeral Mountains under higher pressure conditions, but retrograde mineral assemblages indicate that the difference in mineral assemblages may be due in part to a reduced activity of water during the primary metamorphism.

MEDIUM PRESSURE, BARROVIAN METAMORPHIC TERRAIN, FUNERAL MOUNTAINS

INTRODUCTION

The Funeral Mountains form the eastern boundary of central Death Valley and consist of a core of metamorphosed sedimentary rocks flanked by unmetamorphosed Paleozoic strata. Quite unlike the Panamint Mountains, the metamorphic core of the Funeral Mountains is comprised of a kyanite-bearing terrain, and it has been possible to map "Barrovian"-type isograds which show a range in metamorphic grade from below garnet zone to sillimanite zone. The style of metamorphism developed in the Funeral Mountains contrasts sharply with the low pressure, regional metamorphic style of the Panamint Mountains, and several questions are raised. Are the terrains contemporaneous, or do the different styles imply two, different, unrelated metamorphic episodes?

This section describes the petrography and petrology which define the "style" of the Funeral Mountains terrain, and a later section compares the development of mineral assemblages and contrasts the attendant physical conditions in the Panamint and Funeral Mountains.

The geology of the Funeral Mountains and especially the Chloride Cliff and Big Dune 15' Quadrangles is being mapped by B. W. Troxel and L. A. Wright who kindly provided a copy of the preliminary map. The geology of the southern part of the Funeral Mountains is described by McAllister (1974), and the geology of the Grapevine Mountains which are contiguous with the Funeral Mountains to the north is outlined by Reynolds (1974) (Figure 1). The Grapevine-Funeral Mountains chain is comprised of late Precambrian, Paleozoic and Tertiary sedimentary, metasedimentary, and volcanic rocks.

The oldest rocks consist of a sequence of interbedded pelitic schist, calcite marble, micaceous quartzite, and amphibolite. Pelitic schist comprises about half of this section and is prominent in the lower part and upper part. Micaceous quartzite, calcareous quartzite, and marble make up the middle part of the section. The occurrence of amphibolite in the lower part of the section, and conglomerate in the upper part led to the correlation of these rocks to the Pahrump Group (Troxel and Wright, 1968). The lithologies in this section are not directly correlative to the formations which comprise the Pahrump Group elsewhere in the Death Valley area.

The Pahrump Group is overlain by the Johnnie Formation which consists predominantly of pelitic schist and quartzite. The Stirling Quartzite overlies the Johnnie Formation and is comprised of quartzite, micaceous quartzite, and minor carbonate layers. Pelitic layers occur near the base of the Stirling Quartzite. In the Chloride Cliff Quadrangle, the Stirling Quartzite is locally overlain by argillite and quartzite of the Wood Canyon Formation. This Paleozoic section is overlain by middle and upper Tertiary fluvial, lacustrine, and volcanic rocks. The generalized geology of the Chloride Cliff Quadrangle which encompasses the majority of the metamorphic rocks is shown in Figure 48.

The structure of the Funeral Mountains is dominated by a doubly plunging anticline which culminates in the high grade metamorphic terrain near Chloride Cliff. The high grade metamorphic rocks in this "core" are separated from low grade metasedimentary rocks by a major fault, here called the Boundary Canyon fault, which has a gently

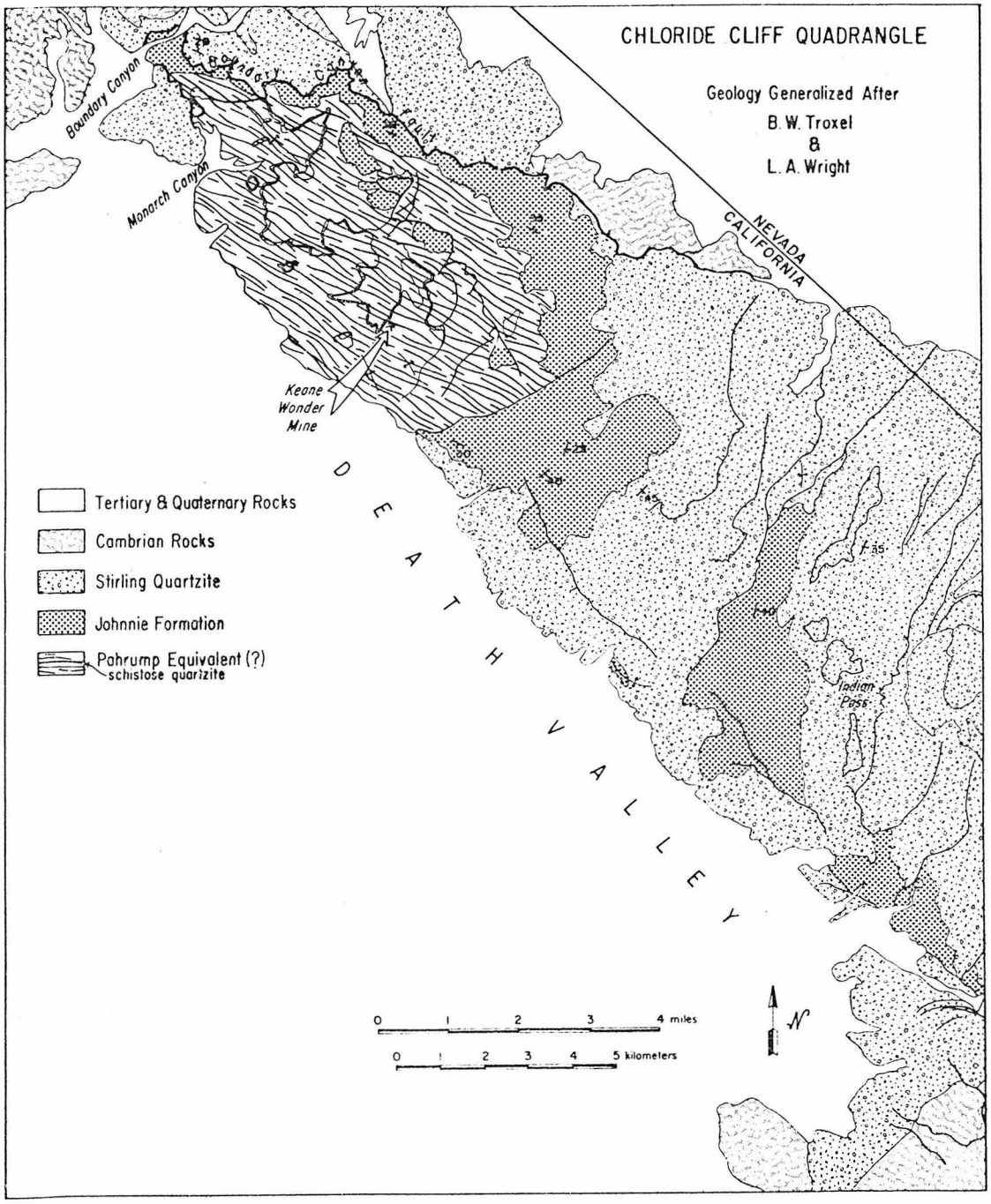

Figure 48: Generalized geology of the Chloride Cliff Quadrangle.

undulating surface and dips generally north. Similar gently north-dipping faults also displace the folded metamorphic terrain. Rocks as young as Oligocene are displaced by these faults and Pliocene strata on the upper plate of the Boundary Canyon fault are warped (Wright and Troxel, personal communication).

Two foliation surfaces are well developed in the metamorphic rocks. The older consists of a schistosity which is defined by the parallel alignment of muscovite and biotite grains and is oriented parallel to the compositional layering. A second foliation developed after the growth of porphyroblasts and consists of microfolds ("strain-slip" cleavage) whose axial planes lie at a high angle to the bedding.

The garnet, staurolite, and kyanite isograds which were mapped in the Funeral Mountains are delineated on Figure 49. Metamorphic grade increases from southeast to northwest, and isograds are cut off by the Boundary Canyon fault. The isograds do cut across the stratigraphy, but, in general, metamorphic grade increases with stratigraphic depth. The highest grade rocks occur in Monarch Canyon, near the culmination of the anticline, where sillimanite-bearing assemblages occur. Migmatites occur in the canyon bottom, and these high grade rocks are intruded by minor bodies of leucocratic, muscovite-bearing, granitic rock.

Extensive retrograde metamorphism has affected the high grade rocks in the Keene Wonder Mine area, Chloride Cliff, and along the Boundary Canyon Fault where most of the mafic minerals are altered to chlorite. The retrograded area corresponds to a mineralized area which was heavily prospected for gold in the early 1900's and to the

post-metamorphic tectonic dislocation.

The age of metamorphism is not well constrained. Metamorphism occurred after the deposition of the affected strata and before the development of the Tertiary Boundary Canyon fault. Wasserburg and others (1959) obtained a K-Ar date of 30 m.y. on muscovite from a pegmatite in Monarch Canyon which may correspond to the time of mineralization and retrograde metamorphism. A tentative hypothesis adopted here is that metamorphism occurred simultaneously in the Panamint and Funeral Mountains at approximately 80 million years ago.

MINERAL ASSEMBLAGES IN PELITIC SCHISTS

Samples were collected from several localities in the Chloride Cliff Quadrangle in order to document the mineral assemblages (metamorphic grade) and the reactions responsible for the change in mineral assemblages with increasing metamorphic grade. Siliceous dolomite and calciferous schist are not as abundant in the Funeral Mountains as they are in the Panamint Mountains, because the majority of the Funeral Mountains terrain is comprised of the Johnnie Formation and Stirling Quartzite. The majority of the rocks collected are pelitic schists from the lower Stirling Quartzite, Johnnie Formation and the Pahrump Group. On the basis of the mineral assemblages in these pelitic schists, garnet, staurolite, and kyanite isograds were mapped.

The garnet isograd is based on the first appearance of garnet (Figure 49). The several mineral assemblages observed in the pelitic rocks south of the garnet isograd include:

biotite + chlorite + muscovite + quartz + plagioclase

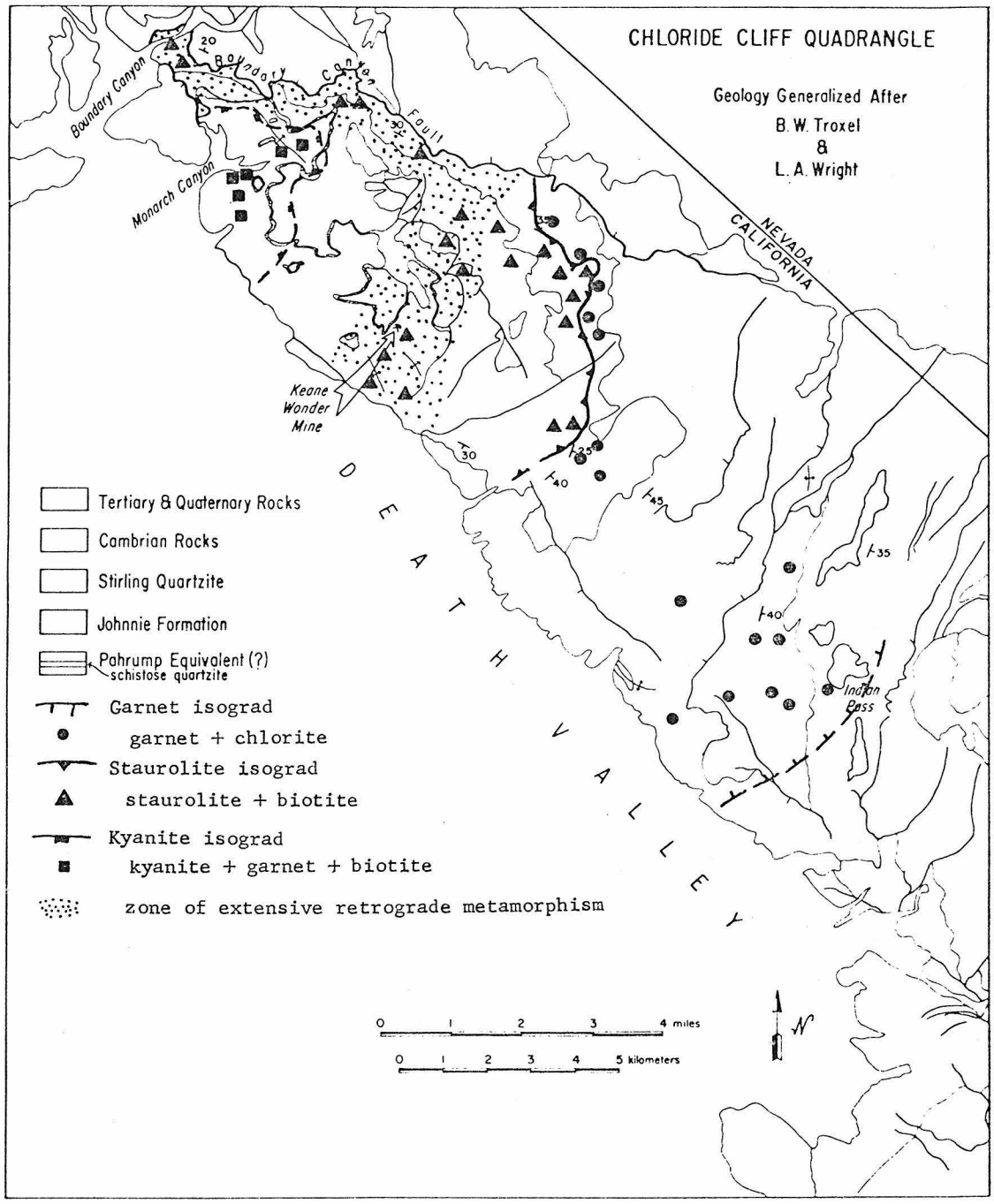

Figure 49: Distribution of diagnostic assemblages and metamorphic isograds in the Funeral Mountains.

chloritoid + chlorite + muscovite + quartz + ilmenite

chloritoid + chlorite + margarite + muscovite + quartz + rutile

chloritoid + chlorite + kyanite + muscovite + quartz + rutile + hematite

Most of these assemblages represent relatively aluminous rock compositions, and the absence of garnet-bearing assemblages may be due in large part to inappropriate rock compositions. These rocks are relatively fine-grained and the largest porphyroblasts, usually kyanite, are less than a few millimeters long. A foliation defined by a preferred orientation of micas is present, and this foliation is oriented approximately parallel to compositional layering. In many samples the foliation is broadly folded on a small scale, and axial planes of these microfolds lie at a high angle to the foliation. Chloritoid and kyanite porphyroblasts are randomly oriented, although in one sample (FML 66) chloritoid plates appear to have been rotated into the folded foliation.

Rocks in the garnet zone also contain a wide variety of mineral assemblages, but the zone is characterized by the coexistence of garnet and chlorite. Chloritoid occurs in rocks just north of the garnet isograd, and the assemblages found in the lower grade part of the garnet zone include:

garnet + chlorite + biotite + muscovite + quartz + plagioclase + ilmenite

garnet + chlorite + chloritoid + muscovite + quartz + ilmenite + paragonite

kyanite + chlorite + chloritoid + muscovite + quartz + hematite +

rutile

kyanite + chlorite + staurolite + musocvite + quartz + hematite +

rutile

The rocks are generally fine-grained and weakly to moderately foliated. Two foliations are apparent. The earlier is defined by a crude parallel alignment of fine-grained micas, oriented approximately parallel to bedding. A second foliation is expressed by gentle crenulation of the first, but in some cases the second foliation is defined by parallel alignment of medium-grained muscovite, oriented at a high angle to the first. The secondary foliation is not penetrative, but micas occur in 1 to 2 mm wide zone separated by 5 mm intervals. Garnet porphyroblasts, less than 3 mm in diameter, contain quartz inclusion trails which are parallel to the first foliation, but the porphyroblasts had grown prior to the development of the secondary foliation (CP 451i, Figure 50).

Retrograde textures were identified only in chloritoid + kyanite + chlorite assemblages in which millimeter-sized magnetite grains are rimmed by hematite, although chloritoid is locally coated by hematite or geothite.

Farther northwest chloritoid-bearing assemblages are absent, and the assemblage garnet + chlorite + staurolite + muscovite + quartz + plagioclase + ilmenite is dominant. Many of the garnet porphyroblasts have inclusions of chloritoid, but chloritoid is absent from the matrix (FML 85a, Figure 50). The grain size is larger than in the lower grade part of the garnet zone and staurolite and garnet porphyroblasts several millimeters in diameter occur. The crenulation cleavage is also better

Figure 50: Textural features of garnet grade pelitic schist, Funeral Mountains.

a) Relic chloritoid (light) included in garnet (black) in a garnet + staurolite (upper right) + chlorite assemblage, FML 85a (crossed nicols).

b) Sigmoidal inclusion trail in garnet (black) in garnet + biotite + chlorite assemblage, CP 451i (crossed nicols).

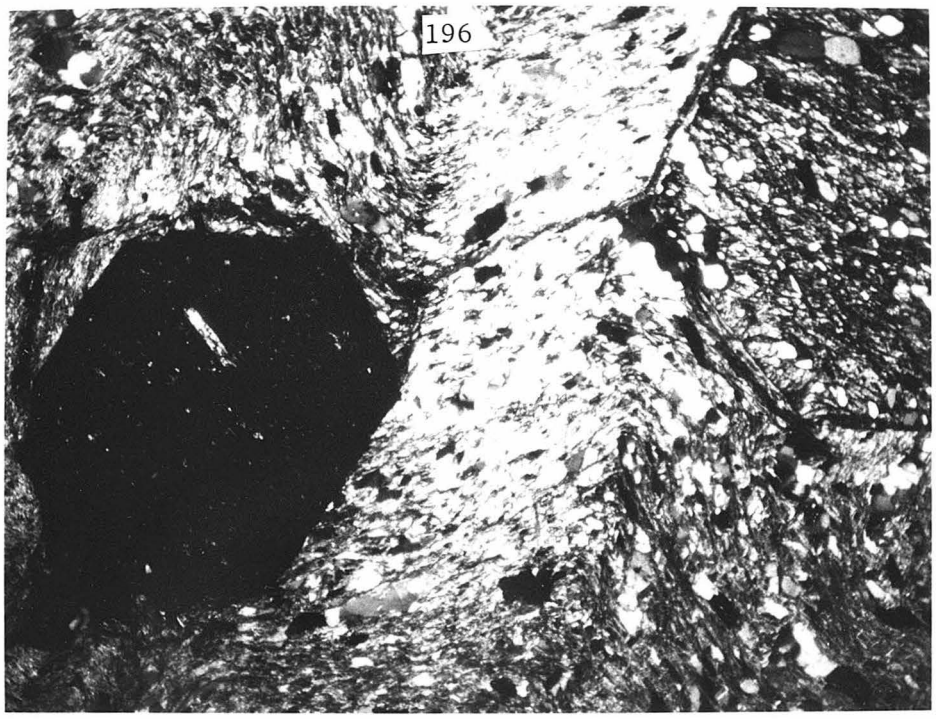

a

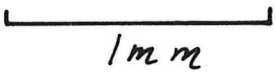

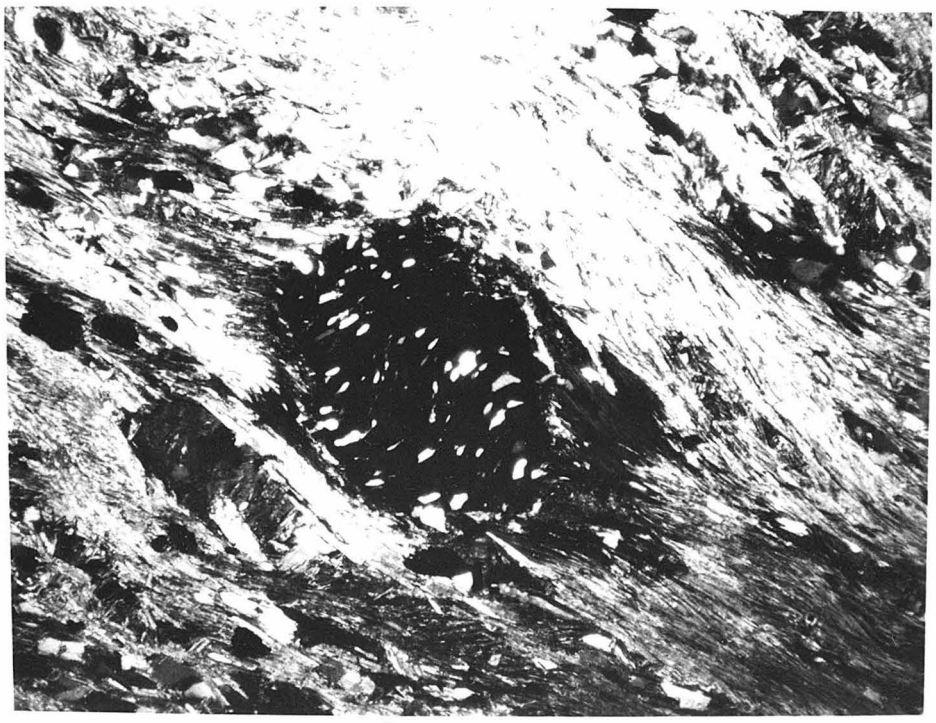

b

developed and the order of development, primary foliation - porphyroblast growth - crenulation, is observed.

Although staurolite is first encountered in what is here called the garnet zone, the staurolite isograd is defined on the basis of the first occurrence of the association staurolite + biotite. The association garnet + chlorite, and Figure 49 illustrates the occurrence of garnet + chlorite versus staurolite + biotite assemblages and the staurolite isograd. The assemblages observed in staurolite-grade schists include:

I garnet + staurolite + biotite + muscovite + quartz + plagioclase + ilmenite

II garnet + staurolite + biotite + chlorite + muscovite + quartz + plagioclase + ilmenite

III garnet + staurolite + biotite + kyanite + muscovite + quartz + plagioclase + ilmenite.

These schists are very coarse-grained and staurolite porphyroblasts several centimeters long are not uncommon. Staurolite and kyanite tend to be aligned in the foliation. Kinking and crenulation in the schistosity is prominent and kyanite grains are kinked and ilmenite grains are bent into the crenulation (Figure 51). Staurolite engulfs and includes garnet, and garnet porphyroblasts which occur in assemblages II and III are greatly embayed, and irregular in form. These textures suggest that garnet is metastable in assemblages II and III and has not been completely digested.

The kyanite isograd is defined by the disappearance of staurolite which is indicated by the stable coexistence of garnet + biotite +

Figure 51: Development of secondary foliation in pelitic schist from Fumeral Mountains.

a) Mica foliation oriented at a high angle to inclusion trails in garnet, CP 451i (crossed nicols).

b) Ilmenite (small black plates) bent into the secondary strain-slip cleavage in garnet + staurolite + chlorite assemblage, FML 92 (plane polarized light).

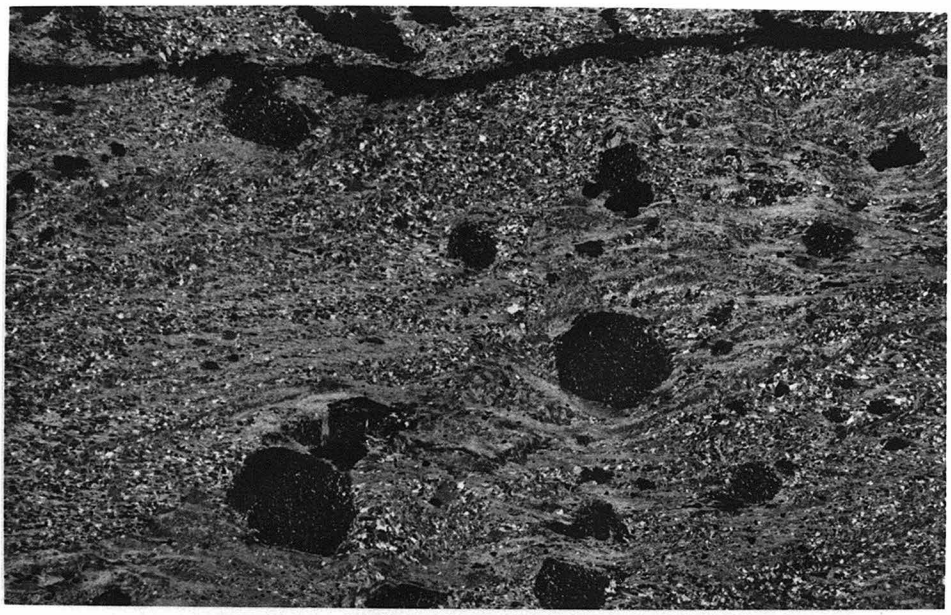

5mm

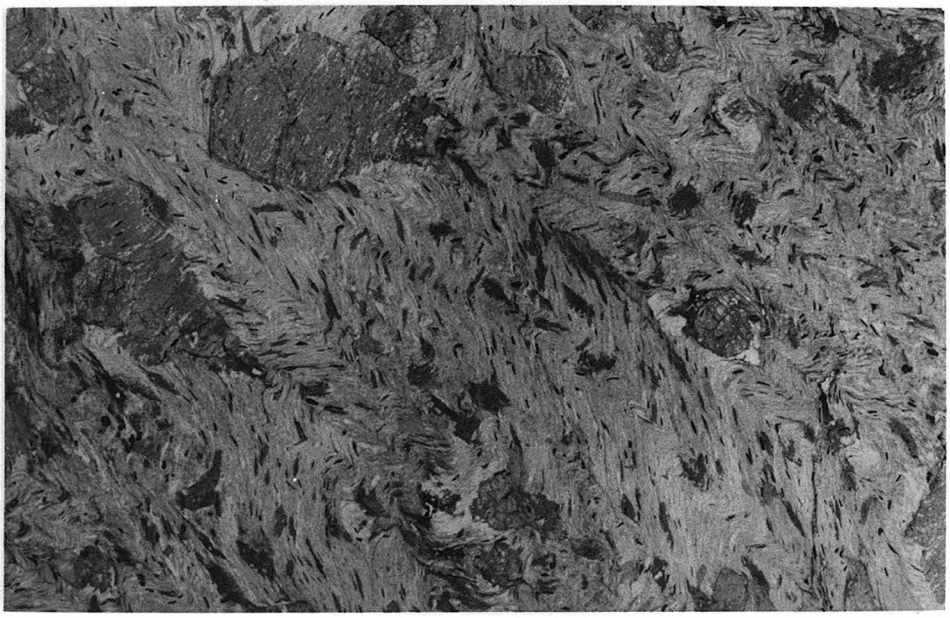

5mm

kyanite (Figure 49). The commonly observed pelitic assemblage is garnet + biotite + kyanite + muscovite + quartz + plagioclase + ilmenite or rutile. In Monarch Canyon sillimanite also occurs in this assemblage. Gneissic foliation characterizes the texture of the highest grade rocks, and migmatites which exhibit passive flow folds and ptygmatic folds occur in Monarch Canyon (Figure 52).

In thin section garnet porphyroblasts contain large inclusions of biotite and some staurolite, and garnet has preserved the relic composition of biotite and staurolite. Sillimanite generally occurs as needles in quartz, in the vicinity of kyanite grains.

The change in mineral assemblages and the preservation of relic minerals as inclusions in porphyroblasts are indicative of prograde metamorphic reactions. The variety in rock compositions which occurs in the Funeral Mountains allows the determination of the distribution of elements in pelitic schists and the elucidation of reactions which alter the stable mineral association with increasing grade.

DISTRIBUTION OF ELEMENTS IN PELITIC SCHISTS

AFM Phases

Most of the phases in these rocks can be described in terms of the oxides SiO_2 - Al_2O_3 - MgO - FeO - H_2O, and the mineral assemblages which occur in quartz + muscovite schists may be represented on the plane Al_2SiO_5 - FeO - MgO. The use of such projection as a phase diagram is discussed by Thompson (1957).

The range in bulk composition is sufficient to allow the determination of the complete facies types for this system at some grades

Figure 52: High grade rocks in the Funeral Mountains.

a) Kyanite + garnet + biotite schist, FML 116b (crossed nicols).

b) Migmatite in Monarch Canyon.

FM-116

TABLE 9: ANALYZED SAMPLES, FUNERAL MOUNTAINS

SAMPLE	QTZ	MUSC	BIO	GA	CH	CTD	ST	KY	SIL	PLAG	ILM	RUT	HEM	MARG	other	location	grade
CP 435c	X	X	X	X				X		X	X					1	K
CP 451e	X	X		X	X	X	X			X	X					12	G
CP 451f	X	X	X	X	X					X	X					12	G
FML 37b	X	X			X	X		X					X	X		9	G
FML 38c	X	X			X	X		X					X			9	G
FML 39b	X	X			X	X		X					X			9	G
FML 54	X	X		X	X	X					X					8	G
FML 55a	X	X						X					X			7	G
FML 55b	X	X			X		X	X				X	X			7	G
FML 56	X	X		X	X					X	X					11	G
FML 57	X	X			X	X		X				X	X	X	par	11	G
FML 58	X	X		X	X	X					X					11	G
FML 60	X	X	X	X	X					X	X					10	G
FML 62	X	X	X	X	X					X	X					10	G
FML 70a	X	X			X	X		X				X	X	X		13	G
FML 72	X	X			X	X						X			marg	13	G
FML 75	X	X			X	X		X					X			6	G
FML 94a	X	X	X	X	X		X			X	X					5	G
FML 101	X	X		X	X		X				X					4	G
FML 104a	X	X	X	X			X	X		X						3	S
FML 104c	X	X	X	X			X	X		X		X				3	S
FML 106a	X	X	X	X			X			X	X					3	S
FML 107a	X	X	X	X			X			X						3	S
FML 109	X	X		X	X		X			X	X					4	G
FML 110	X	X	X	X			X	X	X		X	X				2	K
FML 113a	X	X	X	X				X		X	X					1	K
FML 116b	X	X	X	X				X		X	X					1	K

All minerals except quartz were analyzed
par = paragonite, marg = margarite; K-kyanite S-staurolite G-garnet; locations shown on Figure 53

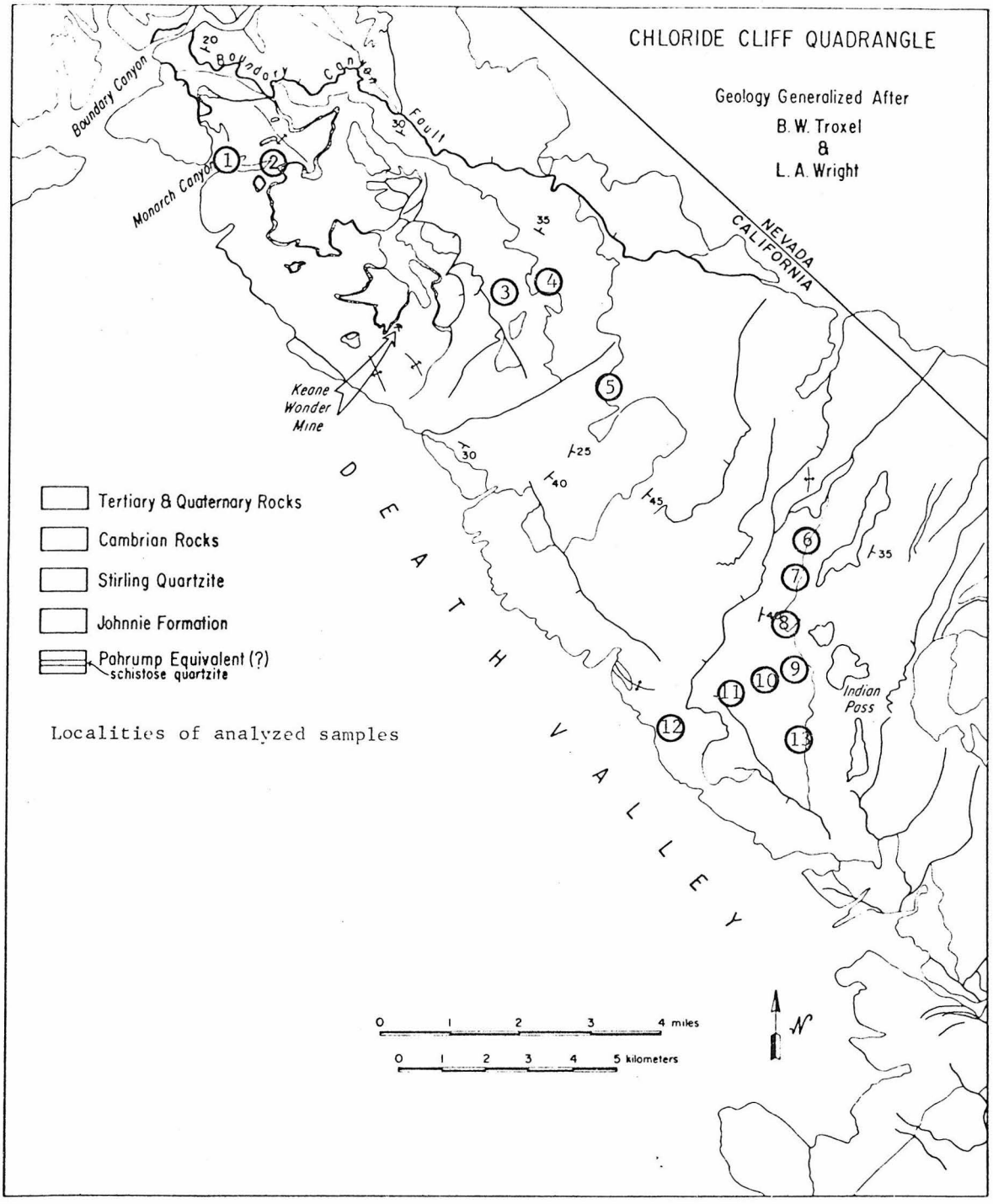

Figure 53: Sample localities, Funeral Mountains.

and of the reactions responsible for the changes in topology with increasing grade.

Analyzed mineral assemblages in pelitic schists from the Funeral Mountains are illustrated in Figures 53 and 54, and Table 9. The relative distribution of iron, magnesium, and aluminum among phases within any one mineral assemblage is consistent in all rocks exhibiting that assemblage. For a given assemblage, tie lines do cross, but these minor inconsistencies are attributed to minor variations in P, T, and a_{H_2O}. For all rocks found within a small area and within the same zone, unlike assemblages do not occupy overlapping regions in composition space, and these changes in mineral assemblage are attributable to changes in bulk composition. Four-phase assemblages occur in some of the higher grade rocks, but the garnet in the staurolite zone assemblage garnet + staurolite + biotite + chlorite appears to be altered and the garnet is believed to be relic. Likewise staurolite in the kyanite zone assemblage garnet + kyanite + biotite + staurolite occurs only as inclusions in garnet or large muscovite plates, and the staurolite also appears to be a relic phase. This apparent consistency in the relative order of element partition and with the Gibbs phase rule suggests that chemical equilibrium was closely approached during metamorphism and invites a closer examination of the mineral chemistry and its relation to rock composition and metamorphic grade.

Chlorite is the most commonly observed mineral in the lower metamorphic grades and its major element chemistry is illustrated in Figure 55. The range in total aluminum is relatively small and aluminum varies from 2.7 to 3.0 cations/formula. Chlorite which coexists

Figure 54a: LOW GRADE ASSEMBLAGES, FUNERAL MOUNTAINS

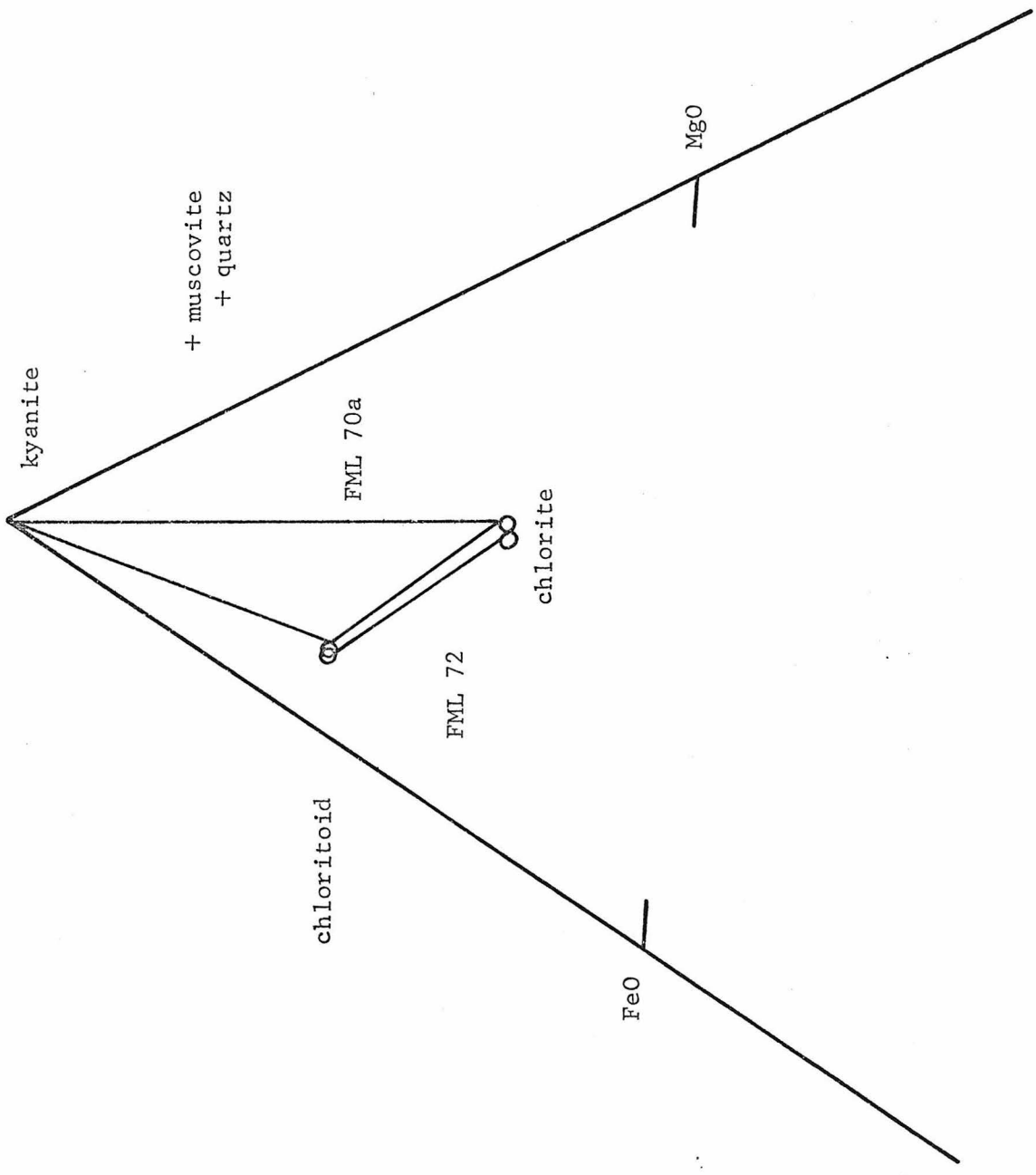

Figure 54b:

ASSEMBLAGES FROM LOWER GRADE PART OF THE GARNET ZONE

FUNERAL MOUNTAINS

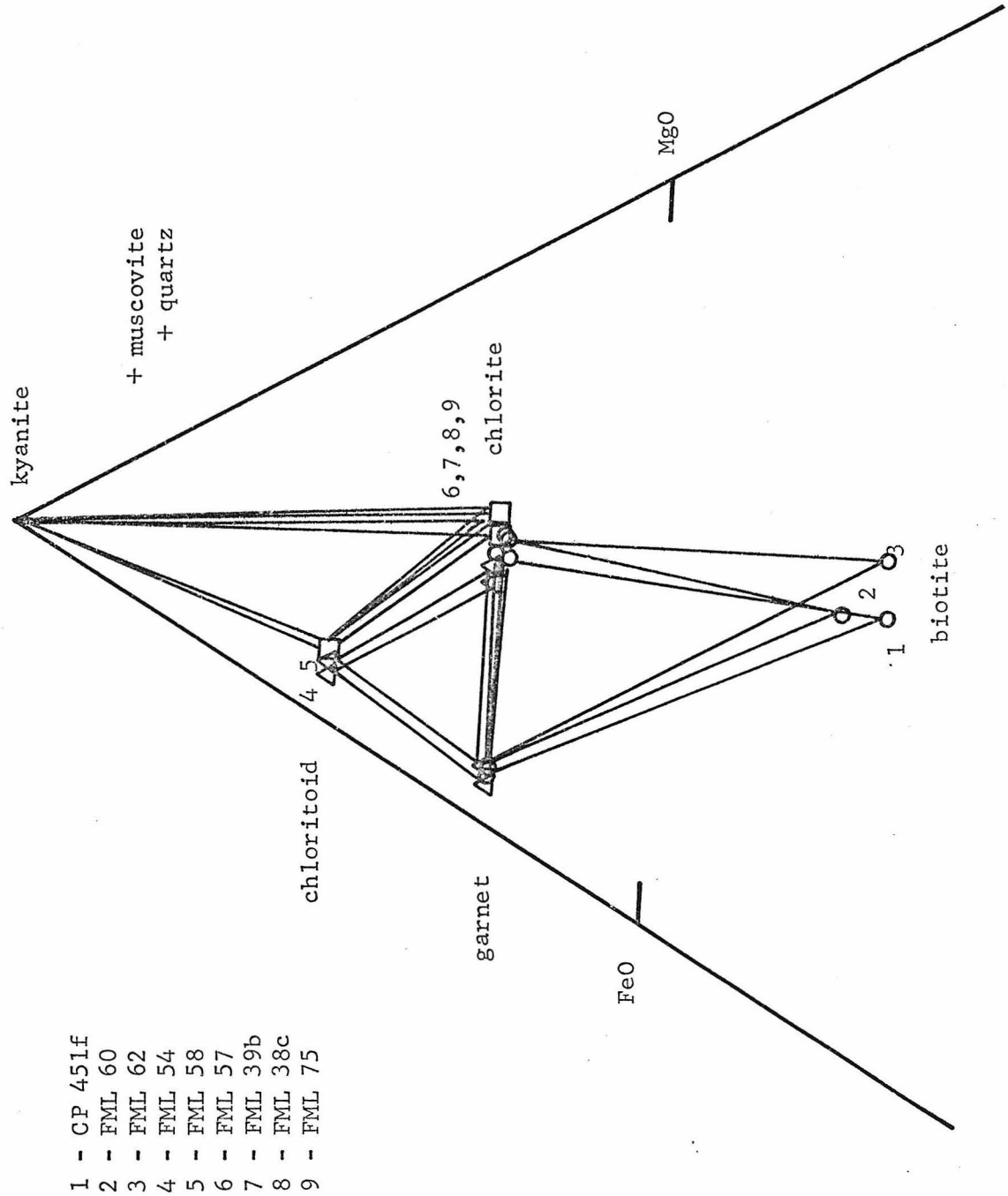

Figure 54c:

ASSEMBLAGES FROM THE HIGHER GRADE PART OF THE GARNET ZONE
FUNERAL MOUNTAINS

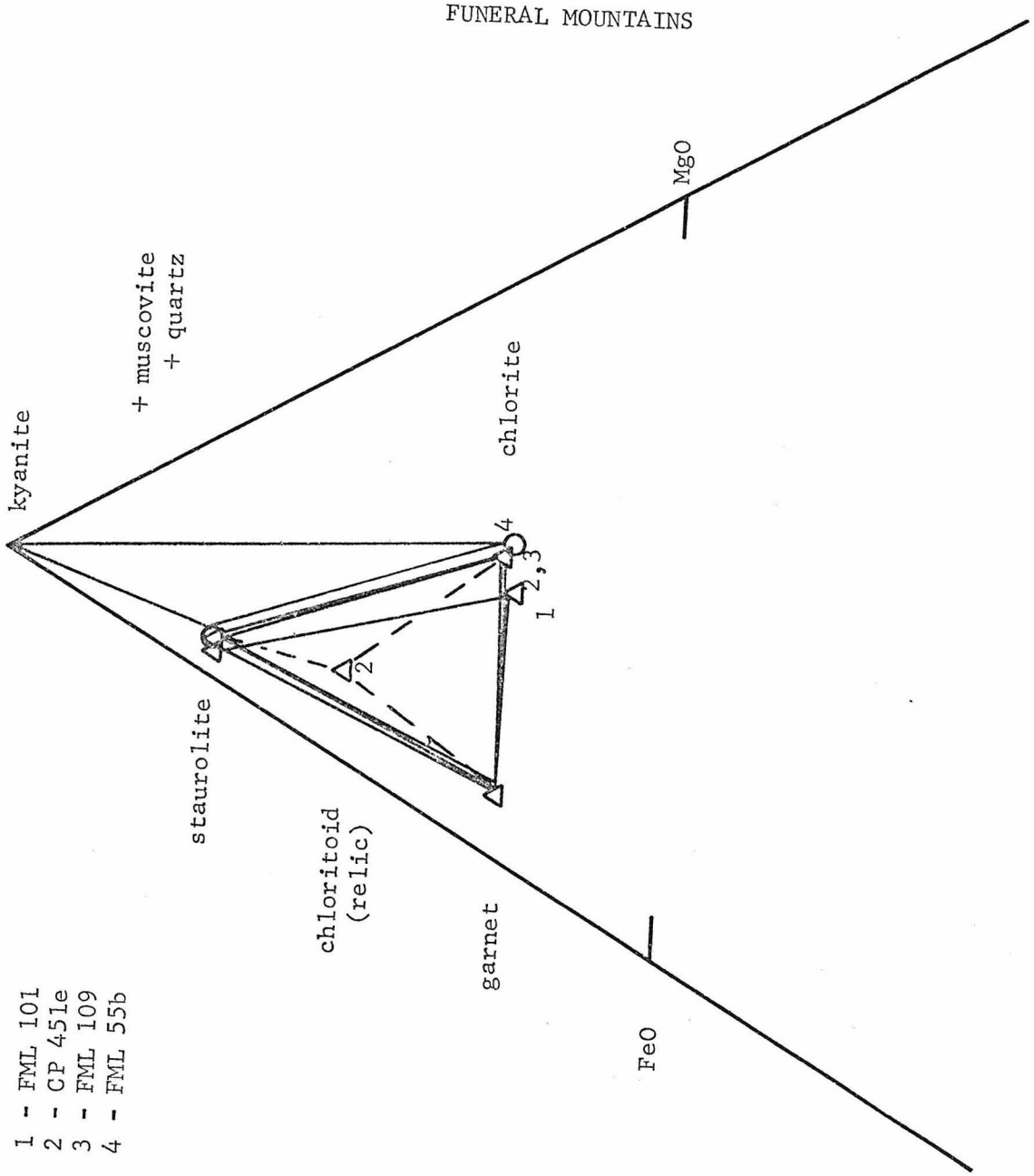

Figure 54d: ASSEMBLAGES FROM THE STAUROLITE ZONE, FUNERAL MOUNTAINS

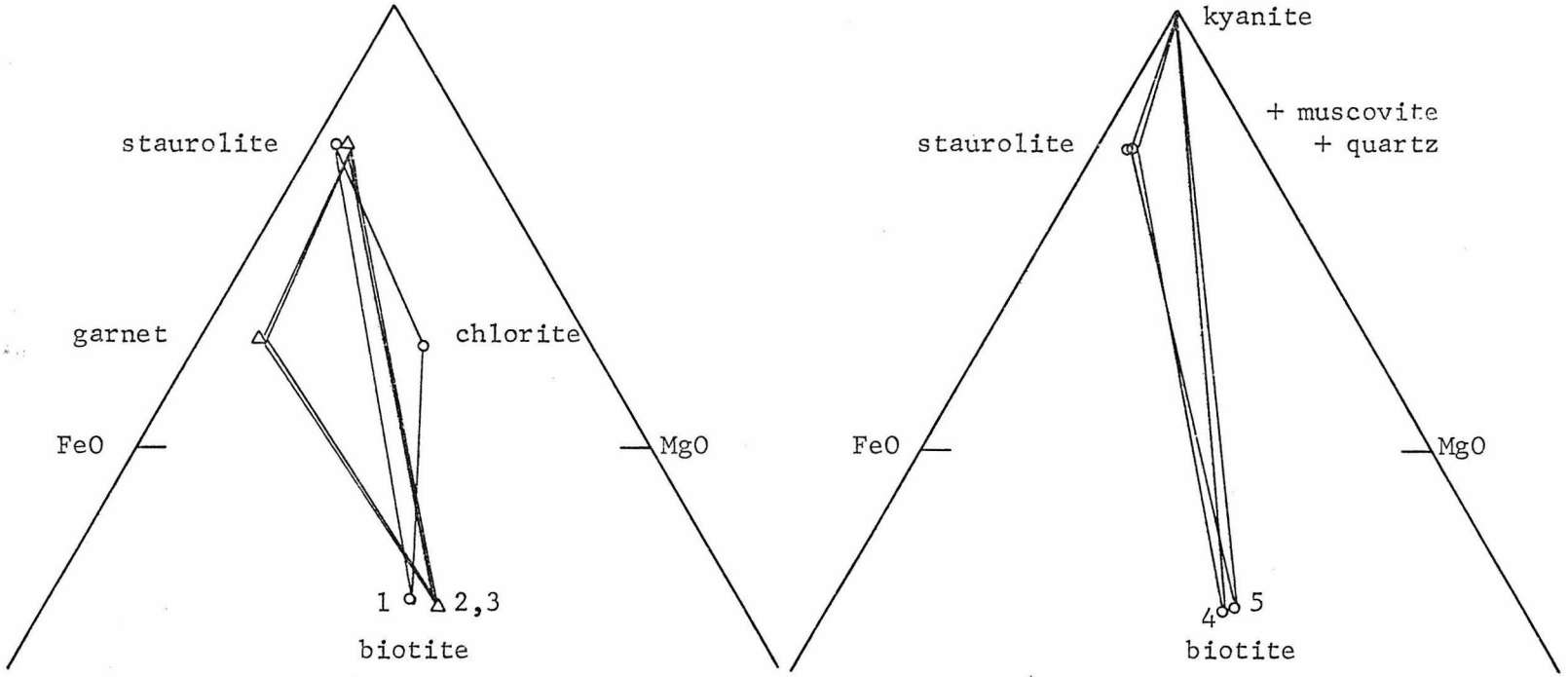

1 - FML 94a
2 - FML 106a
3 - FML 107a

4 - FML 104c
5 - FML 104a

Figure 54e:

ASSEMBLAGES FROM THE KYANITE ZONE, FUNERAL MOUNTAINS

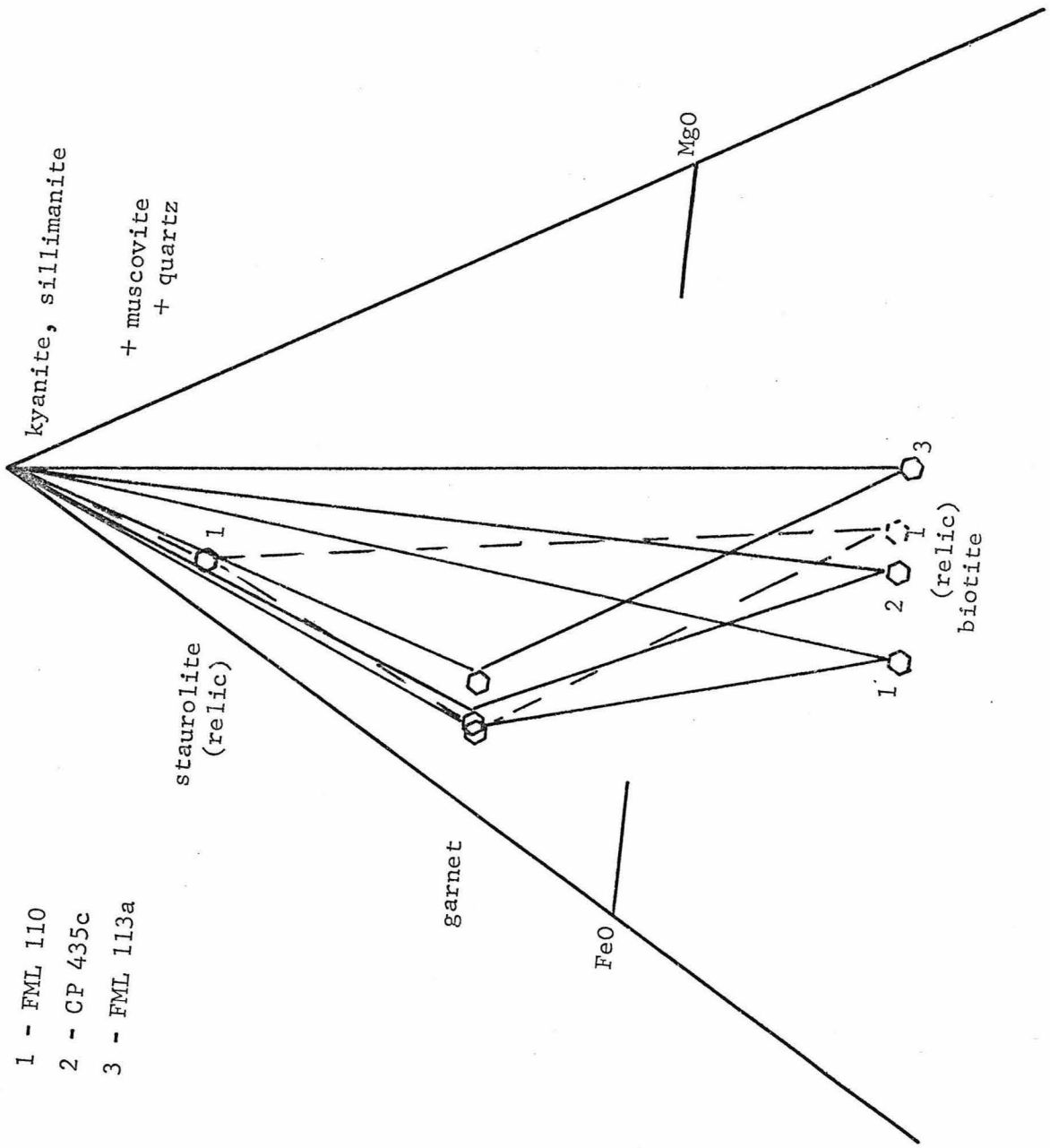

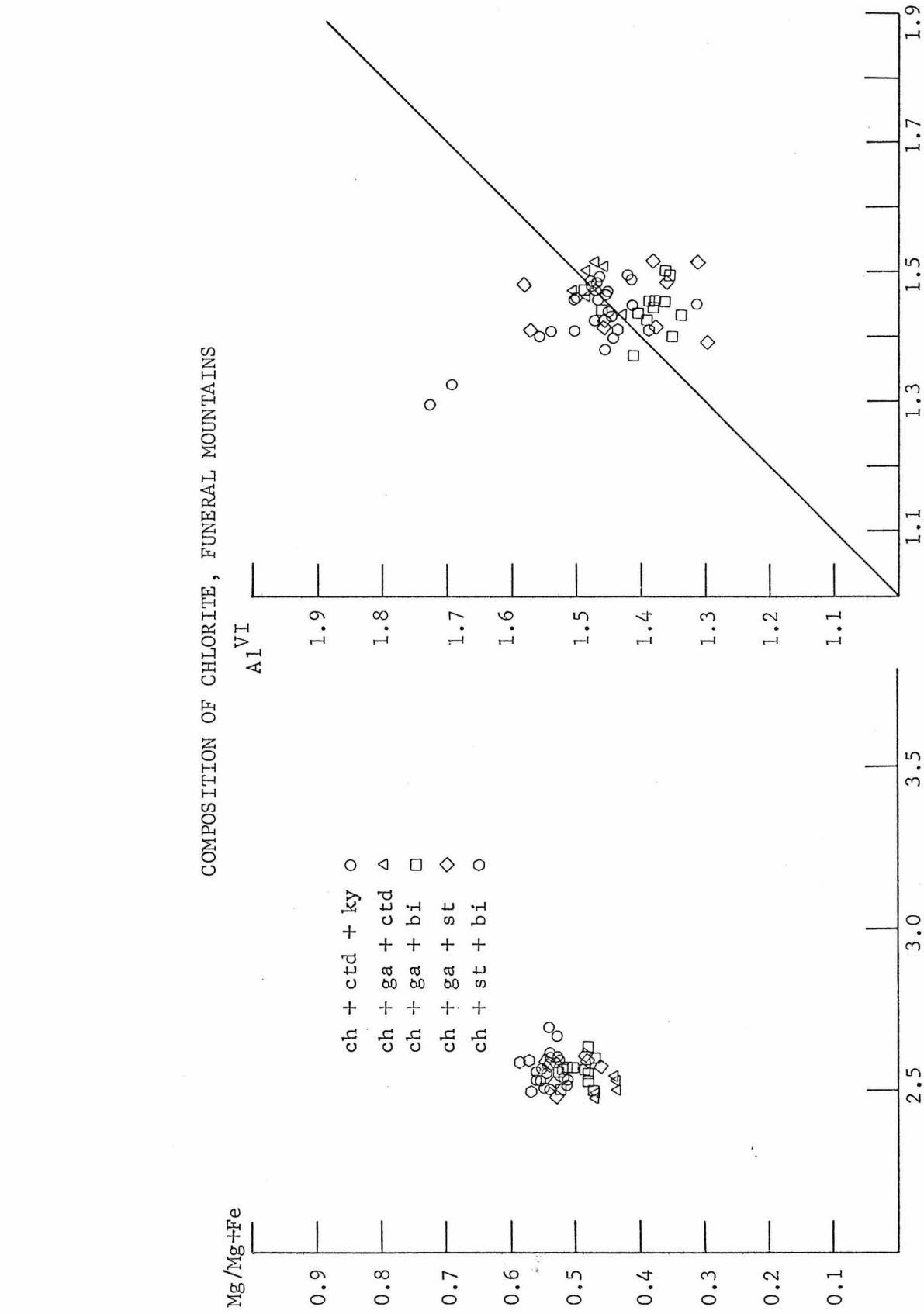
COMPOSITION OF CHLORITE, FUNERAL MOUNTAINS
ch + ctd + ky ○
ch + ga + ctd △
ch + ga + bi □
ch + ga + st ◇
ch + st + bi ○
Mg/Mg+Fe
0.9
0.8
0.7
0.6
0.5
0.4
0.3
0.2
0.1
2.5
3.0
3.5
Si
Al VI
1.9
1.8
1.7
1.6
1.5
1.4
1.3
1.2
1.1
1.1
1.3
1.5
1.7
1.9
Al IV

Figure 55

with biotite tends to be less aluminous than chlorite which coexists with more aluminous minerals. Chlorite with the ideal composition of $(Mg, Fe)_{6-X}Al_X^{VI}(Si_{4-X}Al_X^{IV})O_{10}(OH)_8$ should fall on the line $Al^{IV} = Al^{VI}$. Most analyzed chlorite corresponds to this expectation, but the substitution of up to $0.2Fe^{+3}$ cations/formula for Al^{VI} is indicated for analyses which contain an excess of Al^{IV} over Al^{VI}, and those analyses which shown an excess of Al^{VI} suggest the substitution $2Al^{VI} + \square \rightleftarrows 3FM^{VI}$.

Garnet shows a larger range in composition than chlorite, but this range in composition is principally due to the additional components MnO and CaO. All observed garnets are essentially stoichiometric $(Fe, Mg, Mn, Ca)_3Al_2Si_3O_{12}$; the amounts of TiO_2 and Cr_2O_3 are generally less than can be detected by the probe. Garnet grains are chemically zoned (Figure 56) and the greatest deviations from almandine-pyrope solid solutions are observed in garnet grade samples. The maximum amount of measured grossular is 20 mole % and up to 19 mole % spessartine is observed. The zoning patterns exhibited by garnet are of two types. In both types manganese decreases from core to rim, but calcium is observed to decrease or increase from core to rim.

Nearly all zoning patterns encompass compositional changes of less than 5 mole % for grossular or spessartine components. The change in amount of grossular and spessartine is generally balanced by a complementary change in the almandine component, and pyrope remains relatively constant. The decrease in manganese from core to rim in garnet is most likely attributable to a Rayleigh-fractionation process during garnet growth (Hollister, 1966) because garnet is essentially

Figure 56a:

GARNET FROM GARNET ZONE ASSEMBLAGES

FUNERAL MOUNTAINS

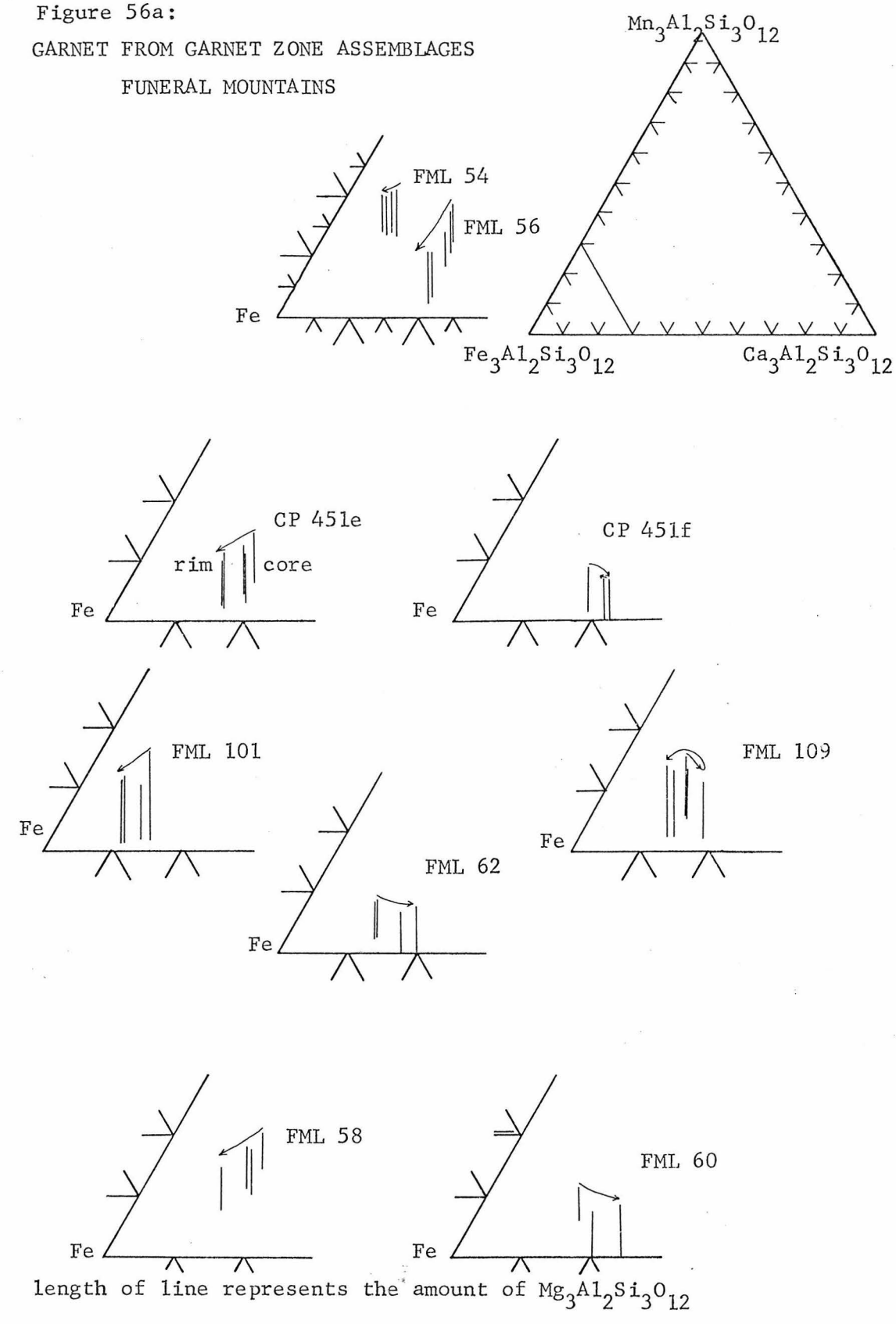

length of line represents the amount of $Mg_3Al_2Si_3O_{12}$

Figure 56b:

GARNET FROM STAUROLITE ZONE ASSEMBLAGES

FUNERAL MOUNTAINS

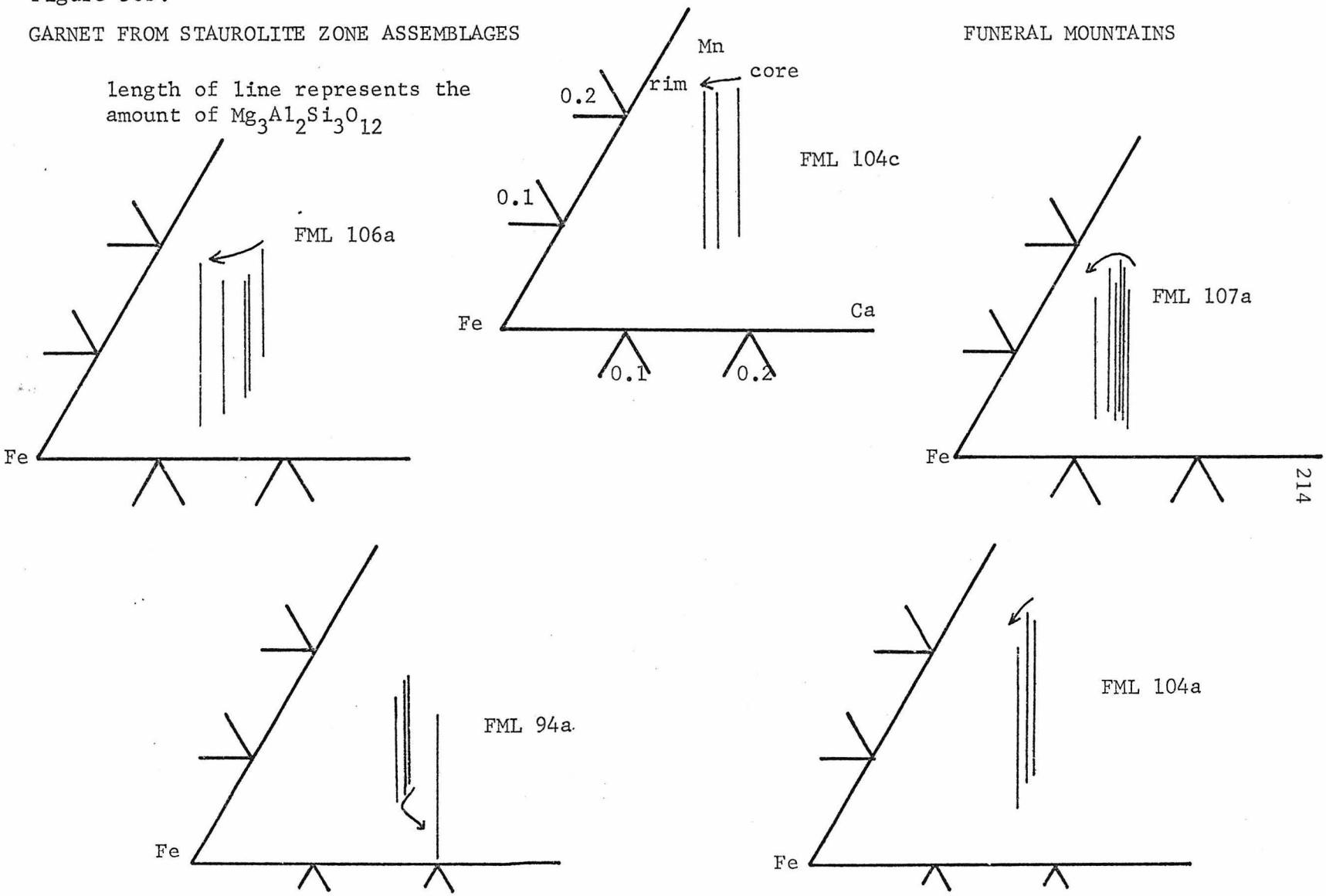

Figure 56c:

GARNET FROM KYANITE ZONE ASSEMBLAGES

FUNERAL MOUNTAINS

length of line represents the amount of $Mg_3Al_2Si_3O_{12}$

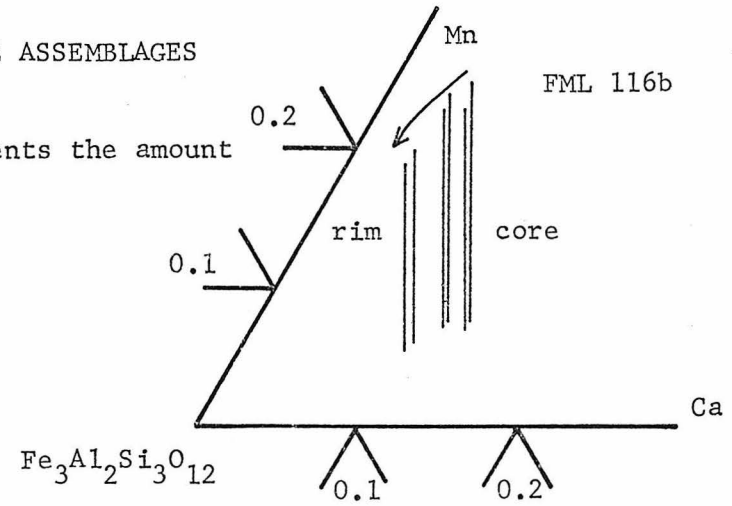

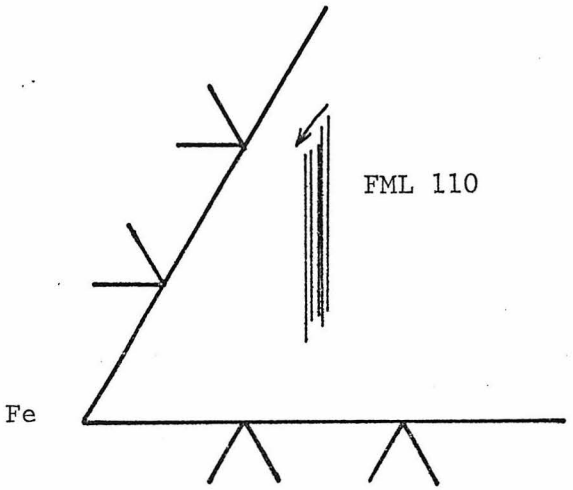

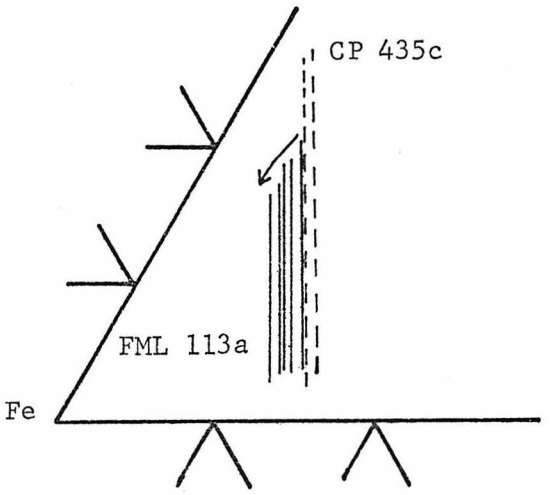

the only Mn-phase present. Ilmenite may contain up to 2 wt % MnO, but all other phases show only barely detectable amounts of manganese; the variations in calcium content may be related to continuous and discontinuous reactions involving plagioclase, and will be examined in greater detail below.

The amount of pyrope increases from about 5 mole % to 20 mole % with increasing grade, and the compositional range encompassed by garnet zoning decreases with increasing grade.

The distribution of Fe, Mg, Mn, and Ca between garnet rims and coexisting chlorite is shown in Figure 57. It was noted above that chlorite consists essentially of Fe and Mg but garnet contains substantial amounts of Ca and Mn as well. In the calcium-free system, the most iron-rich chlorite coexists with garnet which contains no manganese. As the amount of manganese in garnet increases, so does the amount of magnesium in chlorite. Similar relations hold in the manganese-free system. The occurrence of apparently crossing tie lines can arise by the addition of calcium to garnet as well as to the change in the intensive parameters P, T, and a_{H_2O}.

The variations in biotite chemistry are illustrated in Figure 58. The observed range in biotite compositions is quite limited. Mg/(Mg + Fe) varies between 0.40 and 0.60 and the Mg/Fe of biotite depends greatly on metamorphic grade and mineral assemblage (consult Figure 54). The partition of Fe and Mg between garnet and biotite has a strong dependence upon temperature and will be examined more closely in order to estimate the temperature of metamorphism. The aluminum content of biotite is confined to the range 1.6 to 1.7

Figure 57:
PARTITION OF Fe, Mg, Mn, and Ca BETWEEN COEXISTING GARNET AND CHLORITE, FUNERAL MOUNTAINS

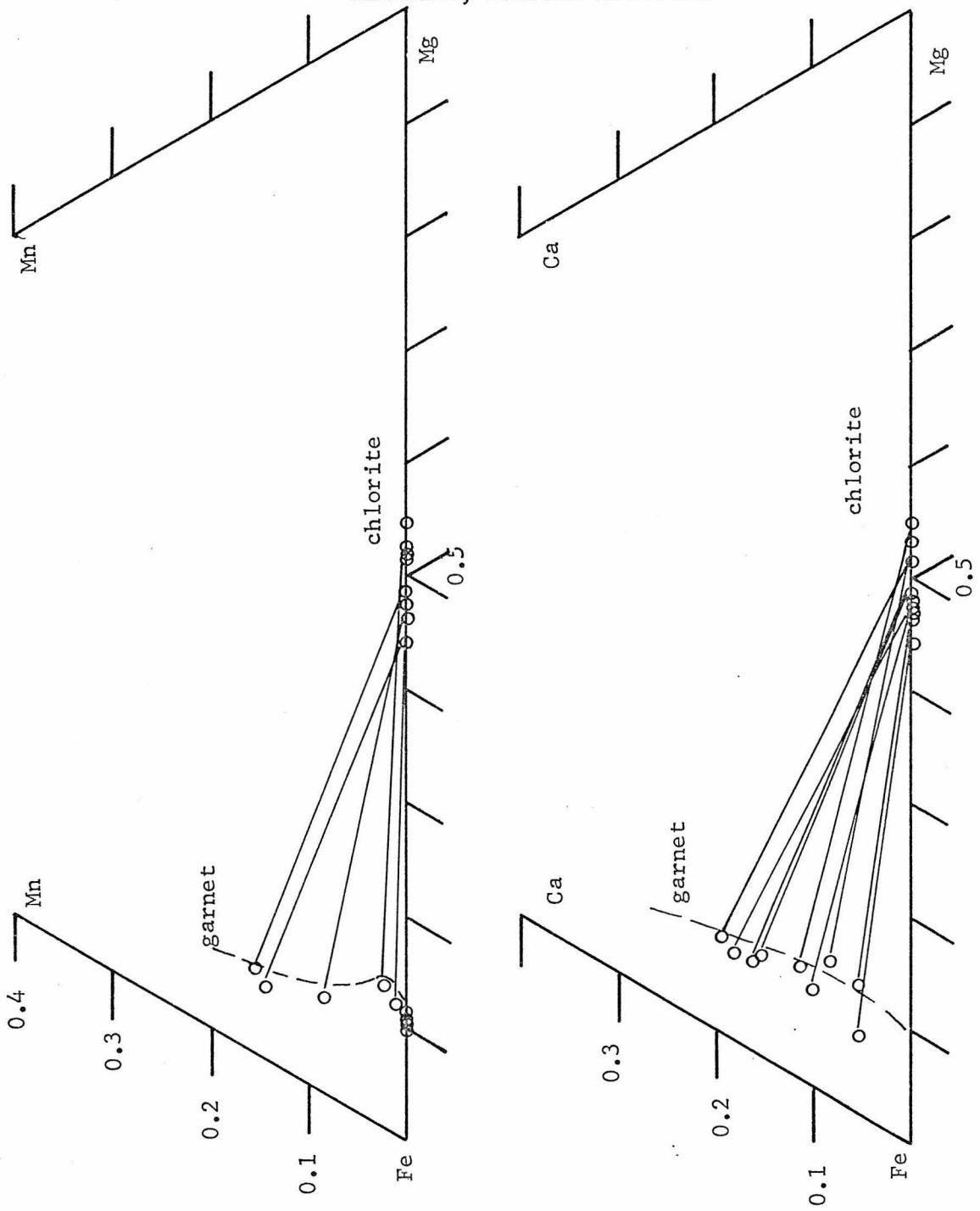

Figure 58: COMPOSITION OF BIOTITE, FUNERAL MOUNTAINS

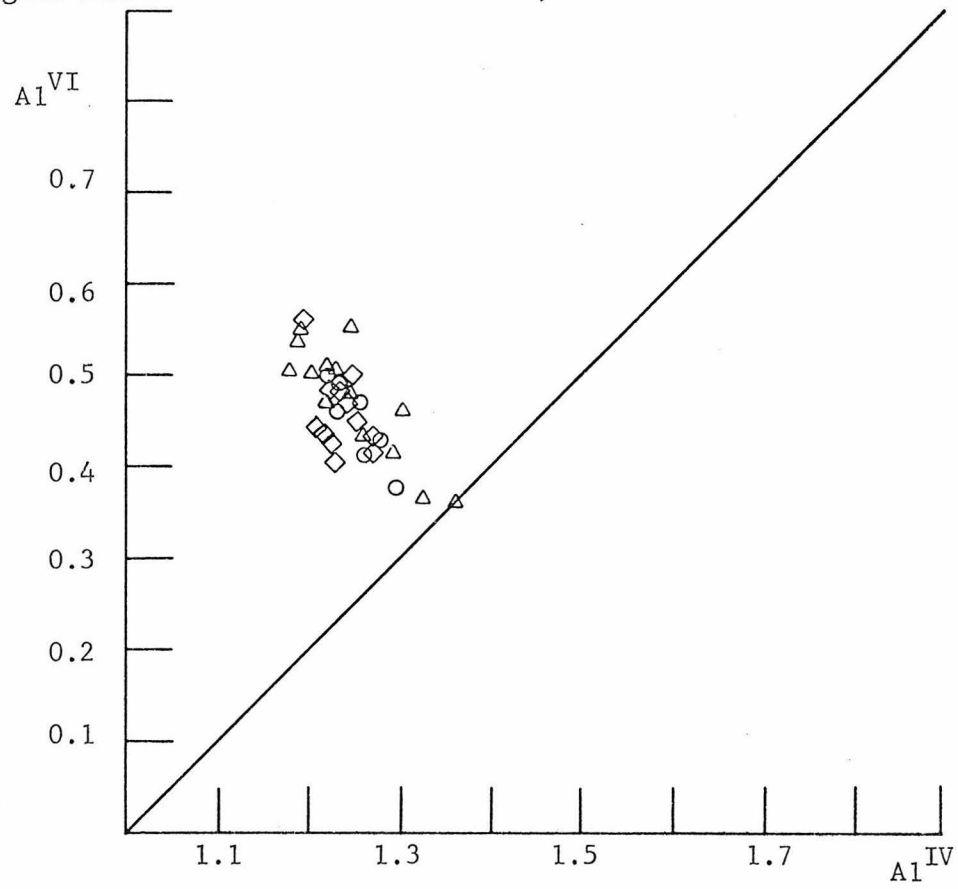

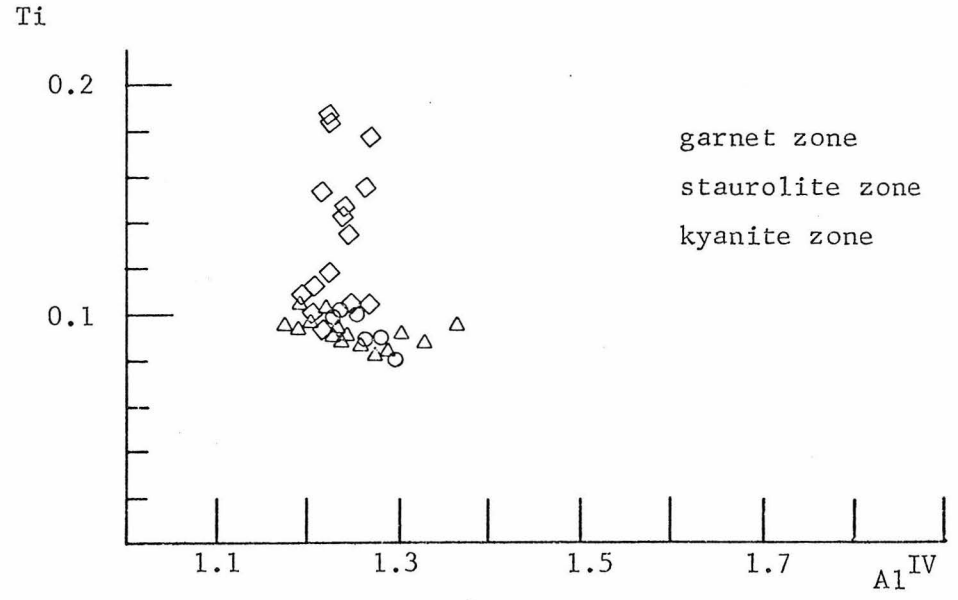

cations/formula, but nearly all analyses show an excess of Al^{VI} over Al^{IV}. There is an observed excess of up to 0.35 Al^{VI}/formula over the amount required by the substitution $Al^{VI} + Al^{IV} \rightleftarrows Fm^{VI} + Si^{IV}$ and a substitution of up to approximately 0.17 mole % dioctahedral mica is suggested.

Biotite from garnet and staurolite grade samples contains a uniform level of titanium, ranging from 0.08 to 0.11 cations/formula ($\sim$1.5 to 2.0 wt % TiO_2). In these assemblages ilmenite is the saturating titanium phase, but kyanite zone biotite from assemblages which contain rutile, contains up to 0.19 cations Ti/formula ($\sim$3.25 wt % TiO_2).

The sodium content in biotite is low and Na/(Na + K) ranges from 0.02 to 0.06 ($Na_2O < 0.4$ wt %). Biotite from staurolite zone assemblages tends to have more Na_2O than biotite from garnet or kyanite zone assemblages. Calcium occurs in amounts below the detection limit of the microprobe.

Chloritoid and staurolite consist essentially of FeO, MgO, Al_2O_3, SiO_2 and H_2O. Manganese usually occurs in amounts less than 0.2 wt % in staurolite, and less than 0.4 wt % in chloritoid. Zinc also occurs in these small amounts except in staurolite from FML 55b in which there is 2.5 wt % ZnO. Up to 0.5 wt % TiO_2 is present in staurolite. The amounts of manganese and zinc are very small (except in garnet cores) so that the ratios Mn/Fe and Zn/Fe encompass the range 0.0 to 0.01. Nothing can be said confidently regarding the relative partitioning of these elements except that garnet concentrates manganese and staurolite concentrates zinc.

The principal variations in the chemistry of these minerals is in the Mg/Fe ratio. Figure 59 illustrates the distribution of iron and magnesium among coexisting mafic phases. The partition of iron and magnesium among coexisting mafic phases is quite regular. Chlorite is always the most magnesium-rich and biotite is always slightly more iron-rich. Garnet is the most iron-rich phase and chloritoid and staurolite have Mg/Fe values intermediate to garnet and biotite. The relative partition of Fe and Mg between chloritoid and staurolite is difficult to assess because coexisting chloritoid and staurolite have not been observed. In one sample (CP 451e) chloritoid occurs as inclusions in garnet in a garnet + staurolite + chlorite assemblage and the staurolite over chloritoid is consistent with the observations in Panamint Mountains assemblages and with the suggestions of Albee (1972). Not only is the order of iron enrichment chlorite < biotite < chloritoid < staurolite < garnet observed, but the distribution coefficients ($K_D \equiv (Mg/Fe)^{\alpha}/(Mg/Fe)^{\beta}$) show only small variations (equal distances between two minerals represents equal K_D because $\log K_D = \log (Mg/Fe)^{\alpha} - \log (Mg/Fe)^{\beta}$). This relative consistency in Fe and Mg partition among coexisting mafic phases and constancy of total aluminum content in biotite and the relatively regular aluminum content in chlorite suggest chemical equilibrium was closely approached during metamorphism. The small variations in K_D (Fe/Mg) are attributable to variations in the intensive thermodynamic parameters or especially in the case of garnet to the addition of calcium and manganese.

It is interesting to note that in sample FML 94a in which on a textural basis garnet is interpreted to be a relic in the assemblage

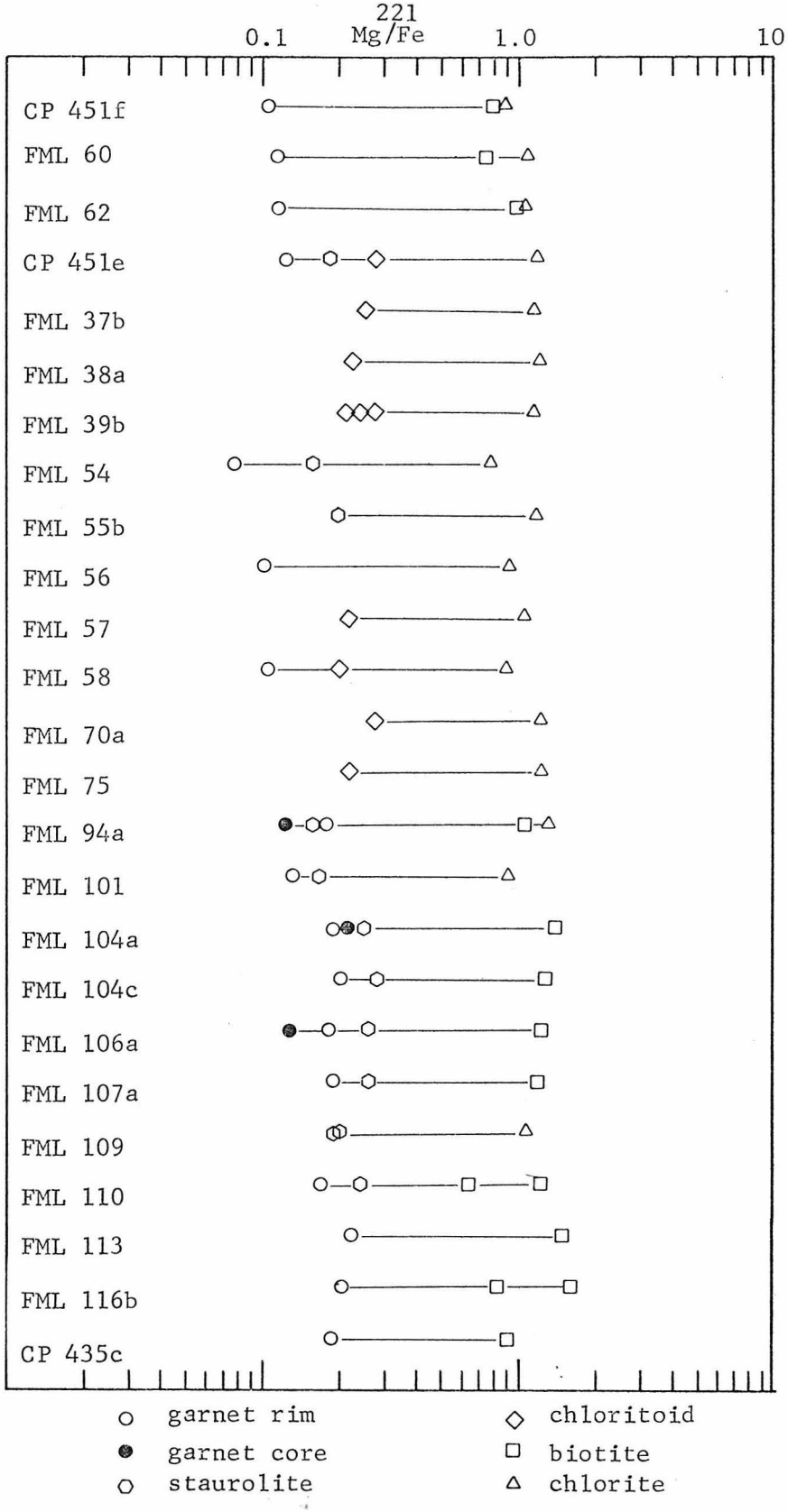

Figure 59a: Distribution of Fe and Mg among coexisting phases, Funeral Mountains.

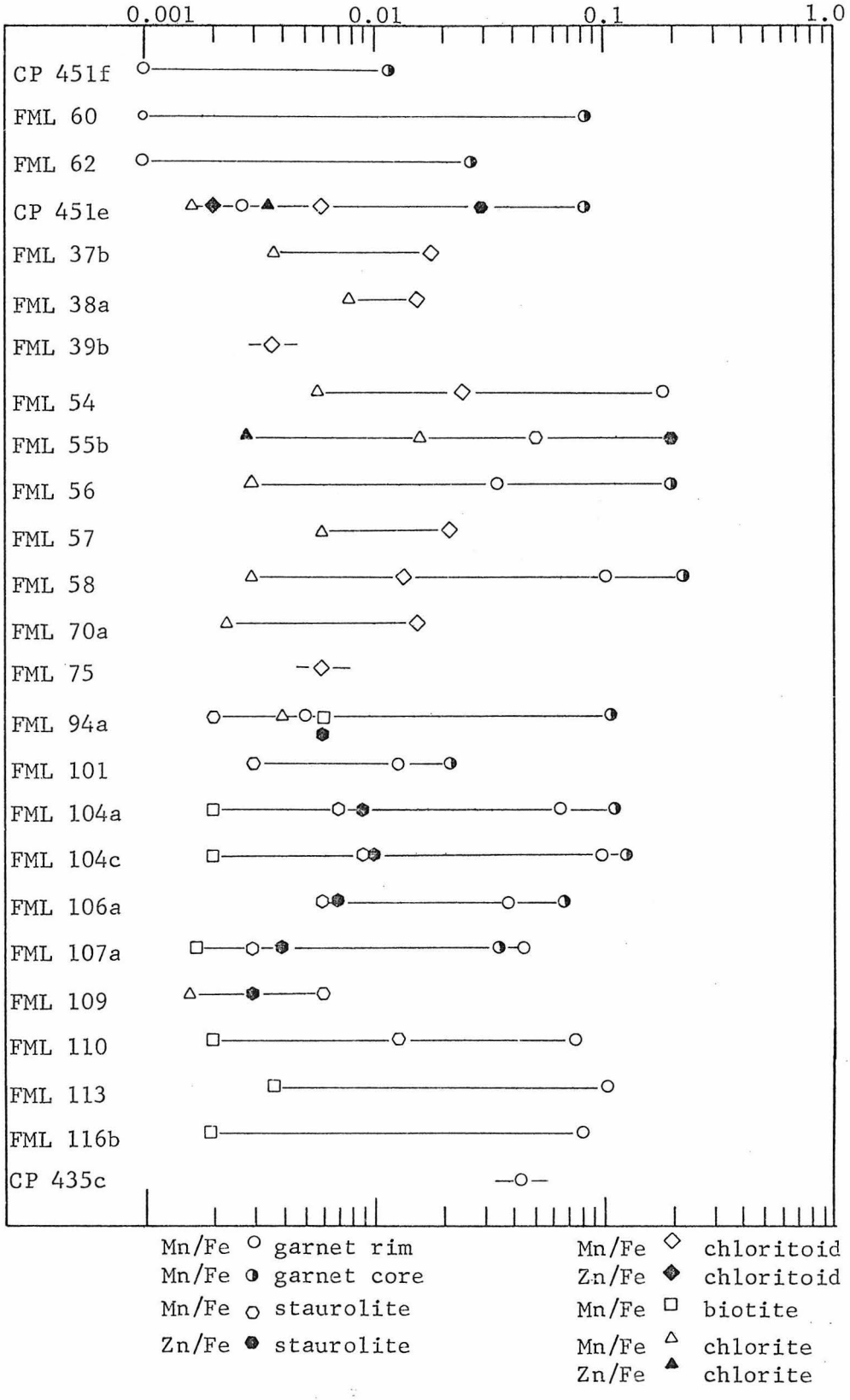

Figure 59b: Distribution of Fe, Mn, and Zn among coexisting phases, Funeral Mountains.

staurolite + chlorite + biotite, the garnet rim is more magnesium-rich than staurolite. This observation is contrary to the common observation that garnet is the more iron-rich mineral, and this apparent reversal in K_D is consistent with the interpretation that garnet is not stable in this assemblage.

A Na K Ca Phases

Most all of the assemblages considered here contain three AFM phases in addition to muscovite and quartz and are invariant to small arbitrary changes in intensive variables. Most all rocks contain sodium and calcium as additional components and here the nature of the saturating phases is considered. In the Funeral Mountains plagioclase, paragonite, and margarite occur as the sodium and calcium saturating phases.

Muscovite occurs in all assemblages in a variety of textures ranging from fine-grained sericite to coarse plates. The composition deviates only slightly from $KAl_3Si_3O_{10}(OH)_2$ as shown in Figure 60. Sodium substitutes for potassium in amounts up to 0.15Na/(Na + K) in lower garnet grade samples and approximately 0.25 in muscovite which coexists with paragonite(?). The sodium content attains values of up to 0.3Na/(Na + K) in the higher grade samples.

The amount of phengite substitution is likewise small. The maximum amount of silicon observed is 3.12/formula garnet grade samples and about 3.06/formula in staurolite and kyanite grade samples. In the low grade assemblages, muscovite which coexists with biotite contains more of the $Si + Mg \rightleftarrows Al^{IV} + Al^{VI}$ substitution than muscovite

SODIUM AND SILICON IN MUSCOVITE, FUNERAL MOUNTAINS

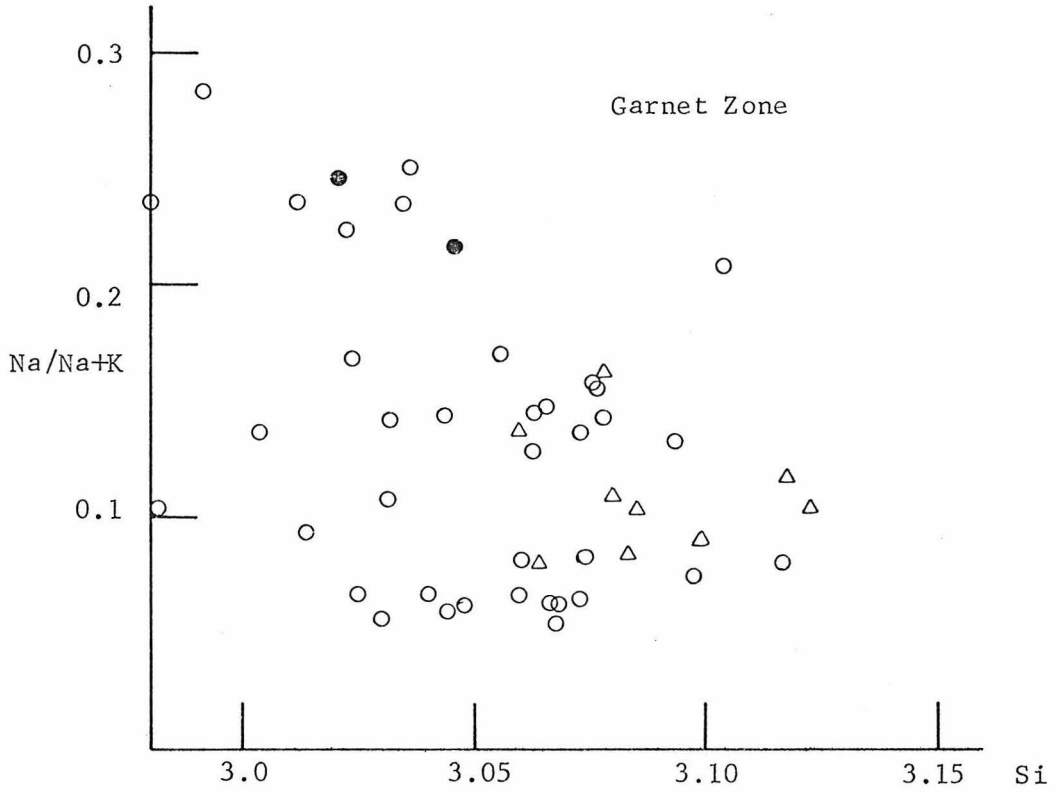

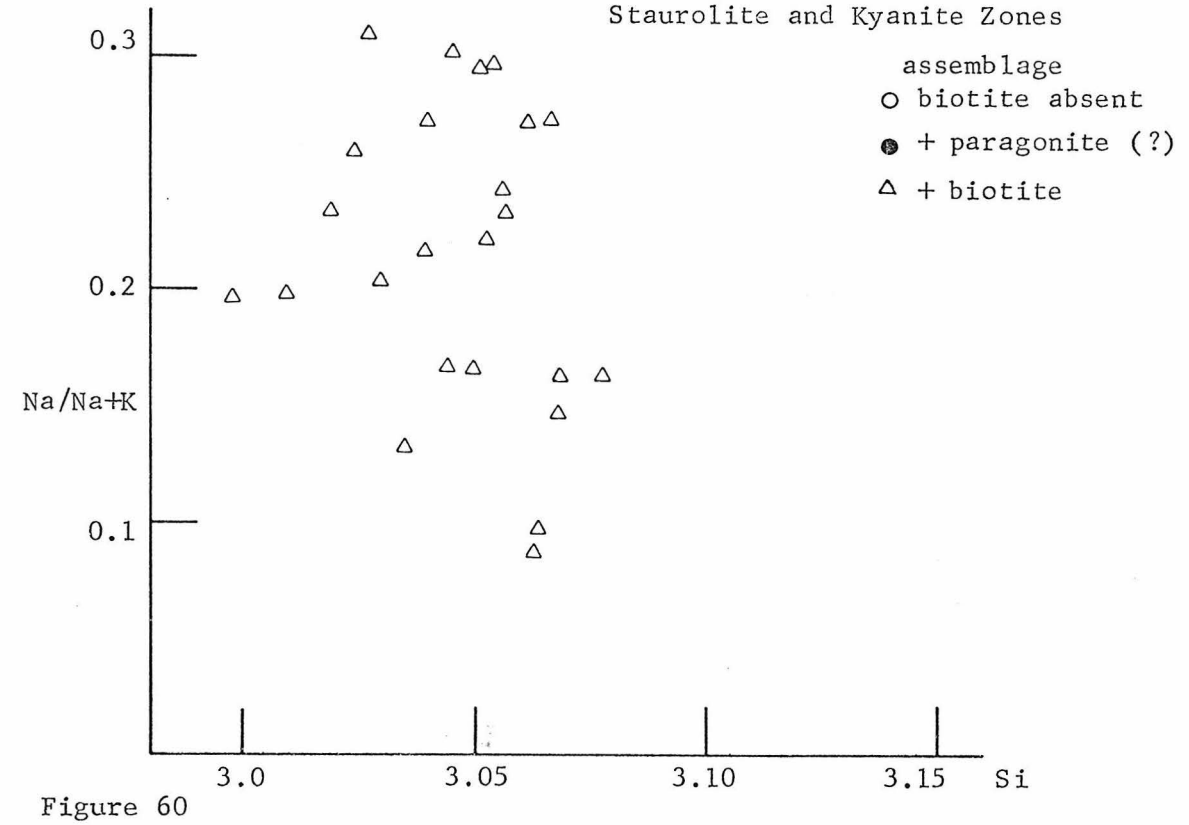

Figure 60

from biotite-absent assemblages. All higher grade assemblages contain biotite which suggests that with increasing grade, the phengite content of muscovite decreases.

The excess silica in muscovite is balanced by the substitution of FeO and MgO for octahedral aluminum. Muscovite analyses indicate 0.5 to 0.6 wt % MgO and 1.0 to 2.5 wt % "FeO". Most of the iron appears to be ferric because the excess silica is nearly balanced by the MgO present and the total positive change indicated is nearly always less than the theoretical value of 22.0. Muscovite from hematite-bearing assemblages tends to contain more "FeO" (nearly all of which must be Fe_2O_3) than muscovite from hematite-free assemblages.

Paragonite has been tentatively identified in FML 58 which contains the assemblage garnet + chloritoid + chlorite. The sample has not been x-rayed, but during microprobe analysis of fine-grained white mica, a sodium-rich, potassium-poor mica was encountered. The cation sum of Na + K + Ca is much less than one, and the ratio Na/(Na + K + Ca) was estimated with the assumption that only sodium was lost during analysis. A systematic search for paragonite has not been done, so its distribution among different assemblages is unknown.

Margarite occurs in one low grade assemblage chloritoid + chlorite (FML 72). The margarite appears as $\sim$2 mm blades in a fine-grained matrix. The distribution of Na, Ca, and K in coexisting white micas is illustrated in Figure 61, which shows that even muscovite which coexists with margarite contains no calcium.

Plagioclase occurs in most assemblages except chloritoid + chlorite + kyanite and garnet + chlorite + chloritoid. Plagioclase in

Figure 61:
COMPOSITION OF COEXISTING WHITE MICA, FUNERAL MOUNTAINS

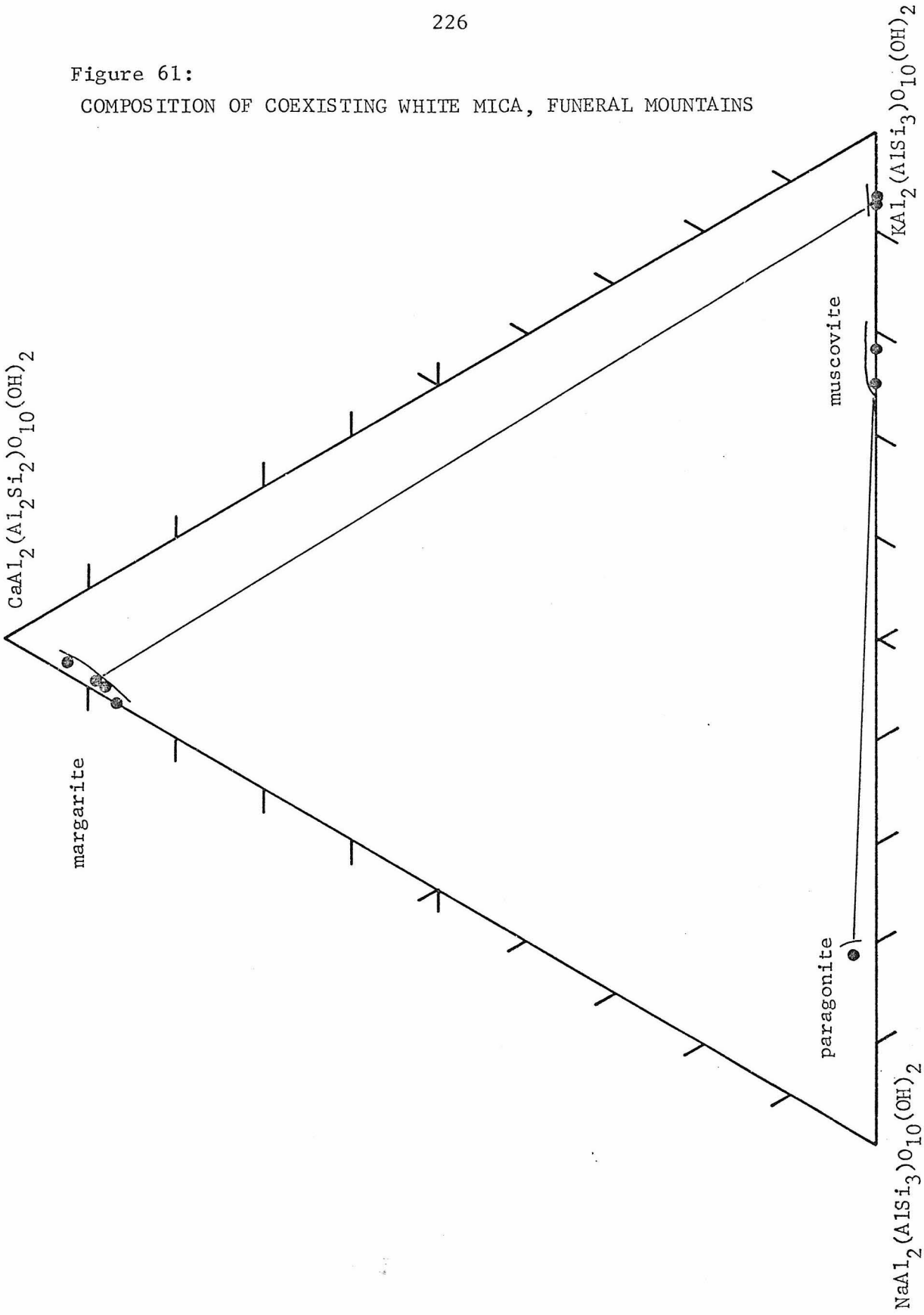

garnet grade samples tends to form rounded porphyroblasts which contain quartz inclusions. Plagioclase in staurolite and kyanite grade samples occurs in twinned grains in a quartz-plagioclase mosaic.

The compositions of plagioclase and coexisting muscovite are shown in Figure 62. Plagioclase contains essentially no potassium and the observed compositional range is An_{60} to An_{8}. Zoning and grain to grain compositional variations are small except as noted below. In FML 56 plagioclase with a composition of An_{35} occurs with plagioclase An_{8}. The plagioclase contains multitudinous inclusions and only one plagioclase of composition An_{8} was observed. Hence it is difficult to determine whether the two compositions coexist due to immiscibility or whether the two are related by zoning or reaction. No other samples were observed which contain the same relation.

The plagioclase in sample FML 60 is the most calcic feldspar observed and does exhibit zoning from a calcium rich core (An_{60}) to a more sodic rim (An_{45}). This sample contains the most calcium-rich garnet and the zoning in garnet (Figure 56) is toward more calcium-rich compositions, opposite to the plagioclase zoning pattern. Figure 63 shows that the more calcium-rich garnets tend to coexist with more calcium-rich plagioclase and that because these are the only calcium phases present the calcium content of both is controlled to some degree by the amount of calcium in the total rock. Among these garnet grade samples there is a fairly regular relation between the Na/(Na + Ca + K) ratios in muscovite and coexisting feldspar. The more sodium-rich muscovites tend to coexist with the more sodium-rich feldspars. Staurolite and kyanite grade samples contain plagioclase

Figure 62:

COMPOSITION OF COEXISTING MUSCOVITE AND PLAGIOCLASE, FUNERAL MOUNTAINS

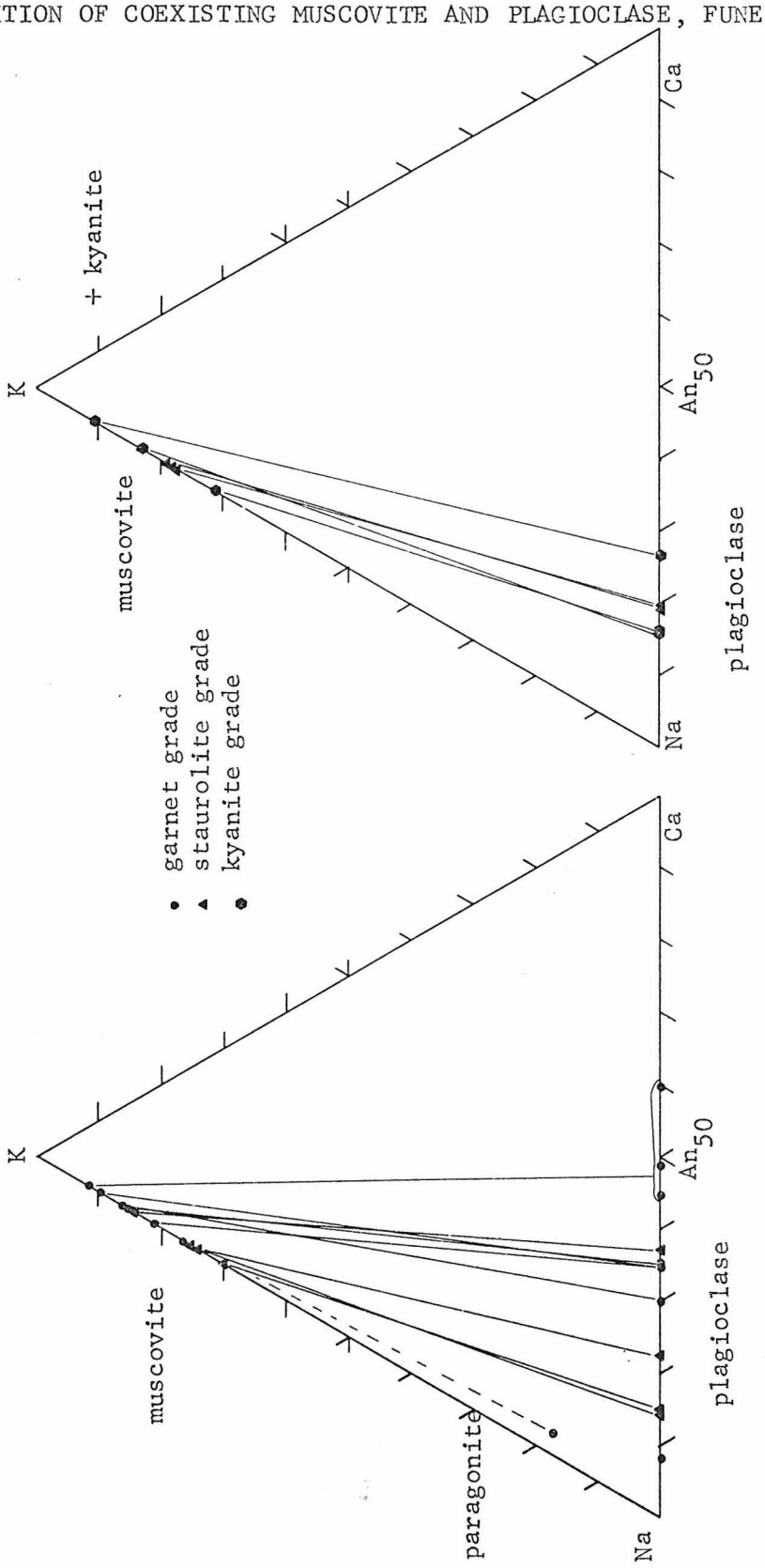

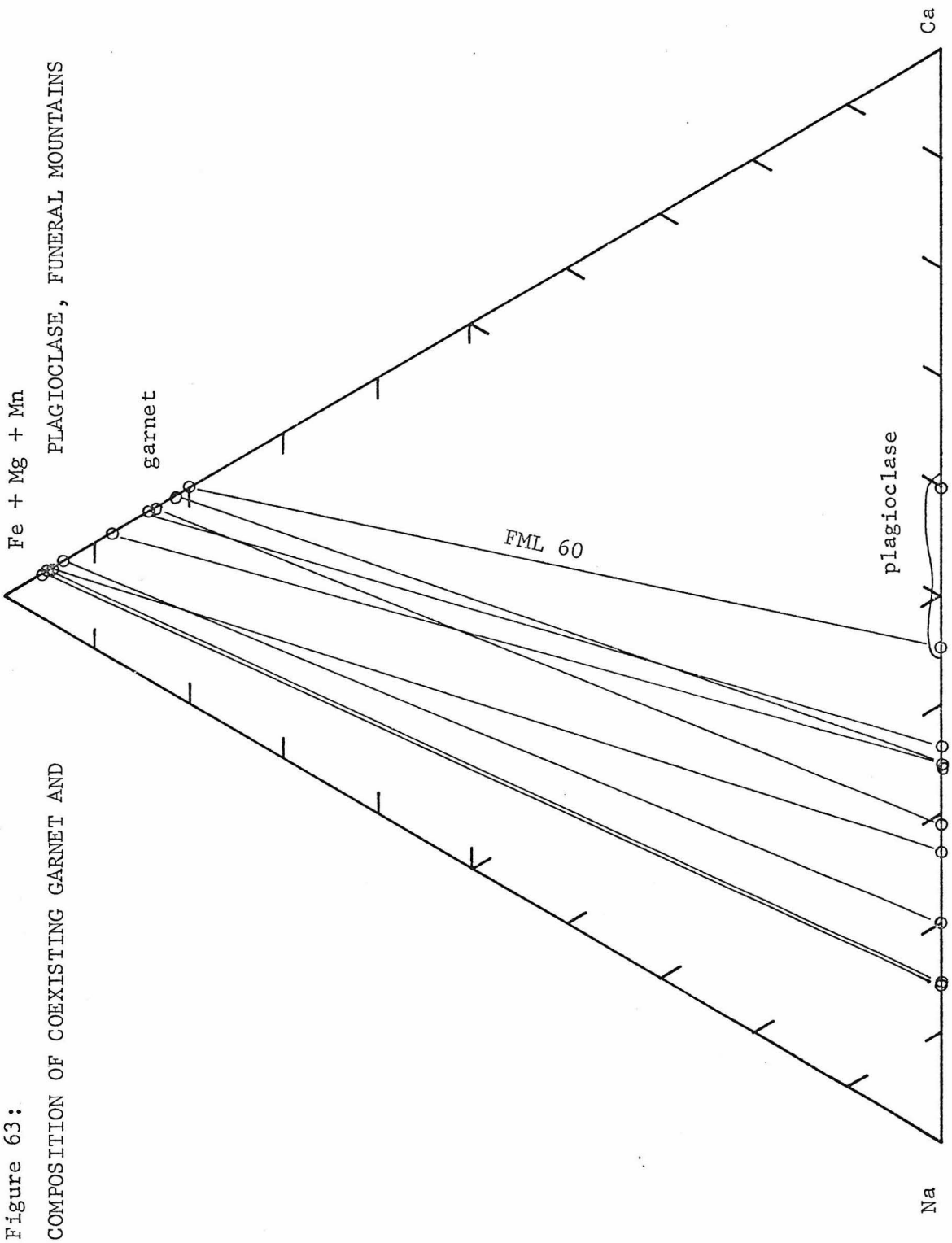

Figure 63:
COMPOSITION OF COEXISTING GARNET AND PLAGIOCLASE, FUNERAL MOUNTAINS

in the compositional range An_{15} to An_{25} and coexisting muscovite is correspondingly more sodium-rich (Figure 62).

Fe-Ti Phases

All mineral assemblages contain Fe-Ti phases. Ilmenite is the most common, and it occurs in the assemblages garnet + chlorite + biotite, garnet + chlorite + chloritoid and garnet + staurolite + chlorite in the garnet zone, and in the higher grade assemblages garnet + staurolite + biotite, staurolite + biotite + chlorite, kyanite + staurolite + biotite, and kyanite + garnet + biotite. Every ilmenite analysis shows more Ti than required by ilmenite, and the presence of minute rutile lamellae is indicated. In general MgO occurs in amounts less than 0.1 wt % and MnO less than 1.0 wt %. The maximum MnO observed is 2.0 wt %.

Rutile occurs in the low grade assemblage kyanite + chlorite + chloritoid, and the high grade assemblages kyanite + staurolite + biotite and kyanite + garnet + biotite.

Ferric iron phases are observed in only the assemblage kyanite + chlorite + chloritoid. Hematite occurs as small (<0.5 mm) plates and as pseudomorphs after magnetite cubes. The remnant magnetite is essentially pure Fe_3O_4 and the hematite rim on magnetite is pure Fe_2O_3. The smaller matrix hematite plates apparently contain up to 50 mole % $FeTiO_3$ (Figure 64). Most of these associations contain rutile in addition. The unusually high TiO_2 content in hematite suggests that there are minute ilmenite lamellae present which may have exsolved during retrograde metamorphism.

Figure 64:

COMPOSITION OF Fe - Ti OXIDE PHASES, FUNERAL MOUNTAINS

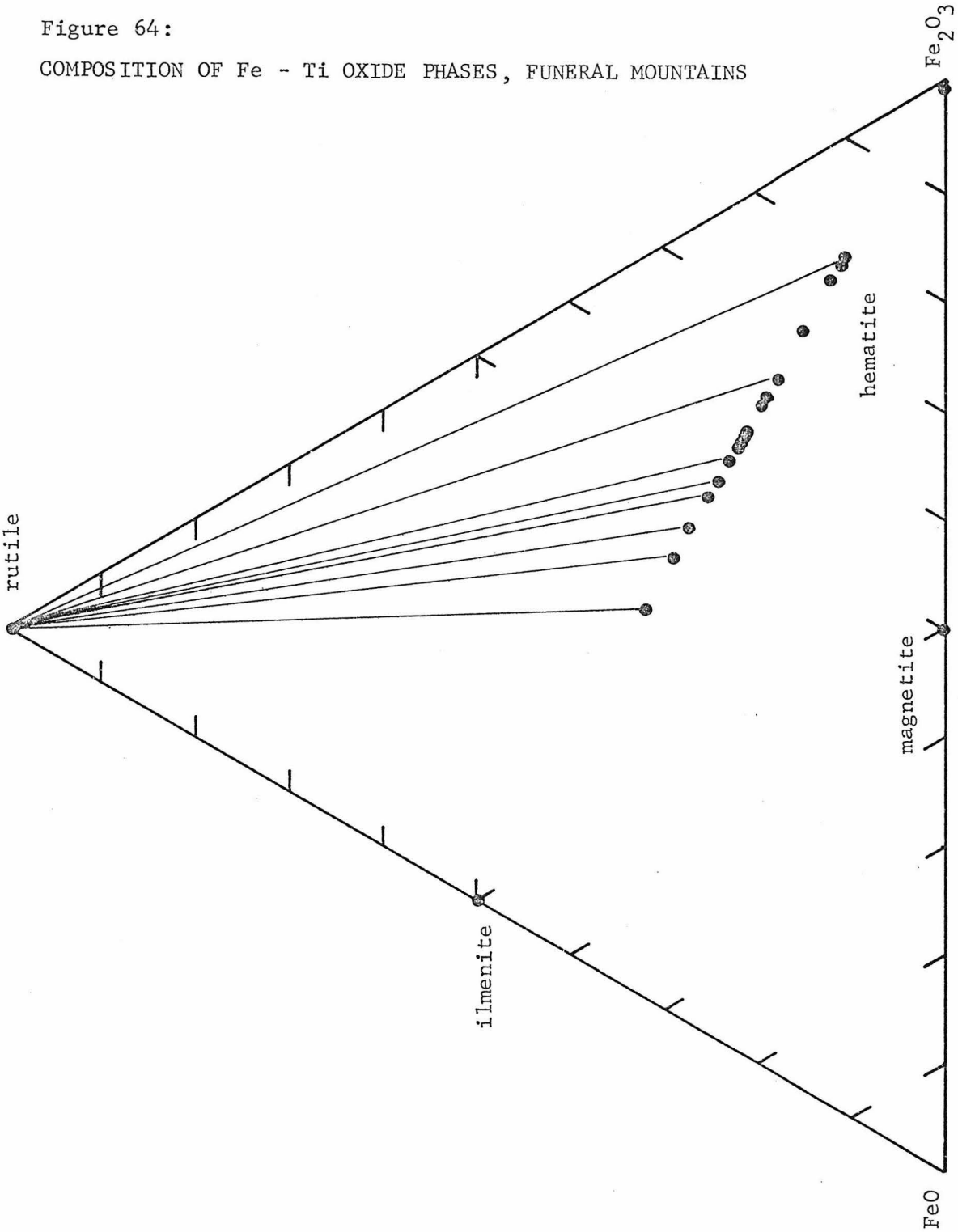

MINERAL FACIES AND REACTIONS

The range in bulk composition and metamorphic grade provide a surprisingly complete determination of mineral facies in a Barrovian metamorphic terrain. The details of the facies types which involve Ca, Na, Fe^{+3} phases are at present only sketchy, but enough information exists to suggest the phase relationships. Figure 65 illustrates the generalized facies types which describe the distribution of elements among coexisting facies during the metamorphism of the Funeral Mountains.

These AKFM mineral facies are very similar to those exhibited by other Barrovian terrains where the complete facies types have been determined, principally in the New England regional metamorphic terrain. The assemblages in garnet grade rocks from Indian Pass are identical to those found at Mt. Grant in Vermont (Albee, 1965a and Figure 65a). Even the incomplete information regarding the saturating Fe^{+3}, Ti, and Na phases is compatible with the Mt. Grant assemblages. By analogy, the undetermined phases may be assigned. Magnetite should occur in the assemblages garnet + chlorite + chloritoid and garnet + chlorite + biotite; paragonite should occur in the assemblage kyanite + chlorite + chloritoid.

The staurolite zone assemblages shown in Figure 65e are very similar to the assemblages exhibited by the Gassetts schist, Vermont (Thompson and others, 1977). Ferric iron phases do not occur in the analyzed samples from the Funeral Mountains and plagioclase rather than paragonite coexists with kyanite.

Titanium phases occur in all observed assemblages. Rutile occurs

AKFM PELITIC SCHIST ASSEMBLAGES

FUNERAL MOUNTAINS

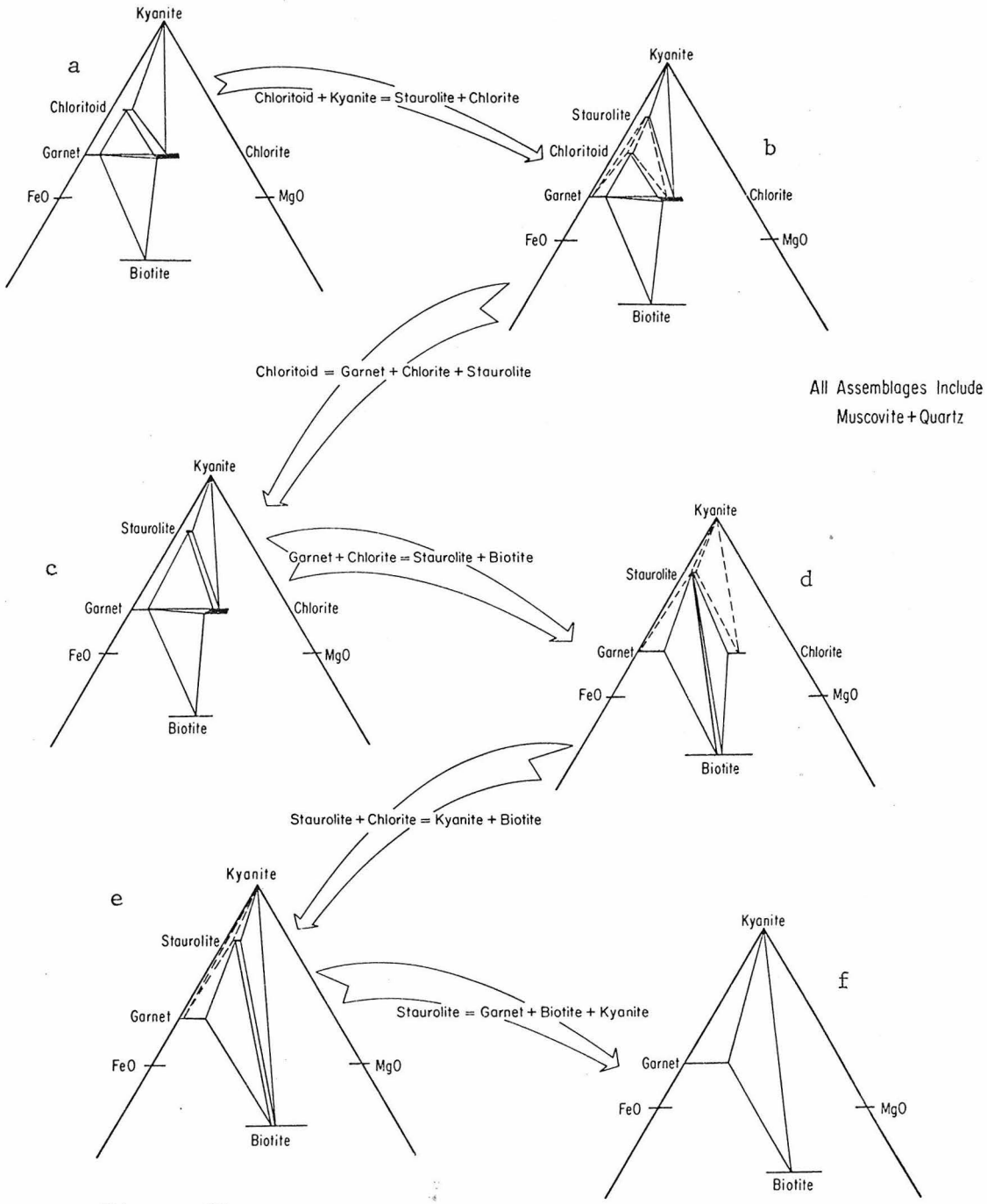

Figure 65

in alumino-silicate-bearing assemblages; whereas, ilmenite occurs in all others. The distribution of Fe^{+3} and Na phases among the assemblages is not well documented but paragonite and magnetite probably may occur in high aluminum and low aluminum assemblages respectively.

All of the assemblages and the sequence of facies types are very similar to those found in the regional metamorphic terrains in northern Vermont (Albee, 1968) and in the Barrovian terrain in Scotland (Harte, 1975) except that staurolite breaks down prior to the kyanite to sillimanite transition. Each facies type is related to another by a discontinuous reaction which either represents a change in mineral compatabilities or a termination of a phase. The reactions which relate the changes in facies in the system AKFM are

1) unknown and probably complex garnet-forming reactions
2) incoming of staurolite by chloritoid + kyanite = staurolite + chlorite
3) breakdown of chloritoid by chloritoid = garnet + chlorite + staurolite
4) break in garnet-chlorite association by garnet + chlorite = staurolite + biotite
5) elimination of chlorite from most rocks by staurolite + chlorite = kyanite + biotite
6) breakdown of staurolite by staurolite = garnet + kyanite + biotite
7) polymorphic inversion of kyanite to sillimanite

The stoichiometry of each discontinuous reaction may be ascertained by the natural composition data for mineral associations which are

stable on either side of an isograd. The present sample density does not permit the details of most reactions, but inclusions of relic mineral phases in garnet suggest the terminal compositions of chloritoid and staurolite.

Sample CP 451e preserves the probable terminal chloritoid as inclusions in garnet in a garnet + chlorite + staurolite assemblage. The compositions of the phases in this sample provide the terminal chloritoid reaction

$$10Fe_{1.57}Mg_{0.43}Al_4Si_3O_8(OH)_4 + 4.923SiO_2 + 1.139CaAl_2Si_2O_8 =$$

chloritoid quartz anorthite

$$3.255Fe_{2.35}Ca_{0.35}Mg_{0.30}Al_2Si_3O_{12} + 3.847Fe_{1.66}Mg_{0.34}Al_{26/3}Si_4O_{22}(OH)_2 +$$

garnet staurolite

$$0.816Fe_{2.04}Mg_{2.47}Al_{1.49}Al_{1.49}Si_{2.51}O_{10}(OH)_8 + 12.889H_2O.$$

chlorite

Anorthite is derived from plagioclase and such a reaction may cause plagioclase to become more sodic (see discussion below).

The termination of staurolite may also be approximated by the composition of staurolite inclusions in garnet in the garnet + kyanite + biotite assemblage from sample FML 110. The composition of biotite inclusions in garnet is also used because the biotite in the matrix has a significantly different Mg/Fe.

$$10Fe_{1.65}Mg_{0.35}Al_{26/3}Si_4O_{22}(OH)_2 + 0.906KAl_3Si_3O_{10}(OH)_2 + 15.552SiO_2 =$$

staurolite muscovite quartz

$$5.942Fe_{2.80}Mg_{0.40}Al_2Si_3O_{12} + 0.906KFe_{1.16}Mg_{1.24}Al_{1.74}Si_{2.74}O_{10}(OH)_2 +$$

garnet biotite

$37.962Al_2SiO_5 + 10H_2O$.

kyanite

The reaction has been simplified by combining Ca and Mn in garnet with Fe. Because muscovite is more sodium-rich than biotite, and because garnet contains significant calcium, any muscovite-consuming, garnet-producing reaction will be accompanied by an increase in the albite component in plagioclase. If both garnet and muscovite are consumed or produced (as in the crossover garnet + muscovite + chlorite = staurolite + biotite) the composition of plagioclase will not necessarily change.

The compositions of all phases in invariant associations is greatly affected by continuous and exchange reactions. The compositions of most mafic phases become more magnesium-rich with increasing grade. Biotite is an exception and once staurolite breaks down, biotite associated with garnet and kyanite becomes more iron-rich. The continuous reactions responsible for the changes in mafic mineral compositions are discussed in the final section.

The compositions of coexisting muscovite and plagioclase are governed by both exchange and continuous reactions. At low grades, the distribution of sodium between muscovite and plagioclase is represented by

$$NaAl_3Si_3O_{10}(OH)_2 + KAlSi_3O_8 = KAl_3Si_3O_{10}(OH)_2 + NaAlSi_3O_8$$

and

$$NaAl_3Si_3O_{10}(OH)_2 + CaAl_2Si_2O_8 = CaAl_4Si_2O_{10}(OH)_2 + NaAlSi_3O_8.$$

Because plagioclase contains essentially no K and muscovite contains

no Ca, the equilibrium constant for the first is very large and for the second very small. At higher grades plagioclase coexists with kyanite and the compositions of plagioclase and muscovite coexisting with kyanite and quartz are controlled by the continuous reaction

$$NaAl_3Si_3O_{10}(OH)_2 + SiO_2 = NaAlSi_3O_8 + Al_2SiO_5 + H_2O.$$

In the kyanite zone the additional reaction

$$3CaAl_2Si_2O_8 = Ca_3Al_2Si_3O_{12} + 2Al_2SiO_5 + SiO_2$$

affects the calcium composition between coexisting plagioclase and garnet.

PHYSICAL CONDITIONS DURING METAMORPHISM

The values of the intensive thermodynamic parameters may be estimated by comparison of natural mineral associations to experimental data, by calculation using mineral compositions and calibrated geothermometer-barometers, and by inference from geologic setting.

The critical observations which define the P-T trajectory during metamorphism is that kyanite is the stable aluminosilicate throughout most of the terrain and that staurolite breaks down before kyanite inverts to sillimanite.

The experimental work of Holdaway (1971), Hoschek (1969), Ganguly (1972) and Richardson (1968) (Figure 66) suggest that within the kyanite stability field minimum conditions at the staurolite isograd are ~550°C, 5 kb; at the kyanite + biotite isograd ~625°C, 6 kb; and at the kyanite isograd ~700°C, 8 kb. These are pressure-temperature conditions where $P_{H_2O} = P_T$ and for P_{O_2} at values within the stability field of magnetite. Higher P_{O_2} conditions restrict apparent staurolite stability (Ganguly,

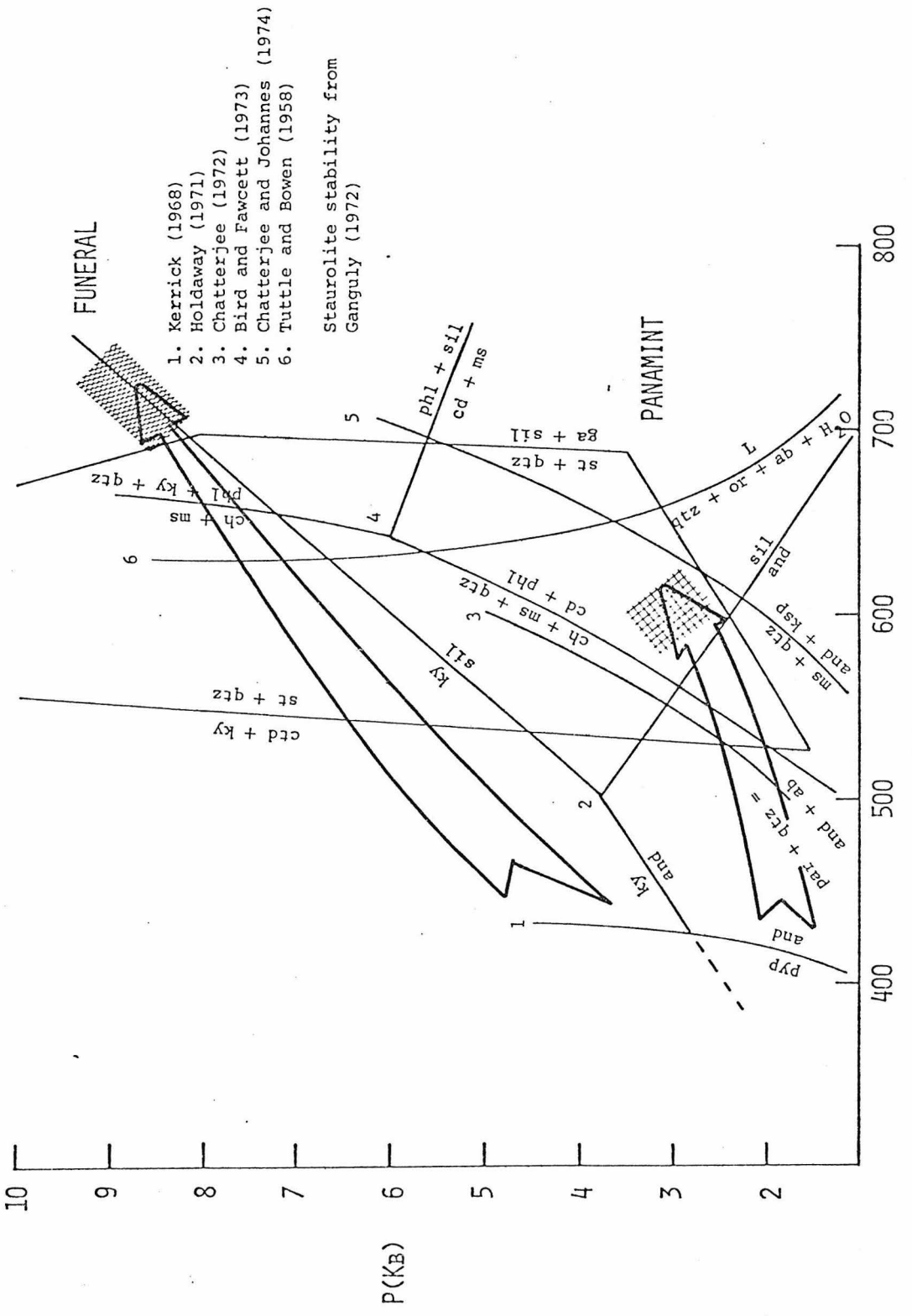

Figure 66:
P/T path of metamorphism, Funeral Mountains.

1972), but none of the high grade rocks contain ferric iron phases so that the values estimated by these experiments are appropriate.

Quantitative estimates on the physical conditions are calculated from existing geothermometers. Temperatures are estimated by the relative partitioning of Fe and Mg between garnet and biotite using the oxygen isotopic calibration of Goldman and Albee (1977). The distribution coefficient provides temperature estimates for all garnet-biotite assemblages because K_D is largely insensitive to pressure (Albee, 1965). Temperatures for garnet-biotite pairs are also calculated with the calibrations of Ferry and Spear (1977) and of A. B. Thompson (1976) for comparison. The results are tabulated in Table 10, and temperatures calculated by the Goldman-Albee calibration correspond well to those calculated by the Ferry-Spear experimental calibration except for three samples collected from the kyanite zone. Temperatures calculated with the A. B. Thompson calibration are in excess of the other two by 75 to 100°C. The high grade pairs CP 435c, FML 110, and FML 116b show better correspondence in temperatures calculated from Ferry-Spear and Thompson. A comparison to experimental data and the correspondence between temperatures calculated by Goldman-Albee and Ferry-Spear for garnet and staurolite grade samples suggest that these may be realistic values. Similarly, temperatures calculated from Thompson for kyanite-sillimanite grade samples seem more appropriate. The suggested temperature in the garnet grade Indian Pass is 470 to 500°C; at the staurolite isograd 500 to 530°C and in the high grade Monarch Canyon area 600°C to 700°C.

The pressure during metamorphism is difficult to estimate for

TABLE 10: GARNET-BIOTITE TEMPERATURES: FUNERAL MOUNTAINS

SAMPLE	GARNET			BIOTITE				TEMPERATURE °C		
	Mg/Fe	X_{Mn}	X_{Ca}	Mg/Fe	X_{Fe}	X_{Ti}	X_{Al}^{VI}	G-A	F-S	T
CP 435c	0.192	0.035	0.050	0.973	0.507	0.056	0.154	538	604	645
CP 451f	0.107	0.0	0.182	0.820	0.550	0.033	0.161	488	483	564
FML 60	0.116	0.0	0.198	0.878	0.533	0.028	0.109	487	486	567
FML 62	0.106	0.0	0.159	1.010	0.495	0.030	0.140	443	432	528
FML 104a	0.198	0.051	0.064	1.416	0.414	0.028	0.138	497	501	578
FML 104c	0.205	0.073	0.051	1.302	0.434	0.027	0.143	521	533	599
FML 106a	0.185	0.030	0.040	1.259	0.443	0.035	0.183	496	514	587
FML 107a	0.191	0.035	0.049	1.249	0.445	0.034	0.183	511	526	594
FML 110	0.176	0.058	0.040	0.653	0.605	0.061	0.136	582	726	717
FML 113a	0.228	0.075	0.033	1.553	0.392	0.036	0.158	513	515	587
FML 116b	0.206	0.060	0.038	0.860	0.538	0.049	0.145	581	676	689

G-A Goldman and Albee (1977)

F-S Ferry and Spear (1977)

T A. B. Thompson (1976)

most mineral assemblages. Estimates based on the probable amount of overburden are unsatisfactory because the Paleozoic section exposed to the north (Reynolds, 1974) and to the south (McAllister, 1974) amounts to 6.2 km and 7.8 km respectively. The thickness of the Mesozoic cover at the presumed time of metamorphism (Cretaceous) is unknown, but if the thickness was comparable to that estimated in the Panamints, perhaps 3 km may be added. A generous estimate of 12 km of cover suggests lithostatic pressures on the order of 4 kb, but the mineral assemblages suggest that pressures may have been approximately 1.5 to 2.0 times this amount.

In the high grade rocks, the coexistence of garnet + plagioclase + kyanite + quartz allows the calculation of pressure, given the temperature. Ghent (1975, 1976) suggested the use of the divariant reaction

$$3 \text{ anorthite} = \text{grossular} + \text{kyanite} + \text{quartz}$$

as a potential geobarometer. The equilibrium constant is given by

$$0 = -\frac{3272}{T} - 8.3969 - \frac{0.3448(P-1)}{T} + \log a^{gar}_{gross} - 3 \log a^{plag}_{an}$$

(Ghent, 1976). The activity of anorthite in plagioclase is $\gamma^{plag}_{an} X^{plag}_{an}$ where $\gamma^{plag}_{an} = 1.28$ for sodic plagioclase (Orville, 1972). The activity of grossular in garnet is given by $(\gamma^{gar}_{gros} X^{gar}_{gros})^3$ assuming random mixing in the three 8-fold sites, γ^{gar}_{gross} is estimated by assuming a regular symmetric solution model for the binary solution grossular-almondine which gives

$$\ln \gamma^{gar}_{gross} = \frac{(1-X^{gar}_{gross})^2}{RT} W \qquad \text{(Ghent, 1975).}$$

W, the regular symmetric solution parameter, derived from the excess free energy of mixing determined by Ganguly and Kennedy (1974) is

TABLE 11: GARNET-PLAGIOCLASE-KYANITE GEOBAROMETER and MUSCOVITE-PLAGIOCLASE-KYANITE GEOTHERMOMETER

SAMPLE	TEMPERATURE C°	X^{plag}_{An}	X^{gar}_{gross}	ln γ_{gross}	P bars	X^{plag}_{ab}	X^{mica}_{Na}	log γ^{mica}_{Na}	f_{H_2O}	a_{H_2O}
CP 435c	538	0.265	0.050	0.560	6109	0.735	0.096	0.884	1639	0.478
	604		0.518	7239				0.842	4838	0.857
	645			0.495	7941			0.818	8761	1.153
FML 113a	513	0.157	0.033	0.599	6064	0.843	0.285	0.651	761	0.254
	515			0.597	6099			0.650	789	0.250
	587			0.547				0.616	2629	0.457
FML 116b	581	0.157	0.038	0.545	7692	0.843	0.168	0.779	2998	0.486
	676			0.491	9408			0.732	11585	0.968
	689			0.484	9643			0.726	13653	1.050

estimated to be +1000 cal/mole.

Pressures were calculated from three samples from the kyanite zone for each temperature calculated by the K_D for coexisting garnet and biotite. The results are shown in Table 11 and show pressures from 6100 to nearly 10,000 bars. The estimated temperature range of 600°C to 700°C, suggests the reasonable pressure range of 7200 to 9600 bars for the high grade terrain in the Funeral Mountains. The large uncertainty in the temperature gives a tremendous uncertainty in pressures.

Despite the great uncertainty, the results calculated for the kyanite zone samples are consistent with the experimental work of Ganguly (1972) and Richardson (1968) for the breakdown of staurolite.

The results of calculation of a_{H_2O} from the three kyanite zone samples by the multi-variant reaction

$$\text{paragonite} + \text{quartz} = \text{albite} + \text{kyanite} + H_2O$$

are inconclusive. Values (Table 11) ranging from 0.250 to essentially 1.0 may be derived from the estimated P-T pairs. The majority of the rocks are pelitic or quartzitic, whereas carbonate rocks are restricted to the high grade regions; the fluid phase was probably rich in H_2O.

The mineral assemblages in the Funeral Mountains are characteristic of Barrovian-style metamorphism and are quite in contrast to the assemblages in the Panamint Mountains. The final section compares and contrasts the development of mineral assemblages and offers tentative explanations for the differences in physical conditions during metamorphism.

CONTRAST IN METAMORPHIC FACIES, PANAMINT AND FUNERAL MOUNTAINS

INTRODUCTION

Both the Panamint and Funeral Mountains exhibit regionally metamorphosed terrains which are comprised of similar age protolith and which are developed in similar structural settings. The affected strata in both ranges encompass the later Precambrian Stirling quartzite, Johnnie Formation and older metasedimentary rocks of the Noonday Dolomite, Pahrump Group and their equivalents. Because the Johnnie Formation is more extensively exposed in the regionally metamorphosed terrain in the Funeral Mountains, pelitic schists are more abundant there. Regional metamorphism preceded major deformation and was accompanied by intrusion of leucocratic granitic rock in the high grade regions of both. Deformation was accommodated by the development of northwest- and north-northwest-trending anticlines and elongate domes which involved basement in the Panamint Mountains. Deformation was accompanied by retrograde metamorphism in the Panamint Mountains and by the development of secondary strain-slip cleavage and kinkbands in the Funeral Mountains. Retrograde metamorphism is also extensive near the culmination of the Funeral Mountains at Chloride Cliff.

The correlation of the tectonic and metamorphic events in the Panamint and Funeral Mountains (Table 12) suggests that the development of the regional metamorphic terrains may have been synchronous. Most aspects, though, of the metamorphic terrains, in particular the mineral assemblages and implied P/T gradients are quite in contrast between the Panamint and Funeral Mountains. Such disparity may indicate that regional metamorphism occurred at different times and record

TABLE 12: CORRELATION OF TECTONIC + METAMORPHIC EVENTS, DEATH VALLEY

PANAMINT MOUNTAINS (TELESCOPE PEAK QUAD)	FUNERAL MOUNTAINS (CHLORIDE CLIFF QUAD)
DEPOSITION OF LATE PRECAMBRIAN THROUGH PALEOZOIC AND (?) TRIASSIC SEDIMENTARY ROCKS ON EARLY (1700 + 1400 MY) PRECAMBRIAN BASEMENT.	DEPOSITION OF LATE PRECAMBRIAN AND PALEOZOIC SEDIMENTARY ROCKS ON UNKNOWN BASEMENT.
MIDDLE MESOZOIC EVENTS NOT APPARENT	
LOW PRESSURE REGIONAL METAMORPHISM AND INTRUSION OF LEUCOCRATIC GRANITE (80 MY), GRADE INCREASES FROM EAST TO WEST.	HIGHER PRESSURE REGIONAL METAMORPHISM WITH MIGMATIZATION AND INTRUSION OF LEUCOCRATIC GRANITE IN HIGHEST GRADE AREA. GRADE INCREASES FROM SOUTHEAST TO NORTHWEST.
FOLDING ALONG NNW AXES AND DEVELOPMENT OF ANTICLINES WITH GENTLY DIPPING EAST LIMBS AND STEEPLY DIPPING WEST LIMBS. ACCOMPANIED BY RETROGRADE METAMORPHISM IN CORES OF FOLDS.	FOLDING ALONG NW AXES AND DEVELOPMENT OF A DOUBLY PLUNGING ANTICLINE WHICH CULMINATES NEAR KEANE WONDER MINE. ACCOMPANIED BY DEVELOPMENT OF SLIP CLEAVAGE AND MICROFOLDS.
DEVELOPMENT OF LOW ANGLE NORMAL FAULTS; UPPER PLATES DISPLACED WESTWARD RELATIVE TO LOWER PLATES. LITTLE CHIEF STOCK (14 MY), INTRUDES FAULTS.	DEVELOPMENT OF LOW ANGLE FAULTS; YOUNGER ROCKS GENERALLY ON UPPER PLATE (BOUNDARY CANYON FAULT SEPARATES STRONGLY METAMORPHOSED FROM WEAKLY METAMORPHOSED ROCKS). OLIGOCENE ROCKS ARE DEFORMED.

two separate tectonic events. Two issues arise from the contrast in facies series; the nature of the response in the rocks in terms of mineral assemblages to the different P/T gradients, and the nature of the tectonic environment of formation of the terrains, whether or not synchronous.

Pelitic schists are used to document the differences in facies series because a multitude of reactions may occur to relate mineral assemblages to one another and because pelitic schists have been intensively studied and used to characterize the P/T regimes in metamorphic terrains.

Differences in the response of pelitic schists to metamorphism under the two different gradients are immediately recognized by the textural development of samples recrystallized at similar grades. The lower pressure Panamint terrain pelitic schists are generally fine-grained. Foliation is very weak, and the overall texture is a hornfels. Andalusite is the only mineral which occurs as large porphyroblasts, whereas staurolite, cordierite, and biotite are fine-grained, almost matrix minerals. The higher pressure Funeral terrain pelitics are much coarser-grained, particularly in the staurolite and kyanite zones. Foliation is well developed and schistose; garnet, chloritoid, staurolite, and kyanite occur as large porphyroblasts and are easily recognized in hand sample.

The second obvious difference is the occurrence of cordierite and andalusite in the Panamint Mountains as opposed to kyanite in the Funeral Mountains. The following discussion reviews the development of mineral assemblage and their implied P/T conditions of formation

for the Panamint and Funeral Mountains and applies these results to the stability of muscovite + quartz + chlorite as a function of pressure. The sequence of observed reactions and estimated physical conditions are used to calibrate a petrogenetic grid for the metamorphism of pelitic schists which predicts a consistent sequence of mineral reactions for observed metamorphic facies series.

AKFM FACIES DEVELOPED IN THE PANAMINT AND FUNERAL MOUNTAINS

The pelitic schists in the Panamint Mountains were shown to be characterized by andalusite and cordierite-bearing assemblages. The assemblages and reactions relating the assemblages are summarized in Figure 67. At low grades pelitic rocks contain the assemblage chlorite + biotite or chlorite + andalusite + chloritoid. Spotted rocks, common in the low grade areas, and rocks with spots which are engulfed by andalusite suggest that at low grades cordierite-bearing assemblages may have also occurred. However, the petrographic evidence which relates the spots to altered cordierite is ambiguous and the low grade phase relations involving cordierite are poorly known.

Within a small change in grade, chlorite compositions are restricted to a narrow interval in Mg/(Mg + Fe) from values of about 0.50 to about 0.65. Rocks having Mg-values outside this range contain assemblages characterized by biotite + aluminous mineral. Fe-rich rocks contain chloritoid + biotite, staurolite + biotite, or andalusite + biotite, and Mg-rich rocks contain cordierite + biotite. At high grades chlorite is restricted to Mg/(Mg + Fe) = 0.55, and then breaks down to an assemblage of andalusite + cordierite + biotite. The

AKFM PELITIC SCHIST ASSEMBLAGES

PANAMINT MOUNTAINS

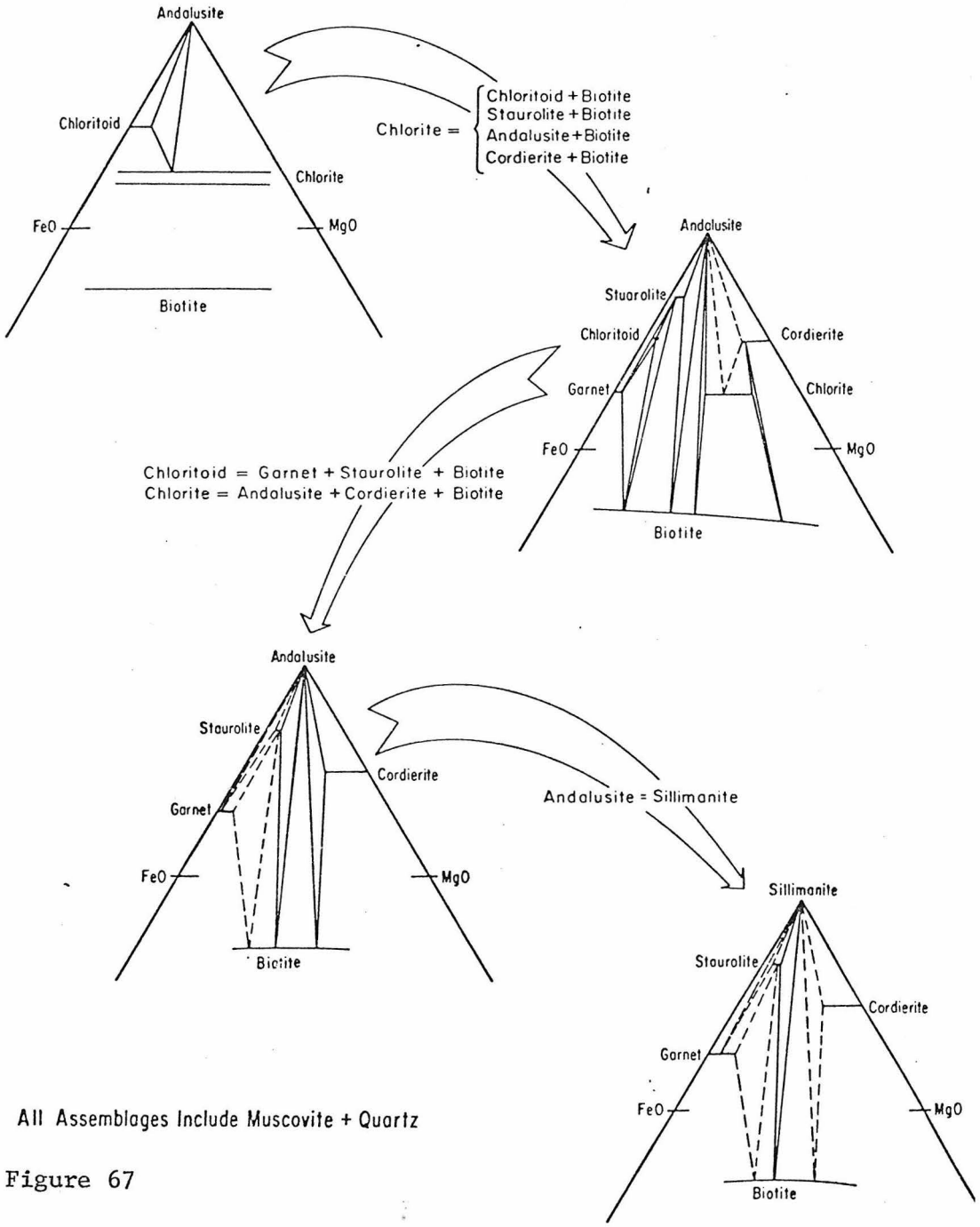

All Assemblages Include Muscovite + Quartz

Figure 67

AKFM PELITIC SCHIST ASSEMBLAGES

FUNERAL MOUNTAINS

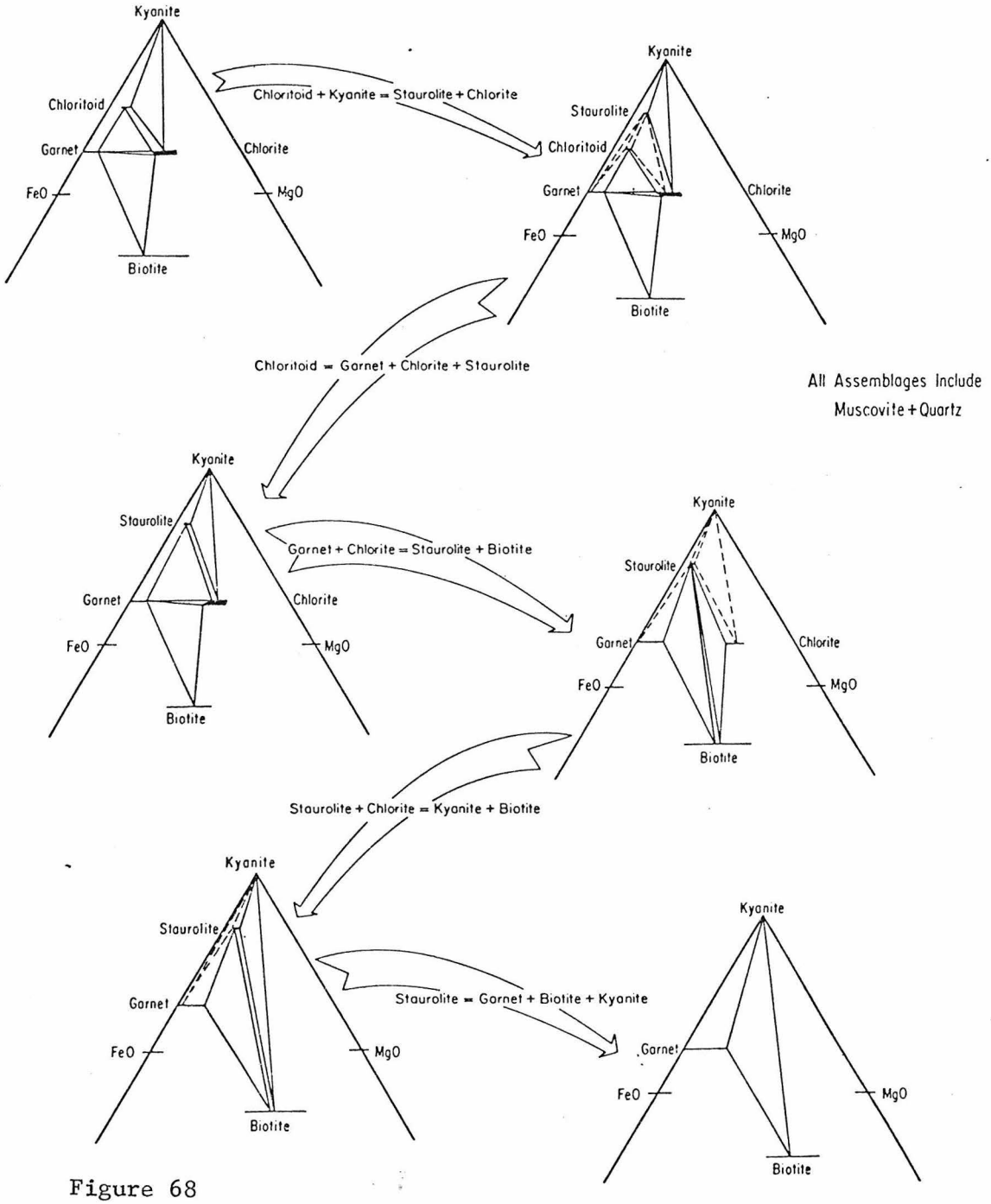

Figure 68

limited occurrence of pelitic schists (i.e. Johnnie Formation) in the Panamint Mountains, particularly chloritoid-bearing schists, prevents the determination of the relation between the breakdown of chloritoid and the breakdown of chlorite.

Estimates of pressure and temperature during metamorphism were made on the basis of assumed stratigraphic cover and the partition of Fe and Mg between coexisting garnet and biotite. The pressure is believed to have been between 2.3 and 3.0 kb, and the temperature is estimated to range from about 420°C in the low grade region to as high as 680°C in the highest grade area.

The Funeral Mountains schists contain assemblages which are characterized by the presence of kyanite and which are commonly exhibited in Barrovian metamorphic terrains. Mineral facies developed in the Funeral terrain are shown in Figure 68. At low grades the garnet-chlorite join is stable and does not break until after chloritoid breaks down. The limitation of chlorite to only magnesium-rich rocks occurs over a much greater change in grade than in the Panamint Mountains and the sequence of reactions

garnet + chlorite = staurolite + biotite

staurolite + chlorite = kyanite + biotite

is reasonably well displayed. Cordierite-bearing assemblages are not observed and cordierite may not be stable under the conditions suggested for the Funeral Mountains. The breakdown of staurolite prior to the transition from kyanite to sillimanite suggests relatively high pressures. Calculations based on garnet-biotite K_D and garnet-plagioclase-kyanite-quartz equilibria suggest that at the highest grade the

temperature was between 600 and 700° C and the pressure was between 7.0 and 9.0 kb.

STABILITY OF CHLORITE + MUSCOVITE + QUARTZ

Progressive metamorphic reactions which are represented in the field by isograds in effect represent the breakdown of chlorite by its limitation to smaller intervals of Mg/(Mg + Fe) in natural rocks. In the majority of pelitic schists this breakdown of chlorite + muscovite + quartz progresses from the formation of garnet, through the isolation of iron-rich compositions from chlorite by the formation of the joins staurolite + biotite and kyanite + biotite. The stability of chlorite is strongly affected by changes in pressure or a_{H_2O}. The sensitivity of chlorite stability on intensive parameters is dramatically illustrated by the facies series exposed in the Panamint and Funeral Mountains.

The radically different physical conditions which prevailed during the metamorphism of the two terrains did not affect the relative partition of Fe and Mg among coexisting phases. Figure 69 illustrates log Mg/Fe for the representative assemblages found in each terrain. Garnet is most iron-rich of all phases, staurolite is slightly more iron-rich than chloritoid, biotite is slightly more iron-rich than chlorite, and cordierite is least iron-rich of all. The order of iron enrichment indicated in the two areas is consistent with the data of Albee (1972) and Guidotti and others (1975).

The aluminum and silicon contents of chlorite encompass the same ranges for both terrains; aluminum occurs in amounts between approxi-

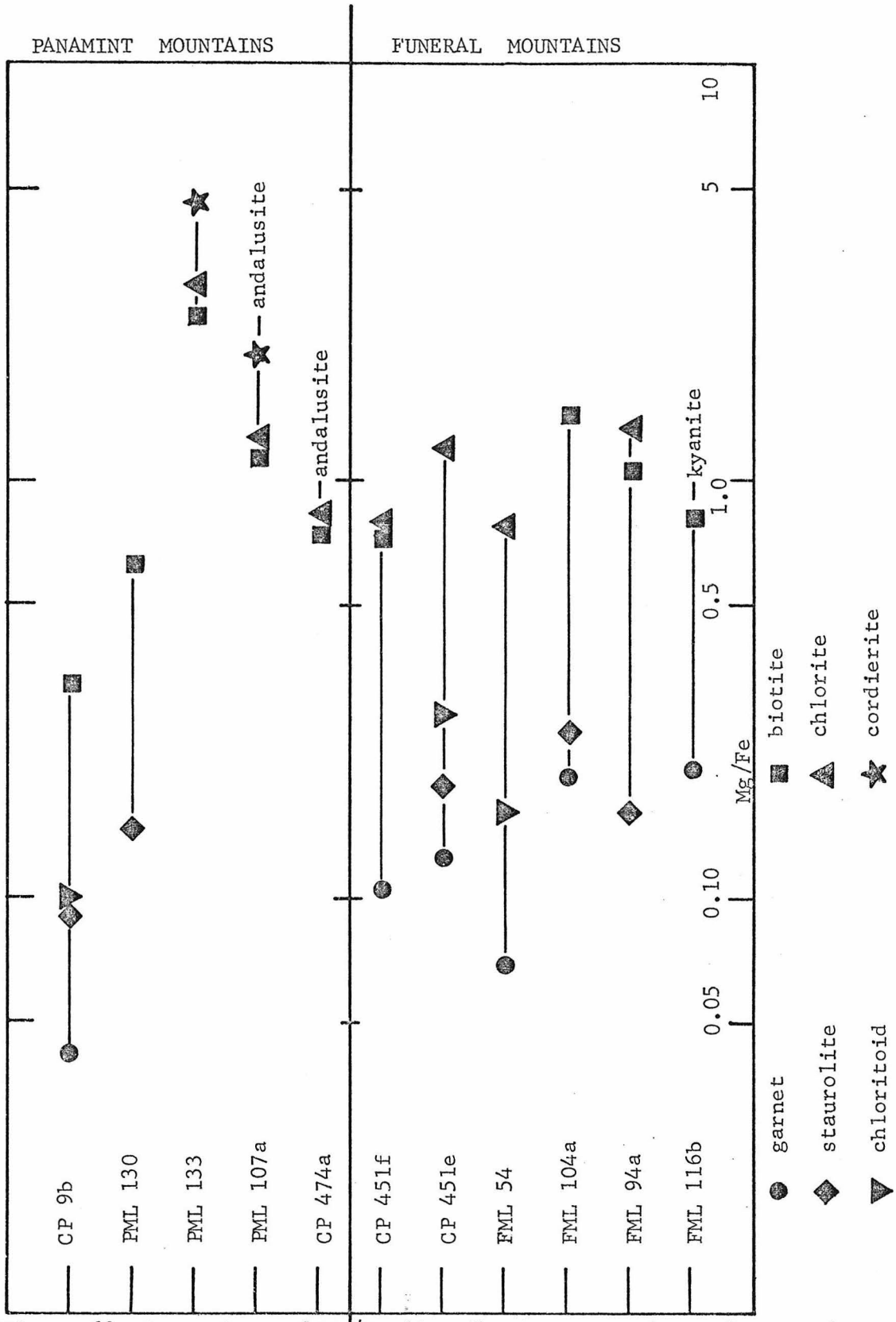

Figure 69: Comparison of Mg/Fe distribution, Panamint and Funeral Mtns.

mately 2.70 and 3.0 cations/formula and silicon between 2.50 and 2.65/ formula. Similarly the aluminum content of biotite and the muscovite are comparable between the Panamint and Funeral Mountains (compare Figures 39 and 40 with Figures 58 and 60). The differences between the Panamint and Funeral Mountains assemblages rest on differences in the sequence of univariant mineral reactions which limit the field of stability of chlorite. Figure 70 illustrates the pseudo-binary phase diagrams which depict the stability of chlorite as a function of temperature for the Panamint and Funeral Mountains.

The differences are obvious. Garnet + chlorite is never observed in the Panamint Mountains and is replaced by chloritoid + biotite whereas chloritoid breaks down prior to the instability of the garnet-chlorite join in the Funeral Mountains. Figure 70 also illustrates that chlorite in the Panamint Mountains becomes unstable over a wide range of Mg/Mg + Fe values within a narrow change in grade. These T-X diagrams are extended to temperatures which exceed those represented by Panamint Mountains assemblages in order to indicate the phase relations which occur beyond the stability of muscovite + quartz. Cordierite is indicated in the Funeral Mountains section, but cordierite may be unstable under such high pressure conditions and another phase such as spinel may replace cordierite.

All analyzed samples containing the pairs chlorite-biotite, chlorite-cordierite, or biotite-cordierite indicate that the relative enrichment of Mg/Fe is biotite < chlorite < cordierite and the enrichment is such that chlorite always occurs on the iron-rich side of the cordierite-biotite tie line. The terminal composition of chlorite

SCHEMATIC PSEUDOBINARY T-X SECTIONS ALONG GARNET-CHLORITE JOIN

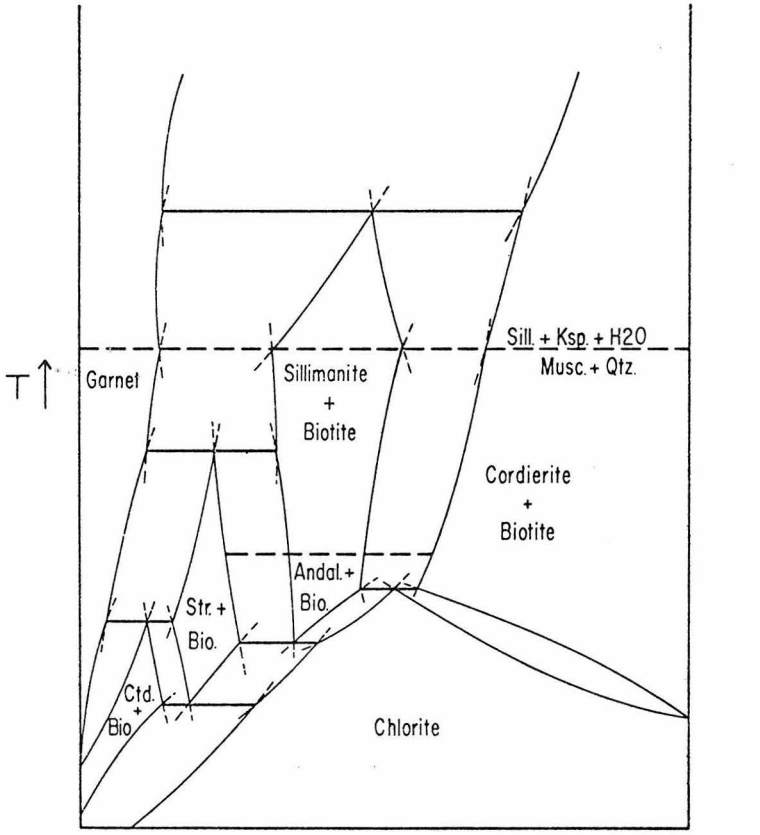

Panamint Mountains

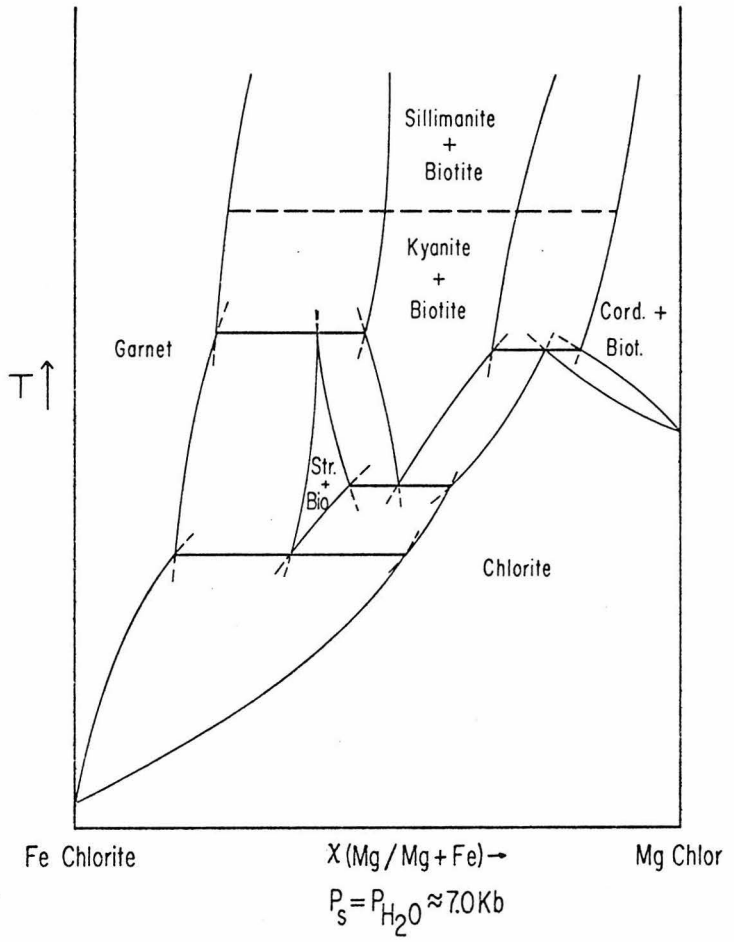

Funeral Mountains

Figure 70

must lie at some intermediate value of Mg/(Mg + Fe) and not at the pure Mg end-member; similar relations were found by Guidotti and others (1975). In no instance is the relative partition of Mg and Fe between any phases reversed and no azeotrope or extremal state is possible (cf. Prigogine and Defay, 1954, and Albee, 1972). Hence chlorite must break down to the assemblage Al-silicate + cordierite + biotite and reactions such as

Al-silicate + chlorite = cordierite + biotite or

chlorite + cordierite = Al-silicate + biotite

cannot occur (Figure 71).

Besides the differences in aluminosilicate phases and the order of the breakdown of staurolite relative to the appearance of sillimanite, the occurrence of chloritoid + biotite in the Panamint Mountains and staurolite + garnet + chlorite in the Funeral Mountains imply that the invariant point [A, Cd] is stable on some section in P-T-a_{H_2O} space. This invariant point relates reactions among the phases garnet-staurolite-chloritoid-biotite-chlorite and separates facies series in which chloritoid breaks down before the garnet + chlorite join from series in which chloritoid + biotite is stable (Albee, 1972). The abundance of carbonate rocks and results from muscovite + albite + andalusite + quartz equilibrium suggest that the activity of water in the Panamint terrain was much less than one. Reduction of the a_{H_2O} favors the product side of the reaction

garnet + chlorite + muscovite = chloritoid + biotite + quartz + H_2O

and Figure 72 illustrates the phase relations of chlorite in an isobaric,

Figure 71: 256

POSSIBLE TERMINAL REACTIONS FOR CHLORITE

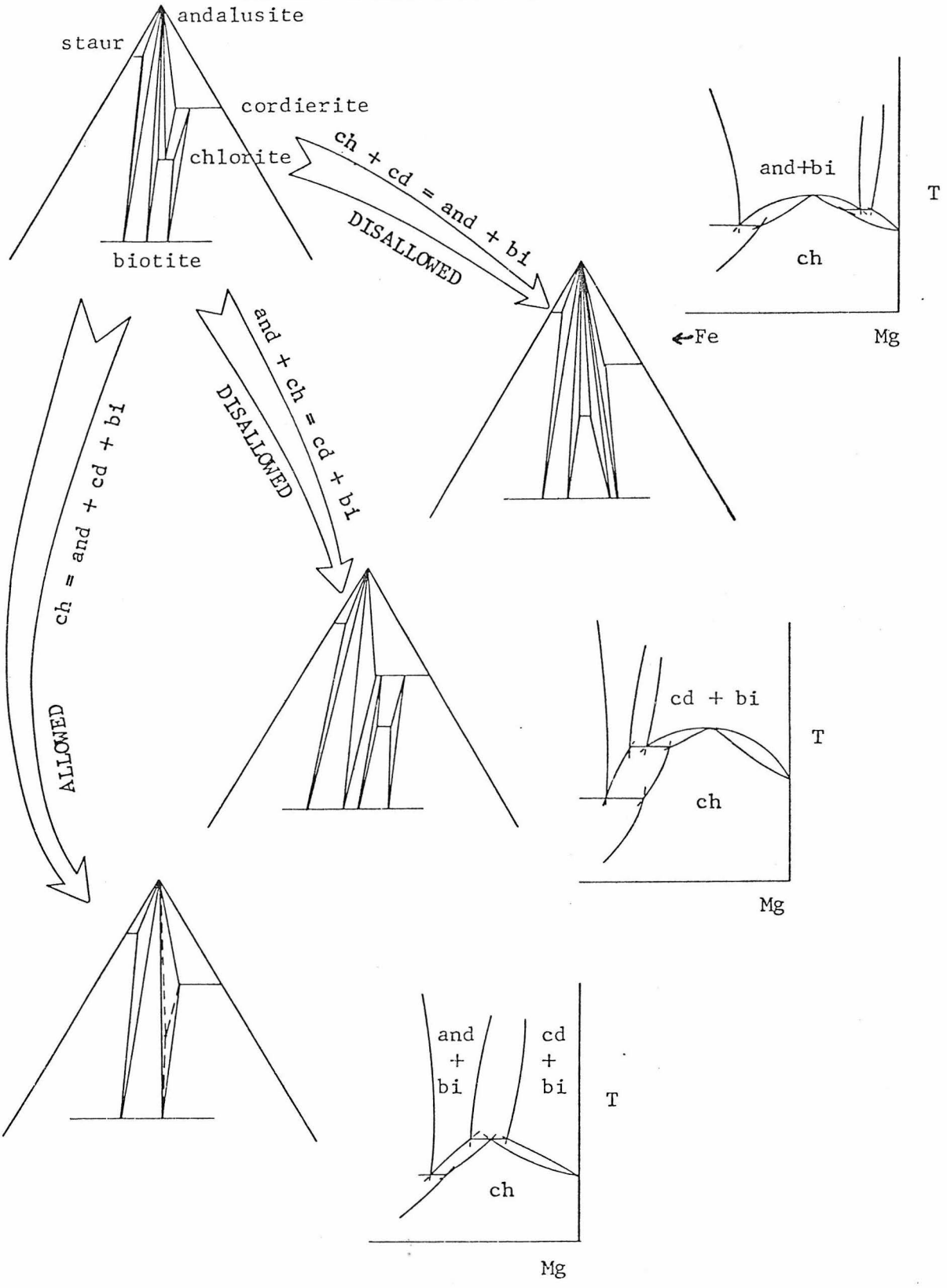

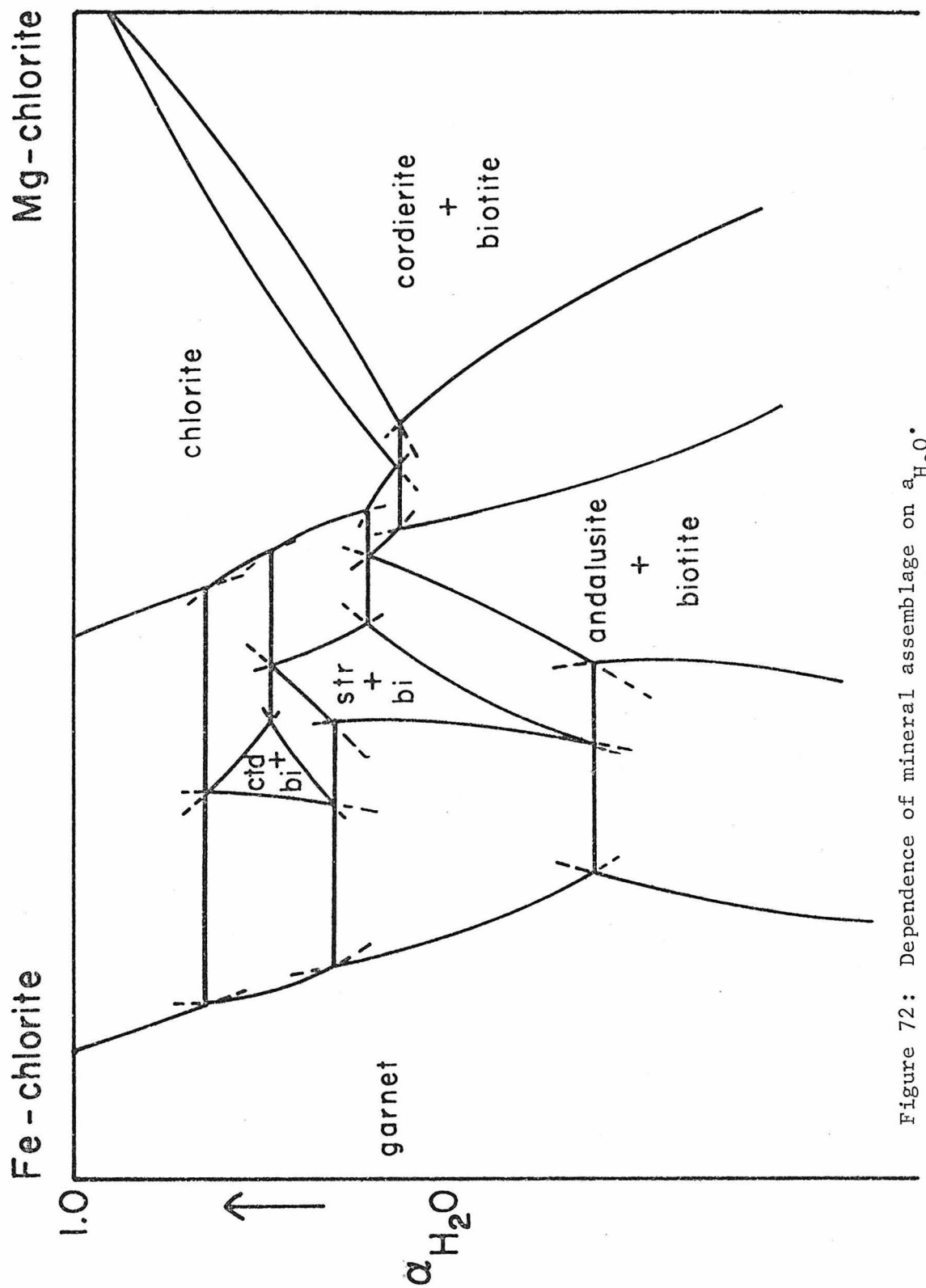

Figure 72: Dependence of mineral assemblage on a_{H_2O}.

isothermal a_{H_2O} - X_{Mg} section. All reactions indicated on Figure 72 are identical to those in Figure 70 because dehydration may be accomplished by either a temperature increase or dilution of H_2O-rich fluid with other constituents (especially CO_2), or a combination of both. In order to construct a petrogenetic grid for pelitic schists which involve chloritoid, it is necessary to know if the [A, Cd] invariant point is stable on the section $P_T = P_{H_2O}$, and if it is stable, if the assemblage chloritoid + biotite is favored at high pressures or low pressures.

The argument for the stability of chloritoid-biotite under low pressure conditions is a generality argument. In all metamorphic terrains which were clearly developed in a low pressure environment, especially in contact aureoles around high level intrusions, chlorite is rare and occurs along the outer fringes or at very low grades, and biotite + aluminous minerals occur instead. The outer aureole in the Steinach area, Germany, is comprised by muscovite + quartz + biotite + andalusite + cordierite (Okrusch, 1969, 1971). In the Comrie area, Scotland, Tilley (1924) reports that regionally metamorphosed muscovite + chlorite slates were altered during intrusion of a diorite to biotite- and biotite + cordierite-bearing assemblages in the outer aureole. Bosma (1964) described the contact metamorphic aureole around a granite in Alsace which is comprised of spotted chlorite-bearing rocks in the outermost part and which contain the assemblage andalusite + biotite in the higher temperature part. Compton (1960) reported assemblages of cordierite + biotite, andalusite + biotite, and staurolite + biotite in the outer and intermediate parts of an aureole around a

stock in the Santa Rosa Range in Nevada. Even in the low pressure regional metamorphic terrains such as the Buchan area in Aberdeenshire (Read, 1952) and in the Abukuma Plateau (Miyashiro, 1958) biotite + aluminosilicate mineral assemblages dominate in the metamorphic rocks over chlorite-bearing assemblages. Never in any of these studies is the assemblage garnet + chlorite observed.

In contrast, the assemblage garnet + chlorite is common in the kyanite-bearing terrains in Vermont (Albee, 1968), in Scotland (eg Harker, 1932), in the Alps (Chatterjee, 1961), and in the Sanbagawa region in Japan (Banno, 1964). In the high pressure Franciscan terrain, biotite does not occur and appears to be replaced by stilpnomelane (Ernst and others, 1970).

Although in each case factors such as lack of proper rock composition, or variations in activity of water may be invoked to explain the observed assemblages, the consistency and preponderance of biotite + aluminous mineral assemblage in low pressure terrains versus chlorite + garnet assemblages in high pressure terrains suggest that the assemblage chloritoid + biotite is stable in low pressure environments.

Furthermore, the occurrence of garnet + chlorite assemblages and staurolite + biotite assemblages in the absence of chloritoid + biotite assemblages in the andalusite-bearing terrain of northern Vermont (Albee, 1968) and Maine (Osberg, 1968) indicate that the invariant point [A, Cd] must occur in the andalusite stability field.

THE PETROGENETIC GRID FOR AKFM PELITIC SCHISTS

Petrogenetic grids for the metamorphism of AKFM pelitic schists

have been presented by Albee (1965c), Hess (1969), A. B. Thompson (1976), and Kepezhinskas and Khlestov (1977). Each falls short in some aspect which separates the Panamint from the Funeral facies series. Neither Hess (1969) nor Thompson (1976) consider chloritoid-bearing assemblages, and one of the noted differences between the Panamint and Funeral Mountains lies with the phase relations which involve chloritoid. Kepezhinskas and Khlestov (1977) do consider chloritoid, but they predict that the stability of chloritoid + biotite lies at high pressures, contrary to the arguments presented above. The grid presented by Albee (1965c) most closely predicts the observed relations, but the phases staurolite-chloritoid-garnet and chlorite-cordierite were assumed to be colinear and kyanite constituted the aluminosilicate phase. Albee (1972) described the non-colinearity of chloritoid-staurolite-garnet and presented the invariant point [A, Cd].

Here the grid of Albee (1965c) is modified by calculation of the slopes of reactions among phases having the compositions observed in the Panamint and Funeral Mountains assemblages. Table 13 lists the compositions and all of the possible reactions among the phases. Slopes for the reactions in $P_S = P_{H_2O}$, T space were estimated by the relation

$$\frac{dp}{dT} = \frac{\Delta S}{\Delta V} = \frac{S_{dehyd/H_2O} + S_{(Al^{VI} \rightarrow Al^{IV})}}{\Delta V_s / n_{H_2O} + \overline{V}_{H_2O}}$$

where S_{dehyd/H_2O} = 14 cal/°K mole H_2O (Fyfe and others, 1958).

$S_{Al^{VI} \rightarrow Al^{IV}}$ = 2.39 cal/°K mole, ΔV_s is the volume change of the solids and $\overline{V}_{H_2O}$ is 0.6682 cal/bar mole H_2O (the value at 2.5 kb, 600°C

TABLE 13: REACTIONS AMONG MINERALS IN AKFM PELITIC SCHSTS

	SiO_2	Al_2O_3	FeO	MgO	K_2O	H_2O	Vol cal/bar	Al^{IV}
Qtz	1.000	0.000	0.000	0.000	0.000	0.000	0.542	0.000
AlSi	1.000	1.000	0.000	0.000	0.000	0.000	1.054*	0.000*
Str	4.000	4.333	1.650	0.350	0.000	1.000	5.400	0.000
Ctd	2.000	2.000	1.570	0.430	0.000	2.000	3.325	0.000
Cord	5.000	2.000	0.600	1.400	0.000	0.000	5.514	1.000
Gar	3.000	1.000	2.650	0.350	0.000	0.000	2.758	0.000
Chl	2.500	1.500	2.000	2.500	0.000	4.000	5.072	1.500
Biot	2.600	0.900	1.300	1.300	0.500	1.000	3.684	1.400
Musc	3.000	1.500	0.000	0.000	0.500	1.000	3.362	1.000
Water	0.000	0.000	0.000	0.000	0.000	1.000	0.000	0.000

*values are for kyanite

Al^{IV} = 1.0 for sillimanite

vol = 1.232 for andalusite

vol = 1.193 for sillimanite

(AlSi, str, ctd)
7.596 biot = - 8.355 cord - 1.000 gar + 8.769 chl + 19.817 qtz
+ 7.596 musc - 35.076 H_2O

(AlSi, str, cord)
1.628 biot = - 1.791 ctd + 1.105 gar + 1.000 chl - 2.884 qtz
+ 1.628 musc - 0.417 H_2O

(AlSi, str, gar)
5.596 biot = - 1.000 ctd - 5.155 cord + 5.969 chl + 10.617 qtz
+ 5.596 musc - 21.876 H_2O

(AlSi, str, chl)
1.000 biot = - 2.350 ctd + 1.251 cord + 1.600 gar - 6.751 qtz
+ 1.000 musc + 4.701 H_2O

TABLE 13 (Continued)

(AlSi, str, biot)
1.000 chl = - 2.036 ctd + 2.036 cord + 1.500 gar - 8.108 qtz
+ 8.072 H_2O

(AlSi, ctd, cord)
2.932 biot = - 1.173 str + 1.000 gar + 1.549 chl - 3.353 qtz
+ 2.933 musc - 5.024 H_2O

(AlSi, ctd, gar)
8.973 biot = - 1.000 str - 7.121 cord + 8.795 chl + 14.032 qtz
+ 8.974 musc - 34.178 H_2O

(AlSi, ctd, chl)
1.355 biot = - 1.000 str + 1.258 cord + 1.003 gar - 5.842 qtz
+ 1.356 musc + 1.000 H_2O

(AlSi, ctd, biot)
1.565 chl = - 1.000 str + 2.750 cord + 1.181 gar - 9.379 qtz
+ 7.261 H_2O

(AlSi, cord, gar)
2.264 biot = - 1.820 str + 2.514 ctd + 1.000 chl - 1.153 qtz
+ 2.265 musc - 7.208 H_2O

(AlSi, cord, chl)
1.000 biot = - 2.860 str + 6.764 ctd - 1.736 gar + 2.720 qtz
+ 1.000 musc - 10.668 H_2O

(AlSi, cord, biot)
1.000 chl = - 4.656 str + 12.805 ctd - 3.932 gar + 7.313 qtz
-16.952 H_2O

(AlSi, gar, chl)
1.536 biot = - 2.107 str + 3.105 ctd + 1.000 cord - 3.394 qtz
+ 1.537 musc - 4.102 H_2O

(AlSi, gar, biot)
1.000 chl = - 1.285 str + 2.062 ctd + 1.474 cord - 3.849 qtz
+ 1.162 H_2O

(AlSi, chl, biot)
2.667 gar = - 2.287 str + 7.289 ctd - 1.000 cord + 7.574 qtz
- 12.290 H_2O

(str, ctd, cord)
9.115 biot = - 13.369 AlSi + 1.000 gar + 4.600 chl - 4.776 qtz
+ 9.115 musc - 18.399 H_2O

TABLE 13 (Continued)

(str, ctd, gar)
1.999 biot = - 1.599 AlSi - 1.000 cord + 1.600 chl + 1.800 qtz
+ 2.000 musc - 6.399 H_2O

(str, ctd, chl)
3.365 biot = - 8.769 AlSi + 2.875 cord + 1.000 gar - 9.951 qtz
+ 3.365 musc

(str, ctd, biot)
2.692 chl = - 6.076 AlSi + 4.558 cord + 1.000 gar - 12.980 qtz
+ 10.769 H_2O

(str, cord, gar)
4.715 biot = - 8.249 AlSi + 1.000 ctd + 2.280 chl - 1.336 qtz
+ 4.715 musc - 11.119 H_2O

(str, cord, chl)
1.000 biot = - 8.223 AlSi + 5.068 ctd - 2.511 gar + 5.224 qtz
+ 1.000 musc - 10.135 H_2O

(str, cord, biot)
1.000 chl = - 13.389 AlSi + 10.042 ctd - 5.194 gar + 11.390 qtz
- 16.084 H_2O

(str, gar, chl)
1.865 biot = - 5.969 AlSi + 1.000 ctd + 1.425 cord - 3.901 qtz
+ 1.865 musc - 2.000 H_2O

(str, gar, biot)
1.492 chl = - 4.476 AlSi + 1.000 ctd + 2.358 cord - 5.580 qtz
+ 3.969 H_2O

(str, chl, biot)
3.288 gar = - 6.576 AlSi + 5.932 ctd - 1.000 cord + 9.576 qtz
- 11.864 H_2O

(ctd, cord, gar)
5.269 biot = - 11.394 AlSi + 1.000 str + 2.600 chl - 1.213 qtz
+ 5.269 musc - 11.399 H_2O

(ctd, cord, chl)
1.000 biot = - 32.787 AlSi + 8.543 str - 4.828 gar + 12.702 qtz
+ 1.000 musc - 8.542 H_2O

(ctd, cord, biot)
1.000 chl = - 62.065 AlSi + 16.929 str - 9.785 gar + 26.209 qtz
- 12.928 H_2O

TABLE 13 (Continued)

(ctd, gar, chl)
2.019 biot = - 8.794 AlSi + 1.000 str + 1.625 cord - 4.138 qtz
+ 2.019 musc - 1.000 H_2O

(ctd, gar, biot)
1.615 chl = - 7.179 AlSi + 1.000 str + 2.635 cord - 5.955 qtz
+ 5.462 H_2O

(ctd, chl, biot)
5.999 gar = - 35.329 AlSi + 10.000 str - 1.000 cord + 18.330 qtz
- 10.000 H_2O

(cord, gar, chl)
1.000 biot = + 18.409 AlSi - 9.262 str + 10.563 ctd - 2.884 qtz
+ 1.000 musc - 11.862 H_2O

(cord, gar, biot)
1.000 chl = + 41.692 AlSi - 19.156 str + 21.406 ctd - 5.379 qtz
- 19.656 H_2O

(cord, chl, biot)
1.000 gar = - 10.602 AlSi + 3.688 str - 2.187 ctd + 3.228 qtz
+ 0.688 H_2O

(gar, chl, biot)
1.000 cord = + 28.288 AlSi - 12.125 str + 13.125 ctd - 1.037 qtz
-14.125 H_2O

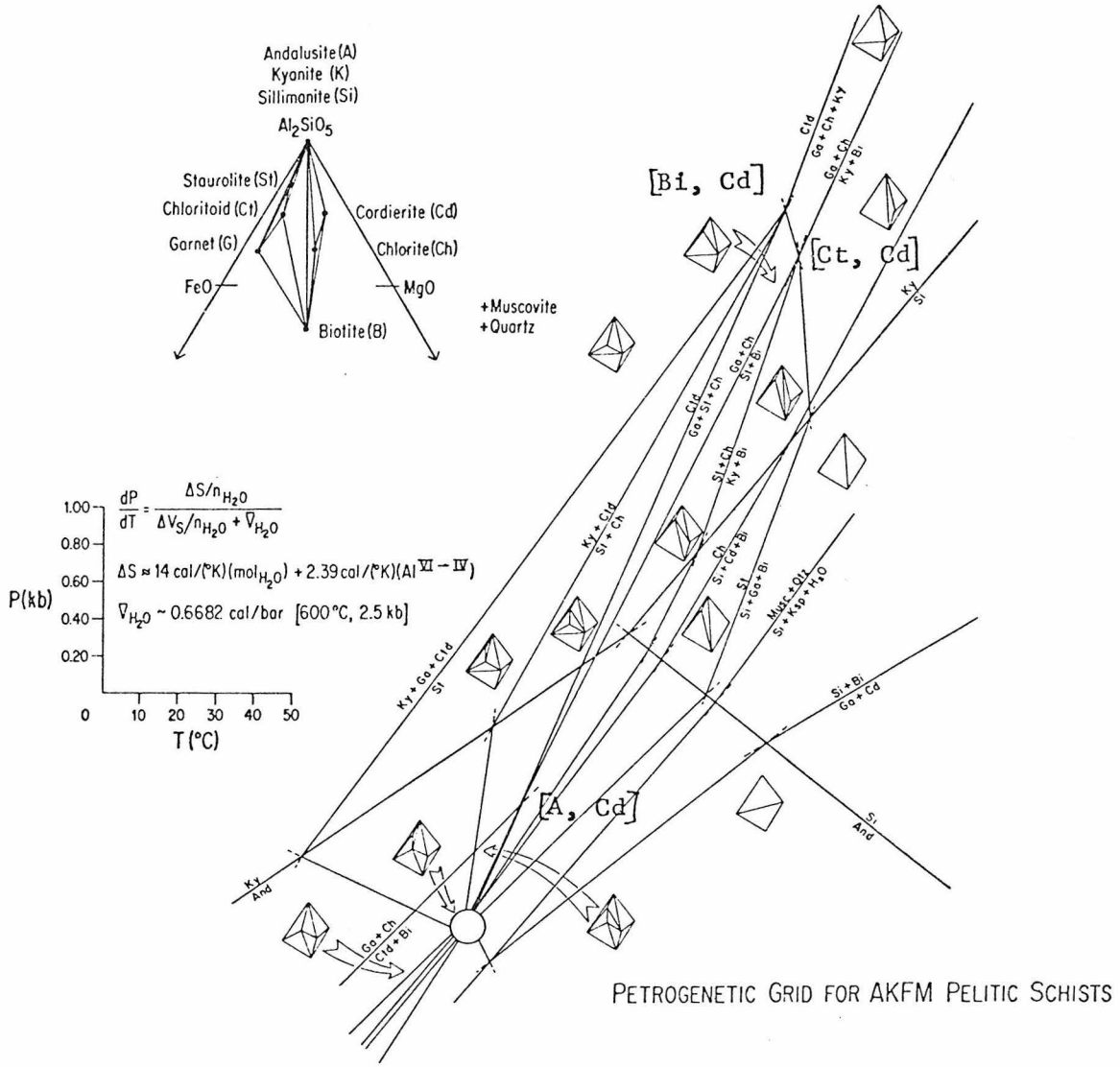

Figure 73a: (small circle enlarged in Figure 73b and 73c).

Figure 73b:

PETROGENETIC GRID FOR AKFM PELITIC SCHISTS: CORDIERITE-PRESENT INVARIANT POINTS

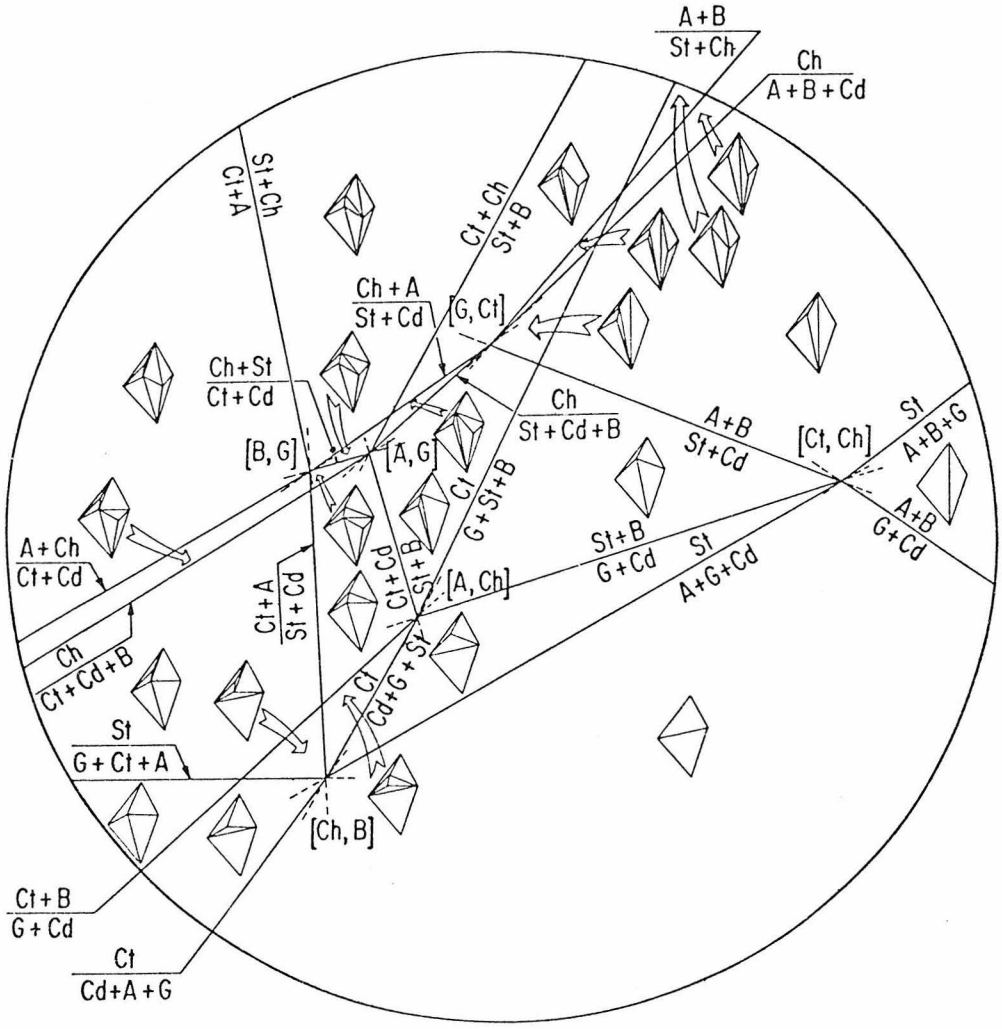

Expansion of Figure 73a; slopes and fields exaggerated for clarity

Figure 73c:
CALCULATED SLOPES FOR CORDIERITE - PRESENT REACTIONS

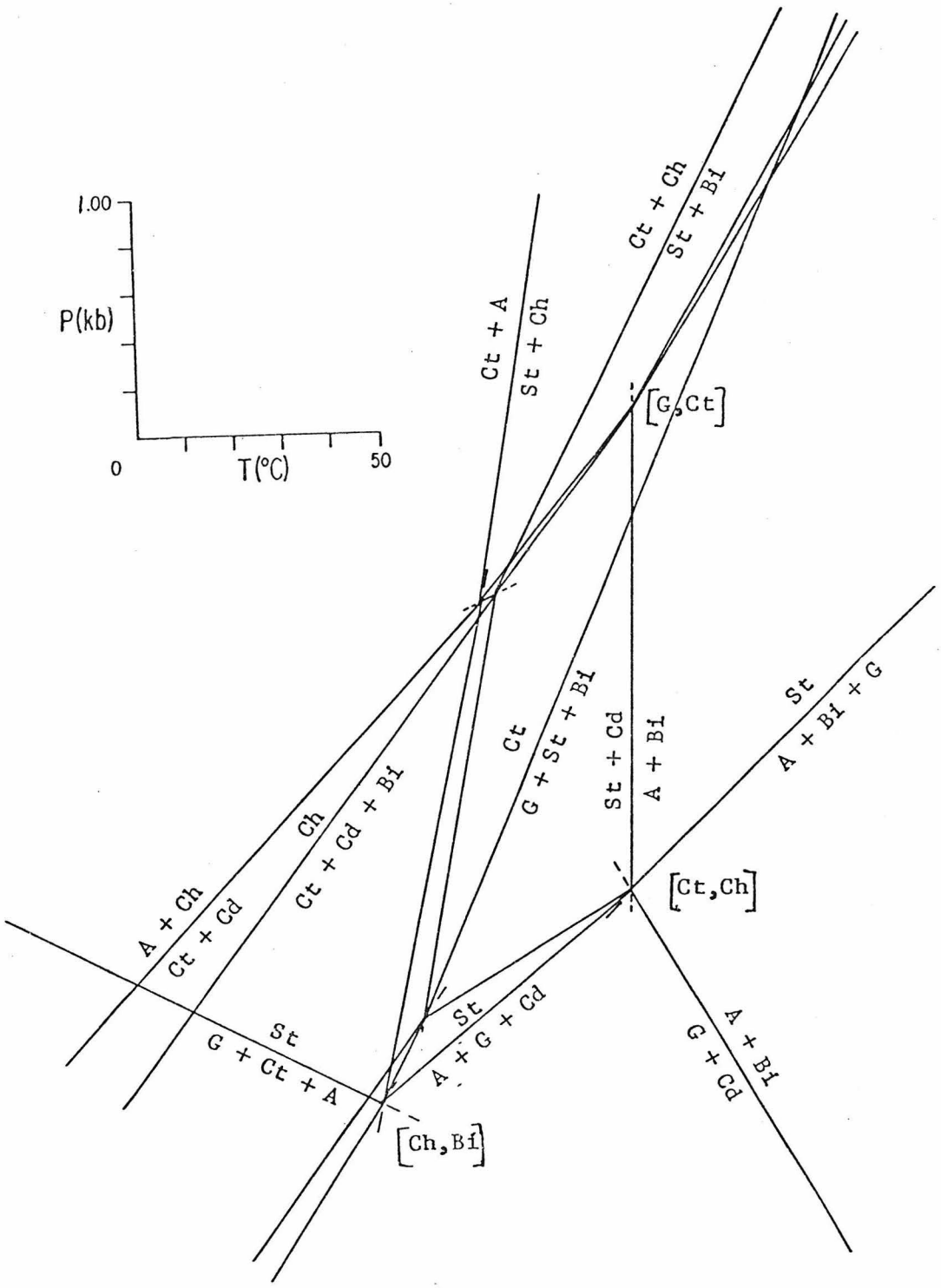

(see Figure 73b for reactions not labeled here)

at which the value 14 cal/°K mole H_2O for dehydration is valid). At high pressures, especially above 1 kb, dehydration reactions have steep, nearly constant slopes. The actual values of the calculated slopes are unimportant and are used only to construct the topology of the petrogenetic grid. Where very steep slopes are indicated, the choice between positive and negative values was allowed to be free in order to construct a self-consistent topology.

The topology of the grid is contrained by the assumptions

1) [A, Cd] is stable and occurs in the andalusite field
2) The Al_2SiO_5 triple point lies between the reactions (A, Cd, Ctd) and (Cd, Ctd, Ga)
3) The invariant point [Ga, Ctd] lies between the reactions (A, Cd, Ga) and (A, Cd, Ch).

Assumption 2 allows the reaction

$$\text{staurolite} + \text{chlorite} = Al_2SiO_5 + \text{biotite}$$

to allow any of the aluminosilicates coexist with biotite early (kyanite in Funeral Mountains, andalusite in Panamint mountains, sillimanite in Maine [Guidotti, 1974]). Assumption 3 allows the coexistence of andalusite + biotite before chloritoid breaks down, a possible, but undetermined relation in the Panamint Mountains.

Figure 73 is a useful extension of Albee (1965c) because it successfully predicts all reactions which are observed or inferred in the Panamint and Funeral Mountains. The majority of the P-T field, except at low pressures, is dominated by reactions which do not involve cordierite. In fact, the steep-sloped reactions which span most of the field correspond to naturally occurring isograds mapped in meta-

morphic field studies. The staurolite isograd corresponds to garnet + chlorite = staurolite + biotite, and the kyanite-in isograd corresponds to staurolite + chlorite = kyanite + biotite, and so on.

The P-T trajectory traversed by the Panamint Mountains metamorphism passes on the low pressure side of the invariant point [A, Cd], into the sillimanite field within the stability limit of staurolite. The trajectory crosses reactions which limit the stability of chlorite over a small increment of temperature. The occurrence of andalusite + biotite assemblages is realized at relatively low temperatures, as is apparent from field observations. The slope of the reactions (A, Cd, St) is relatively low and the assemblage garnet + chlorite may never have been stable.

The Funeral P-T trajectory crosses chlorite-limiting reactions over a much greater temperature interval, and staurolite breaks down within the kyanite stability field. Garnet + chlorite is stable over a large temperature range.

An attempt to quantify this petrogenetic grid is shown in Figure 74. Quantifying the grid so that calculated slopes and relative positions of reactions are consistent with experimental data proved very frustrating. The actual calculated slopes were abandoned except that the relative topology remains the same. The grid was fixed by the aluminosilicate triple point of Holdaway (1971), by the assumption that the [A, Cd] invariant point is in the vicinity of 2.5 kb, 475°C, and by the relation between the stability of staurolite and the calculated maximum temperature noted for the Panamint and Funeral Mountains.

Figure 74 cannot be taken too seriously, because it is largely con-

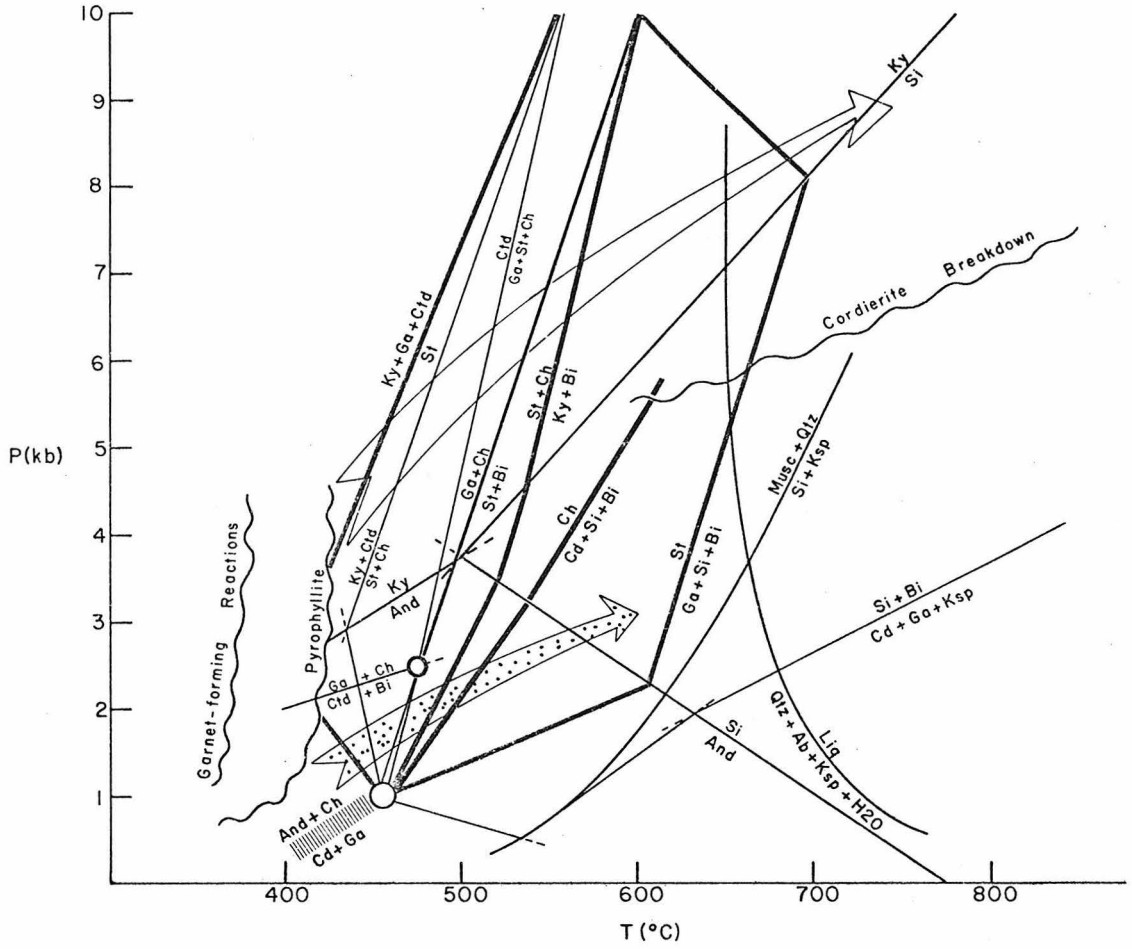

Figure 74: Approximate orientation of petrogenetic grid in p - T space.

structed on a topologic basis. It is useful, though, to illustrate the gross differences in P/T exhibited by the Panamint and Funeral Mountains. The geothermal gradient recorded in the Panamint Mountains is a relatively hot 60° C/km whereas the Funeral Mountains terrain found is a gradient of approximately 28° C/km.

RECONCILIATION: GEOLOGICAL ENVIRONMENT DURING METAMORPHISM

The working assumption throughout is that metamorphism in the Panamint and Funeral Mountains was synchronous and occurred about 80 m.y. ago. If regional metamorphism is directly related to magmatism, metamorphism may have occurred during the Jurassic when most of the granitic rocks were emplaced in the White-Inyo Mountains area (Evernden and Kistler, 1970). It is difficult, based upon presently available maps and dates, to determine the distribution of Cretaceous and Jurassic granitic plutons in relation to the regionally metamorphosed terrains in the Panamint and Funeral Mountains. The most likely location for a heat source lay in the vicinity of the Argus Range which is comprised predominantly of Jurassic plutons (Moore, 1974) and Jurassic plutons occur in the Butte Valley area in the Panamints (Johnson, 1957; Armstrong and Suppe, 1973).

Metamorphism has occurred under a flattened dP/dT for both the Panamint and Funeral Mountains relative to estimates for "normal" geothermal gradients (Figure 75 and Clark and Ringwood, 1964). Metamorphic isograds in both the Panamint and Funeral Mountains cut across the stratigraphy, and, for example, the Kingston Peak Formation in the Panamint Mountains is highly metamorphosed at the western edge of the

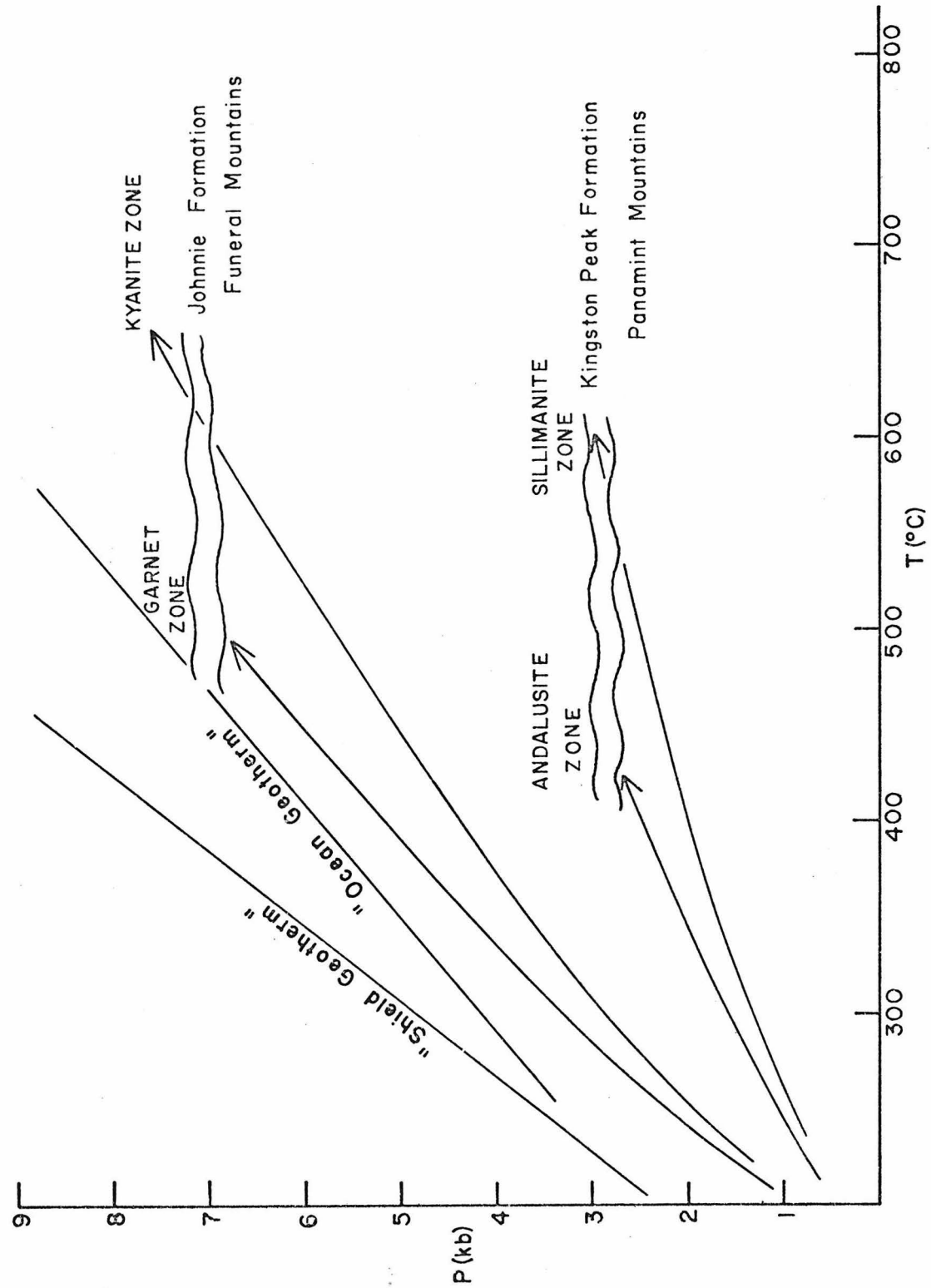

Figure 75: P/T gradients exposed in the metamorphic terrains.

range, but it is essentially unmetamorphosed east of the range crest. Similarly in the Funeral Mountains the Johnnie Formation occurs in the garnet zone and in the staurolite zone. If the depth of burial was constant over these differences in grade and if increase in grade indicates increase in temperature, then the thermal gradient must change over these distances. Figure 75 illustrates the change in gradient over the Panamint and Funeral Mountains.

A cartoon reconstruction of the thermal regime is shown in Figure 76 in which enough displacement on the Death Valley-Furnace Creek fault zone is replaced so that central Death Valley is closed (Burchfiel and Stewart, 1966). A high heat source is provided by production and/or emplacement of batholithic rocks in the Argus Range area. With distance from the source, the thermal gradient will decrease to the relatively low values suggested by the Funeral Mountains.

The approximate doubling in thickness of cover in the Funeral Mountains remains an enigma. The only feasible method appears to be selective burial of the Funeral Mountains by thrust sheets. Pre-Middle Jurassic thrusts are evident in the northern Grapevine Mountains (Reynolds, 1974), in the northwest Panamint Mountains (Hall, 1971) and the Cottonwood Mountains (McAllister, 1956).

It is possible to conceive a geologic model to explain the variations in the styles of metamorphism in the Panamint and Funeral Mountains. Several hypotheses and relations remain to be tested and determined. The ages of the terrains are not yet determined to be the same, nor is the age of metamorphism in the Panamints conclusively

POSSIBLE RECONSTRUCTION FOR SIMULTANEOUS DEVELOPMENT OF REGIONAL METAMORPHIC TERRAIN, DEATH VALLEY CALIFORNIA

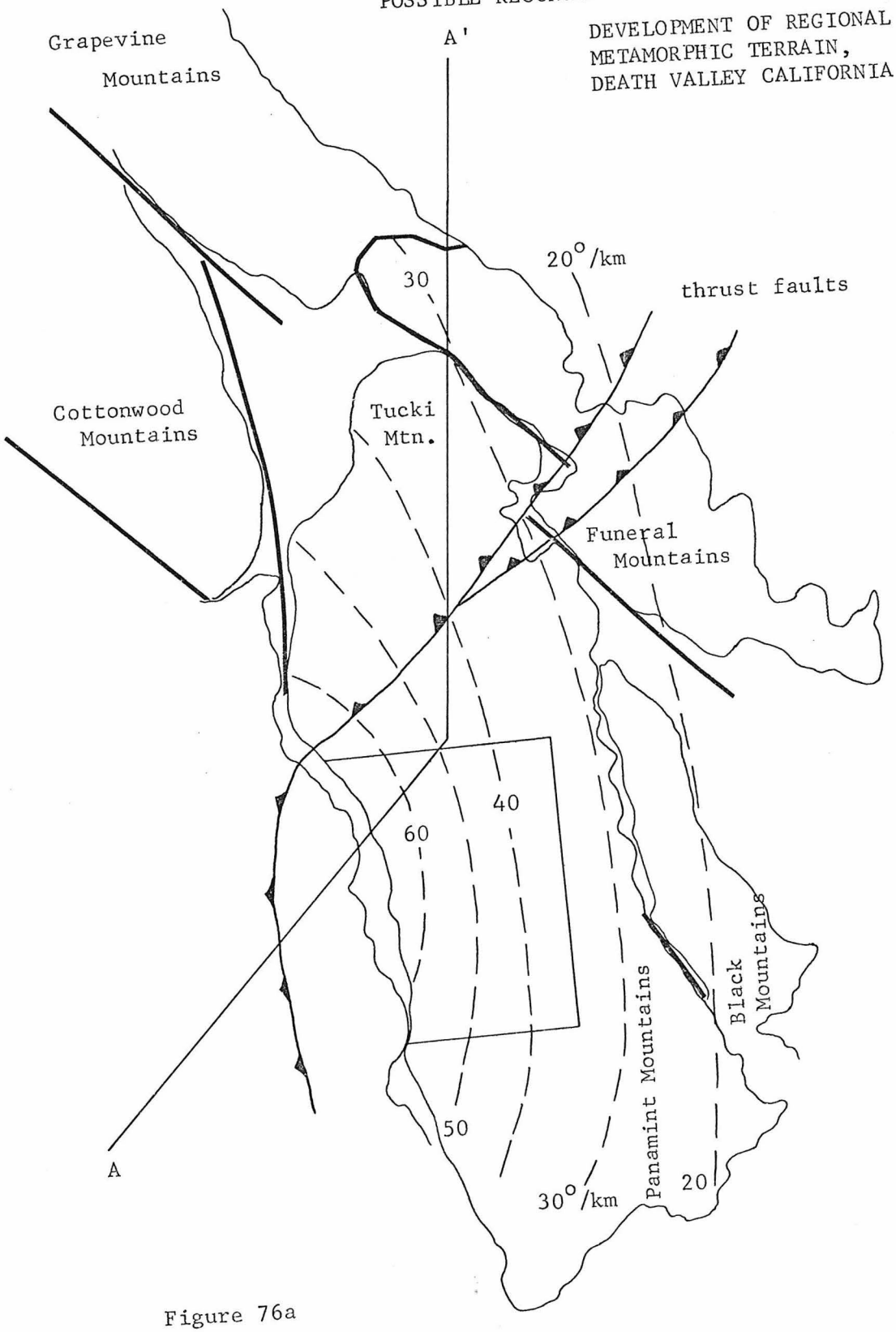

Figure 76a

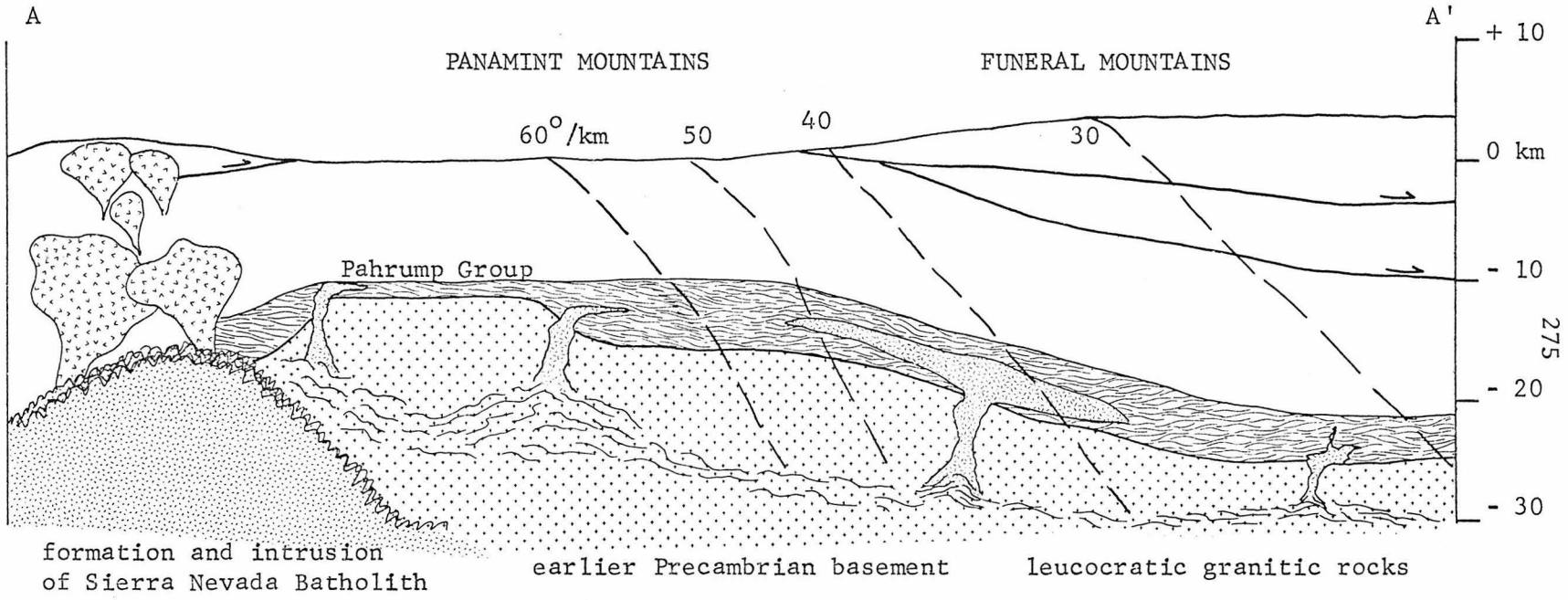

Figure 76b: Schematic cross section indicated in Figure 76a.

determined to be Jurassic or Cretaceous. In addition, the relation between metamorphism and plutonism is unclear, particularly if the granitic rocks in the Argus-Inyo-White Mountains are all Jurassic and metamorphism is Cretaceous. Regional metamorphism affected the Precambriam strata in which there is a dearth of granitic rocks, and yet the granitic rocks in the Argus and Cottonwood Mountains intrude upper Paleozoic strata which occur in large part as roof pendants. As indicated in part I, the structural relation between the Panamint Mountains and the regions to the west of the Panamint Valley fault zone are unclear. The Panamint Mountains are comprised of a folded metamorphic terrain and the regions to the west consist of rocks greatly involved in thrust faulting. Whatever the ultimate origin of the metamorphic terrain two constraints are imposed by the facies series exposed in the Panamint and Funeral Mountains. First, a region of high heat flow existed in the area now occupied by Panamint Valley and Argus Range, and second, the Funeral Mountains were buried to a depth greater than about twice the apparent stratigraphic thickness.

LOW PRESSURE METAMORPHISM OF CALCIFEROUS SCHIST, PANAMINT MOUNTAINS

INTRODUCTION

Calciferous schists are abundant in both the tremolite and diopside zones in the low pressure regional metamorphic terrain of the Panamint Mountains, particularly in the widespread Kingston Peak Formation. The most common assemblage is epidote + biotite + plagioclase + quartz, but calcic amphibole is an additional constituent in many assemblages. This section describes the distribution of elements among phases during progressive low-pressure metamorphism of calciferous schist.

The calciferous schists are generally fine-grained, and compositional inhomogeneities, sedimentary bedding, and clasts in conglomerates are well preserved, even in the diopside zone. Unlike most other constituent phases, amphiboles in calciferous schists occur as porphyroblasts several millimeters in size, and rocks in which amphibole is abundant are medium- to coarse-grained. These large amphibole grains are optically zoned and show evidence for polymetamorphism. In most cases hornblende shows patchy alteration to actinolite, but in some samples discontinuous zoning is developed. Typical of these samples, CP 470 contains dark green hornblende with colorless actinolite rims, and CP 349 contains colorless actinolite with green hornblende rims (Figure 77). Such samples also contain smaller, matrix amphibole with optical characteristics similar to those of the rims on larger amphiboles. The compositional range of amphibole preserved in these polymetamorphosed samples in some cases matches the total compositional range of amphibole developed during the primary metamorphism. This wide range allows the determination of substitutional

Figure 77: Polymetamorphic textures in calciferous schist, Panamint Mountains.

a) Dark hornblende rims on actinolite (light) core in hornblende + plagioclase + quartz assemblage, CP 349 (plane polarized light).

b) Pale actinolite rim on dark hornblende core in biotite-rich matrix, CP 470 (plane polarized light).

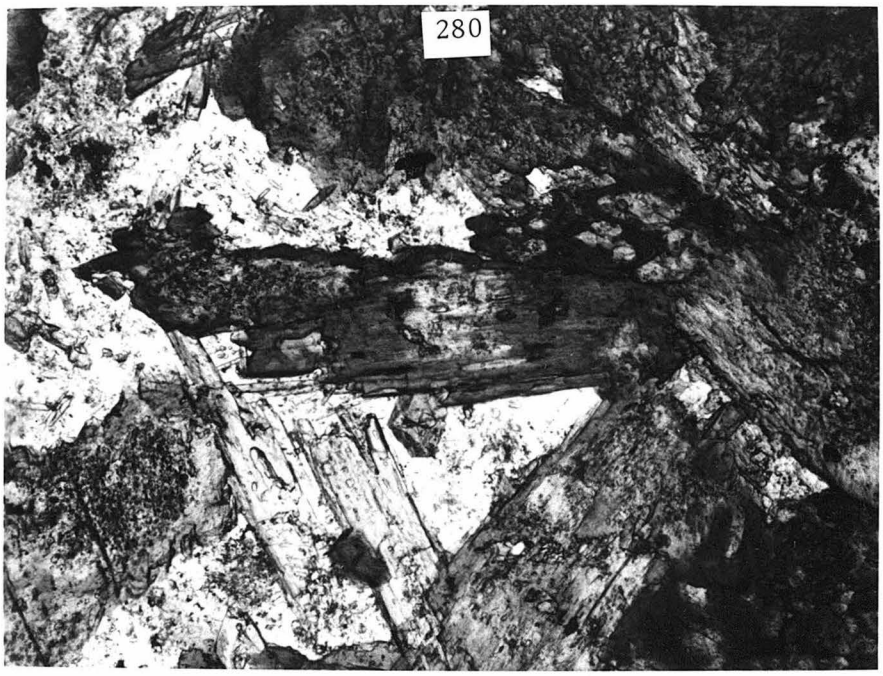

a

0.5 mm

b

50 μm

mechanisms responsible for compositional variations in these amphiboles, but the effects of polymetamorphism have made difficult the determination of equilibrium mineral assemblages in calciferous schists and of equilibrium element partition among these phases. A large number of phases coexist with calcic amphibole, and it was hoped that several progressive metamorphic reactions would be displayed. The superposition of the second metamorphism has confused the phase relations of the first. Nevertheless, the gross characteristics of the phase relations in calciferous schists can be deciphered, and a potentially useful generalization of the phase relations in potassium-rich calciferous schists is proposed. The compositional variations in calcic amphiboles are outlined, and the substitutional mechanisms are described.

MINERAL FACIES IN CALCIFEROUS SCHISTS

Numerous samples of calciferous schist were analyzed by electron microprobe techniques. Samples were chosen to provide assemblages representative of a wide range in bulk composition. The analyzed samples, their mineral assemblages, and locations are tabulated in Table 14 and Figure 78. Complete chemical analyses may be obtained from the author upon request.

In general, the relative partition of iron over magnesium in coexisting mafic phases is small and mineral assemblages in calciferous schist may be represented on the plane $Al_2O_3 + Fe_2O_3$, CaO, FeO + MnO + MgO (ACF). The compositions of minerals in selected tremolite zone assemblages are illustrated in Figure 79. The characteristic

TABLE 14: ANALYZED SAMPLES, CALCIFEROUS SCHIST, PANAMINT MOUNTAINS

SAMPLE	QTZ	EPID	PLAG	CA-AMP	FM-AMP	CHL	GAR	DIOP	BIO	MUSC	MICR	GROSS	PREHN	CAL	ILM	SPH	MAG	OTHER*	LOCATION
Tremolite Zone																			
P 46	X	X	X	X		X			X		X						X		EQ
P 230	X	X		X					X		X					X		goeth	EQ
P 256	X	X				X			X	X				X				graph	EQ
P 272	X	X	X			X			X	X				X		X			EQ
CP 156	X		X	X					X						X				1
CP 183	X	X	X	X		X			X	X				X	X	X			2
CP 332a	X		X	X					X						X				3
CP 349	X		X	X		X			X						X			goeth	4
CP 401	X	X	X				X		X	X					X			unk	5
CP 414	X		X	X			X		X		X				X				6
CP 446	X		X	X		X									X				7
CP 463	X					X			X		X			X		X		scap	8
CP 470	X	X	X	X					X	X	X			X		X			9
PML 141c	X	X	X	X					X		X			X					10
PML 214b		X	X	X					X					X		X			11
PML 242	X		X	X	X	X	X		X									stilp	12
PML 255	X	X	X	X		X			X	X	X			X		X			13
PML 268	X	X	X	X		X			X	X								graph	EQ
Diopside Zone																			
McD 350a	X	X	X	X			X		X	X					X				14
P 99		X		X				X								X			15
P 101			X	X		X		X	X							X			15
CP 128	X	X	X				X		X	X			X	X	X				16
CP 422a	X		X			X	X		X		X			X					17
CP 478b	X		X	X		X		X	X				X	X	X				18
CP 482		X		X						X	X				X	X			19
CP 483a				X		X		X							X				19
CP 483b	X	X	X	X		X									X				19
CP 485	X	X	X	X					X							X			20
PML 24a	X	X	X	X		X		X	X	X									21
PML 37a	X		X	X	X	X			X						X				22
PML 37b	X	X	X	X		X			X	X					X				22
PML 39	X	X	X	X			X		X	X			X	X	X	X			22
PML 52b	X	X	X				X		X	X			X		X			goeth	23
PML 61	X	X	X	X				X	X	X	X					X		rut	24
PML 112		X		X		X			X						X	X			25
PML 157a	X		X	X	X		X		X									stilp	26
PML 163	X	X	X	X		X			X	X			X					rut	27
PML 166b			X	X				X	X						X	X			28
PML 167c	X	X		X		X					X				X	X			28
PML 182a	X	X	X	X		X				X	X					X			14
PML 189c	X	X	X					X			X	X						fluor	29
PML 190b	X	X	X	X				X			X								29
PML 195a	X	X	X	X			X		X	X			X		X	X			20
PML 219a	X	X		X		X			X					X	X	X			30
PML 225a	X			X	X	X	X		X						X		X	stilp	31
PML 225b	X	X	X	X			X		X						X				31
PML 232	X			X			X		X		X					X		graph	32
PML 234a	X	X	X	X				X	X	X	X					X			32
PML 234b	X	X	X	X		X	X		X	X				X	X	X			32

*goeth = goethite, graph = graphite, unk = unknown phase, scap = scapolite, stilp = stilpnomelane, fluor = fluorite, rut = rutile EQ - Wildrose Canyon, Emigrant Canyon Quadrangle

All minerals except quartz, goethite, graphite, and rutile are analyzed; location refers to Figure 78.

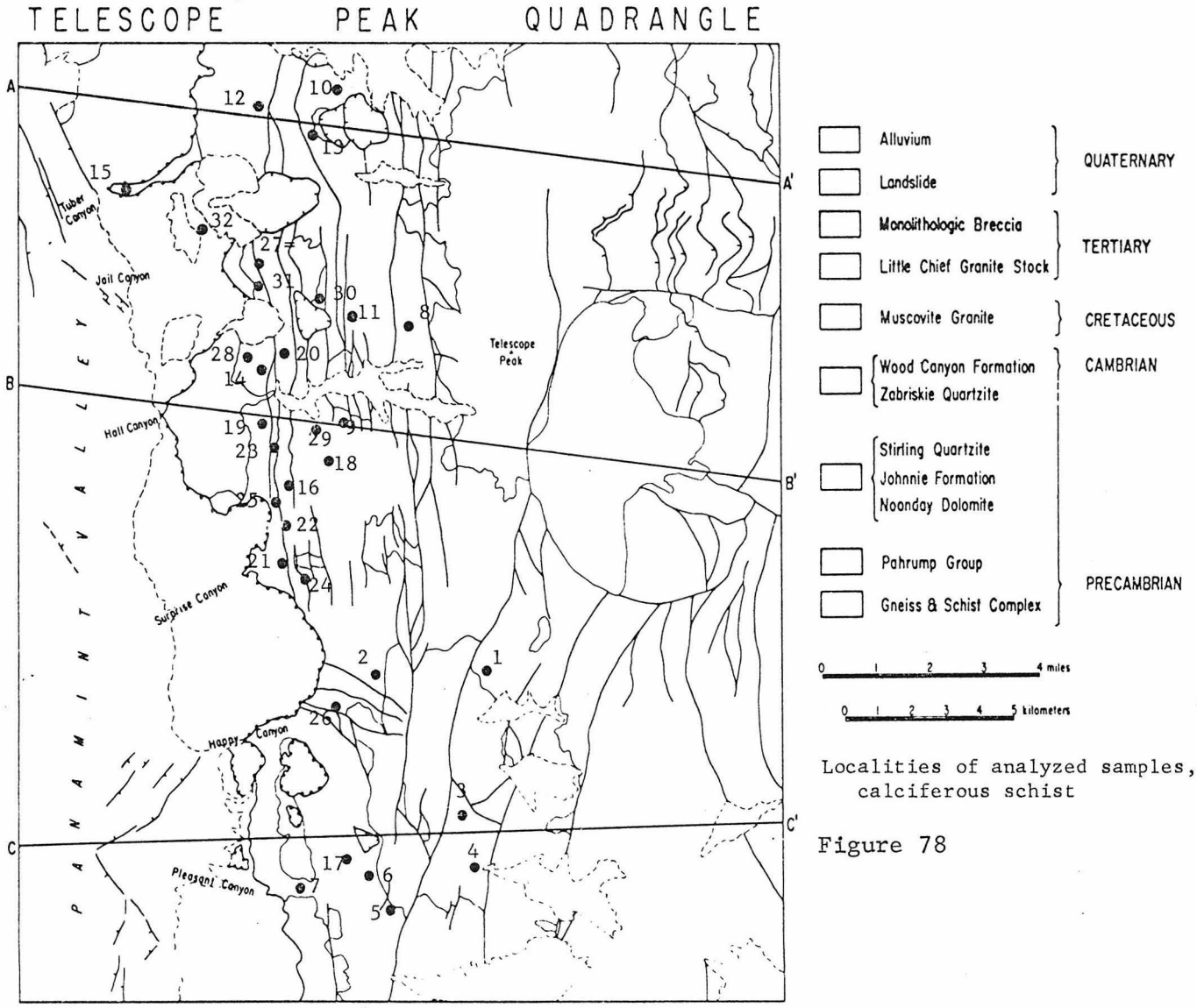

Localities of analyzed samples, calciferous schist

Figure 78

assemblage exhibited in the tremolite zone is quartz + epidote + calcic amphibole + chlorite + plagioclase + calcite + biotite + (ilmenite or sphene). PML 268 was collected near the tremolite isograd, and this relatively low grade rock contains actinolite. In the higher grade portions of the tremolite zone represented by CP 183 and P 46, amphibole contains substantially more aluminum. The composition of plagioclase which coexists with amphibole and epidote is also shown in Figure 79. There is a general correlation between the composition of amphibole and plagioclase; the more aluminous the hornblende is, the more aluminous (anorthitic) the coexisting plagioclase. The actinolite in the lower grade sample PML 268 coexists with An_8 plagioclase, and the hornblende from the higher grade sample CP 183 coexists with An_{39} plagioclase. One sample, PML 214b, which was collected in the vicinity of the diopside isograd contains plagioclase with the composition An_{97}. PML 214b contains no quartz and the very aluminous nature of the plagioclase may be the result of undersaturation in SiO_2.

The greater variety of mineral assemblages which occur in the diopside zone are illustrated in Figure 80. The diagnostic magnesium-rich assemblages, shown in Figure 80a, include

quartz + epidote + Ca-amphibolte + chlorite

quartz + epidote + Ca-amphibole + diopside

quartz + epidote + diopside + grossular

quartz + chlorite + Ca-amphibole + cummingtonite.

The Ca-amphibole which coexists with chlorite and epidote is more aluminous than amphibole which coexists with diopside or cummintonite,

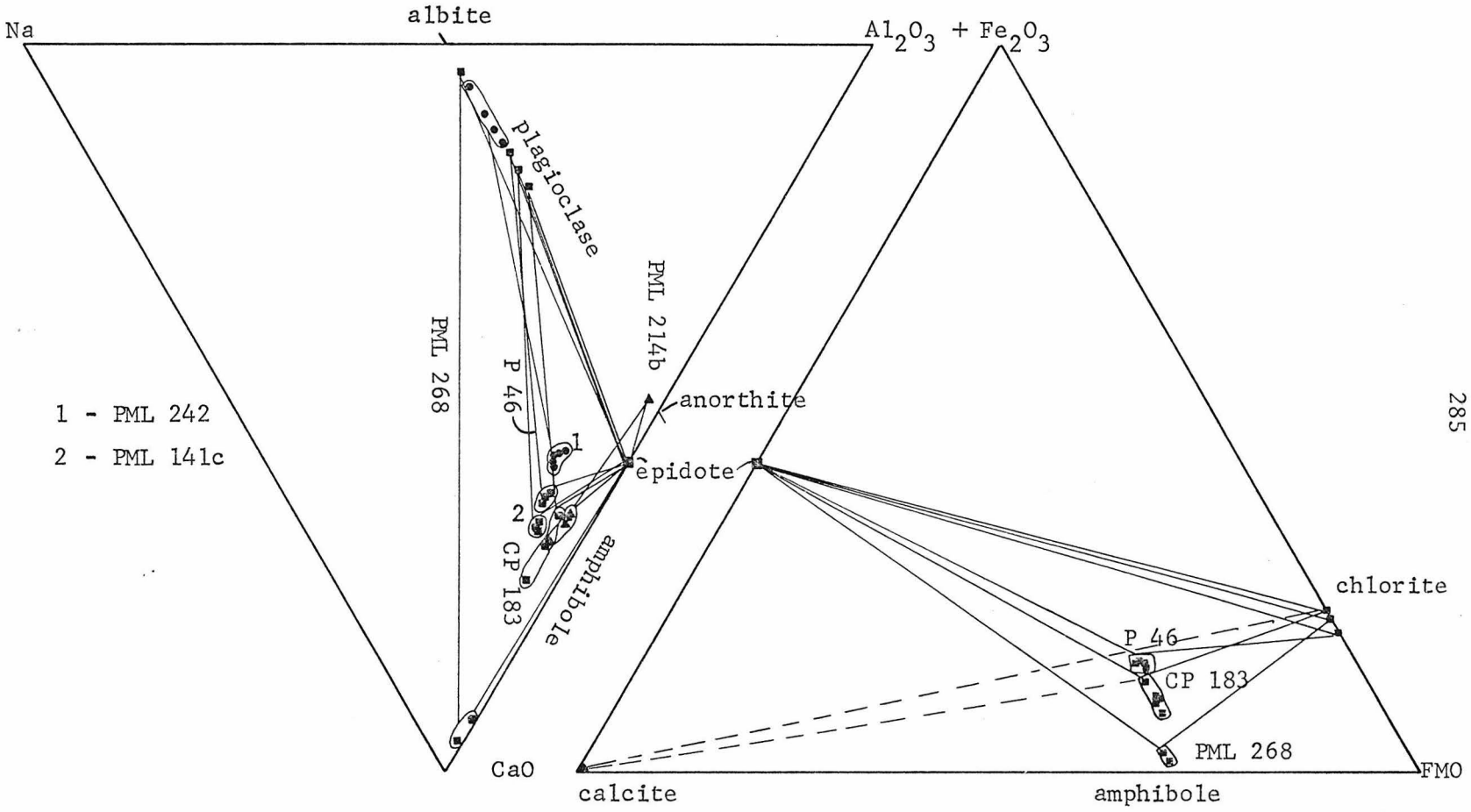

Figure 79: Mineral assemblages in calciferous schist, Panamint Mountains. Tremolite zone.

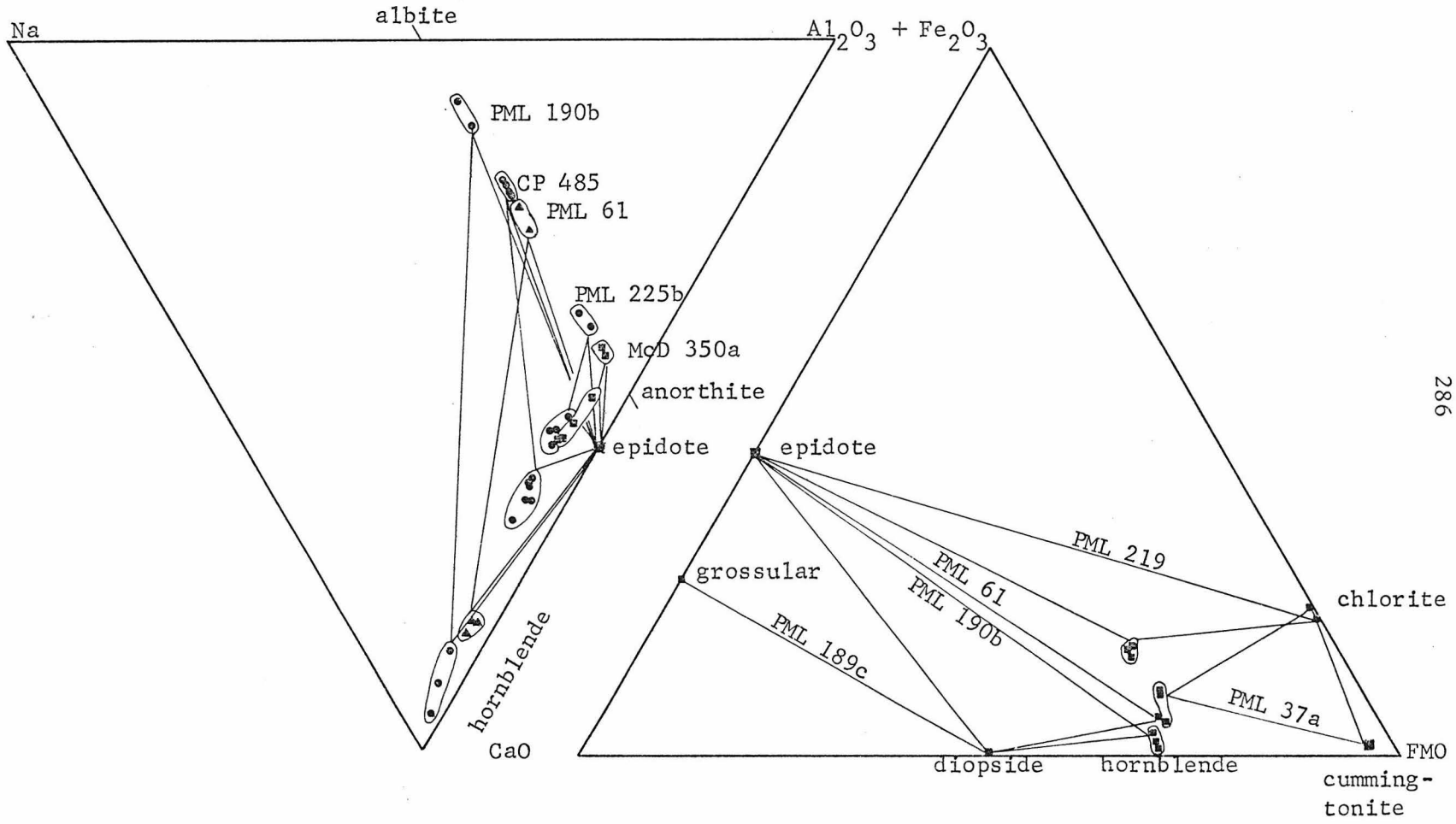

Figure 80a: Mineral assemblages in Mg-rich calciferous schist, Panamint Mountains, diopside zone.

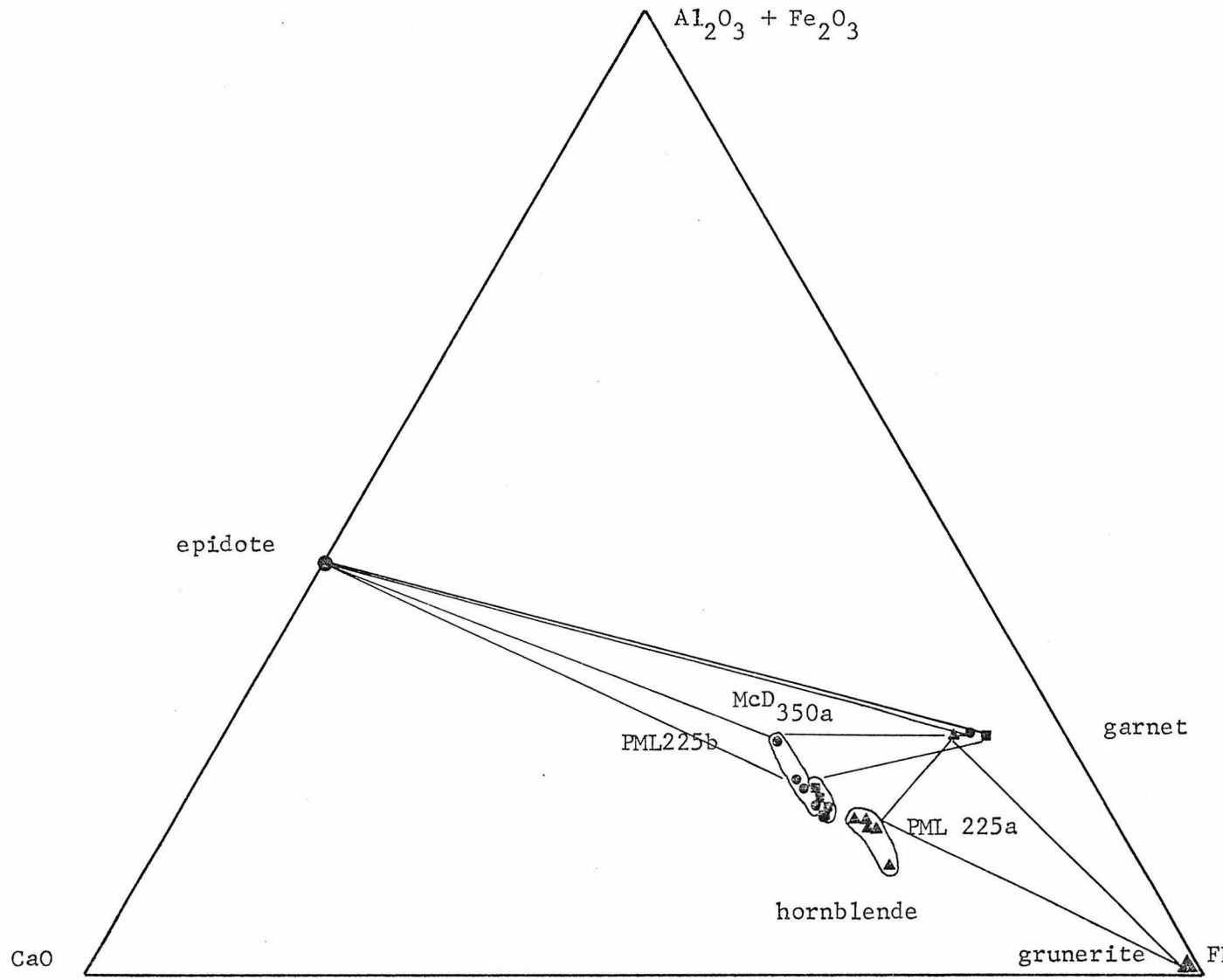

Figure 80b: Mineral assemblages in Fe-rich calciferous schist, Panamint Mountains, diopside zone.

and calcic amphibole which coexists with cummingtonite appears to be richer in Mg + Fe than amphibole which coexists with diopside. These relations are also observed in the more iron-rich assemblage

quartz + epidote + hornblende + garnet

quartz + hornblende + garnet + grunerite

(Figure 80b). The distribution of iron, magnesium, and calcium between coexisting diopside + hornblende, and hornblende + Fe-Mg amphibole is shown in Figure 81. The pyroxene compositions fall in the diopside-hedenbergite series and tend to be slightly more magnesium-rich than coexisting hornblende, although the Fe^{2+}-Mg distribution coefficient is very nearly one. Hornblende which coexists with cummingtonite or grunerite contains slightly less calcium than amphibole which coexists with diopside. Hornblende is more magnesium-rich than coexisting cummingtonite, but hornblende is slightly more ferrous iron-rich than coexisting grunerite. However, this effect may be due to the procedure for estimating the amount of ferric iron in amphibole; an inaccurate estimate of Fe^{3+} will change the Fe^{2+}/Mg ragio in amphibole and may cause the apparent reversal in distribution.

The composition of plagioclase in these diopside zone assemblages is also shown in Figure 80a. The generality observed in tremolite zone samples holds. In epidote + quartz assemblages, the more calcic plagioclase coexists with the more aluminous hornblende. The most aluminous hornblende observed occurs in McD 350a, and the amphibole coexists with garnet and An_{89} plagioclase. Only well-behaved samples are plotted in Figure 80a. Most others contain a large range in plagioclase composition (consult Figure 43) which is due to the super-

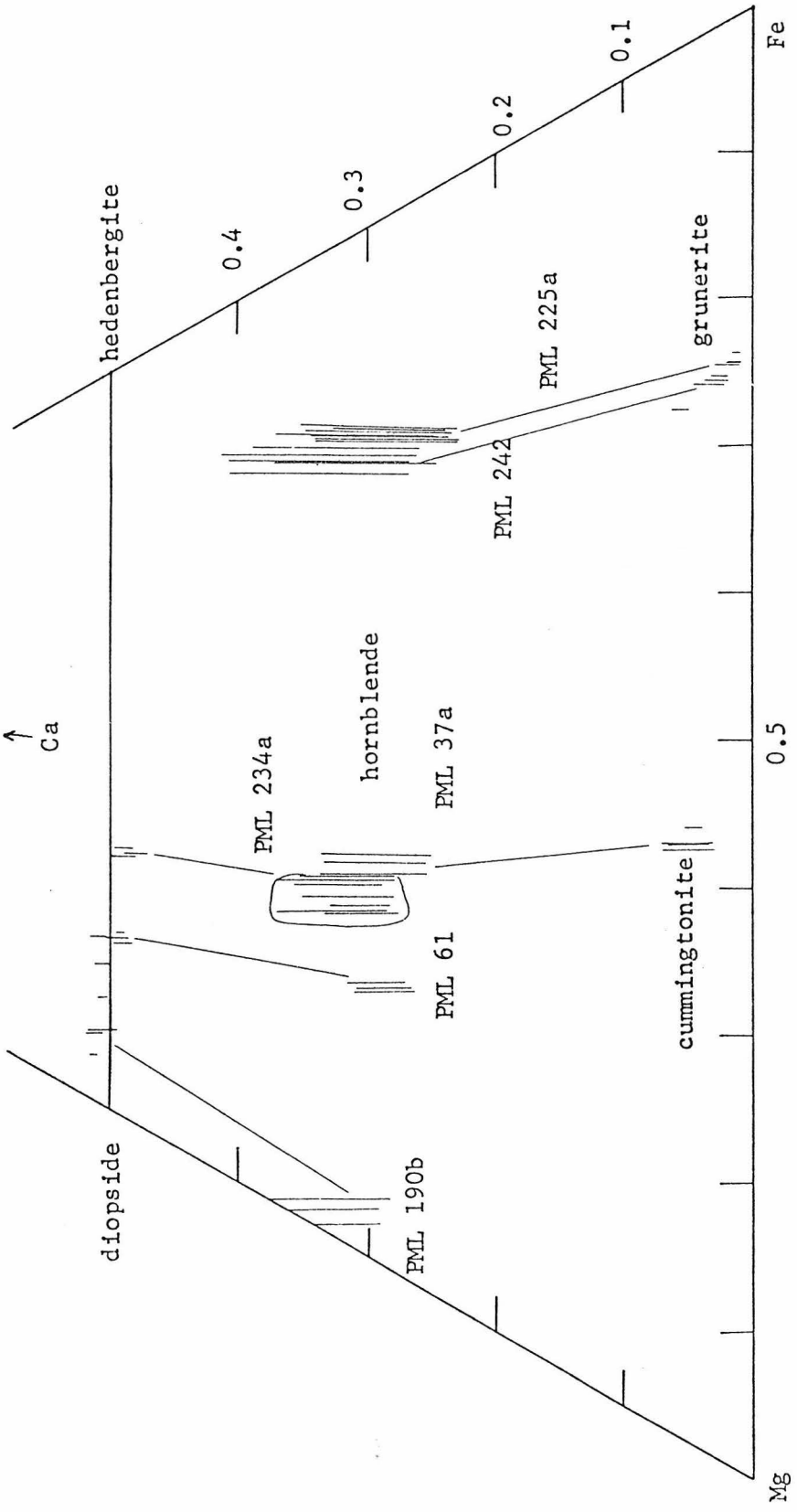

Figure 81: Distribution of Ca, Mg, and Fe between coexisting hornblende and diopside, and coexisting hornblende and Fe-Mg amphibole, Panamint Mountains. Length of line represents the amount of other components (principally aluminum) in six- and eight-fold sites.

position of the retrograde metamorphism. These selected samples which appear to have been minimally affected by retrograde metamorphism do show a consistent sense of partition of the major elements and indicate the approach to equilibrium.

DISTRIBUTION OF POTASSIUM PHASES IN CALCIFEROUS SCHIST

Almost all assemblages in calciferous schist contain biotite, and several contain either muscovite or microcline in addition. In these assemblages it is possible to illustrate the relative partition of iron, magnesium, and aluminum among coexisting phases through two projections. The first projects from quartz + epidote + muscovite onto the plane $KAlSi_3O_8$ - FeO - MgO, and the second projects from quartz + epidote + microcline onto the plane $KAl_3Si_3O_{10}(OH)_2$ - FeO - MgO. The coordinates of phases on these planes were calculated by linear algebraic methods described by Greenwood (1975). These projections are phase diagrams if

1) Plagioclase is the principal Na-phase; Na does not stabilize hornblende
2) Ferric iron only rarely stabilizes an extra phase, but it does occur in significant amounts in epidote and amphibole. The lack of a ubiquitous ferric phase complicates the use of epidote as a projection point (analogous to Mn in garnet). Here ferric iron is considered inconsequential to the intrinsic stability of a phase and it is combined with aluminum.
3) Titanium is a trace element or occurs principally in ilmenite

or sphene.

4) Manganese occurs in substantial quantities in garnet. Because of its major role in garnet, a garnet analysis is represented by the altitude of a triangle whose size represents the amount of MnO. MnO occurs only in trace amounts in other phases.

5) Calcite presence is due to CO_2. Calcite is a very common phase and it is nearly always an "extra" phase. That is, when calcite is present there is always one more phase present than expected for an arbitrary choice of P and T and if a a_{CO_2} is a boundary value component. a_{CO_2} appears to be buffered by the rock, and its presence is indicated by the presence of calcite (see Zen, 1963, and 1974).

6) H_2O is a boundary value component.

7) All other components occur in extra phases; Zr in zircon, B in tourmaline, P in apatite, and REE in allanite.

The locations of phases in the two projections are shown in Figure 82.

Assemblages observed in the tremolite zone are shown in Figure 83 and include

quartz + epidote + muscovite + biotite + chlorite + Ca-amphibole

quartz + epidote + muscovite + biotite + garnet + unknow Ca-rich phase

quartz + epidote + muscovite + microcline + biotite + Ca-amphibole

quartz + epidote + microcline + biotite + chlorite + amphibole.

Biotite occurs in all assemblages and the apparent order of enrichment in Mg/Fe is garnet < biotite < chlorite < hornblende. Hornblende in

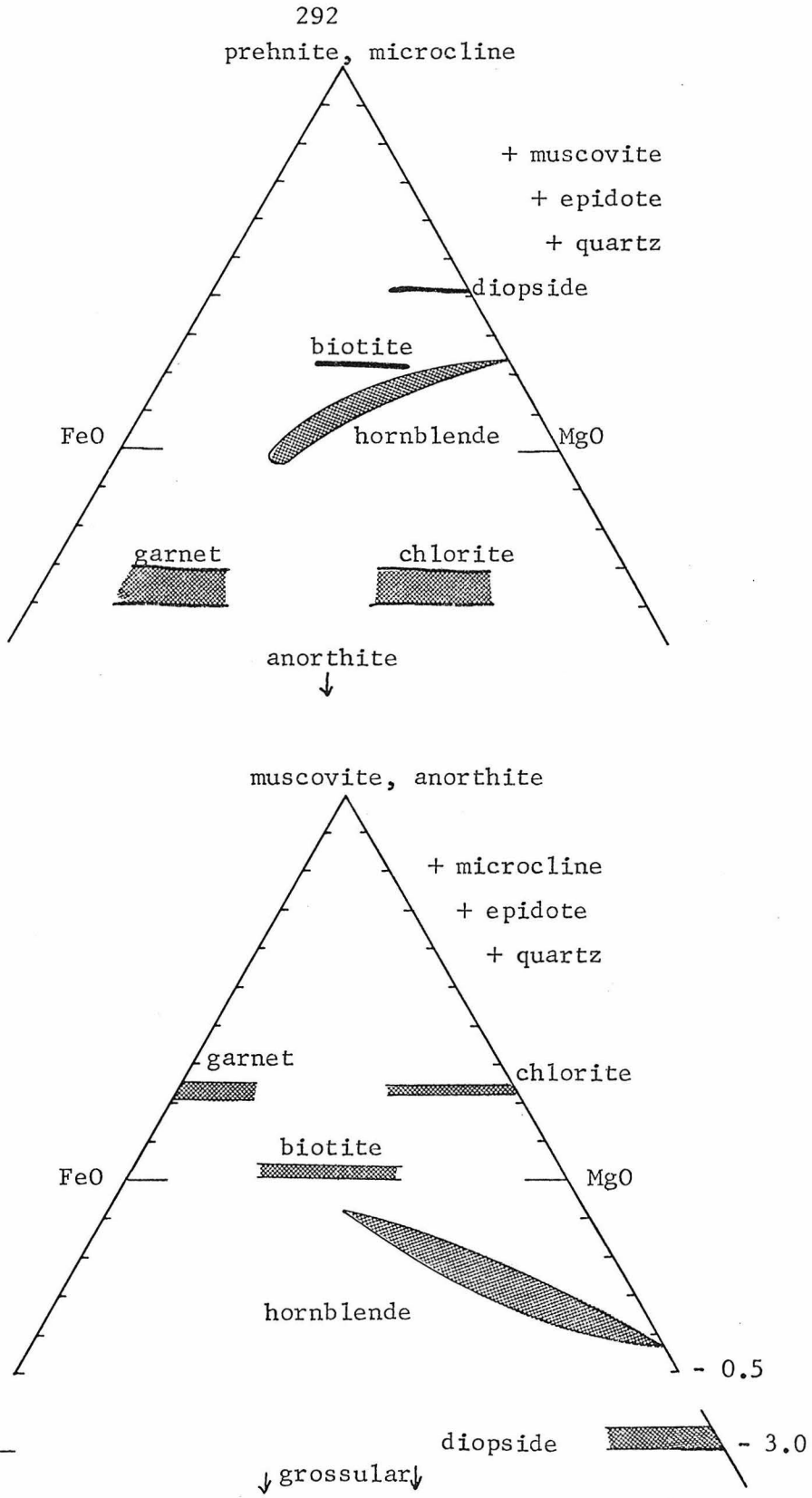

Figure 82: Locations of phases in projections used for potassium-rich, calciferous schist.

Figure 83: POTASSIUM - RICH CALCIFEROUS SCHIST, PANAMINT MOUNTAINS, TREMOLITE ZONE

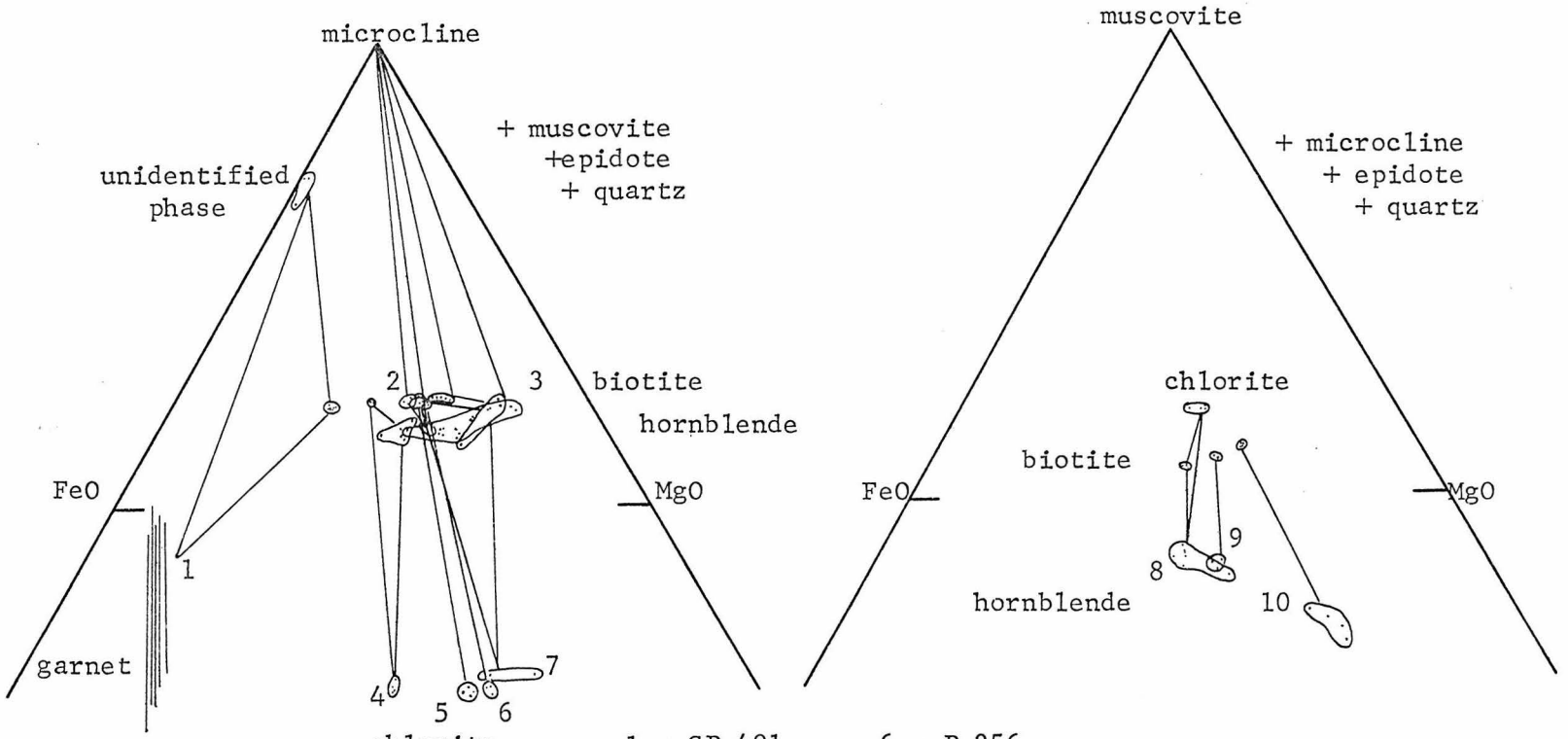

1 - CP 401
2 - PML 255
3 - CP 470
4 - CP 183
5 - P 272
6 - P 256
7 - PML 268
8 - P 46
9 - PML 141c
10 - P 230

CP 470 preserves a range in Mg/Fe which encompasses the Mg/Fe of both chlorite and biotite. The rims are magnesium-rich, and it appears that during retrograde metamorphism, amphibole only partially reacts with its matrix, but biotite and chlorite reequilibrate readily to the lower grade conditions. Because hornblende preserves a range in composition, the magnitude of the partition coefficient between amphibole and biotite is not certain.

Sample CP 401 contains an unidentified mineral in the assemblage garnet + biotite + muscovite + epidote + quartz. The mineral has a habit and optical properties similar to chlorite but its composition has the cation proportions

$$Si_{0.361}Al_{0.162}Ti_{0.010}Mg_{0.005}Fe_{0.090}Mn_{0.004}Ca_{0.367}$$

and contains 0.90 wt % fluorine. Because of the small grain size and low modal abundance, the mineral has not been x-rayed and its nature is uncertain, but its composition is indicated on Figure 83.

Potassium-rich assemblages from the diopside zone are shown in Figure 84. Retrograde metamorphism has strongly affected most diopside zone assemblages, and assemblages which are believed to represent equilibration during the primary metamorphism are illustrated in Figure 84a and 84b. Retrograde assemblages are shown in Figure 84c. The primary assemblages include

quartz + epidote + muscovite + garnet + biotite + hornblende

quartz + epidote + muscovite + microcline + diopside + hornblende

quartz + epidote + muscovite + microcline + biotite + hornblende

quartz + epidote + microcline + diopside + grossular.

Figure 84a: POTASSIUM - RICH CALCIFEROUS SCHIST, PANAMINT MOUNTAINS, DIOPSIDE ZONE

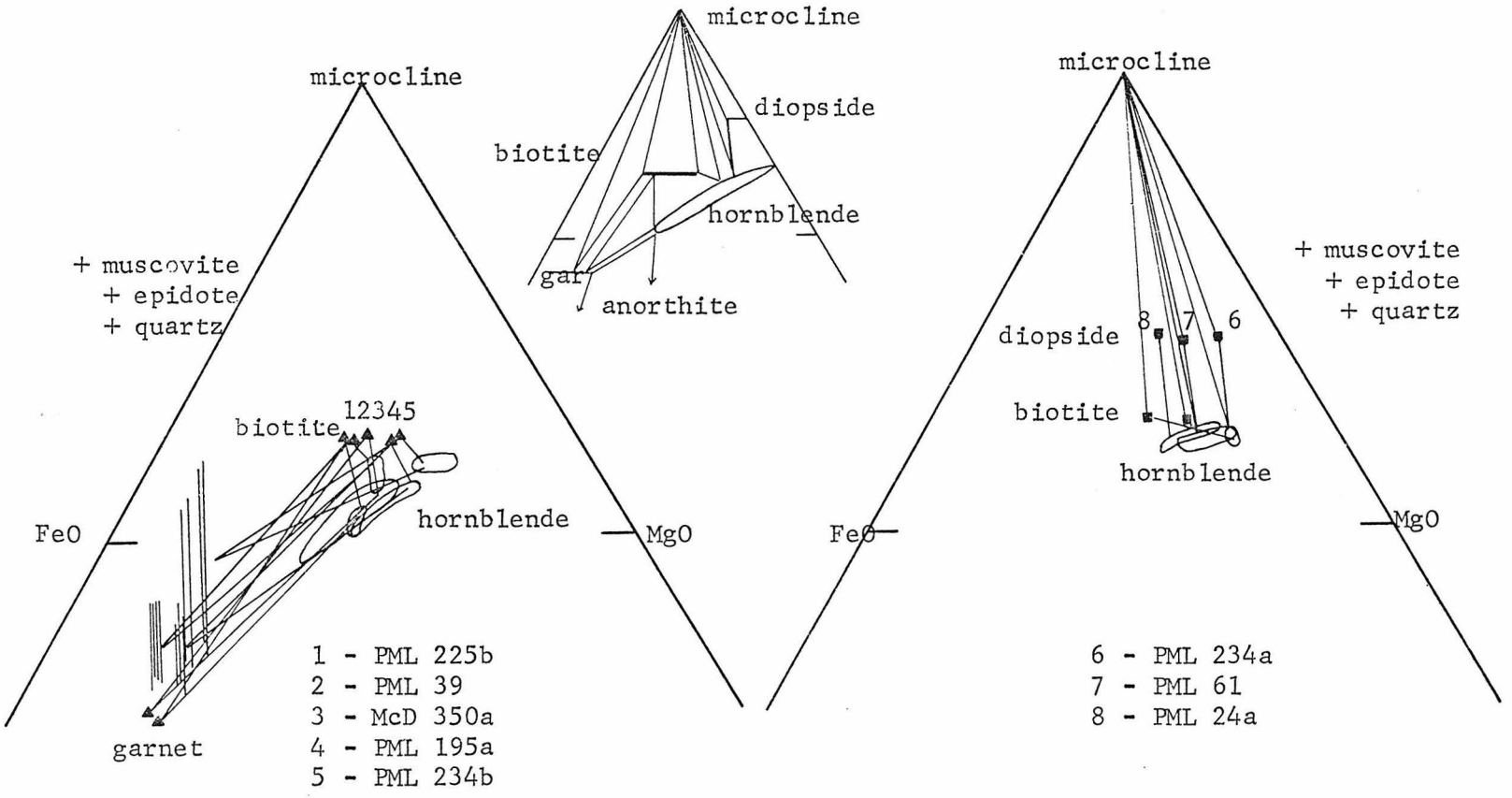

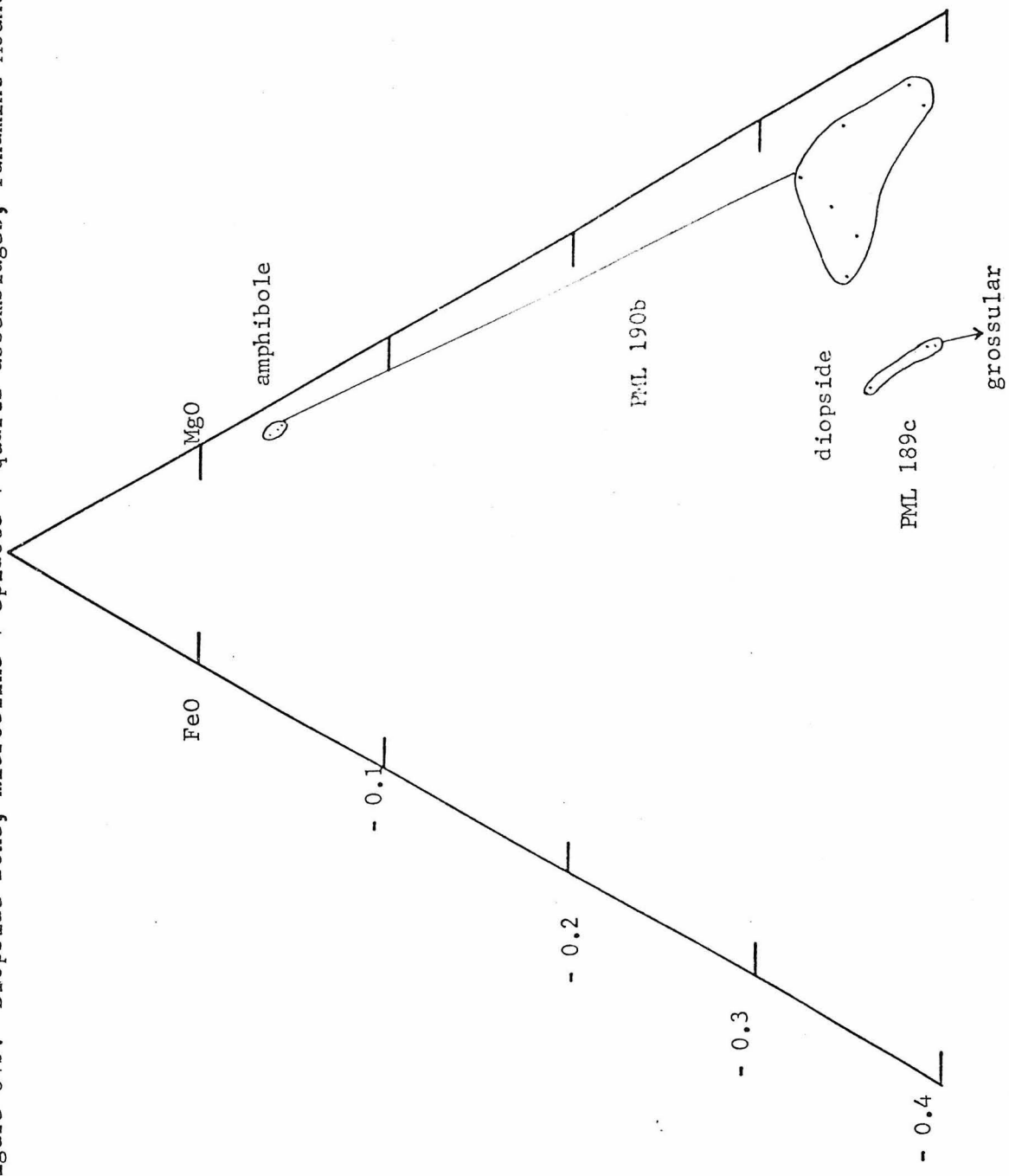

Figure 84b: Diopside zone, microcline + epidote + quartz assemblages, Panamint Mountains

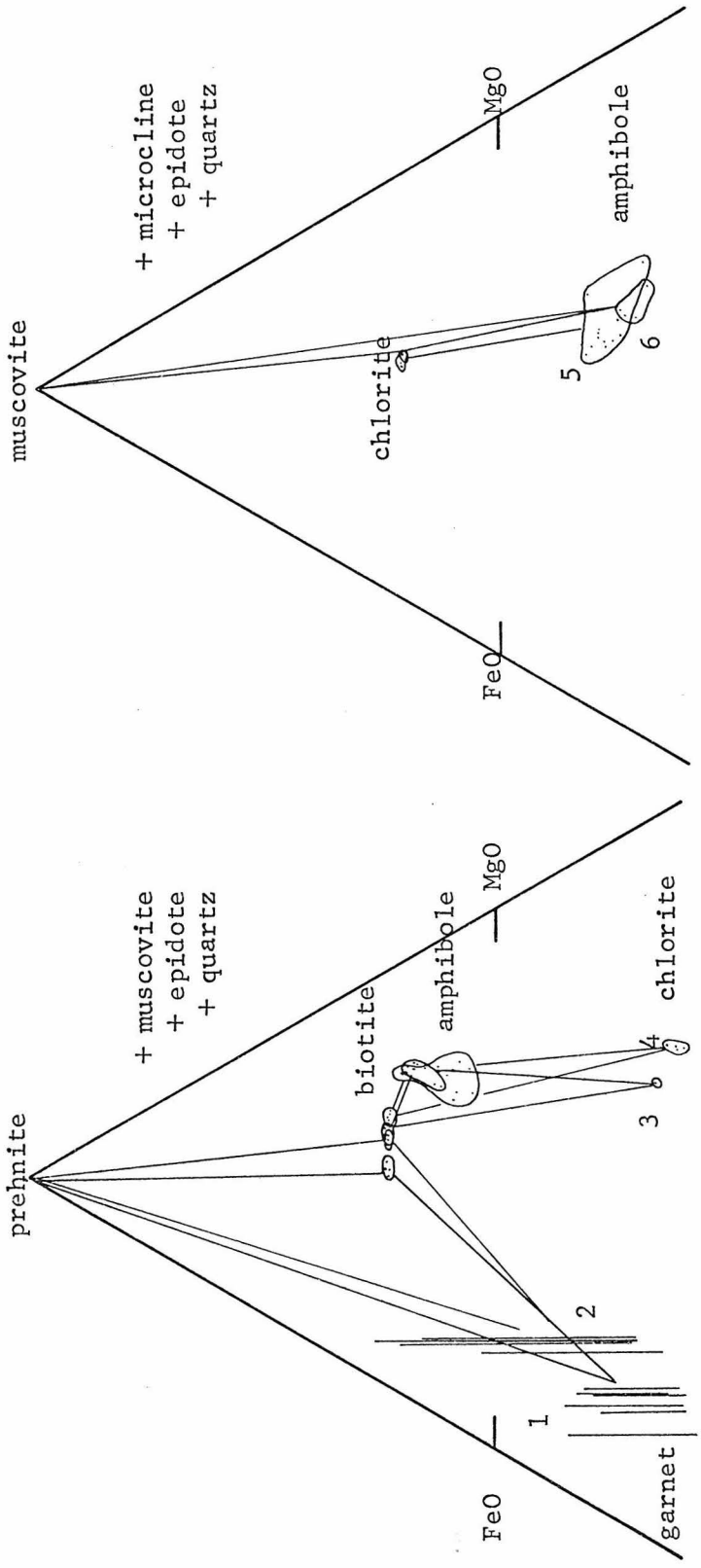

1 - CP 128
2 - CP 52b
3 - PML 37b
4 - PML 163
5 - PML 167c
6 - PML 182a

Figure 84c: Retrograde assemblages from the diopside zone, Panamint Mountains.

As in the tremolite zone, there is a large range in amphibole composition, an effect of retrograde metamorphism. Garnet also shows a large range in composition which is in part due to variations in the manganese content. Figure 85 illustrates the compositions of garnet from a variety of assemblages. Most garnet is very rich in manganese and calcium, and complex zoning patterns are exhibited. Garnet which coexists with hornblende + epidote generally contains less manganese + calcium and shows very little zoning. Garnet which coexists with hornblende + grunerite contains almost no manganese. The distribution of Fe, Mg, Mn, and Ca among these phases is poorly understood, in great part due to the range in amphibole composition developed during retrograde metamorphism, but one generality is noted. The most iron-rich hornblende coexists with grunerite and manganese-free garnet (samples PML 199, 225a, 242). The hornblende which coexists with the most manganese + calcium-rich garnet (PML 234b) has the highest Mg/(Mg + Fe) value of all hornblende which coexists with garnet (Figure 84a). A regularity in distribution is suggested, i.e., the more iron-rich garnet coexists with the more iron-rich hornblende.

Retrograde assemblages are shown in Figure 84c, and are similar to tremolite grade assemblages shown in Figure 83. The more iron-rich assemblages CP 128 and CP 52b contain prehnite which is intergrown with biotite, and in chlorite-bearing assemblages, chlorite is replacing biotite. Sample PML 182a exhibits a texture which suggests equilibrium, but the rock is comprised of the tremolite grade assemblage quartz + muscovite + epidote + microcline + chlorite + actino-

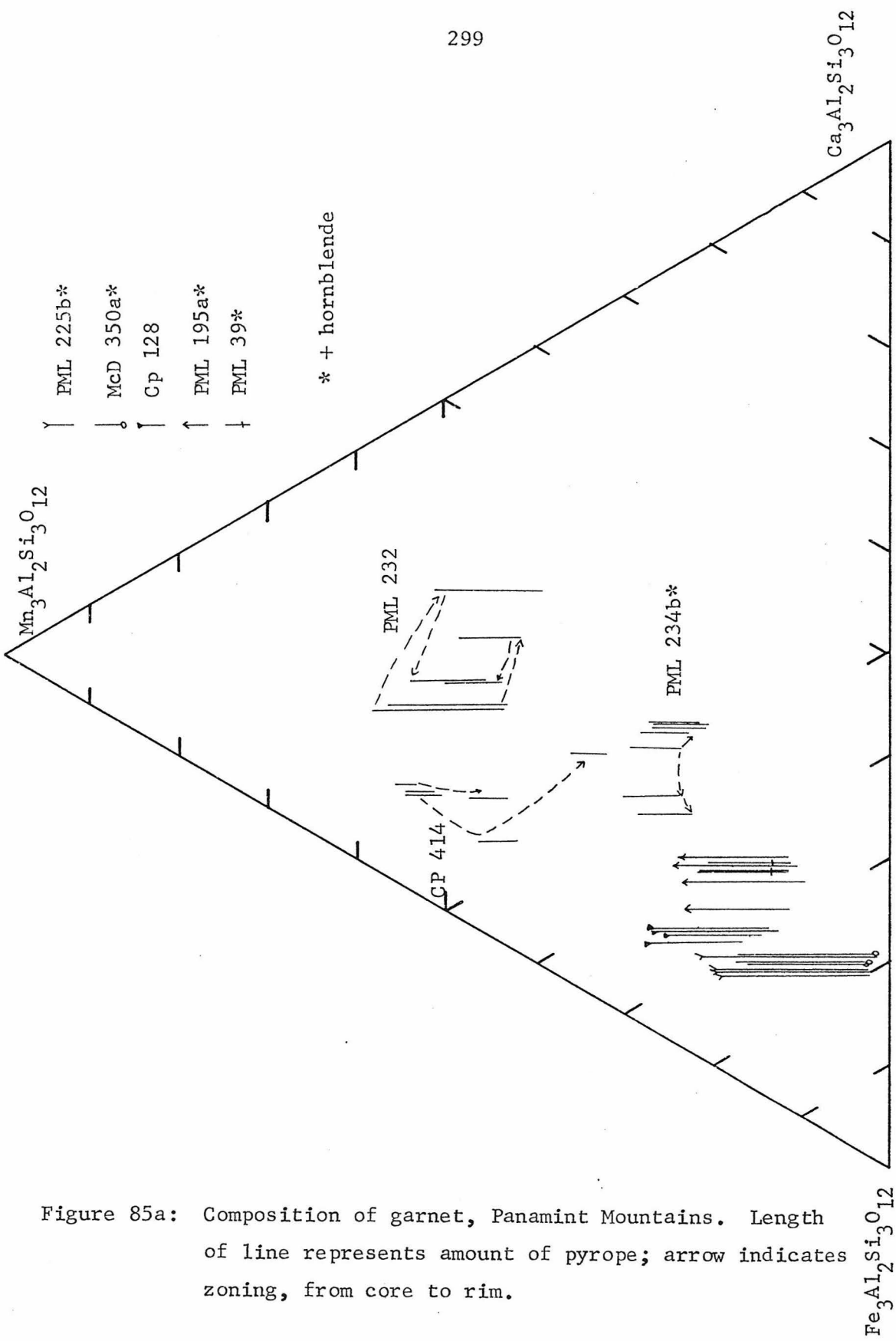

Figure 85a: Composition of garnet, Panamint Mountains. Length of line represents amount of pyrope; arrow indicates zoning, from core to rim.

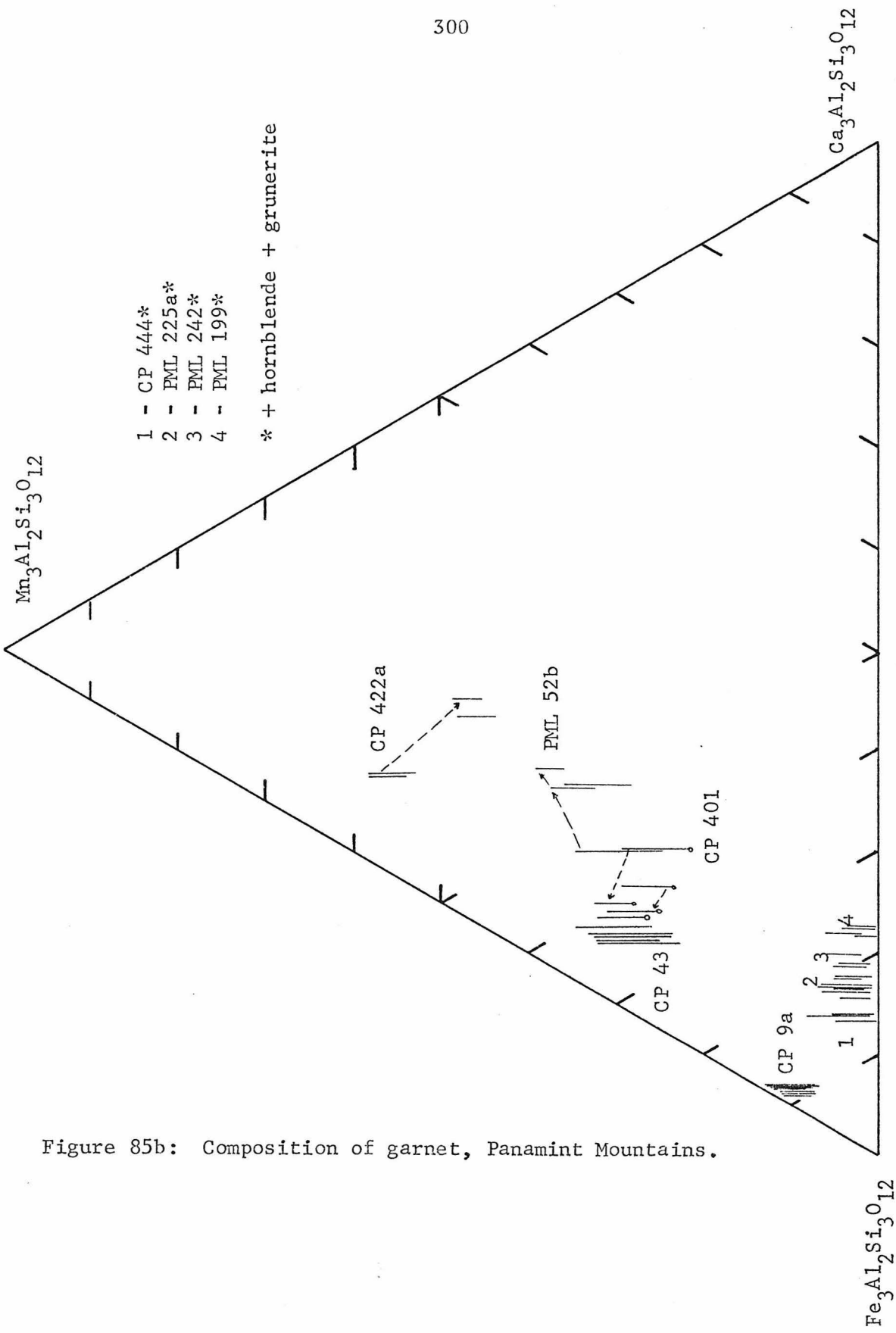

Figure 85b: Composition of garnet, Panamint Mountains.

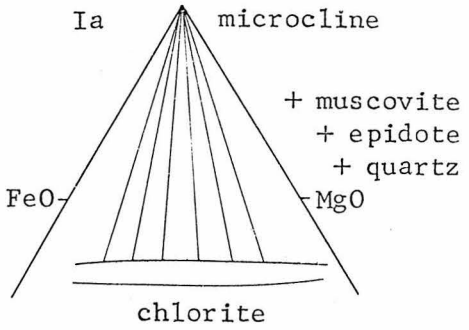

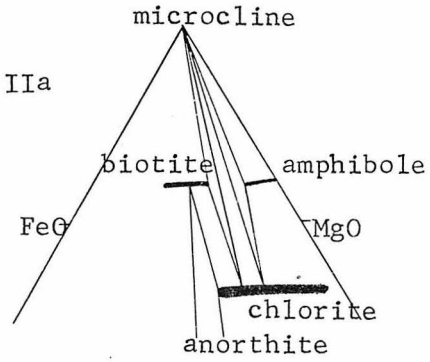

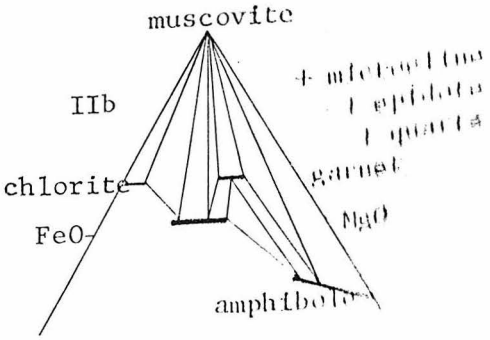

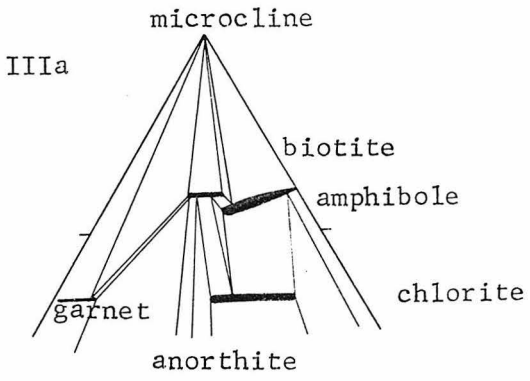

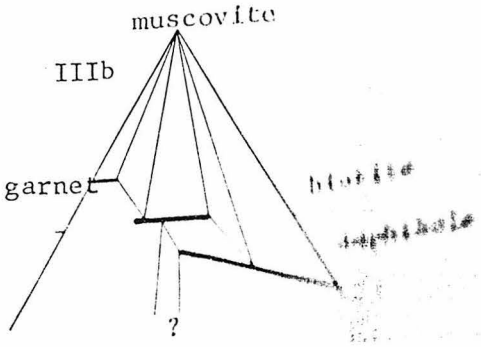

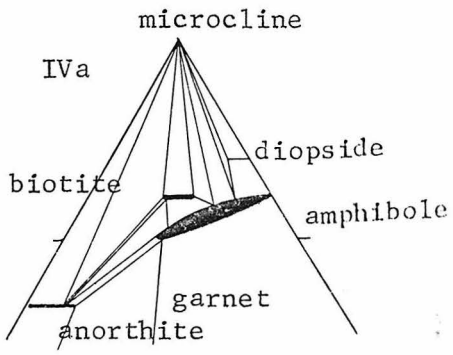

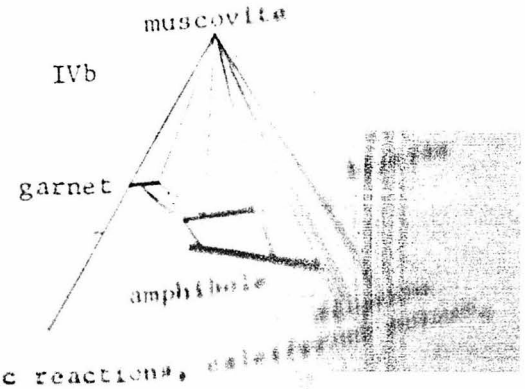

Figure 86: Progressive metamorphic reactions, [illegible] Panamint Mountains (see text).

lite.

Retrograde metamorphism has affected most rocks, but the nature of the distribution of potassic phases is suggested. Biotite occurs in all assemblages except those which contain diopside. Microcline is generally observed in assemblages which contain diopside, but it also occurs in hornblende + chlorite + biotite assemblages. Muscovite may coexist with almost every phase, but muscovite + chlorite + epidote + quartz is unstable in the diopside zone. A sequence of prograde reactions is proposed in Figure 86 which is based on the observations in calciferous schist from the Panamint Mountains. Figure 86 is drawn so that garnet + chlorite + muscovite + quartz does not occur and so that prehnite does not occur. These associations appear to occur in the retrograde metamorphism, but not in the primary. The order of increasing Mg/Fe is garnet < biotite < chlorite < hornblende < diopside.

Figure 86 indicates the sequence of reactions which occurs in muscovite + epidote + quartz assemblages in I, IIa, IIIa, and IVa, and the corresponding sequence in microcline + epidote + quartz rocks is shown in IIb, IIIb, and IVb. Calcite is a possible additional phase in each assemblage due to the additional component CO_2. At low grades the assemblage quartz + epidote + muscovite + microcline + chlorite ± calcite commonly occurs (I). As grade increases, biotite and actinolite become stable. In muscovite + epidote + quartz rocks biotite is introduced by

chlorite + microcline = biotite + muscovite.

The assemblages in quartz + muscovite + epidote rocks (IIa) are microcline + biotite + chlorite and microcline + actinolite + chlorite. In microcline-bearing rocks which contain no muscovite, biotite and actinolite must have first been introduced by some reaction such as:

chlorite + carbonate + microcline = biotite + epidote

and chlorite + carbonate = actinolite + epidote.

Microcline + epidote + quartz rocks may contain the assemblage biotite + chlorite + actinolite (IIb). Garnet-bearing assemblages are possible in iron-rich compositions.

With increasing grade, chlorite continues to break down, and in stage III, chlorite is isolated from microcline-bearing assemblages:

chlorite + microcline + epidote = biotite + amphibole + muscovite.

Chlorite now occurs only in the muscovite-bearing assemblages biotite + amphibole + chlorite, biotite + chlorite + anorthite, and amphibole + chlorite + anorthite. Chlorite is eliminated from muscovite + epidote + quartz assemblages by the reaction

chlorite + muscovite + epidote = biotite + amphibole + anorthite.

In muscovite assemblages the observed garnet + biotite + hornblende assemblage (IVa) is created by the tie line crossover

biotite + anorthite = garnet + hornblende + muscovite,

and diopside is introduced by

microcline + epidote + amphibole = diopside + muscovite.

In IVb the associations muscovite + amphibole + diopside and garnet + hornblende + biotite (+ microcline + epidote + quartz) are shown. Grossular plots at $-\infty$ and the assemblage grossular + diopside occurs in the Panamint Mountains, but it is uncertain whether grossular may

coexist with amphibole or almandine garnet.

In metamorphic terrains formed under different conditions, other reactions and assemblages may occur. In particular, garnet + chlorite + muscovite does not seem to occur in the low pressure environment of the Panamint Mountains, but this association is common in medium pressure pelitic schists elsewhere. Hence, a different sequence of reactions in calciferous schist may occur under higher pressure conditions where garnet + chlorite are stable. Similarly, biotite + diopside may coexist under conditions not attained in the Panamint Mountains. The large number of reactions which may occur in potassium-rich calciferous schists makes these rocks potentially useful for elucidation of metamorphic grade. This potential is difficult to realize in the Panamint Mountains, though, because of the superposition of two metamorphic events. In addition, different sequences of reactions may occur in different dp/dT environments, and K-rich calciferous schist is potentially useful for distinguishing higher from lower pressure facies series.

SUBSTITUTIONAL MECHANISMS IN CALCIC AMPHIBOLE

Calcic amphibole exhibits a wide range in chemical composition; large amphibole grains are chemically zoned and smaller amphibole grains have compositions which vary from grain to grain. This chemical zoning is attributable to the superposition of metamorphic episodes. The composition of cores of amphibole grains is believed to most closely represent the composition of amphibole formed during the earlier metamorphism and the composition of amphibole rims and of

small matrix amphiboles are believed to represent the composition of amphibole formed during the second metamorphic event. The application of compositional zoning in amphiboles as an index to polymorphism is described in detail by Laird (1977). In particular, Laird found that despite the range in amphibole composition, the compositions of amphibole from the common assemblage quartz + epidote + calcic amphibole + chlorite + K-phase + plagioclase + Ti-phase + Fe^{+3}-phase defined a trend which is dependent upon the P/T gradient during formation. Laird (1977) found that the parameters Na/(Na + Ca) and Al/(Al + Si) separated amphiboles formed in low, medium, and high pressure facies series environments. Figure 87 illustrates the compositional ranges for the different facies series as depicted by Laird (1977). Amphiboles from high pressure environments have higher Na/(Na + Ca) values than those from low pressure environments.

Figure 88 illustrates the compositions of amphiboles from the Panamint Mountains. The compositions of amphiboles from the tremolite zone are shown in Figure 88a, and from the diopside zone in Figure 88b. Tremolite zone amphiboles coexist with epidote + quartz + plagioclase + chlorite and much of the variation seen in Figure 88a may be due to differences in metamorphic grade. Samples P 230 and PML 268 are located just inside of the tremolite isograd, and amphiboles from these rocks are very rich in calcium and silicon (actinolite). Samples located near the diopside isograd (CP 470, P 46) contain amphiboles which are very rich in aluminum (∿20-25% Al/Al + Si) and contain a modest amount of sodium (∿20% Na/Na + Ca), but CP 470 shows a wide

Figure 87: Dependence of amphibole composition on facies series (from Laird, 1977)

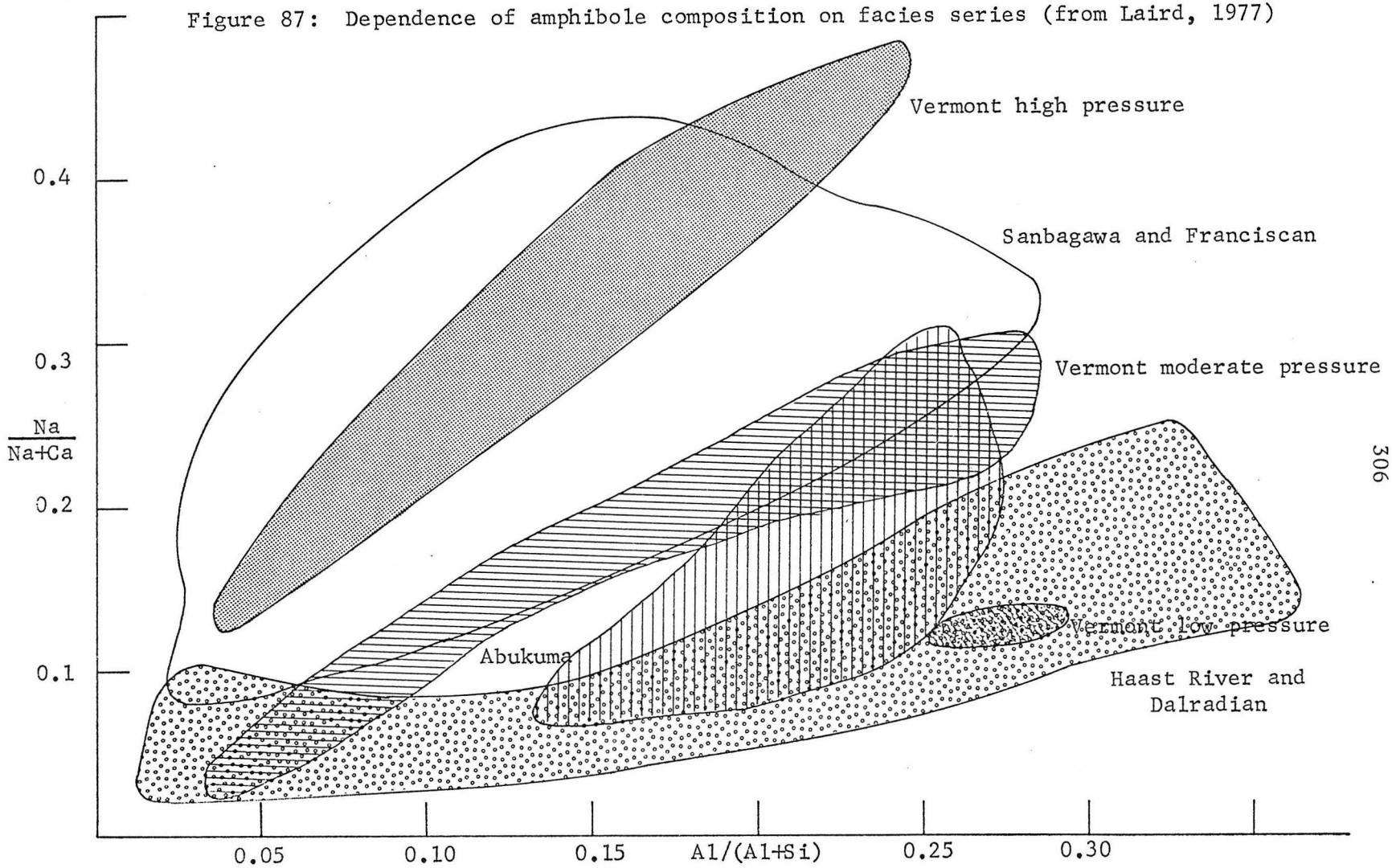

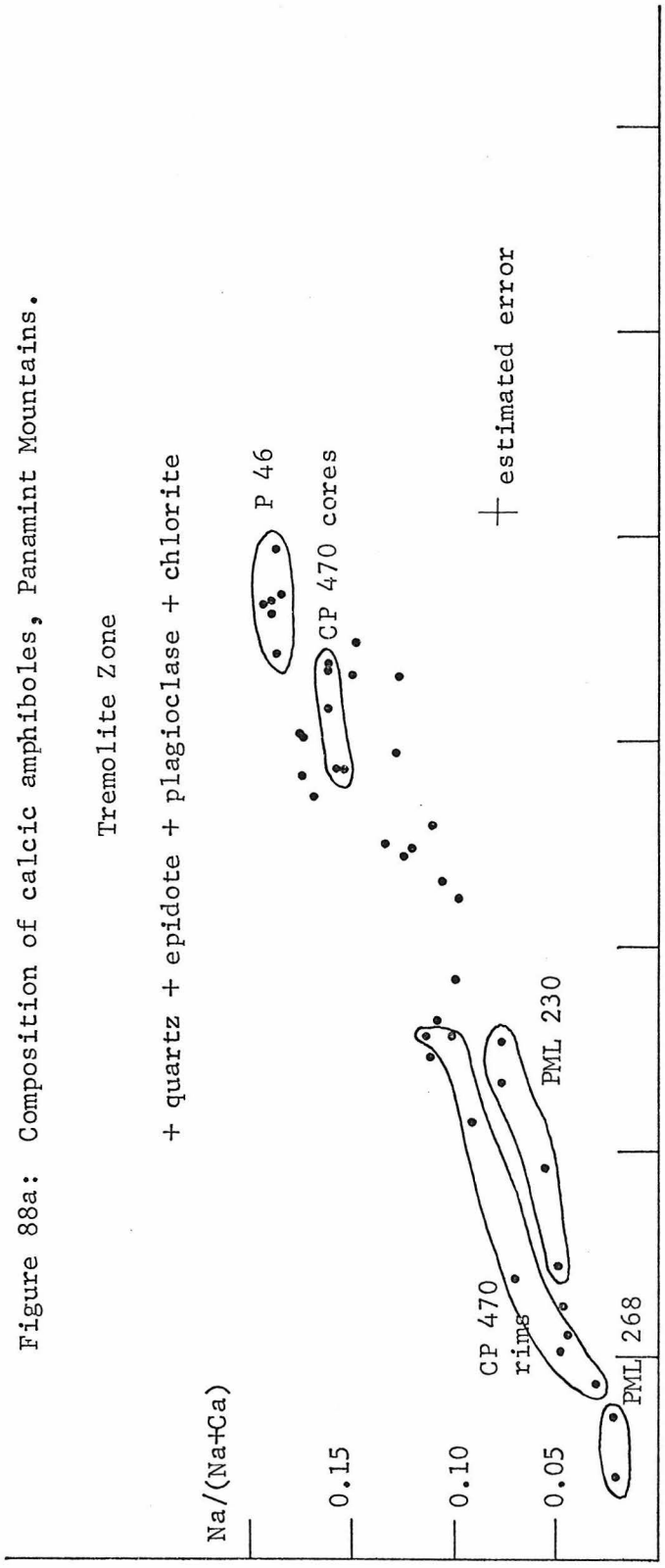

Figure 88a: Composition of calcic amphiboles, Panamint Mountains.

Figure 88b: Composition of amphibole, Panamint Mountains, diopside zone

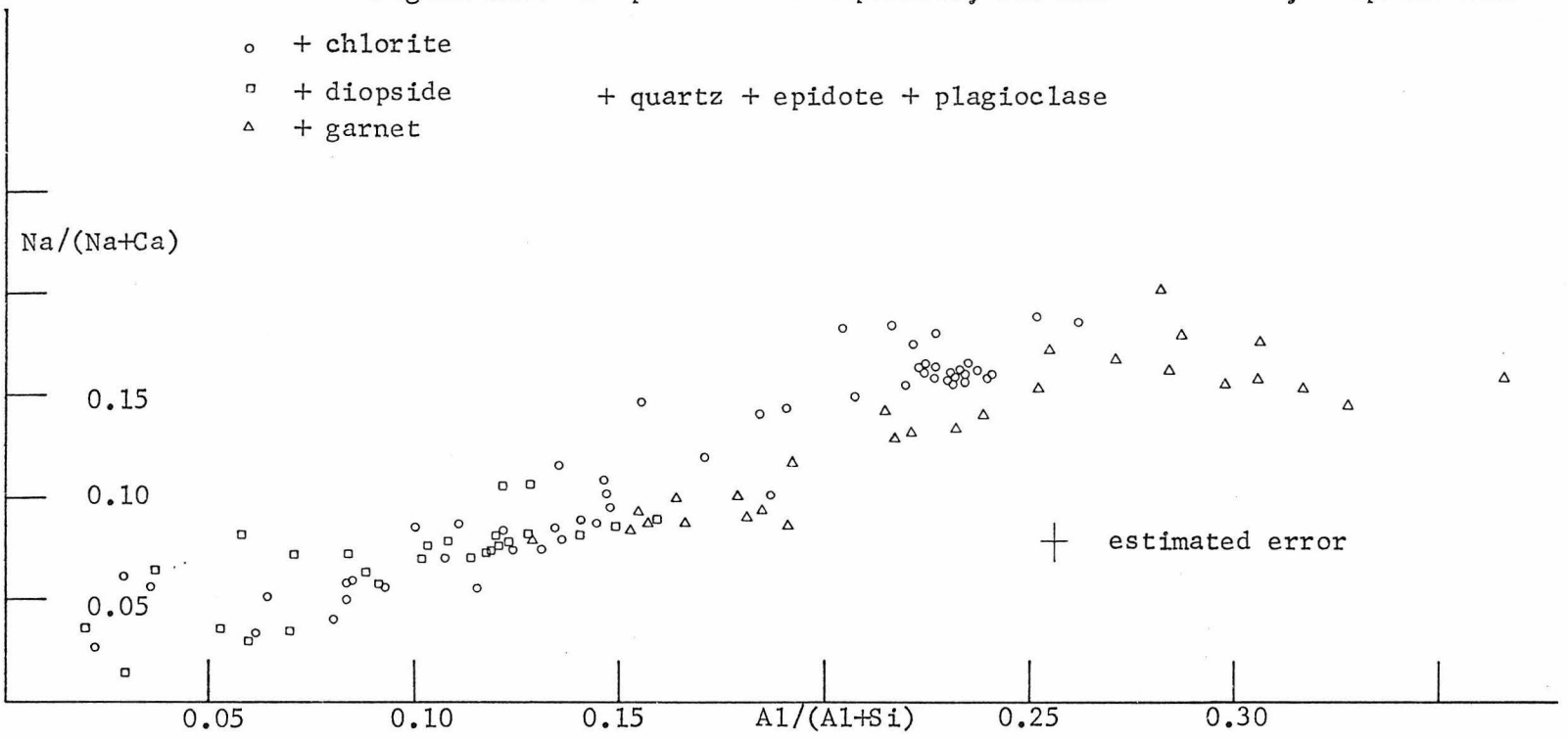

Figure 88c: Composition of amphiboles, Panamint Mountains.

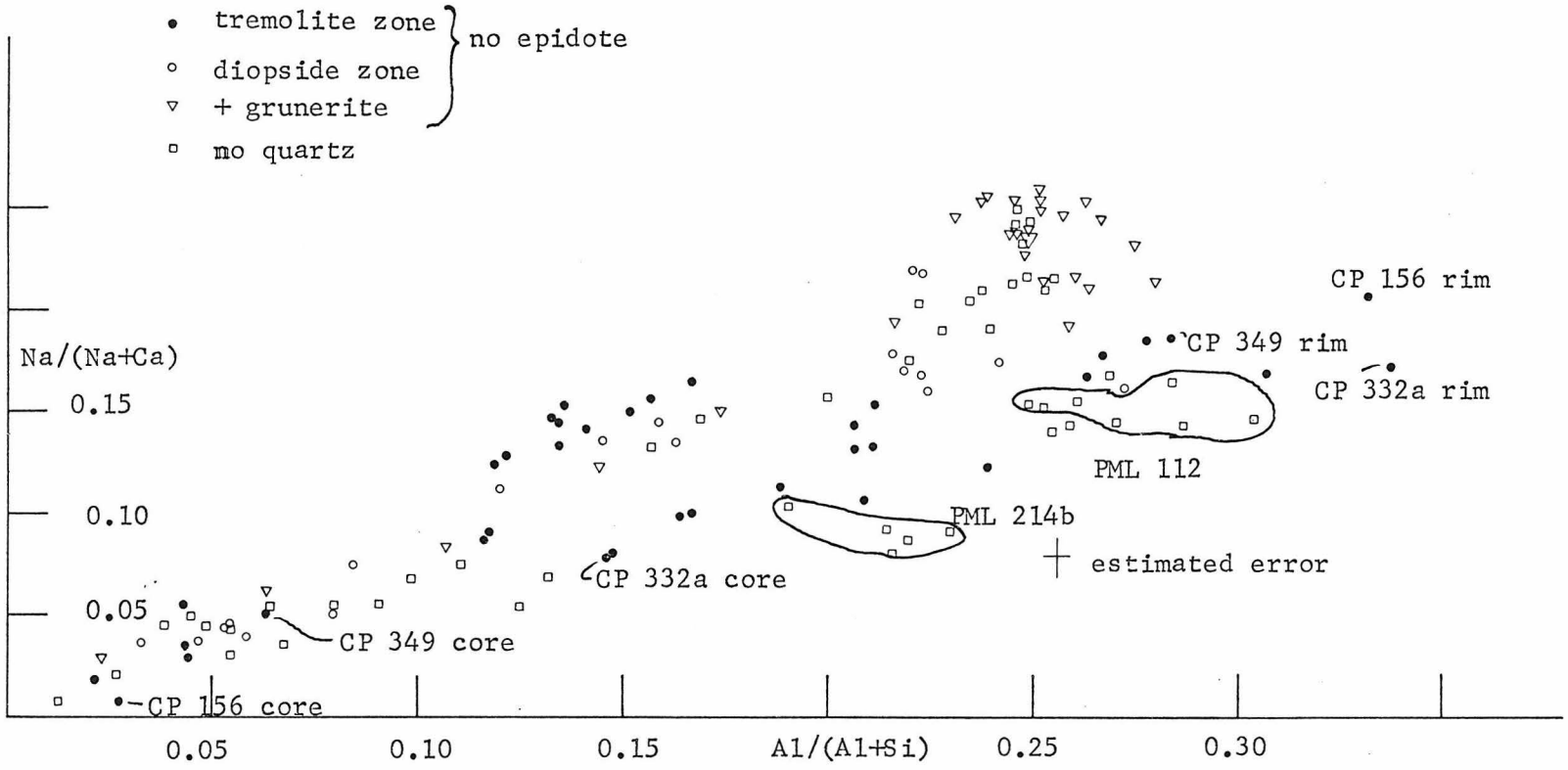

range in amphibole composition due to retrograde metamorphism.

Diopside zone amphiboles from quartz + epidote assemblages show a slightly greater range in composition (Figure 88b), but much of the variation appears to be due to differences in rock composition. Amphiboles which coexist with garnet are much more aluminous than those which coexist with calcic clinopyroxene, and the two groups are almost mutually exclusive. Chlorite-bearing assemblages contain amphiboles which overlap the two groups, but chlorite in most of these assemblages is believed to be secondary.

Amphiboles from epidote-free assemblages show a larger range in composition (Figure 88c), and many are more sodium-rich than those from epidote-bearing assemblages. Hence, amphiboles from epidote-bearing assemblages are saturated in calcium for a given amount of aluminum. The spread in compositions from tremolite zone assemblages completely overlap the spread from diopside zone assemblages, but many of the aluminous tremolite zone amphiboles occur as rims on actinolite cores (samples CP 156, 349, 332a). These aluminous compositions are believed to be the result of the second metamorphism which has upgraded these amphibolites.

Amphiboles from quartz-free assemblages also show a wider range in composition than those from quartz + epidote assemblages (Figure 88c). Some, PML 214b and PML 112, contain less silicon for a given amount of calcium than those from quartz + epidote assemblages.

The compositions of amphiboles which coexist with quartz + epidote + plagioclase from the tremolite and diopside zones form a well defined trend, and this trend is consistent with that indicated

by Laird for low pressure terrains. Those amphiboles which do not coexist with either quartz or epidote have compositions which are not constrained to lie on the trend.

In order to determine the major substitutional mechanisms responsible for the observed variation in amphibole composition, it is necessary to normalize the chemical analysis to a formula. The generalized formula for amphibole is $A_{0-1}X_2Y_5Z_8O_{22}(OH, F, Cl)_2$ where A may be Na, K; X (the M4 site) may be Na, Ca, Fe, Mg; Y may be Fe^{+2}, Mg, Ti Al^{VI}; and Z may be Si or Al^{IV}. Because of the occurrence of vacancies in the large A site, and the inability of the probe to determine the ferric iron and hydroxyl content, a formula cannot be defined uniquely. The three schemes which have proved most useful involve the assumptions: I All sodium occurs in the M4 site, II No iron + magnesium occurs in the M4 site, or III No sodium occurs in the M4 site. Normalization I is designed to accommodate glaucophane ($Na_2Fm_3Al_2Si_8O_{22}(OH)_2$). Normalization II allows accumulation of M4 sodium in calcic amphiboles ($Ca_xNa_{2-x}FM\ Al_{2-x}(Si_8)O_{22}(OH, F, Cl)_2$), and normalization III accounts for the presence of Fe + Mg in the M4 site. Ferric iron is calculated from the positive charge deficiency from 46, and potassium and excess sodium (if any) are assigned to the A site. Normalization I predicts a maximum amount of ferric iron, and normalization III a minimum.

The substitutions which give rise to the major compositional variation in amphiboles are

$$Na^{M4} + Al^{VI} \rightleftarrows Ca^{M4} + Mg^{VI} \qquad \text{(glaucophane)}$$

$$Na^{A} + Al^{IV} \rightleftarrows \square + Si^{IV} \qquad \text{(edenite)}$$

$$Al^{IV} + Al^{VI} \rightleftarrows Si^{IV} + Mg^{VI} \qquad \text{(tschermakite)}$$

$$Mn,\ Fe^{+2} \rightleftarrows Mg$$

$$Cr,\ Fe^{+3} \rightleftarrows Al$$

$$K^{A} \rightleftarrows Na^{A}.$$

Because glaucophane occurs in high pressure terrains (Ernst and others, 1970), the glaucophane substitution is favored by an increase in pressure. Normalization I was not used to produce any amphibole formulae from the Panamint Mountains. Both normalizations II and III predict realistic amphibole formulae. In some cases, though, the calculated positive charge by normalization III is greater than 46 which suggests that some sodium occurs in the M4 site. In Figure 89, Al^{IV} is plotted against the sum $Al^{VI} + Cr + Fe^{+3}$, and normalization II and III are compared. The difference in composition indicated by the two normalization schemes is small for tremolite zone samples, but becomes significant for diopside zone amphiboles. In most analyses the ferric iron calculated by normalization II is equal to or greater than the amount of Al^{VI}, and the principal substitution indicated is the tschermakite $[(Al + Fe^{+3})^{VI} + Al^{IV} = Mg^{VI} + Si^{IV}]$. The compositions of amphiboles normalized by II fall into fields on Figure 89 which are populated by amphiboles from medium to high pressure terrains (Leake, 1965; Raase, 1974; Laird, 1977). Because of the low pressure nature of the metamorphic terrain and the low ferric iron content of most assemblages (magnetite is rare and hematite never occurs in Panamint amphibolitic schists - see Table 13) normalization III more closely

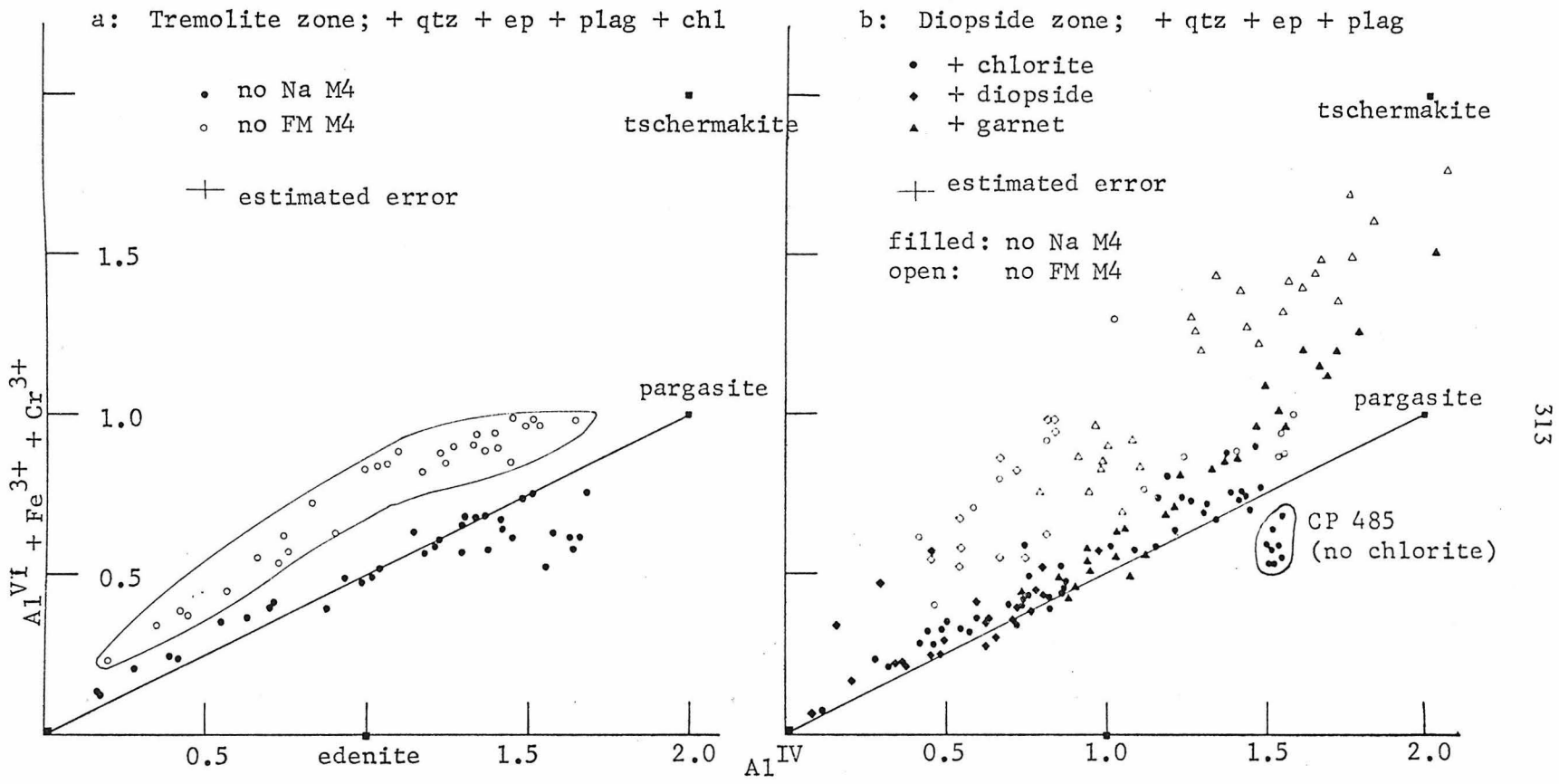

Figure 89: Al^{IV} versus $Al^{VI} + Fe^{+3} + Cr^{+3}$ in amphibole, Panamint Mountains.

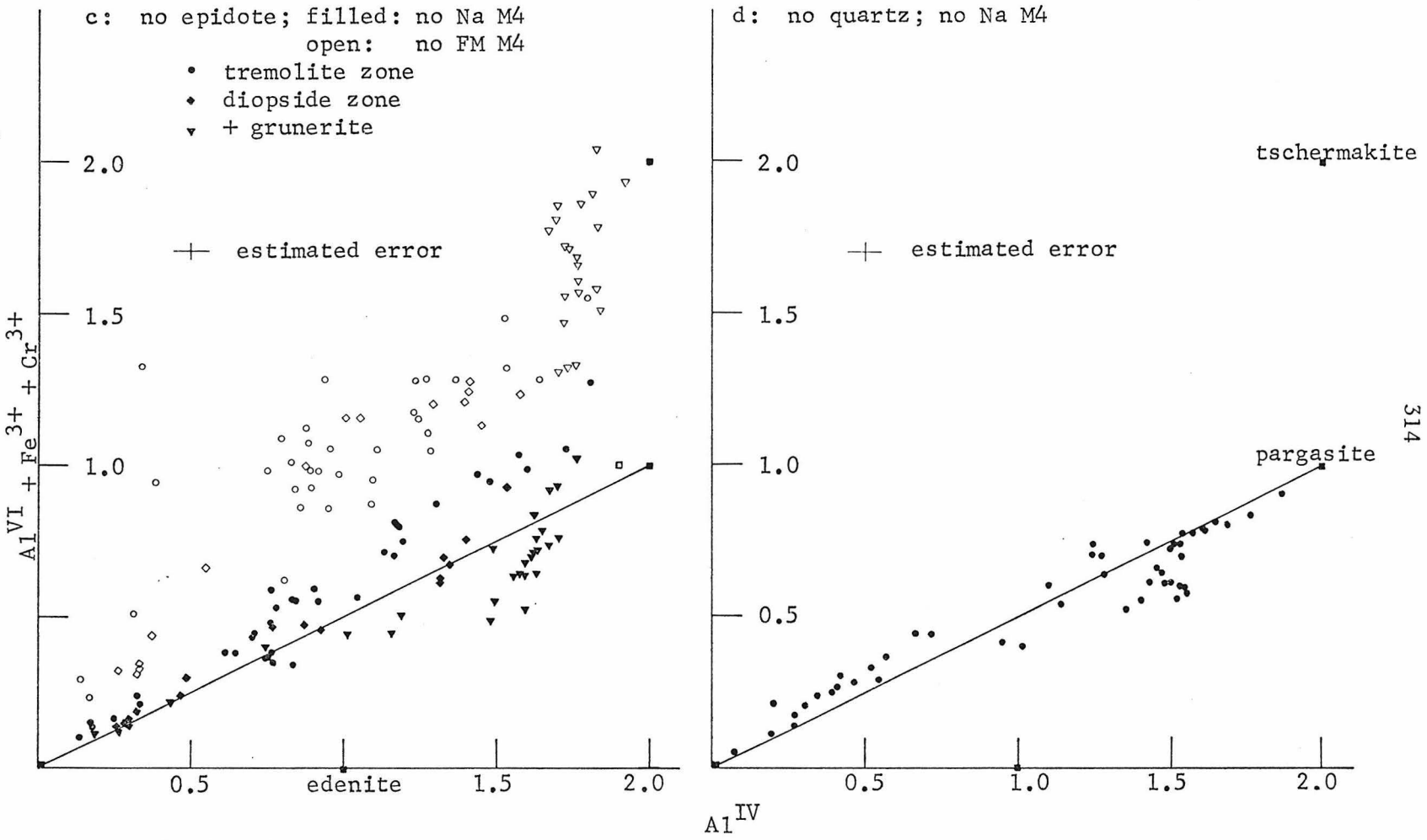

Figure 89: (continued).

represents the formulae of calcic amphiboles from the Panamint Mountains.

This normalization procedure eliminates the glaucophane substitution as a possible mechanism for the chemical variations in amphibole. Amphibole analyses from tremolite zone samples in Figure 89a follow a trend with a slope of 1/2. The equal importance of the tschermakite and edenite substitutions is indicated, and the analyses fall on a line from tremolite ($\square Ca_2FM_5Si_8O_{22}(OH)_2$) to pargasite ($NaCa_2FM_4Al^{VI}(Al_2^{IV}Si_6)O_{22}(OH)_2$). Diopside zone amphiboles (Figure 89b) also follow this trend for amphiboles with less than about 1.5 Al^{IV}, although the points are displaced to somewhat high values of $Al^{VI} + Fe^{+3} + Cr^{+3}$. A break in slope at $Al^{IV} = 1.5$ is noted, and amphiboles with greater amounts of Al^{IV} (generally those which coexist with garnet) fall on a trend with a slope of approximately 1. Here the tschermakite substitutions becomes dominant. CP 485 contains neither chlorite nor garnet and the amphibole composition falls below the pargasite trend. Amphiboles from epidote-free assemblages show a less well defined trend but also fall about the tremolite-pargasite line. Amphiboles from quartz-free assemblages exhibit a behavior similar to that of tremolite zone amphiboles.

If the principal substitutional mechanism is the coupled edenite and tschermakite ("pargasite"), the amount of sodium plus potassium should equal half the tetrahedral aluminum. Figure 90 shows that in all cases for less than about 1.5 Al^{IV}/formula, the amount of sodium + potassium is only 0.35 that of aluminum. For Al^{IV} values greater than 1.5, amphiboles from garnet-bearing assemblages have less Na + K which

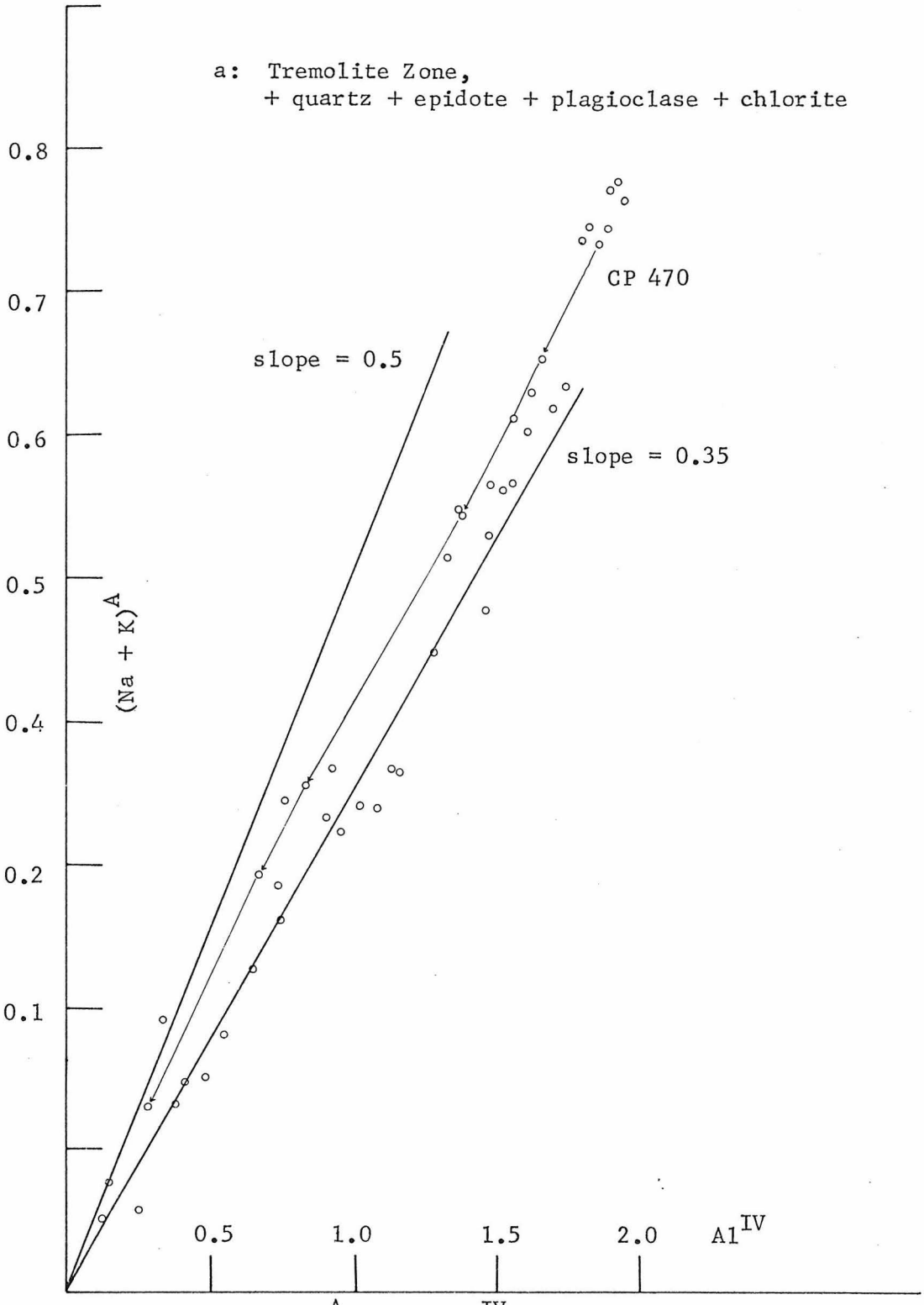

Figure 90: $(Na + K)^A$ versus Al^{IV} in amphibole, Panamint Mountains.

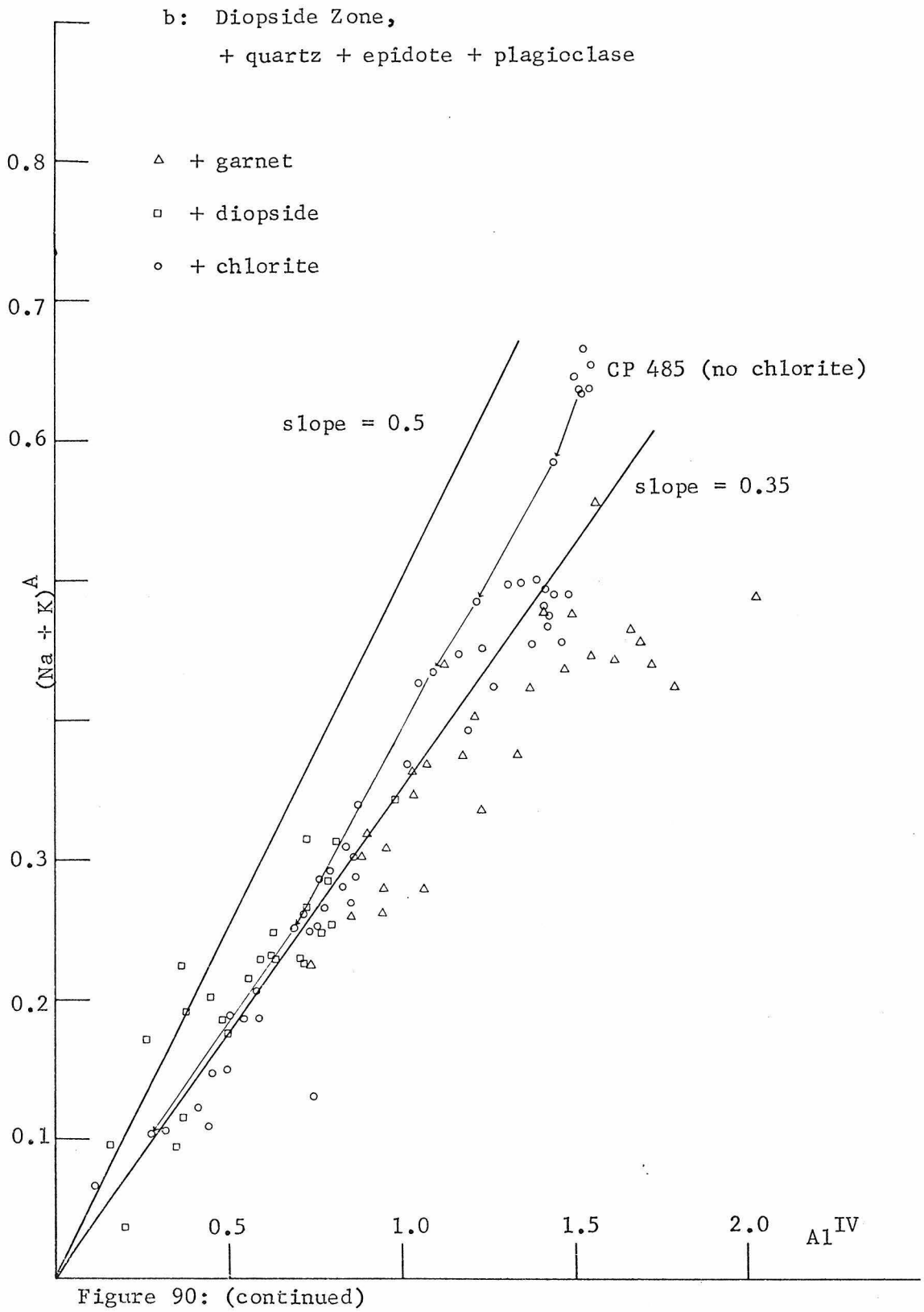

Figure 90: (continued)

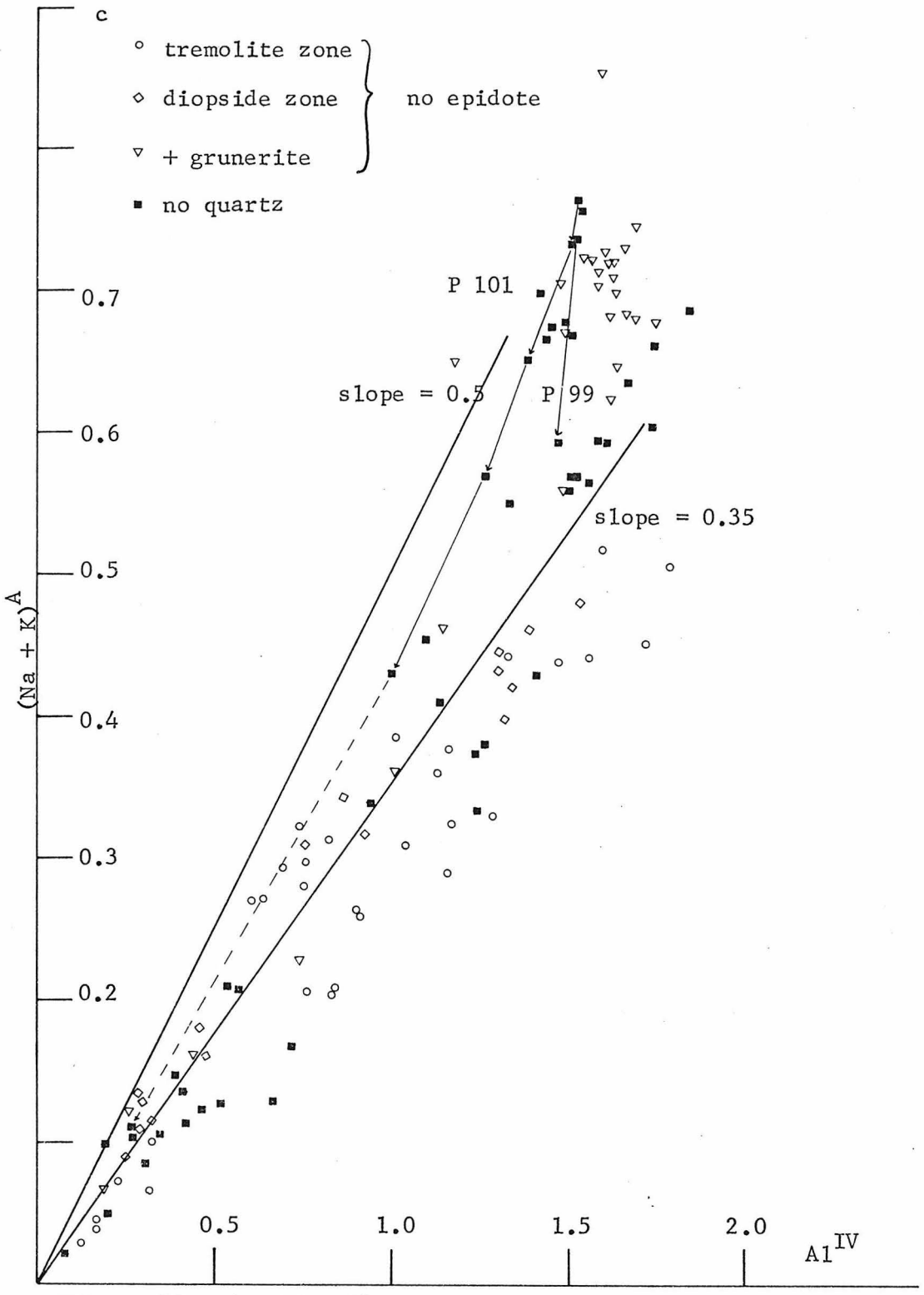

Figure 90: (continued)

reflects the importance of the tschermakite substitution. Most other amphiboles contain more Na + K and approach the ideal value of 1/2 Al^{IV}.

Thus it is suggested that the pargasite substitution does occur but A-site occupancy is affected by an additional substitution. Because Cr^{+3} and Fe^{+3} can proxy for aluminum in any of the previously described substitutions without need for any additional charge balance requirements, titanium is suspect. In Figure 91 titanium is plotted as a function of Al^{IV}. There is a less clear correlation between these two parameters, particularly for Al^{IV} values greater than about 1.25/formula, but a trend which has a slope of 0.075 is suggested; that is, $2Ti = 0.15\ Al^{IV}$. The information from Figure 90 coupled with that from Figure 91 indicate that $(Na + K)^{A} + 2Ti = 0.5\ Al^{IV}$ and that titanium is accommodated in amphibole by the coupled substitution $2\square + Ti = 2(Na + K)^{A} + Mg$. The "edenite" substitution now becomes $0.70(Na + K)^{A} + 0.15Ti^{VI} + Al^{IV} = 0.70\square^{A} + 0.15Mg^{VI} + Si^{IV}$ and the mechanism responsible for the variation in amphibole composition is $0.70(Na + K)^{A} + 0.15Ti^{VI} + 2Al^{IV} + Al^{VI} = 0.70\square^{A} + 1.15Mg^{VI} + 2Si^{IV}$ ("pargasite").

Substitutions which may occur within the framework of this "pargasite" substitution are $Fe^{+2} = Mn^{+2} = Mg^{+2}$, $K^{A} = Na^{A}$, and $Fe^{+3} = Cr^{+3} = Al^{+3}$. Chromium occurs in negligible amounts. Ferric iron content varies unsystematically and most likely represents variations in ferric iron content of the total rock. Figure 92 illustrates the degree to which the A-site is occupied by potassium. Almost all amphiboles

Figure 91: Titanium in amphibole, Panamint Mountains

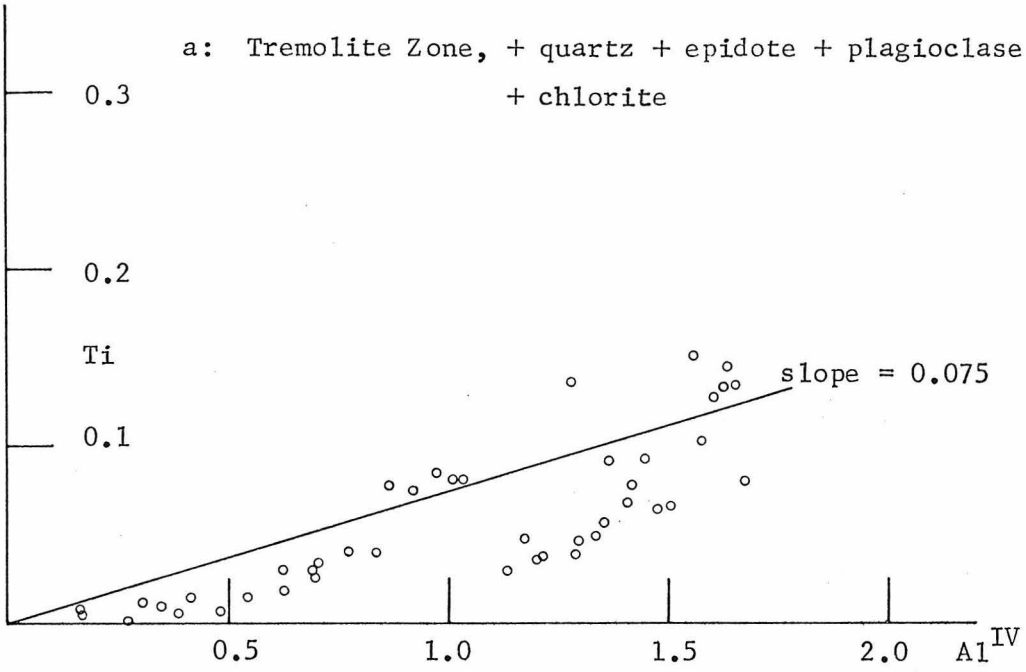

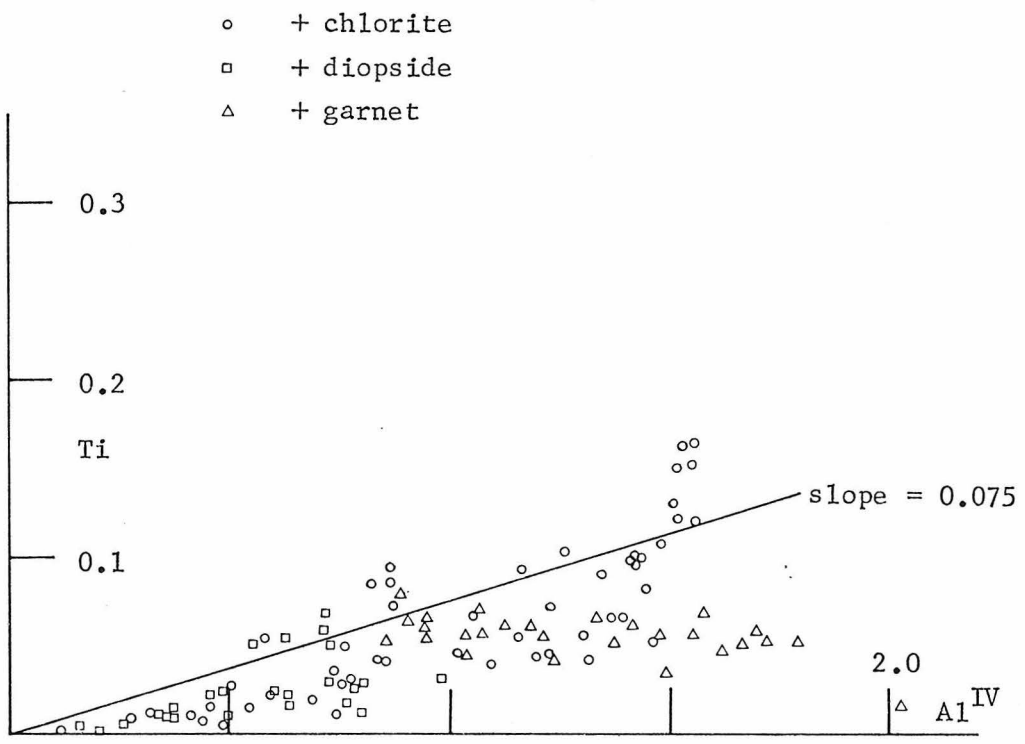

Figure 91: (continued)

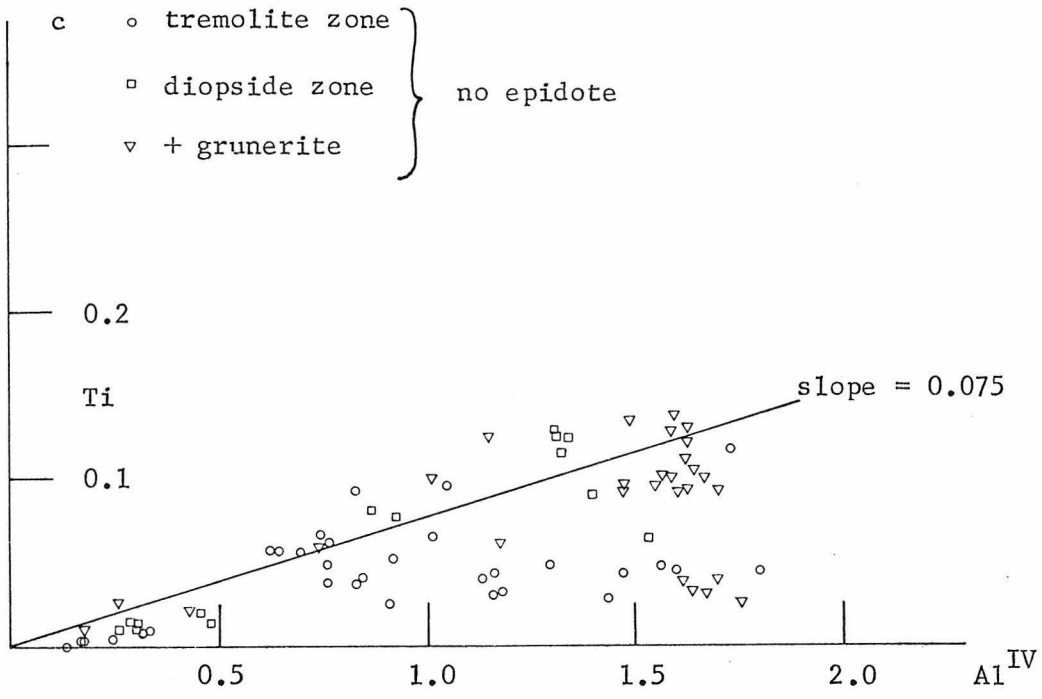

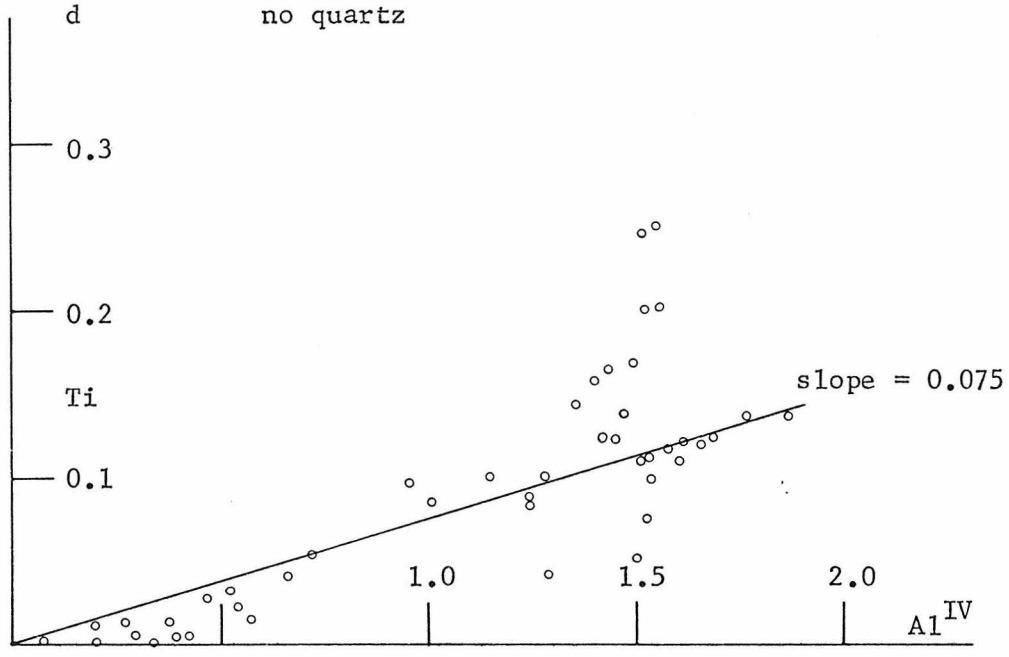

Figure 92: Potassium in amphibole, Panamint Mountains.

a: Tremolite Zone, + qtz + ep + plag + chl

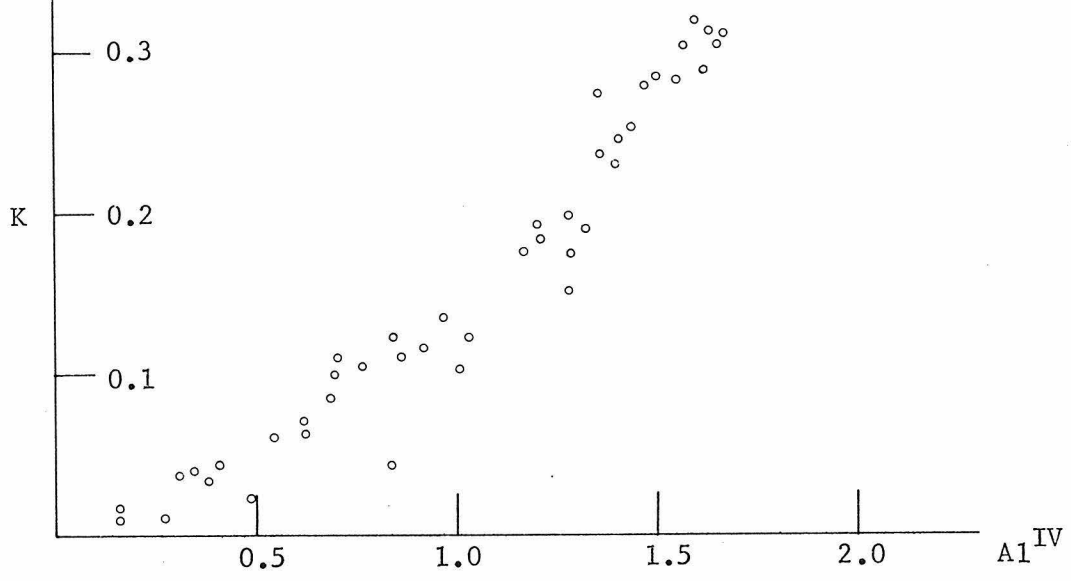

b: Diopside Zone, + qtz + ep + plag

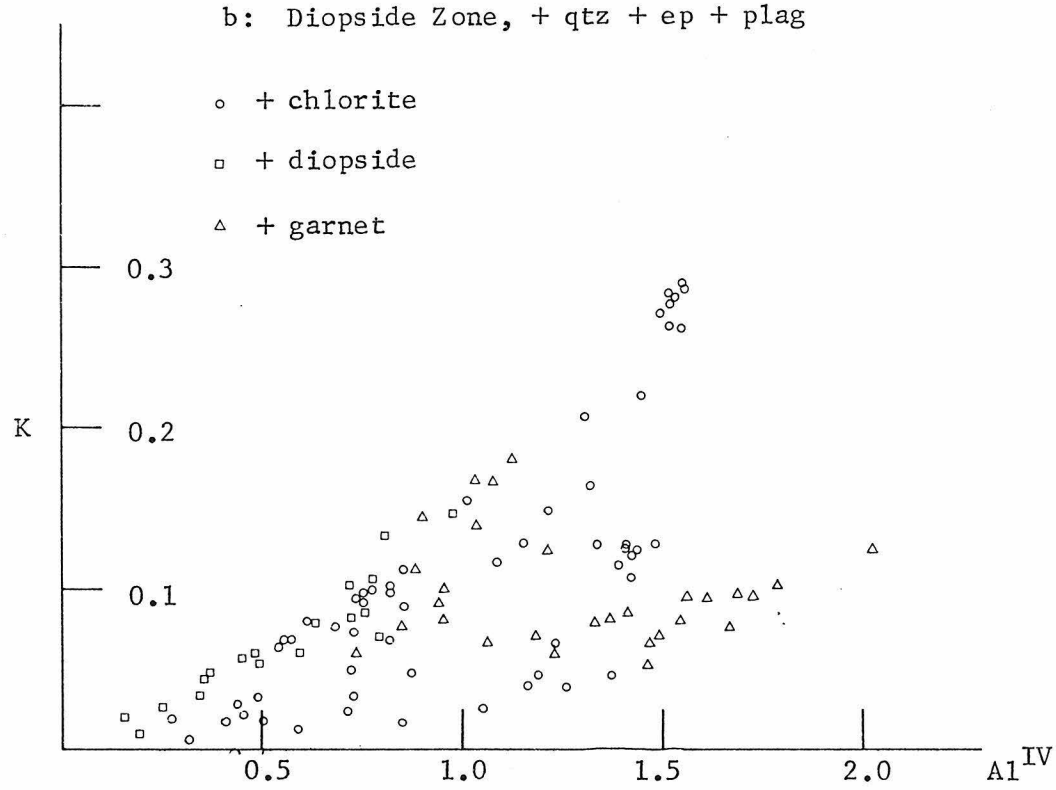

Figure 92: (continued)

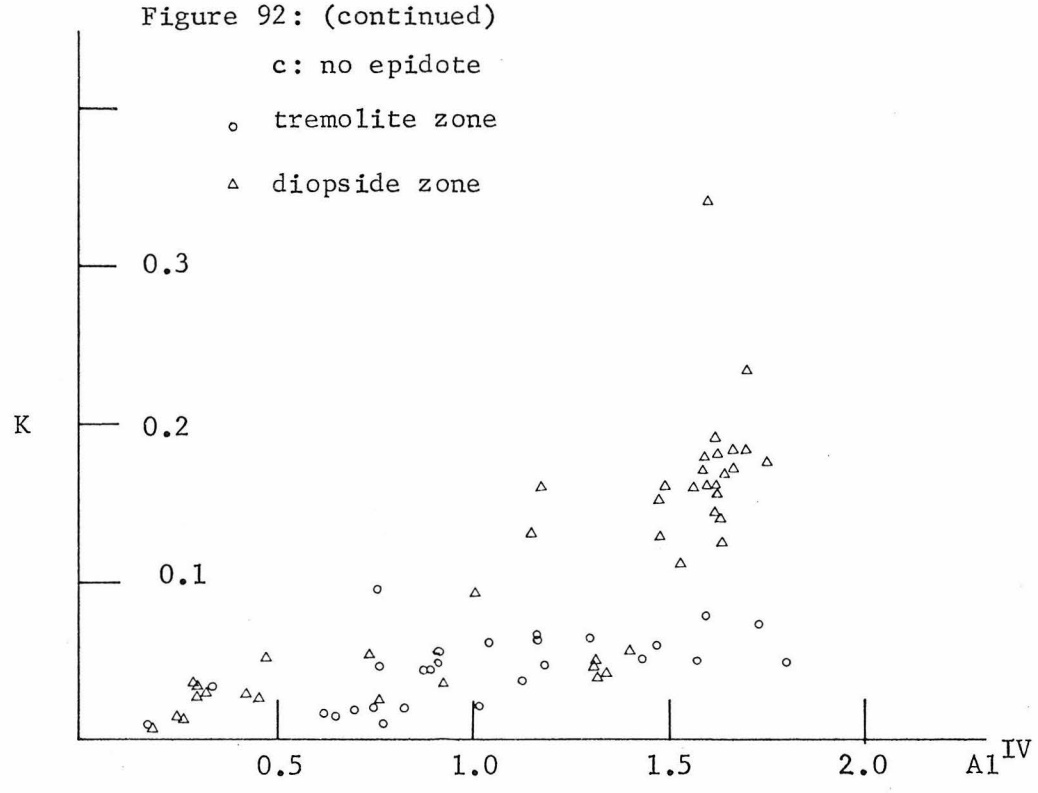

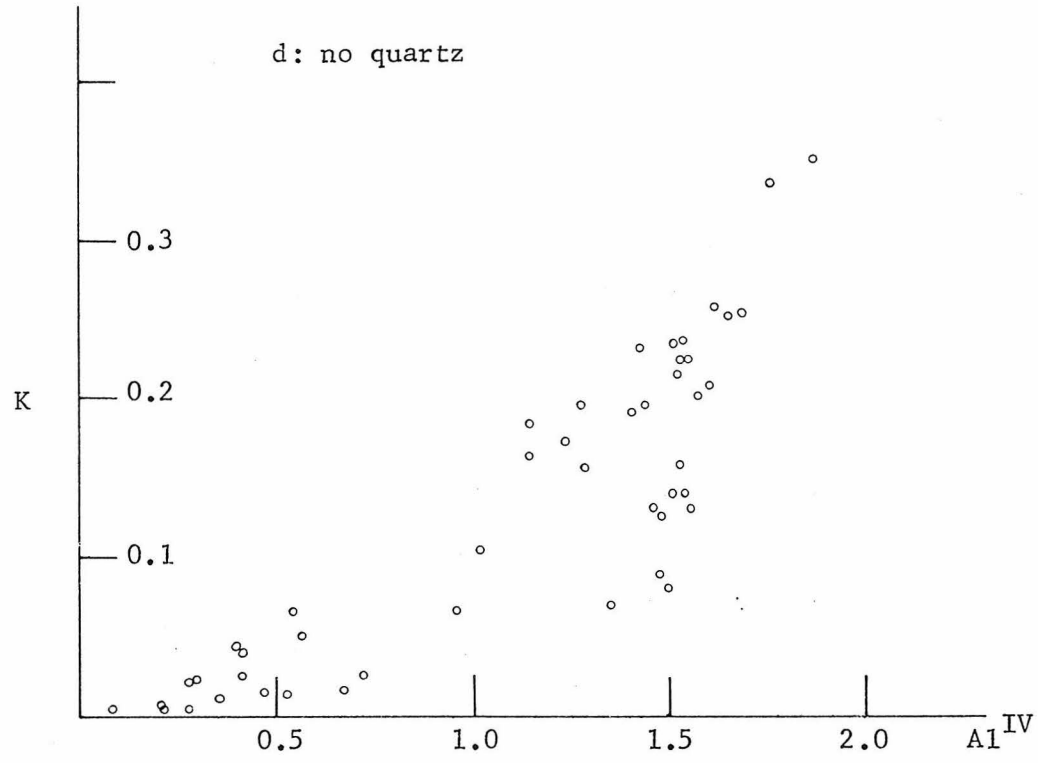

coexist with biotite and many in addition coexist with either muscovite or microcline. These amphiboles are relatively potassium-rich and as much as 0.35 K/formula was observed. There appears to be a saturation limit for potassium which is about $1/3(Na + K)^A$ for $Al^{IV} < 1.0$/formula and about $1/2(Na + K)^A$ for $Al^{IV} > 1.0$/formula. The absolute amount of potassium depends upon the degree to which Al^{IV} is accumulated by the edenite substitution, and amphibole from garnet-bearing assemblages show less potassium because of the importance of the tschermakite substitution.

Figure 93 depicts Mg/(Mg + Fe) versus Al^{IV}. This calculated Mg-value depends greatly on the estimated amount of ferric iron, and an inaccurate estimate may be responsible for some of the range in values. There is a general tendency for amphiboles from quartz + epidote + chlorite + plagioclase assemblages to have decreasing Mg-values for increasing Al^{IV}. Amphiboles from epidote- or quartz-free assemblages show little correlation between Mg/(Mg + Fe) and Al^{IV}, and the Mg/Fe values in these amphiboles is in large part determined by the Mg/Fe value of the bulk rock.

SUMMARY

The composition of amphibole changes with increasing metamorphic grade through continuous reactions which involve the breakdown of epidote and chlorite. The amphibole which occurs in quartz-free or epidote-free assemblages has compositions which may not be governed by such reactions and may reflect the bulk composition of the rock. The composition of amphibole from the assemblage quartz + epidote +

Figure 93: Mg/(Mg + Fe) in amphibole, Panamint Mountains

a: Tremolite Zone, + qtz + ep + plag + chl

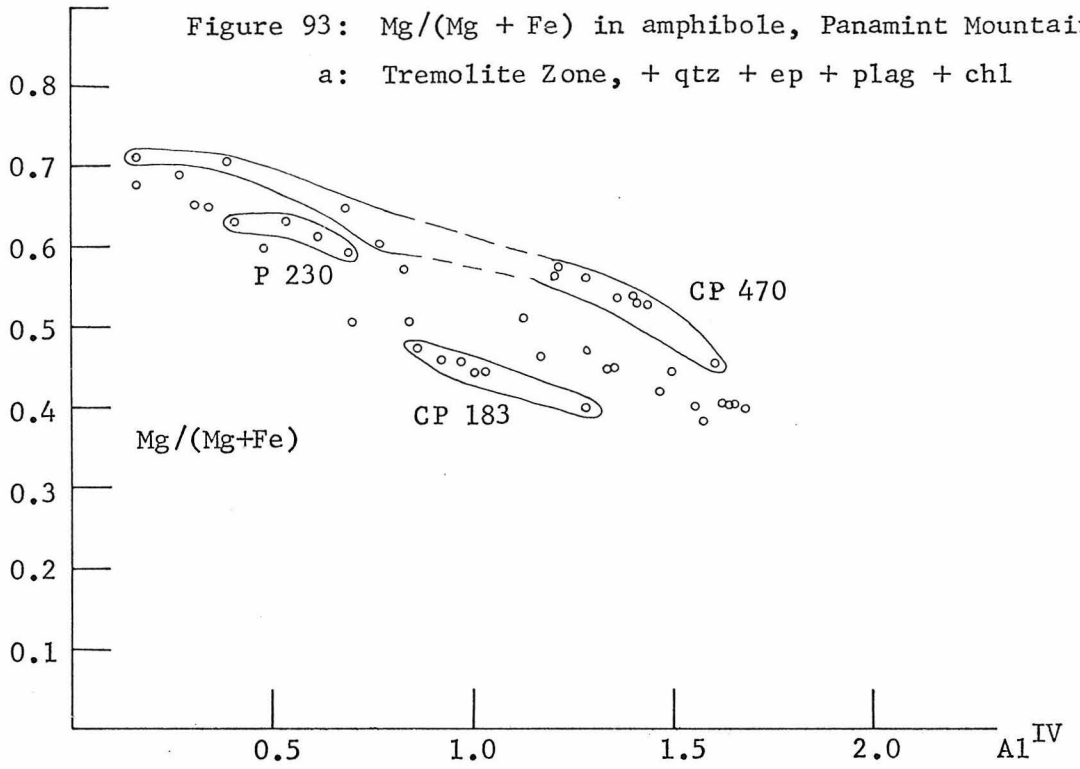

b: Diopside Zone, + qtz + ep + plag

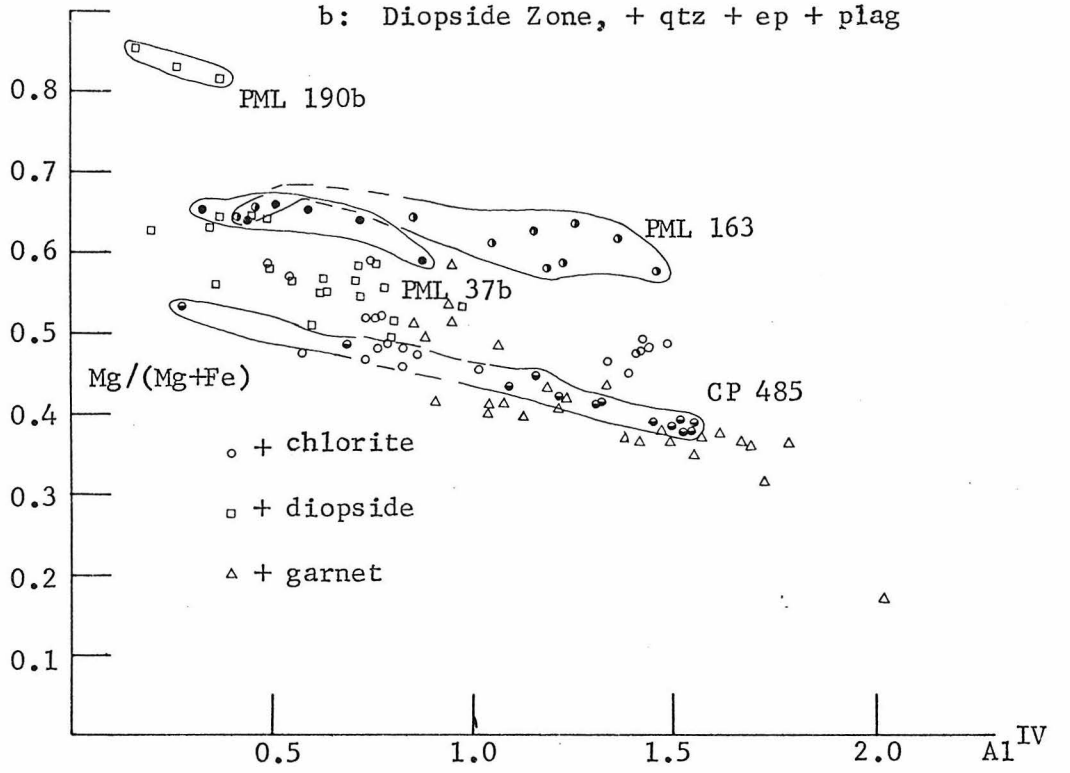

Figure 93: (continued)

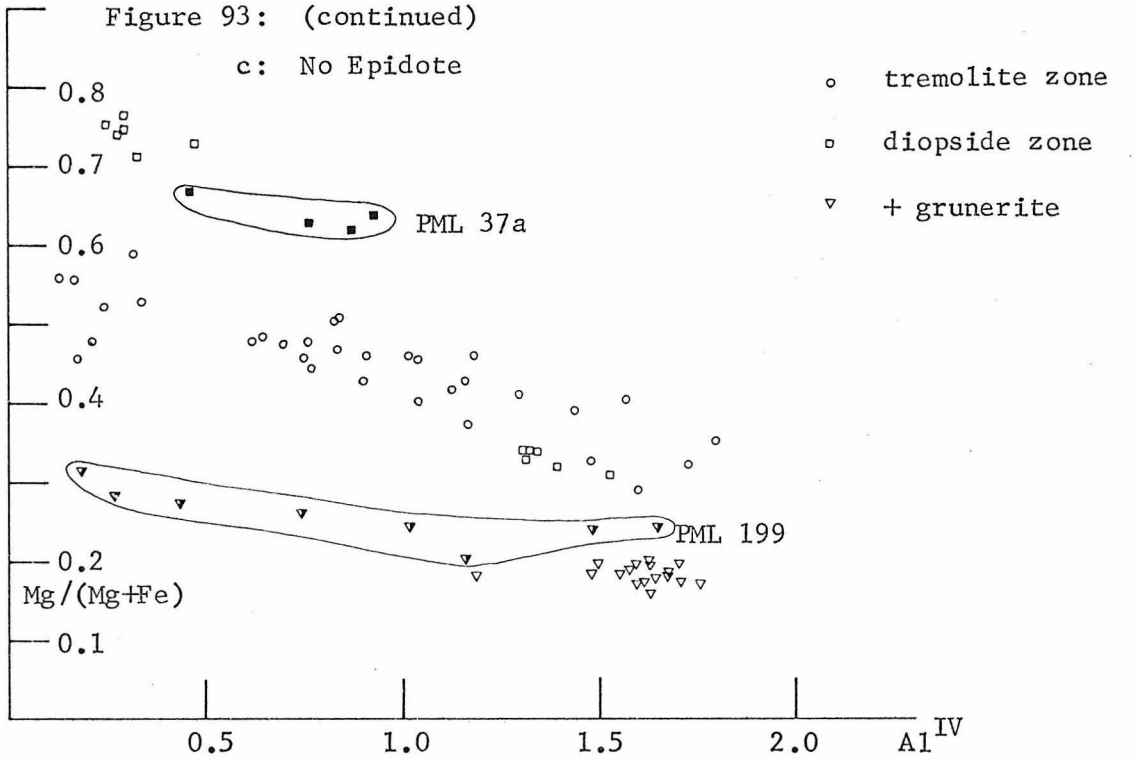

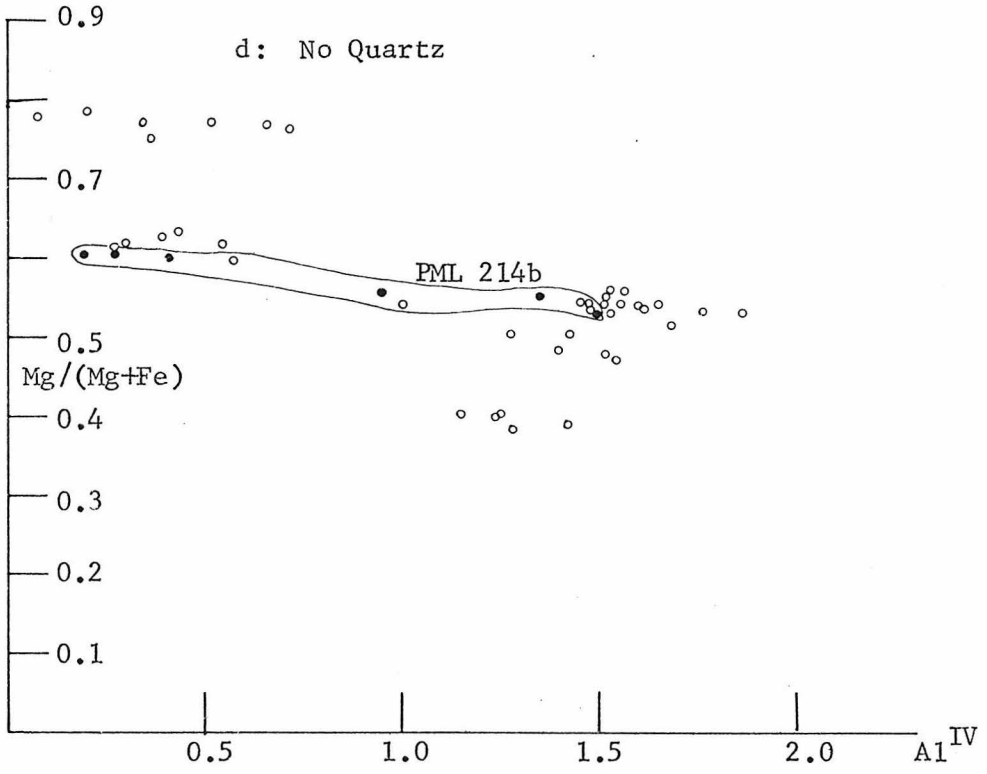

plagioclase + (chlorite or diopside or garnet) is constrained in general to the trend tremolite-pargasite. This "pargasite" substitution is modified by an unexpected and somewhat complex substitution involving titanium:

$$2Na^{A} + Mg \rightleftarrows 2\square^{A} + Ti,$$

and potassium may account for as much as one-half of the occupied A-site. Very aluminous amphibole generally coexists with very calcium-rich plagioclase and garnet and exhibits compositional variations dominated by the tschermakite substitution. Aluminous amphibole from the chlorite-free assemblage exhibited by CP 485 shows an increased importance in the edenite substitution. The glaucophane substitution is deemed unimportant but may occur to a minor degree.

The total amount of aluminum in amphibole depends on the assemblage. Diopside-bearing assemblages contain low aluminum amphibole; garnet-bearing assemblages contain high aluminum amphibole. There is a similar correlation with Mg/Fe values. Amphibole in diopside assemblages are magnesium-rich, and amphibole in garnet assemblages is iron-rich.

The "pargasite" substitution (neglecting the effects of Ti, K, and Fe^{+3}) in amphibole from the assemblage quartz + epidote + plagioclase + chlorite arises from the continuous reaction

$$23.2Ca_2Al_3Si_3O_{11}(OH) + 5NaAlSi_3O_8 + 4.25FM_{4.7}Al_{2.6}Si_{2.7}O_{10}(OH)_8 +$$

epidote albite chlorite

$$6.7SiO_2 = 36.4CaAl_2Si_2O_8 + 5NaCa_2FM_4Al(Si_6Al_2)O_{22}(OH)_2 + 23.6H_2O$$

quartz anorthite pargasite

and is similar to one determined by Laird (1977) in a more quantitative study of the variations in amounts and compositions of phases during prograde metamorphism of amphibolitic schists on a medium pressure gradient. At higher grades in iron-rich rocks, garnet becomes stable and an increase in the pargasite substitution can be accomplished by

$$14Ca_2Al_3Si_3O_{11}(OH) + 3NaAlSi_3O_8 + 4FM_3Al_2Si_3O_{12} = 22CaAl_2Si_2O_8 +$$

epidote albite garnet anorthite

$$3NaCa_2FM_4Al(Al_2Si_6)O_{22}(OH)_2 + SiO_2 + 4H_2O.$$

pargasite

These reactions account for the increase in "pargasite" content in hornblende, an increase in the anorthite content in plagioclase, and because both garnet and chlorite are more iron-rich than coexisting amphibole, an increase in Fe/(Fe + Mg) in hornblende.

If the albite component is totally consumed by these reactions then an increase in aluminum in amphibole may be accomplished by

$$14Ca_2Al_3Si_3O_{11}(OH) + 4FM_3Al_2Si_3O_{12} + 11SiO_2 = 22CaAl_2Si_2O_8 +$$

epidote garnet anorthite

$$3\square Ca_2FM_4Al(AlSi_7)O_{22}(OH)_2 + 4H_2O.$$

"tschermakite"

The plagioclase which coexists with garnet and amphibole which exhibits the greater tschermakite substitution (eg McD 350a) is very anorthitic (up to An_{90}). Hence in these samples, the "pargasite"-producing reaction occurred until the sodium was consumed and then the tschermakite-producing reaction became dominant.

Analogously, the chlorite and garnet-free assemblage amphibole increased its aluminum by

$$NaAlSi_3O_8 + Ca_2FM_5Si_8O_{22}(OH)_2 =$$

albite tremolite

$$NaCa_2FM_5(AlSi_7)O_{22}(OH)_2 + 4SiO_2.$$

edenite

In the sample CP 485 the "pargasite"-producing reaction ceased when chlorite (or garnet) was consumed, and an increase in aluminum was accomplished by the breakdown in albite component in plagioclase.

Potassium-rich calciferous schists in the Panamint Mountains are comprised of a variety of mineral assemblages which include quartz + epidote + muscovite or microcline. The large number of possible assemblages and reactions makes this rock type potentially useful for determining metamorphic grade and perhaps even distinguishing lower pressure from higher pressure facies series.

REFERENCES

Albee, A. L. (1965a) Phase equilibria in three assemblages of kyanite-zone pelitic schists, Lincoln Mountain Quadrangle, central Vermont. Jour. Petrology, vol. 6, p. 246-301.

Albee, A. L. (1965b) Distribution of Fe, Mg, and Mn between garnet and biotite in natural mineral assemblages. Jour. Geology, vol. 73, p. 155-164.

Albee, A. L. (1965c) A petrogenetic grid for the Fe-Mg silicates of pelitic schists. American Jour. Sci., vol. 263, p. 512-536.

Albee, A. L. (1968) Metamorphic zones in northern Vermont. In Zen, E-An, White, W. S., Hadley, J. B., and Thompson, J. B. (eds.) Studies of Appalachian Geology: Northern and Maritime, Interscience Publishers, New York, p. 329-342.

Albee, A. L. (1972) Metamorphism of pelitic schists: reaction relations of chloritoid and staurolite. Geol. Soc. America Bull., vol. 83, p. 3249-3268.

Albee, A. L., and Lanphere, M. A. (1962) Distribution of earlier and later Precambrian rocks in the central Panamint Range (abs). Geol. Soc. America Spec. Paper 72, p. 19.

Albee, A. L., Lanphere, M. A., and McDowell, S. D. (1971) Geology of the Telescope Peak Quadrangle compiled for Geologic Atlas of California, Death Valley Sheet, Calif. Div. Mines (in press).

Albee, A. L., and Ray, L. (1970) Correction factors for electron probe microanalysis of silicates, oxides, carbonates, phosphates, and sulfates. Analytical Chemistry, vol. 42, p. 1408-1414.

Anderson, P. A. M., Newton, R. C., and Kleppe, O. J. (1977) The enthalpy change of the andalusite-sillimanite reaction and the Al_2SiO_5 diagram. American Jour. Sci., vol. 277, p. 585-593.

Armstrong, R. L., and Suppe, J. (1973) Potassium-argon geochronometry of Mesozoic igneous rocks in Nevada, Utah, and southern California. Geol. Soc. America Bull., vol. 84, p. 1375-1392.

Banno, S. (1964) Petrologic studies on Sanbagawa crystalline schists in the Bessi-Ino district, central Shikoku, Japan. Tokyo Univ. Fac. Sci. J., Sec. II, vol. 15, p. 203-319.

Bence, A. E., and Albee, A. L. (1968) Empirical correction factors for the electron microanalysis of silicates and oxides. Jour. Geology, vol. 76, p. 382-403.

Bird, G. W., and Fawcett, J. J. (1973) Stability relations of Mg-chlorite-muscovite and quartz between 5 and 10 kb water pressure. Jour. Petrology, vol. 14, p. 415-428.

Bosma, W. (1964) The spots in the spotted slates of Stiege (Vosges) and Vogtland (Saxony). Geol. en Mijnbouw, vol. 43, p. 476-489.

Burchfiel, B. C., and Davis, G. A. (1971) Clark Mountain thrust complex in the Cordillera of southeastern California: geologic summary and field trip guide. Calif. Univ., Riverside, Campus Mus. Contr., no. 1, p. 1-28.

Burchfiel, B. C., and Davis, G. A. (1975) Nature and controls of Cordilleran orogenesis, western United States: extensions of an earlier synthesis. American Jour. Sci., vol. 275-A, p. 363-396.

Burchfiel, B. C., and Davis, G. A. (1977) Geology of the Sagamore Canyon-Slaughterhouse Spring area, New York Mountains, California. Geol. Soc. America Bull., vol. 88, p. 1623-1640.

Burchfiel, B. C., and Stewart, J. H. (1966) "Pull apart" origin of the central segment of Death Valley, California. Geol. Soc. America Bull., vol. 77, p. 439-442.

Champion, D. E., Albee, A. L., and Chodos, A. A. (1975) Reproducibility and operator bias in a computer controlled system for quantitative electron microprobe analysis. Proc. Tenth Annual Microbeam Analysis Soc. Conf., p. 55A-55F.

Chatterjee, N. D. (1961) The Alpine metamorphism in the Simplon area, Switzerland and Italy. Geologische Rundschau, vol. 51, p. 1-62.

Chatterjee, N. D. (1972) The upper stability limit of the assemblage paragonite + quartz and its natural occurrences. Contr. Min. Petrology, vol. 34, p. 288-303.

Chatterjee, N. D. and Johannes, W. (1974) Thermal stability and standard thermochemical properties of synthetic $2M_1$- muscovite $KAl_2[AlSi_3O_{10}(OH)_2]$. Contr. Min. Petrology, vol. 48, p. 89-114.

Chodos, A. A., Albee, A. L., Gancarz, A. J., and Laird, J. (1973) Optimization of computer-controlled quantitative analysis of minerals. Proc. Eighth National Conf. Electron Probe Analysis, p. 45A-45C.

Clark, S. P., and Ringwood, A. E. (1964) Density distribution and constitution of the mantle. Rev. Geophysics, vol. 2, p. 35-88.

Compton, R. R. (1960) Contact metamorphism in the Santa Rosa Range, Nevada. Geol. Soc. America Bull., vol. 71, p. 1383-1416.

Crittenden, M. D., Schaeffer, F. E., Trimble, D. E., and Woodward, L. E. (1971) Nomenclature and correlation of some upper Precambrian and basal Cambrian sequences in western Utah and southeastern Idaho. Geol. Soc. America Bull., vol. 82, p. 581-602.

Dalrymple, G. B., and Lanphere, M. A. (1971) $^{40}Ar/^{39}Ar$ technique of K-Ar dating: a comparison with the conventional technique. Earth Plan. Sci. Letters, vol. 12, p. 300-308.

Diehl, P. (1974) Stratigraphy and sedimentology of the Wood Canyon Formation, Death Valley area, California. In Guidebook: Death Valley Region, California and Nevada, Shoshone, Death Valley Pub. Co., p. 37-48.

Dunne, G. C., Gulliver, R. M., and Sylvester, A. G. (1978) Mesozoic evolution of rocks of the White, Inyo, Argus, and Slate Ranges, eastern California. In Howell, D. G., and McDougall, K. (eds.) Mesozoic Paleogeography of the Western United States, Soc. Econ. Paleontologists and Mineralogists, Pacific sec., Pacific Coast Paleogeography Symposium 2 (in press).

Ernst, W. G., Seki, Y., Onuki, H., and Gilbert, M. C. (1970) Comparative study of low grade metamorphism in the California Coast Ranges and the outer metamorphic belt of Japan. Geol. Soc. America Memoir 124.

Eugster, H. P., Albee, A. L., Bence, A. E., Thompson, J. B., and Waldbaum, D. R. (1972) The two-phase region and excess mixing properties of paragonite-muscovite crystalline solutions. Jour. Petrology, vol. 13, p. 147-179.

Evernden, J. F., and Kistler, R. W. (1970) Chronology of emplacement of Mesozoic batholithic complexes in California and western Nevada. U.S. Geol. Survey Prof. Paper 623, 42 p.

Ferry, J. M., and Spear, F. S. (1977) Experimental calibration of the partitioning of Fe and Mg between biotite and garnet (abs). Geol. Soc. America Abstracts with Programs, vol. 9, p. 974.

Fyfe, W. S., Turner, F. J., and Verhoogen, J. (1958) Metamorphic reactions and metamorphic facies. Geol. Soc. America Mem. 73.

Gabrielse, H. (1972) Younger Precambrian of the Canadian Cordillera. American Jour. Sci., vol. 272, p. 521-536.

Ganguly, J. (1972) Staurolite stability and related parageneses: theory, experiments, and applications. Jour. Petrology, vol. 13, p. 335-365.

Ganguly, J., and Kennedy, G. C. (1974) The energetics of natural garnet solid solution I. mixing of the aluminosilicate end-members. Contr. Min. Petrology, vol. 48, p. 137-148.

Ghent, E. D. (1975) Temperature, pressure, and mixed volatile equilibria attending metamorphism of staurolite-kyanite-bearing assemblages, Esplanade Range, British Columbia. Geol. Soc. America Bull., vol. 86, p. 1654-1660.

Ghent, E. D. (1976) Plagioclase-garnet-Al_2SiO_5-quartz: a potential geobarometer-geothermometer. American Min., vol. 61, p. 710-714.

Goldman, D. S., and Albee, A. L. (1977) Correlation of Mg/Fe partitioning between garnet and biotite with $^{18}O/^{16}O$ partitioning between quartz and magnetite. American Jour. Sci., vol. 277, p. 750-767.

Greenwood, H. J. (1975) Thermodynamically valid projections of extensive phase relationships. American Min., vol. 60, p. 1-8.

Guidotti, C. V. (1974) Transition from staurolite to sillimanite zone, Rangeley Quadrangle, Maine. Geol. Soc. America Bull., vol. 85, p. 475-490.

Guidotti, C. V., Cheney, J. T., and Conatori, P. (1975) Coexisting cordierite + biotite + chlorite from upper staurolite to lower sillimanite zone rocks in the Rumford Quadrangle, Maine. Geology, vol. 3, p. 147-148.

Hall, W. E. (1971) Geology of the Panamint Butte Quadrangle, Inyo County, California. U.S. Geol. Survey Bull. 1299, 67 p.

Harrison, J. E., Griggs, A. B., and Wells, J. D. (1974) Tectonic features of the Precambrian Belt basin and their influence on post-Belt structures. U.S. Geol. Survey Prof. Paper 886, 15 p.

Harrison, J. E., and Reynolds, M. W. (1976) Western U.S. continental margin: a stable platform dominated by vertical tectonics in the late Precambrian (abs). Geol. Soc. America Abstracts with Programs, vol. 8, p. 905.

Harker, A. (1932) Metamorphism: A Study of the Transformation of Rock Masses. London, Meuthen.

Harte, B. (1975) Determination of a pelitic petrogenetic grid for the eastern Scottish Dalradian. Carn. Inst. Washington Year Book 74, p. 438-446.

Hazzard, J. C. (1937) Paleozoic section in the Nopah and Resting Spring Mountains, Inyo County, California. Calif. Jour. Mines and Geology,

vol. 33, p. 273-339.

Hess, P. C. (1969) The metamorphic paragenesis of cordierite in pelitic rocks. Contr. Min. Petrology, vol. 24, p. 191-207.

Hewett, D. F. (1940) New formation names to be used in the Kingston Range, Ivanpah Quadrangle, California. Wash. Acad. Sci. Jour., vol. 30, p. 239-240.

Hewett, D. F. (1956) Geology and mineral resources of the Ivanpah quadrangle, California and Nevada. U.S. Geol. Survey Prof. Paper 275, 172 p.

Hewitt, D. A. (1973) Stability of the assemblage muscovite-calcite-quartz. American Min., vol. 58, p. 785-791.

Hewitt, D. A. (1975) Stability of the assemblage phlogopite-calcite-quartz. American Min., vol. 60, p. 391-397.

Holdaway, M. J. (1971) Stability of andalusite and the aluminum silicate phase diagram. American Jour. Sci., vol. 271, p. 97-131.

Hollister, L. S. (1966) Garnet zoning: an interpretation based on the Rayleigh fractionation model. Science, vol. 154, p. 1647-1651.

Hooke, R. L. (1965) Alluvial fans (Ph.D. thesis). California Institute of Technology, Pasadena, 192 p.

Hopper, R. H. (1947) Geologic section from the Sierra Nevada to Death Valley, California. Geol. Soc. America Bull. 58, p. 393-432.

Hoschek, G. (1969) The stability of staurolite and chloritoid and their significance in metamorphism of pelitic rocks. Contr. Min. Petrology, vol. 22, p. 208-232.

Hoschek, G. (1973) Die Reaktion Phlogopit + Calcit + Quartz = Tremolit + Kalifeldspat + H_2O + CO_2. Contr. Min. Petrology, vol. 39, p. 231-237.

Hunt, C. B., and Mabey, D. R. (1966) Stratigraphy and structure, Death Valley, California. U.S. Geol. Survey Prof. Paper 494-A, 162 p.

Johnson, B. D. (1957) Geology of a part of the Manly Peak Quadrangle, southern Panamint Range, California. U. California Pub. Geol. Sci., vol. 30, p. 353-424.

Kepezhinskas, K. B., and Khlestov, V. V. (1977) The petrogenetic grid and subfacies for middle-temperature metapelites. Jour. Petrology, vol. 18, p. 114-143.

Kerrick, D. M. (1968) Experiments on the upper stability limit of phyrophyllite at 1.8 kilobars and 3.9 kilobars water pressure. American Jour. Sci., vol. 266, p. 204-214.

Kretz, R. (1961) Some applications of thermodynamics to coexisting minerals of variable composition. Examples: orthopyroxene-clinopyroxene and orthopyroxene-garnet. Jour. Geology, vol. 69, p. 361-387.

Labotka, T. C., and Albee, A. L. (1976) Paleogeography and Paleotectonics of the Late Precambrian Pahrump Group, Panamint Mountains, California (abs). Geol. Soc. America Abstracts with Programs, vol. 8, p. 996-997.

Labotka, T. C., and Albee, A. L. (1977) Late Precambrian depositional environment of the Pahrump Group, Panamint Mountains, California. Calif. Div. Mines and Geology, Spec. Paper 129, p. 93-100.

Laird, J. (1977) Phase equilibria in mafic schist and the polymetamorphic history of Vermont (Ph.D. thesis). California Institute of Technology, Pasadena, 445 p.

Lanphere, M. A. (1962) I. Geology of the Wildrose area, Panamint Range, California. II. Geochronologic studies in the Death Valley-Mojave Desert region, California (Ph.D. thesis). California Institute of Technology, Pasadena, 171 p.

Lanphere, M. A., and Dalrymple, G. B. (1967) K-Ar and Rb-Sr measurements on P-207, the U.S.G.S. interlaboratory standard muscovite. Geochim. Cosmochim. Acta, vol. 31, p. 1091-1094.

Lanphere, M. A., Wasserburg, G. J., Albee, A. L., and Tilton, G. R. (1964) Redistribution of strontium and rubidium isotopes during metamorphism, World Beater Complex, Panamint Range, California. In Craig, H., Miller, S. L., and Wasserburg, G. J. (eds.) Isotopic and Cosmic Chemistry, North Holland Publishing Co., Amsterdam, p. 269-320.

Leake, B. E. (1965) The relationship between tetrahedral aluminum and the maximum possible octahedral aluminum in natural calciferous and sub-calciferous amphiboles. American Min., vol. 50, p. 843-851.

Maxson, J. H. (1950) Physiographic features of the Panamint Range, California. Geol. Soc. America Bull. 61, p. 99-114.

McAllister, J. F. (1956) Geology of the Ubehebe Peak Quadrangle, California. U.S. Geol. Survey Map GQ 95.

McAllister, J. F. (1974) Geologic maps and sections of a strip from

Pyramid Peak to the southeast end of the Funeral Mountains, Ryan Quadrangle, California. In Guidebook: Death Valley Region, California and Nevada, Shoshone, Death Valley Pub. Co., p. 81-83.

McDowell, S. D. (1967) The intrusive history of the Little Chief granite porphyry stock, central Panamint Range, California. I. Structural relationships. II. Petrogenesis, based on electron microprobe analysis of the feldspars (Ph.D. thesis). California Institute of Technology, Pasadena, 282 p.

McDowell, S. D. (1974) Emplacement of the Little Chief stock, Panamint Range, California. Geol. Soc. America Bull. 85, p. 1535-1546.

McDowell, S. D. (1978) Little Chief granite porphyry: feldspar crystallization history. Geol. Soc. America Bull. 89, p. 33-49.

Miyashiro, A. (1958) Regional metamorphism in the Gosaisyo-Takanuki district in the central Abukuma Plateau. Tokyo Univ. Fac. Sci. J., Sec. 2, vol. 11, p. 219-272.

Miyashiro, A. (1961) Evolution of metamorphic belts. Jour. Petrology, vol. 2, p. 277-318.

Moore, S. C. (1974) Syn-batholithic thrusting of Jurassic? age in the Argus Range, Inyo Co., California (abs). Geol. Soc. America Abstracts with Programs, vol. 6, p. 223.

Murphy, F. Mac (1930) Geology of the Panamint Silver District, California. Econ. Geol., vol. 25, p. 305-325.

Murphy, F. Mac (1932) Geology of a part of the Panamint Range, California. Calif. Div. Mines, 28th Report State Mineralogist, p. 329-355.

Nolan, T. B. (1929) Notes on the stratigraphy and structure of the northwest portion of Spring Mountain, Nevada. American Jour. Sci., 5th series, vol. 17, p. 461-472.

Okrusch, M. (1969) Die Gneishornfelse um Steinach in der Oberpfalz. Eine phasenpetrologische Analyse. Contr. Min. Petrology, vol. 22, p. 32-72.

Okrusch, M. (1971) Garnet-cordierite-biotite equilibria in the Steinach aureole, Bavaria. Contr. Min. Petrology, vol. 32, p. 1-23.

Orville, P. M. (1972) Plagioclase cation exchange equilibria with aqueous chloride solution: results at 700°C and 2000 bars in the presence of quartz. American Jour. Sci., vol. 272, p. 234-272.

Pyramid Peak to the southeast end of the Funeral Mountains, Ryan Quadrangle, California. In Guidebook: Death Valley Region, California and Nevada, Shoshone, Death Valley Pub. Co., p. 81-83.

McDowell, S. D. (1967) The intrusive history of the Little Chief granite porphyry stock, central Panamint Range, California. I. Structural relationships. II. Petrogenesis, based on electron microprobe analysis of the feldspars (Ph.D. thesis). California Institute of Technology, Pasadena, 282 p.

McDowell, S. D. (1974) Emplacement of the Little Chief stock, Panamint Range, California. Geol. Soc. America Bull. 85, p. 1535-1546.

McDowell, S. D. (1978) Little Chief granite porphyry: feldspar crystallization history. Geol. Soc. America Bull. 89, p. 33-49.

Miyashiro, A. (1958) Regional metamorphism in the Gosaisyo-Takanuki district in the central Abukuma Plateau. Tokyo Univ. Fac. Sci. J., Sec. 2, vol. 11, p. 219-272.

Miyashiro, A. (1961) Evolution of metamorphic belts. Jour. Petrology, vol. 2, p. 277-318.

Moore, S. C. (1974) Syn-batholithic thrusting of Jurassic? age in the Argus Range, Inyo Co., California (abs). Geol. Soc. America Abstracts with Programs, vol. 6, p. 223.

Murphy, F. Mac (1930) Geology of the Panamint Silver District, California. Econ. Geol., vol. 25, p. 305-325.

Murphy, F. Mac (1932) Geology of a part of the Panamint Range, California. Calif. Div. Mines, 28th Report State Mineralogist, p. 329-355.

Nolan, T. B. (1929) Notes on the stratigraphy and structure of the northwest portion of Spring Mountain, Nevada. American Jour. Sci., 5th series, vol. 17, p. 461-472.

Okrusch, M. (1969) Die Gneishornfelse um Steinach in der Oberpfalz. Eine phasenpetrologische Analyse. Contr. Min. Petrology, vol. 22, p. 32-72.

Okrusch, M. (1971) Garnet-cordierite-biotite equilibria in the Steinach aureole, Bavaria. Contr. Min. Petrology, vol. 32, p. 1-23.

Orville, P. M. (1972) Plagioclase cation exchange equilibria with aqueous chloride solution: results at 700°C and 2000 bars in the presence of quartz. American Jour. Sci., vol. 272, p. 234-272.

Osberg, P. H. (1968) Stratigraphy, structure, and metamorphism of the Waterville-Vassalboro area, Maine. Maine Geol. Survey Bull. 20.

Prigogine, I., and Defay, R. (1954) Chemical Thermodynamics, Longman, Green and Co. Ltd., London, 543 p.

Raase, P. (1974) Al and Ti contents of hornblende, indicators of pressure and temperature of regional metamorphism. Contr. Min. Petrology, vol. 45, p. 231-236.

Read, H. H. (1952) Metamorphism and migmatisation in the Ythan Valley, Aberdeenshire. Trans Edin. Geol. Soc., vol. 15, p. 265-279.

Reynolds, M. W. (1974) Geology of the Grapevine Mountains, Death Valley, California: a summary. In Guidebook: Death Valley Region, California and Nevada, Shoshone, Death Valley Pub. Co., p. 91-97.

Richardson, S. W. (1968) Staurolite stability in a part of the system Fe-Al-Si-O-H. Jour. Petrology, vol. 9, p. 467-488.

Roberts, M. T. (1974) Stratigraphy and depositional environments of the Crystal Spring Formation, Death Valley area, California. In Guidebook: Death Valley Region, California and Nevada, Shoshone, Death Valley Pub. Co., p. 49-58.

Ryan, B. D., and Belkinsop, J. (1971) Geology and geochronology of the Hellroaring Creek stock, British Columbia. Canadian Jour. Earth Sci., vol. 8, p. 85-95.

Silver, L. T. (1960) Age determinations on Precambrian diabase differentiates in the Sierra Ancha, Gila County, Arizona (abs). Geol. Soc. America Bull., vol. 71, p. 1973-1974.

Silver, L. T., Anderson, C. A., Crittenden, M., and Robertson, J. M. (1977) Chronostratigraphic elements of the Precambrian rocks of the southwestern and far western United States (abs). Geol. Soc. America Abstracts with Programs, vol. 9, p. 1176.

Silver, L. T., McKinney, C. R., and Wright, L. A. (1961) Some Precambrian ages in the Panamint Range, Death Valley, California (abs). Geol. Soc. America Spec. Paper 68, p. 55.

Skippen, G. B. (1974) An experimental model for low pressure metamorphism of siliceous dolomitic marble. American Jour. Sci., vol. 274, p. 487-509.

Slaughter, J., Kerrick, D. M., and Wall, V. J. (1975) Experimental and thermodynamic study of equilibria in the system CaO-MgO-SiO_2-H_2O-CO_2. American Jour. Sci., vol. 275, p. 143-162.

Smith, G. I., Troxel, B. W., Gray, C. H., von Huene, R. (1968) Geologic reconnaissance of the Slate Range, San Bernardino and Inyo Counties, California. California Div. Mines and Geology Spec. Report 96, 33 p.

Smith, R. S. U. (1976) Late-Quaternary pluvial and tectonic history of Panamint Valley, Inyo and San Bernardino Counties, California (Ph.D. thesis). California Institute of Technology, Pasadena, 295 p.

Stern, T. W., Newell, M. F., and Hunt, C. B. (1966) Uranium-lead and potassium-argon ages of parts of the Amargosa thrust complex, Death Valley, California. U.S. Geol. Survey Prof. Paper 550-B, p. 142-147.

Stevens, C. H., and Olson, R. C. (1972) Nature and significance of the Inyo thrust fault, eastern California. Geol. Soc. America Bull., vol. 83, p. 3761-3768.

Stevens, C. H., Wrucke, C. T., and McKee, E. H. (1974) Directions and amount of movement on the Butte Valley thrust, southeastern California (abs). Geol. Soc. America Abstracts with Programs, vol. 6, p. 261.

Stewart, J. H. (1970) Upper Precambrian and Lower Cambrian strata in the southern Great Basin, California and Nevada. U.S. Geol. Survey Prof. Paper 620, 206 p.

Stewart, J. H. (1972) Initial deposits in the Cordilleran Geosyncline: evidence of a Late Precambrian (<850 m.y.) continental separation: Geol. Soc. America Bull., vol. 83, p. 1345-1360.

Stewart, J. H., Ross, D. C., Nelson, C. A., and Burchfiel, B. C. (1966) Last Chance thrust - a major fault in the eastern part of Inyo County, California. U.S. Geol. Survey Prof. Paper 550-D, p. 23-34.

Storre, B., and Nitsch, K-H (1972) Die Reaktion 2 Zoisit + 1 CO_2 = 3 Anorthit + 1 Calcit + 1 H_2O. Contr. Min. Petrology, vol. 35, p. 1-10.

Tilley, C. E. (1924) Contact metamorphism in the Comrie area of the Perthshire Highlands. Q. J. Geol. Soc. London, vol. 80, p. 22-70.

Thompson, A. B. (1976) Mineral reactions in pelitic rocks: I. Prediction of P-T-X(Fe-Mg) phase relations. II. Calculation of some P-T-X(Fe-Mg) phase relations. American Jour. Sci., vol. 276, p. 401-454.

Thompson, A. B., Lyttle, P. T., and Thompson, J. B. (1977) Mineral reactions and A-Na-K and A-F-M facies types in the Gassetts Schist, Vermont. American Jour. Sci., vol. 277, p. 1124-1151.

Thompson, J. B. (1957) The graphical analysis of mineral assemblages in pelitic schists. American Min., vol. 42, p. 842-858.

Troxel, B. W., and Wright, L. A. (1968) Precambrian stratigraphy of the Funeral Mountains, Death Valley, California (abs). Geol. Soc. America Spec. Paper 121, p. 574-575.

Tuttle, O. F., and Bowen, N. L. (1958) Origin of granite in light of experimental studies in the system $NaAlSi_3O_8$-$KAlSi_3O_8$-SiO_2-H_2O. Geol. Soc. America Mem. 74.

Wasserburg, G. J., Wetherill, G. W., and Wright, L. A. (1959) Ages in the Precambrian terrane of Death Valley, California. Jour. Geology, vol. 67, p. 702-708.

White, D. E. (1940) Antimony deposits of the Wildrose Canyon area, Inyo County, California. U.S. Geol. Survey Bull. 922-K, p. 307-325.

Williams, E. G., Wright, L. A., and Troxel, B. W. (1974) The Noonday Dolomite and equivalent stratigraphic units, southern Death Valley region, California. In Guidebook: Death Valley Region, California and Nevada, Shoshone, Death Valley Pub. Co., p. 73-77.

Wright, L. A. (1968) Talc deposits of the southern Death Valley-Kingston Range region, California. California Div. Mines and Geol. Spec. Report 95, 79 p.

Wright, L. A., and Troxel, B. W. (1966) Strata of late Precambrian-Cambrian age, Death Valley region, California-Nevada. American Assn. Petroleum Geologists Bull., vol. 50, p. 846-857.

Wright, L. A., and Troxel, B. W. (1973) Shallow-fault interpretation of Basin and Range structure, southwestern Great Basin. In deJong, K. A., and Scholten, R. (eds.) Gravity and Tectonics, John Wiley and Sons, New York, p. 397-407.

Wright, L. A., Troxel, B. W., Williams, E. G., Roberts, M. T., and Diehl, P. E. (1974) Precambrian sedimentary environments of the Death Valley region, eastern California. In Guidebook: Death Valley Region, California and Nevada, Shoshone, Death Valley Pub. Co., p. 27-35.

Wright, L. A., Williams, E. G., and Cloud, P. (1978) Algal and cryptalgal structures and platform environments of the late pre-Phanerozoic Noonday Dolomite, eastern California. Geol. Soc. America, vol. 89, p. 321-333.

Wrucke, C. T., and Shride, A. F. (1972) Correlation of Precambrian diabase in Arizona and southern California (abs). Geol. Soc. America Abstracts with Programs, vol. 4, p. 265-266.

Zen, E-An (1963) Components, phases, and criteria of chemical equilibrium in rocks. American Jour. Sci., vol. 261, p. 929-942.

Zen, E-An (1974) Prehnite- and pumpellyite-bearing mineral assemblages, west side of the Appalachian metamorphic belt, Pennsylvania to Newfoundland. Jour. Petrology, vol. 15, p. 197-242.

APPENDIX

DESCRIPTION OF MAP UNITS

Qa ALLUVIUM AND TALUS (Quaternary)

Qp PLAYA LAKE DEPOSITS (Quaternary)

Qoa OLDER ALLUVIUM (Quaternary) Uplifted and dissected alluvial gravels and sand

LANDSLIDE DEPOSITS (Quaternary)

Qlc Landslide debris composed of Crystal Spring Formation

Qlb Landslide debris composed of Beck Spring Dolomite

Qlk Landslide debris composed of Kingston Peak Formation

Qln Landlside debris composed of Noonday Dolomite

Qlj Landslide debris composed of Johnnie Formation

Ql Landslide, undifferentiated

Tn NOVA FORMATION (Pliocene) Gravel, sand, and silt. A thin limestone occurs at its base.

MONOLITHOLOGIC BRECCIA (Pliocene?) -- Consists of deposits of greatly crushed and fragmented rock derived from older metasedimentary and granitic rocks. Divided into:

Tbb Breccia composed of Beck Spring Dolomite

Tbk Breccia composed of Kingston Peak Formation

Tbn Breccia composed of Noonday Dolomite

Tbh Breccia composed of Hall Canyon pluton

Tbm Breccia composed of mixed granodiorite and Kingston Peak Formation

LITTLE CHIEF STOCK (Miocene?) -- Leucocratic, hornblende-biotite granite porphyry which contains phenocrysts of sanidine and complexly zoned plagioclase up to 10 mm in diameter. The groundmass is composed of 0.5 mm grains of quartz, alkali feldspar, and minor plagioclase. The stock is a composite of a north and a south phase. The north phase has a slightly higher mafic mineral content (10%) than the south (5%), and has a chilled margin against the south phase. The emplacement of the stock is described by McDowell (1974), and the crystallization history is described by McDowell (1977).

Tln North phase

Tls South phase

Td FELSIC SILLS AND DIKES (Miocene?) -- Dikes and sills similar in composition to the Little Chief stock which preceded and accompanied the emplacement of the stock.

Khc HALL CANYON PLUTON (Cretaceous) -- Medium-grained leucocratic granodiorite which consists of sodic plagioclase, quartz, microcline, and muscovite. Locally, a minor amount of biotite and a trace of garnet are observed. In Wildrose Canyon this unit contains abundant microcline, and the dominant rock type is granite.

$\epsilon p\epsilon w$ WOOD CANYON FORMATION (Cambrian and Precambrian) -- Mostly thin-bedded siltstone and quartzite

s STIRLING QUARTZITE (Precambrian) -- Mostly quartzite throughout. Contains arkosic quartzite and conglomerate at the base, and two purple argillite layers about 150 m above the base which locally contain andalusite porphyroblasts. Minor siltstone and thin-bedded dolomite occur near the top.

ju JOHNNIE FORMATION (Precambrian)

Upper member -- 700 m of argillite and calcareous argillite. The lower portion consists of very thinly laminated, micaceous, green argillite with rare sandy dolomite and limestone layers. The upper part is characterized by thin-bedded, blue-gray argillite and gray-green silty limestone. Sedimentary bedforms are abundant and include ripple marks, climbing ripples, and flaser structures. Thin quartzite beds are common near the top. Locally, the contact between the lower green argillite and the upper blue-gray calcareous argillite is mapped. Locally includes:

jud Sandy dolomite unit -- Occurs at top of the upper member in the northeast corner of the quadrangle where it is about 50 m in thickness.

jl Lower member -- Thick-bedded dolomite and sandy dolomite interbedded with quartzite and dolomitic quartzite and overlain by dark reddish brown-weathering quartzite and pelite. Thickness ranges from 150 to 300 m. The more highly metamorphosed equivalent of the member contains tremolite-dolomite marble and andalusite-staurolite-biotite schist.

NOONDAY DOLOMITE (Precambrian) -- Dominantly dolomite and dolomitic limestone. West of the range crest the Noonday Dolomite is metamorphosed and consists of marble.

nrl Redlands Member -- 125 to 250 m of thick-bedded to massive, light gray dolomite with minor, thin argillite beds near the top. In the southeast part of the quadrangle the member is dominantly clastic, consisting of dolomitic sandstone, quartz-dolomite calcarenite, and quartzite.

nr Radcliff Member -- 100 to 250 m of thinly-bedded, grey, pink, green, or brown limestone interbedded with thin laminae of grey-green argillaceous limestone and argillite. The lower part consists almost entirely of argillite, but it includes lenses of conglomerate containing clasts of argillite and dolomite in an argillaceous dolomite matrix.

nsp Sentinel Peak Member -- 3 to 150 m of light gray, massive dolomite containing thinly-laminated, siliceous limestone in the lower part. Thin laminae, eyes, and tubes of probable biologic origin are common in this member. In many places the Sentinel Peak Member is too thin to be mapped separately.

PAHRUMP GROUP (Precambrian)

KINGSTON PEAK FORMATION

ksp South Park Member -- The lower part consists of up to 130 m of thin-bedded argillite. Locally, the argillite has a spotted appearance due to the presence of altered cordierite porphyroblasts. The argillite is overlain by up to

35 m of stretched pebble conglomerate which consists of quartzite clasts in a black argillaceous matrix. The conglomerate is overlain by about 70 m of feldspathic quartzite and up to 30 m of pebbly argillite. These upper units are variably truncated by the disconformity at the base of the Noonday Dolomite.

ksd Sourdough Limestone Member -- 5 to 30 m of thinly-laminated, light and dark grey, micaceous limestone. In places, slump folds occur at the top of the member and fold the argillite of the overlying South Peak Member into the Sourdough Limestone. In most places the limestone is too thin to be mapped separately and is represented by the contact between the South Park Member and the Surprise Member of the Kingston Peak Formation.

ks Surprise Member -- 250 to 1000 m of clastic rocks. South of Surprise Canyon the unit consists of massive to unbedded, trimodal to unsorted pebbly mudstone and diamictite. Clasts several meters across are observed, but generally the largest clasts are less than 10 cm in diameter. Clast lithologies include quartzofeldspathic gneiss, quartzite, dolomite, argillite, and diabase. Graded argillite beds which contain exotic "lonestones" also occur in the member. North of Surprise Canyon this member consists of thin-bedded argillite and fine-grained metagreywacke. Diamic-

tite is absent and conglomeratic layers are uncommon. Interbeds of thinly-laminated, grey siliceous marble occur in Jail and Tuber Canyons. Basalt and amphibolite with pillow structures are interbedded with the Surprise Member in upper Pleasant Canyon and along the western margin of the range.

kb Pillow basalt and amphibolite

km Siliceous calcite marble

Limekiln Spring Member -- Includes a variety of rock types which interfinger with the upper part of the Beck Spring Dolomite, but locally lie unconformably on top of Beck Spring Dolomite, Crystal Spring Formation, and earlier Precambrian gneiss. The thickness varies from 50 to 500 m, and the member consists primarily of fine-grained metagreywacke, pelitic schist, and amphibolititc schist. Conglomeratic layers are locally abundant and contain clasts of the earlier Precambrian basement or clasts of Beck Spring Dolomite up to several meters in diameter. Interbeds of dolomite, lithologically similar to the Beck Spring Dolomite, are common in the lower part, and in many places the unit interfingers with the Beck Spring Dolomite. North of Surprise Canyon the lower part of the member also contains numerous interbeds of metamorphosed arkose and arkosic conglomerate. The top of the unit is marked by 60

to 100 m of thin-bedded calcareous quartzite and quartz arenite. Divided into:

ka Argillite, schist, amphibolite, and metamorphosed conglomerate

kq Quartzite and calcareous quartzite

kd Dolomite. Only thick units are mapped

kar Arkose and arkosic conglomerate. Also contains interbeds of dolomite, dolomite-clast conglomerate, and gneiss-clast conglomerate.

da DIABASE AND AMPHIBOLITE -- Sills and dikes of metamorphosed mafic rock. May include intrusions of several ages.

bs BECK SPRING DOLOMITE -- 200 to 300 m of blue-gray to buff, massive siliceous dolomite and its metamorphosed equivalent, tremolite-dolomite marble. Thin, wavy laminae and stromatolites are preserved on Sentinel Peak. Where the top interfingers with clastic rocks of the overlying Kingston Peak Formation, interbeds of intraformation conglomerate and argillite occur.

cs CRYSTAL SPRING FORMATION -- Consists primarily of 200 to 300 m of marble and schist. A quartzite-clast conglomerate occurs at the base in upper Happy Canyon where the formation consists of dolomitic marble overlain by argillite. Elsewhere

dark brown-weathering, micaceous calcite marble occurs at the base, and the upper part consists of biotite schist. In Tuber Canyon the formation is over 1000 m thick and is divided into a lower unit of marble, a middle unit of quartzite interbedded with pelitic schist, and an upper unit of garnet-chlorite schist interbedded with micaceous quartzite.

In Tuber Canyon, divided into:

css Garnet-chlorite-biotite and garnet-chlorite-chloritoid schist interbedded with micaceous quartzite

csq Micaceous quartzite

csm Marble -- Dark brown-weathering and locally containing chert nodules

wb WORLD BEATER COMPLEX (Precambrian)-- Gray biotite augen gneiss (approximately 1700 m.y., Lanphere and others, 1964) intruded by gray porphyritic quartz monzonite (approximately 1400 m.y., Lanphere and others, 1964). These rock types occur in the World Beater dome in Pleasant and Happy Canyons.

qf QUARTZOFELDSPATHIC GNEISS COMPLEX (Precambrian) -- Thickly-foliated, leucocratic, quartz-plagioclase-microcline-muscovite gneiss. Compositional layering is parallel to foliation, and the leucocratic gneiss overlies with apparent conformity a sequence of metasedimentary rock. This metasedimentary sequence consists dominantly of leucocratic quartz-rich schist

and micaceous quartzite. Dark biotite-rich and amphibole-rich layers are locally abundant.

Contact. Long dash where approximately located. Short dash where inferred.

Contact between different clast lithologies within megabreccia and landslide deposits.

Landslide contact.

Fault, showing dip. Long dash where approximately located. Short dash where inferred. Dotted where concealed.

Zone of intense disharmonic folding.

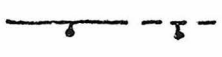

Scarp in alluvium. Ball on lower side. Short dash where inferred.

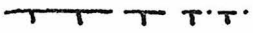

Low angle normal fault. Hatchures on upper plate.

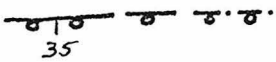

Lower boundary of monolithologic breccia, showing dip. Beads on upper plate.

Strike and dip of bedding

inclined

vertical

horizontal

overturned

Strike and dip of foliation

Plunge of mineral or stretched cobble lineation

Plunge of minor fold axis

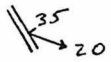

Strike and dip of axial plane and plunge of axis of fold

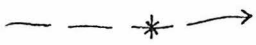

Approximate location of trace of synclinal axial surface showing direction of plunge